TECHNICAL REPORT STANDARD TITLE PAGE

1. Report No.	2. Government Accession No.	3. Recipient's Catalog No.
FHWA/TX-83/15+254-1		

4. Title and Subtitle	5. Report Date
VERIFICATION OF ANALYSIS PROGRAMS FOR SOLID AND HOLLOW CONCRETE BRIDGE PIERS	September 1983
	6. Performing Organization Code

7. Author(s)	8. Performing Organization Report No.
T. E. Gilliam, Y. Yamamoto, R. W. Poston, and J. E. Breen	Research Report 254-1

9. Performing Organization Name and Address	10. Work Unit No.
Center for Transportation Research The University of Texas at Austin Austin, Texas 78712-1075	11. Contract or Grant No. Research Study 3-5-79-254

12. Sponsoring Agency Name and Address	13. Type of Report and Period Covered
Texas State Department of Highways and Public Transportation; Transportation Planning Division P. O. Box 5051 Austin, Texas 78763	Interim
	14. Sponsoring Agency Code

15. Supplementary Notes

Study conducted in cooperation with the U. S. Department of Transportation, Federal Highway Administration. Research Study Title: "Design of Slender Nonprismatic or Hollow Bridge Piers or Columns"

16. Abstract

In this report the details and results of an experimental investigation of the stiffness and strength of typical solid and hollow cross section reinforced concrete bridge piers is summarized. The piers were subjected to combinations of axial load and biaxial moments typical of bridge pier applications. Stiffness measurements from the current series as well as measured behavior from solid pier tests previously reported in the literature were compared to analytical predictions based on a generalized fiber model used with computer code BIMPHI. In addition force displacement relationships computed using computer codes PIER and FPIER were compared to previously reported test results for a wide variety of columns, beams and frames. The comparisons showed these programs to be accurate, yet conservative, programs for prediction of stiffness, strength and behavior of solid, hollow and multi-cell bridge piers and bents.

17. Key Words	18. Distribution Statement
reinforced concrete, bridge, piers, solid, hollow, stiffness, strength, axial load	No restrictions. This document is available to the public through the National Technical Information Service, Springfield, Virginia 22161.

19. Security Classif. (of this report)	20. Security Classif. (of this page)	21. No. of Pages	22. Price
Unclassified	Unclassified	188	

Form DOT F 1700.7 (8-69)

VERIFICATION OF ANALYSIS PROGRAMS FOR SOLID AND HOLLOW CONCRETE BRIDGE PIERS

by

T. E. Gilliam
Y. Yamamoto
R. W. Poston
and
J. E. Breen

Research Report Number 254-1

Design of Slender Nonprismatic or Hollow Bridge Piers or Columns

Research Project 3-5-79-254

Conducted for

Texas
State Department of Highways and Public Transportation
in cooperation with the
U. S. Department of Transportation
Federal Highway Administration

by the

CENTER FOR TRANSPORTATION RESEARCH
BUREAU OF ENGINEERING RESEARCH
THE UNIVERSITY OF TEXAS AT AUSTIN

September 1983

The contents of this report reflect the views of the authors who are responsible for the facts and accuracy of the data presented herein. The contents do not necessarily reflect the views or policies of the Federal Highway Administration. This report does not constitute a standard, specification or regulation.

PREFACE

In this report, the experimental and verification phases of a study on "Design of Slender Nonprismatic or Hollow Bridge Piers or Columns" is presented. The basic objectives of the overall study was to develop design-oriented procedures for slender reinforced concrete bridge piers with special attention to tapered and hollow bridge piers. A major subsidiary objective was to verify components of the design method not previously authenticated such as the stiffness of hollow cross sections. In this report, test results from both previously reported and current physical model tests are compared with the predictions of several computer codes developed as a part of this project. The current test series was designed to reflect actual prototype hollow pier cross sections and variables as determined from the results of responses to a state-of-the-art questionnaire and from plans of actual bridges submitted with those responses. The test results validate the analytical methods used in the design phase of this project.

In the final report on this project, the specific design procedures and computer codes developed will be reported. The present report documents the accuracy of several of these routines when applied to typical hollow bridge pier cross-sections.

The work was sponsored by the Texas State Department of Highways and Public Transportation and the Federal Highway Administration, and administered by the Center for Transportation Research at the University of Texas at Austin. Close liaison with the State Department of Highways and Public Transportation has been maintained through Mr. Dave McDonnold, the contact representative during the project. Mr. Gary Johnson has provided similar liaison for the Federal Highway Administration.

The project was conducted in the Phil M. Ferguson Structural Engineering Laboratory located at the Balcones Research Center of The University of Texas at Austin. The authors are particularly indebted to Professors J. O. Jirsa and J. Roesset for their valuable assistance in the overall study.

IMPLEMENTATION

The results of the detailed physical tests and the comparisons with the analytical programs reported herein are important in establishing the applicability of the programs PIER and FPIER for analysis of a wide variety of solid and hollow concrete piers. Comparative design studies between solid and cellular tall piers for bridges in the 200 ft span range have indicated that provision of a cellular pier with the same approximate stiffness as a solid pier can result in substantial dead load reductions resulting in important foundation cost savings as well as savings in pier material costs. The verification of the design programs provided by the comparison with test results will lead to acceptance by designers and make it easier for them to utilize these possible savings. In addition, the use of the programs should simplify analysis of tapered and flared piers which may be desirable for economic or aesthetic reasons.

SUMMARY

In this report the details and results of an experimental investigation of the stiffness and strength of typical solid and hollow cross section reinforced concrete bridge piers is summarized. The piers were subjected to combinations of axial load and biaxial moments typical of bridge pier applications. Stiffness measurements from the current series as well as measured behavior from solid pier tests previously reported in the literature were compared to analytical predictions based on a generalized fiber model used with computer code BIMPHI. In addition force displacement relationships computed using computer codes PIER and FPIER were compared to previously reported test results for a wide variety of columns, beams and frames. The comparisons showed these programs to be accurate, yet conservative, programs for prediction of stiffness, strength and behavior of solid, hollow and multi-cell bridge piers and bents.

C O N T E N T S

Chapter

Page

TABLES

F I G U R E S

N O T A T I O N

A_s = area of steel in section

A_{st} = total area of longitudinal reinforcement

b = width of compression face

b_{eff} = effective flange width

b_{oH} = one-half of difference between effective flange width and web width

b_w = web width

e = eccentricity of axial load from neutral axis of a compression member

E_c = concrete modulus

E_s = steel modulus

f'_c = compressive strength of concrete (determined with 6 in. × 12 in. cylinders)

f_y = yield point of steel

H = lateral load

k = effective length factor

K = constant

ℓu = unsupported length of a column

L = length of member

M = moment

M_N = nominal ultimate strength for moment

M_{STR} = moment about strong axis

M_{WK} = moment about weak axis

M_x = moment about x-axis

M_y = moment about y-axis

P = axial load

P_N = nominal ultimate strength for axial load

P_o = pure axial load strength

P_u = axial load at ultimate

r = radius of gyration of a cross section of a compression member

R = capacity reduction factor used in conjunction with the R-method (ACI 318-63)

t = time; thickness of wall of hollow section; width of section

$\bar{x}$ = mean value

X_u = longest dimension of the hollow portion of a section

z = shear span

Δ = deflection

ϵ = strain

ϵ_u = strain at ultimate

μ = microstrain (1×10^{-6} in./in.)

ρ''_h = volumetric ratio of hoop reinforcement to confined concrete

σ = standard deviation

ϕ = curvature

CHAPTER 1

INTRODUCTION

1.1 Bridge Pier Design Trends

Current trends in bridge construction indicate increasing use of slender compression members. This is primarily due to the growing utilization of higher compressive strength concretes. In addition, sensitivity to bridge aesthetics has increased utilization of flared and tapered bridge piers such as shown in Fig. 1.1.

Many successful bridge projects have utilized slender piers and columns of cellular cross section to provide adequate stiffness and strength but with substantial saving of dead load. This dead load reduction results in reduced material and foundation costs. Such savings can be quite substantial, depending upon the geometric configuration of the cross section. When a hollow cross section exceeds a width to depth ratio of 3, the cost of extra formwork probably exceeds the material savings, but the reduction in dead load can still produce appreciable savings in foundation cost. Slip form construction techniques are well-suited to hollow or cellular pier construction. Use of these methods in hollow pier construction could produce even greater savings due to reduced formwork costs.

1.2 Needs of the Designer

Designers are facing increasing difficulty with bridge pier ddsign as slender nonprismatic or hollow piers become more commonplace. Recent revisions to the AASHTO Specifications [1] base the design of slender concrete compression members on the slender column design procedures of the ACI Building Code (ACI 318-77) [2,3]. These procedures are applicable over a wide range of slenderness ratios and are considerably

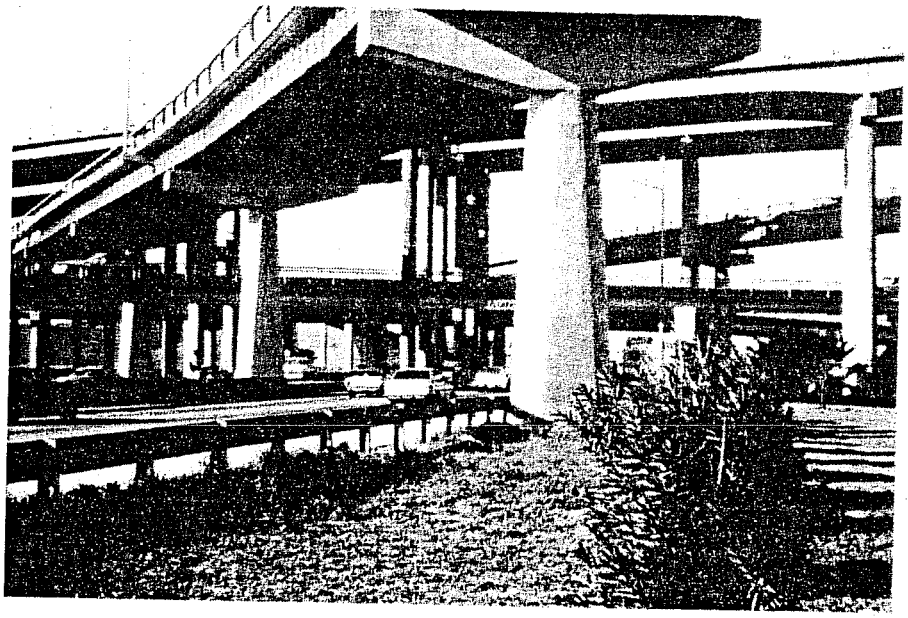

(a) In a busy highway exchange

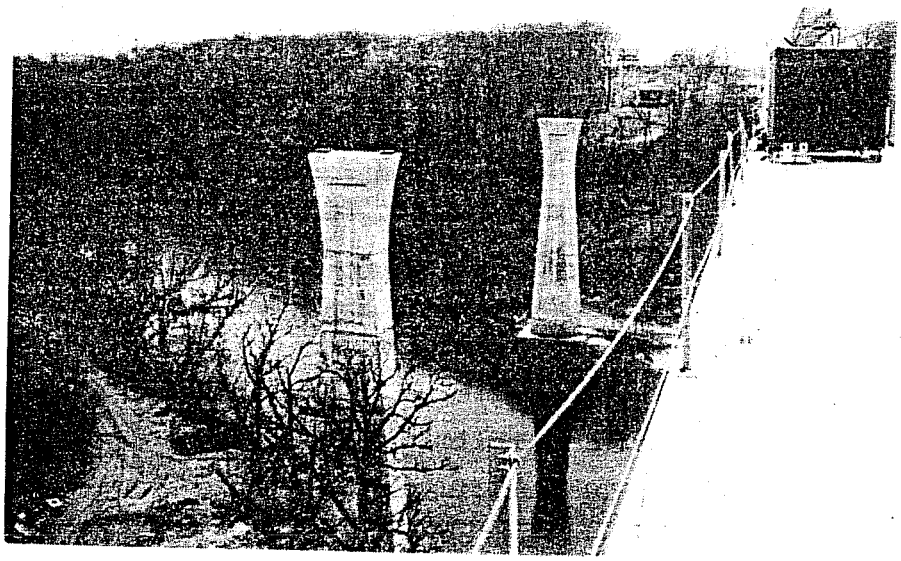

(b) As a part of a river crossing

Fig. 1.1 Tapered bridge piers

more accurate for unbraced piers. The basic provisions of Article 1.5.34(A)(1) require a second order analysis which is based on realistic moment-curvature relationships considering the effects of cracking, reinforcement, and time effects. Such second order analyses have not been previously verified for hollow cross sections. In lieu of such an analysis, Article 1.5.34(A)(2) requires an approximate evaluation of slenderness effects using the moment magnification procedure of Article 1.5.34(B).

The revised AASHTO Specification [1] rules for concrete column slenderness only include the ACI Code [2] provisions without the Code Commentary provisions. This complicates slender compression member design by the moment magnification method, since many of the guidelines for using this method were presented in the Commentary. However, even with adequate explanatory material concerning the use of the moment magnification procedures, the application of the procedures to tall bridge pier design is difficult in some cases.

Both the second order analysis and the moment magnification procedure are very time-consuming when they are used apart from computer codes or suitable design aids. In addition, the important empirical equations for stiffness used in the moment magnification procedure were developed based on solid prismatic column tests. No consideration was given to hollow piers; therefore, the validity of the approximate magnification procedure for those cases is unchecked. Some promising analytical procedures have been developed to treat irregular sections, but they have not been verified by experimental evidence other than tests of typical solid prismatic piers. In addition, all basic parameters for the slenderness procedures were based on typical building values with no regard for typical bridge values.

1.3 A Feasible Solution

Recent studies [4,5] have indicated that the design of slender compression members can be achieved more efficiently by using a second

order structural analysis procedure than by using the moment magnification procedures. These second order analysis procedures are more efficient when design programs are developed for implementation on electronic digital computers. With such analysis procedures, the deflection limits as well as the strength limits can be programmed in, and a design produced which will meet both limits.

Based on these designer needs, Poston, et al. [6,7] developed refined second order structural analysis programs for bridge piers. The key element is a computer routine which would calculate the biaxial P-M-ϕ relationship of an arbitrary section. That routine, called BIMPHI, was used as a major component of program PIER which predicts the space behavior of a single reinforced concrete bridge pier subjected to static loads. The pier may be of arbitrary section and longitudinal configuration. The programs can analyze circular, rectangular, or oval sections. The circular and rectangular sections can be solid or hollow. The piers can have cross sections of varying linear geometry and end conditions. Poston verified the accuracy and applicability of the routines for solid section piers. The present report summarizes the verification for solid cross sections and extends the verification to hollow and cellular cross sections.

1.4 Purpose of the Investigation

A primary purpose of this investigation was the verification of the accuracy of program BIMPHI in calculating the P-M-ϕ behavior of hollow cross sections. Examples of solid section behavior selected from the engineering literature were checked to verify the overall accuracy of the programs. Comparisons are presented in this report. Very limited data were available on hollow sections. To provide this information, four model column specimens were fabricated and tested cross sections varied from solid sections through three cell cross sections. Each column had a realistic bridge pier cross section but had negligible slenderness effects. The tests in this study investigated only the P-M-ϕ

behavior and strength of these cross sections. There is little question that verified results of section stiffness can then be validly integrated to determine member behavior. Typical examples of such verifications for solid cross sections using PIER are summarized. In addition, program FPIER was developed to handle multiple bay and multiple story bents. It is also compared with data from the literature.

One of the primary assumptions used in developing program BIMPHI was that plane sections remain plane before and after bending. This assumption has been previous verified for solid sections [8]. A possibility exists that with biaxial bending in thin-walled hollow sections, some nonplanar action might occur. Very few hollow compression member tests have been conducted. Thus, it was felt that this basic assumption needed to be examined for validity in this application. For this reason, the check of the applicability of the plane sections assumption in typical hollow pier sections was a major purpose of this study.

1.5 Report Contents

A very brief review of the analytical procedures used is included in Chapter 2. Detailed information on these procedures is given in Ref. 7. Comparisons of the analytical results with test results previously reported in the literature are also given in Chapter 2. Details of the fabrication, instrumentation, and loading of the hollow pier test series are given in Chapter 3. Test results from the hollow pier test series are summarized in Chapter 4 and compared to analytical predictions. Chapter 5 gives the conclusions determined from comparisons with the hollow section test series results as well as other pier tests previously reported in engineering literature.

CHAPTER 2

REVIEW OF PREVIOUS ANALYTICAL METHODS AND EXPERIMENTAL VERIFICATIONS

2.1 Brief Review of Analytical Methods

A more detailed review of analytical approaches and the development of the selected fiber model is given in the companion report (Ref. 7). This report includes only enough description so a reader will understand the general nature of the method chosen.

There are a large number of methods for analytically determining the behavior of bridge piers. Some can be classified as hand computation methods, while others are more complex and are practical only as electronic computation methods. This review will explain the need for an electronic computation based method and the reasons for the choice of the fiber model formulation.

2.1.1 Hand Computation Methods. Within this category the two most widely recognized methods for bridge pier design are the moment magnifier design method of the present AASHTO Specifications and the long column reduction factor design method previously used by AASHTO.

2.1.1.1 Moment Magnifier Design Method (AASHTO, ACI 318-77). This method is based on a moment magnifier which approximates the amplification of the column moments in order to account for the effect of axial loads on these moments, commonly called the PΔ effect. The moment magnifier is a function of the ratio of the column axial load to the Euler buckling load (which empirically considers column stiffness), the ratio of the column end moments, and the deflected shape of the column [3]. The method is particularly difficult to use with biaxial loading. Unfortunately, many of the empirical values used in this

method were selected based on typical building columns and their loading conditions and not based on typical bridge piers. Also, the basic studies used in developing and verifying this method were all based on solid prismatic columns without any consideration of hollow, cellular, or tapered cross sections. Finally, the design of a bridge pier may be controlled by a deflection limit rather than a strength limit, and this method presently does not have the capability of imposing such limits.

2.1.1.2 Long Column Reduction Factor Design Method (ACI Building Code Commentary) [3]. This method is based on a reduction factor R which is a linear function of the $k\ell_u/r$ ratio. The short column strengths, P_n and M_n, are each divided by R to obtain the allowable long column strength. This method is the easiest to use of the methods, but it has serious shortcomings [9]. One of the most serious is that moment values computed by the reduction factor method may be substantially less than what really exists. If these moments are used in designing the restraining members, they may be seriously in error. In addition, computer analyses and physical tests have shown the failure loads calculated by this method to be unsafe for many unbraced column or pier cases [10].

2.1.2 Electronic Computation Methods. Review of the approximate hand computation methods showed that they were inadequate for predicting the behavior of all bridge piers. Two options exist to solve this problem. One solution is to expand one of the approximate methods or to develop a new hand computation method to represent all bridge pier behavior. However, extensive test data of hollow, cellular, and nonprismatic piers under various loadings is required to develop such a method. Therefore, this option is not practical at this point. The second option is to develop a more exact second order structural analysis which, in accordance with AASHTO Article 1.5.34(A)(1), would use realistic moment-curvature relationships based on accurate material stress-strain relationships and consider the effects of axial load, variable moment of inertia along the member, creep due to sustained loads, and the effects

of lateral deflections on moments and forces. Such an analysis should be verified by experimental results.

Second order structural analysis methods are only practical when programmed for an electronic computer. A number of methods were reviewed in detail, as reported in Ref. 7. The selected method will be described in more detail in a following section.

There are two general methods for such an analysis [6]. The first technique is an iterative search procedure. This procedure would first establish a relationship between the axial load, moment, and curvature of a section. Then it determines the plane of strains at that section. Once the plane of strains is determined, the curvatures can be calculated, and by using the previously established P-M-ϕ relationship, the axial load and moment can also be determined. The iterative search procedure was not chosen because it would be difficult to extend to hollow or nonprismatic members.

All of the other methods considered are variations of the second technique and are based on stiffness formulations. A general nonlinear stiffness solution would involve formulating the member stiffnesses, assembly of a total system matrix, and then solving the equilibrium equations for the unknown displacements. The drawback of this technique is usually the great amount of computer storage and time needed to execute such an analysis. However, the fiber model can accomplish the analysis with greatly reduced storage and time requirements [6]. This is due to the way it handles material nonlinearities when some simplifying assumptions can be made.

To handle axial load-moment-curvature relationships, the grid method, variations of the grid method, and the fiber model were reviewed. The fiber model was felt to be superior due to its ease of handling boundary conditions for hollow sections [6,7]. In the fiber model, incremental curvatures are applied about the strong and weak axes, and from these incremental curvatures, changes in strain are calculated.

Then incremental stiffness parameters are found, which in turn are used to calculate the incremental moments about the strong and weak axes.

Several methods of load-deflection analysis were reviewed. The first method involved assuming a sine curve for the deflected shape while another assumed several shapes until the deformed shape was found [6]. Other techniques reviewed were the finite difference method and the finite element method. Again, the fiber model was felt to be the best method for analyzing bridge pier behavior. This decision was based primarily on the fiber model's adaptability to handle arbitrary cross sections and arbitrary longitudinal configurations. Also, the problems of material nonlinearities and slenderness effects are easily handled by the fiber model [6,7].

Using the fiber model for a load-deflection analysis is merely an extension of the previously discussed P-M-ϕ analysis using the fiber model. Fig. 2.1 shows how a pier is divided into longitudinal segments and the segments into sections. Each section is divided into fibers. Loads are then incrementally applied, and the incremental displacements and forces are calculated. After new stiffness parameters are found, the procedure is repeated. Then the total stiffness matrix for the pier is assembled, and the equations of equilibrium are solved [6,7].

2.2 Fiber Model Programs

The fiber model was chosen by Poston [6,7] as the best method to use in predicting the behavior of slender nonprismatic or hollow bridge piers. He used this model to develop two computer programs. The first program, BIMPHI, was developed to predict the behavior of a cross section by calculating the values of the P-M-ϕ relationship for that section. The second program, PIER, utilizes BIMPHI as a subroutine and can compute the behavior of a single pier element (uniform, tapered, solid, hollow, etc.) under realistic highway-type loadings. A third program, FPIER, treats single or double story pier bents of multiple columns and was developed

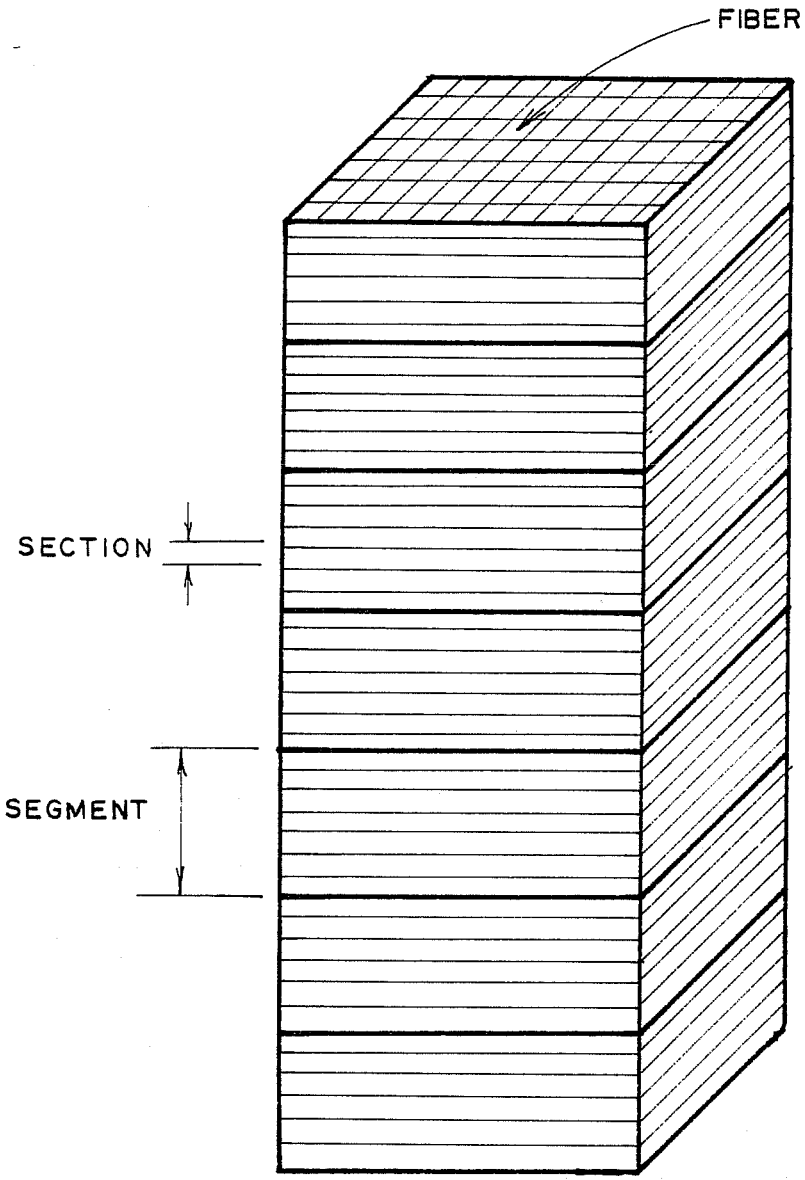

Fig. 2.1 Fiber model representation of a rectangular solid prismatic bridge pier

by Diaz using BIMPHI and PIER as subroutines. Users guides for all three programs are presented in Ref. 7.

2.2.1 The Fiber Model. A detailed formulation of the fiber model is presented in Refs. 6 and 7 and is not repeated here. However, the model can be summarized as follows:

The principal assumption of the method is that small changes in displacement can be linearly related to small changes in force. In order for this to be true, a segment or member must be analyzed in the undeformed position, thus individual member stability is not considered, but only overall pier stability.

Each member is divided into a series of cross sections and each cross section into fibers. The first step in assembling the stiffness matrix is calculation of flexibility coefficients from the fiber dimensions and stress state of each cross section. The integration over the cross section is accomplished by summing over each fiber for all fibers of a cross section. Once these flexibility coefficients have been determined, the flexibility matrix is formed by summing the appropriate flexibility term for each cross section over all the cross sections of the segment or member. The member flexibility matrix is then inverted to form the member stiffness matrix. The member stiffness matrix is then rotated into global coordinates and added to the total pier stiffness matrix.

After the new joint displacements and forces have been computed by the stiffness method, the inverse of the original member force-strain assumption is used to calculate the incremental strains at each cross section. From these strains, the strain of each fiber in the cross section can be computed. This now makes it possible to recalculate the stiffness coefficients and the procedure begins again.

In summary, the assumption made in the fiber model is that small changes in member force can be linearly related to small changes in member strains, and the geometry of the member in the deformed position

is a straight line. A method of generating cross sections and fiber is used to assemble the stiffness matrix and monitor the strains. The stiffness matrix is reassembled for every load increment and the cycle is continued until all increments of load have been applied to the pier, or there is a material or stability failure of the pier. P-delta, geometrical, and material nonlinearities are included in the formulation.

2.2.2 Program BIMPHI Details. Program BIMPHI was developed for the purpose of calculating the axial load-moment-curvature relationship of a section subjected to axial loads and biaxial bending moments. The program will allow the user to load the section by incrementing moments about both axes, by incrementing curvatures about both axes, or by incrementing curvatures about one axis and moments about the other axis. Additionally, axial load may be held constant or incremented, or an axial strain may be incremented instead. If moments are incremented, curvatures are calculated, and if curvatures are incremented, moments are calculated. BIMPHI assumes that the ratio of the two incremented values remains constant. This is important in the case of a biaxially loaded column if second order deflections become significant. Due to these increased lateral deflections, the applied moments will not equal the actual total moments at various cross sections along the member. BIMPHI does not account for these second order effects, so the user must be careful to only use BIMPHI for section behavior as is needed in short columns. For slender columns a program like PIER should be used in which second order effects are accounted for. One of the favorable aspects of being able to increment curvatures is that the descending portion of the moment-curvature curve can be obtained. This is important when the criteria for design may be a deflection limit as is possible with slender bridge piers.

A general flowchart of BIMPHI is shown in Fig. 2.2. The cycle shown is repeated until a material failure occurs. A compressive failure is assumed if the specified limiting strain of the concrete is exceeded. A tensile failure is assumed if the strain in any of the steel fibers exceeds 1%.

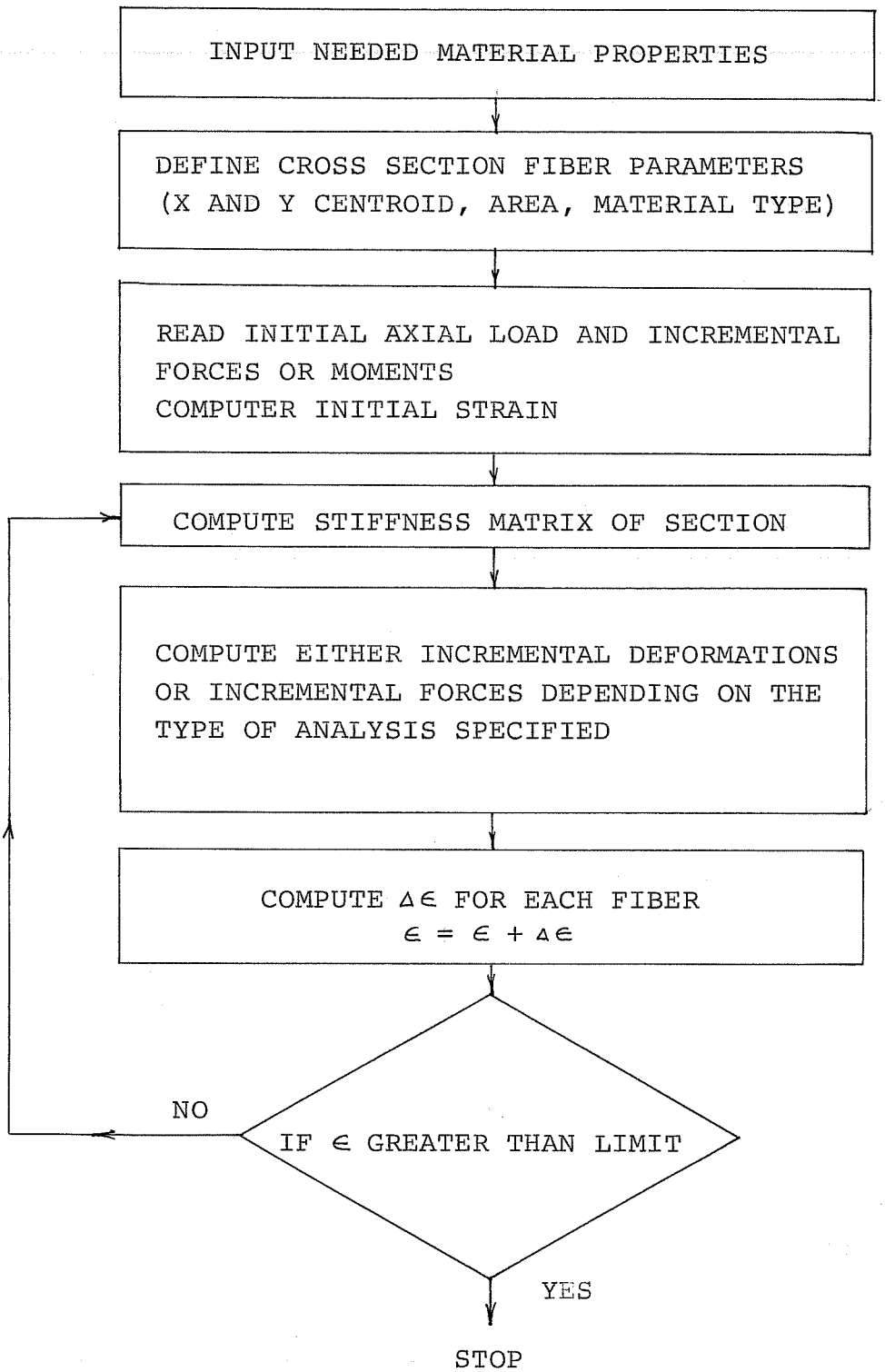

Fig. 2.2 Flowchart of program BIMPHI

Only a small amount of input is required to initiate the operation of BIMPHI. The program generates the concrete and steel fibers, allowing up to 200 fibers for each of the two materials. The steel is modeled as a ring of steel, as shown in Fig. 2.3, unless the user opts to input the location of each reinforcing bar. Actually, the user is only required to input the basic section geometry, material properties, and the type of analysis. The program can consider creep effects by modifying the short-term stress-strain relationship of the concrete. Presently the program can generate the P-M-ϕ behavior of any of the cross sections shown in Fig. 2.4.

The output given by BIMPHI is in the form of axial load, moment about the x-axis, moment about the y-axis, curvature about the x-axis, and curvature about the y-axis. This is given twice for each applied increment. The first line of these values is calculated from the strains, and the second line of values is calculated from equilibrium. Usually a minimum of 50 increments is used for accurate results.

2.2.3 Limitations. The user should be aware of the limitations of BIMPHI. It deals only with the axial load-moment-curvature relationship of a cross section. Variation in cross section along a pier requires that a higher level program like PIER be utilized. The assumptions of the fiber model, such as small changes in strain are linearly related to small changes in force and plane sections before bending remain plane after bending, must be true for the case being analyzed. BIMPHI is also limited to closed symmetrical sections and a maximum of 200 fibers each of concrete and steel. Finally, a maximum of three rings of steel is allowed to model the reinforcement, and a maximum of five interior walls is permitted for a cellular section.

2.3 Comparison of Analysis with Previously Reported Tests

In order to verify the method of analysis developed, results of several previous investigators were compared with predictions using BIMPHI, PIER, and FPIER. BIMPHI was checked against several uniaxial and

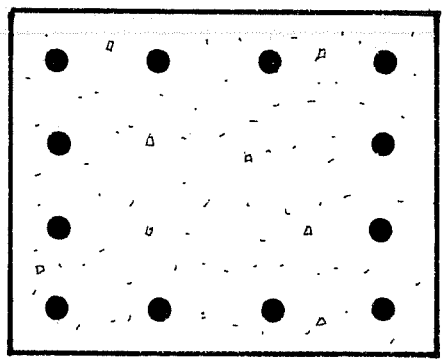

ACTUAL CONCRETE SECTION

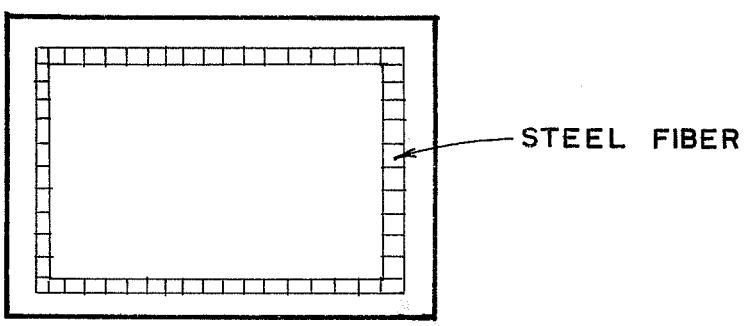

SECTION SHOWING REINFORCING STEEL
MODELLED AS MANY STEEL FIBERS
IN A RING

Fig. 2.3 Modeling of reinforcing bars

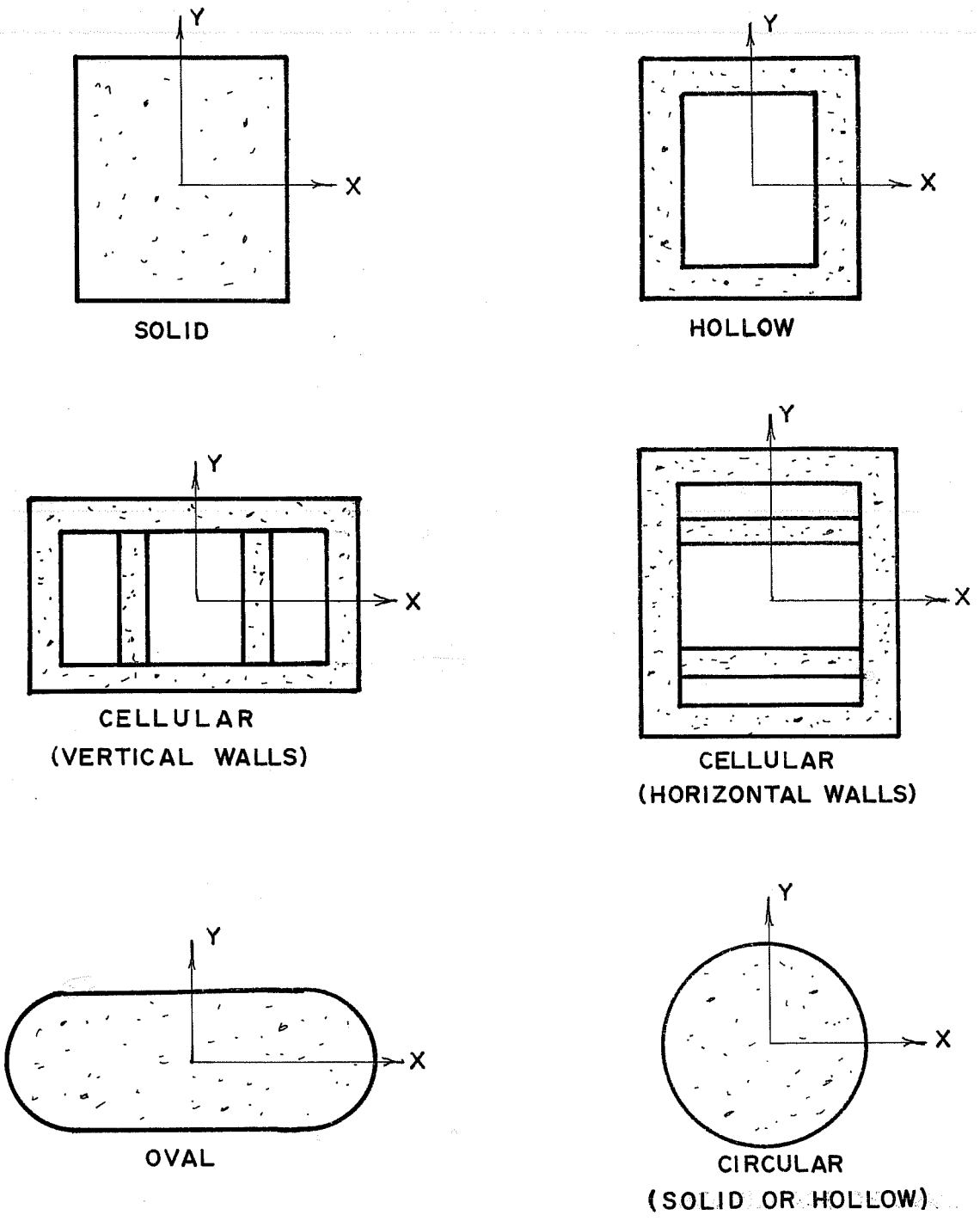

Fig. 2.4 Sections handled by BIMPHI at present

biaxial moment-curvature cases. Predictions from PIER were checked for both planar and space behavior of a beam-column. Predictions from FPIER were checked for beam-columns and frame conditions. The test specimens checked were arbitrarily selected for the study to give reasonable range and scope.

2.3.1 Check of Program BIMPHI

2.3.1.1 Breen. BIMPHI was used to investigate the moment-curvature relationship of two column sections subject to a constant axial load and single axis bending. The column sections analyzed were from two columns previously analyzed and tested by Breen [11]. The two column cross sections and pertinent material properties are shown in Fig. 2.5. A Hognestad-type stress-strain curve was used in the analysis, since no moment gradient existed along the column. However, a maximum compressive stress of 0.95 f'_c was used because the columns were horizontally cast. A least squares fit of the test data obtained by Breen is shown in Figs. 2.6 and 2.7. The bending was about the y-axis.

Figures 2.6 and 2.7 present the results of the comparisons. As can be seen, the predicted results from BIMPHI are very close to the experimental results, certainly within the range of the original scattered data. The results are closer than those originally predicted by Breen because the effect of some residual tension after cracking of concrete was accounted for in this program and because the assumption of maximum compressive stress of 0.95 f'_c was made for a horizontally cast member. The major difference in the two columns examined was the level of constant axial load. Column C5 failed by crushing of concrete before yielding of the reinforcement, whereas Column C7 failed by yielding of reinforcement before crushing of concrete.

2.3.1.2 Ford. Ford [12] tested his columns with a controlled deformation procedure. The columns were subject to single axis bending. In addition to the axial loads, the columns were laterally loaded at a pin in the center of the column. Both ends were fixed, thus the specimen

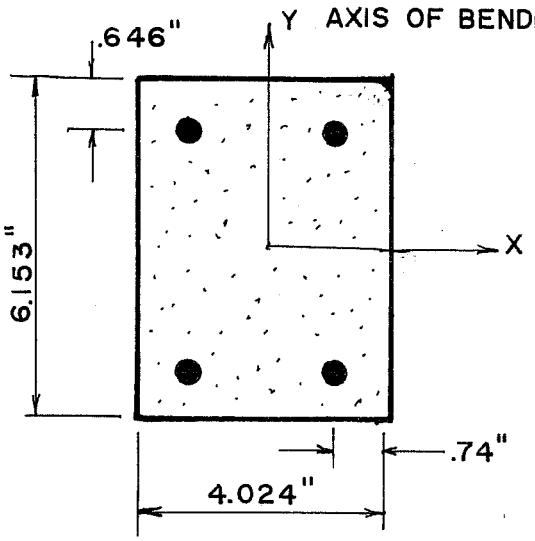

f'_c = 3005 psi

f_y = 52100 psi

E_s = 29×10^6 psi

A_{st} = $4 \times 0.11 = 0.44$ in.^{2}

P/P_o = 0.524

BREEN COLUMN SECTION C5

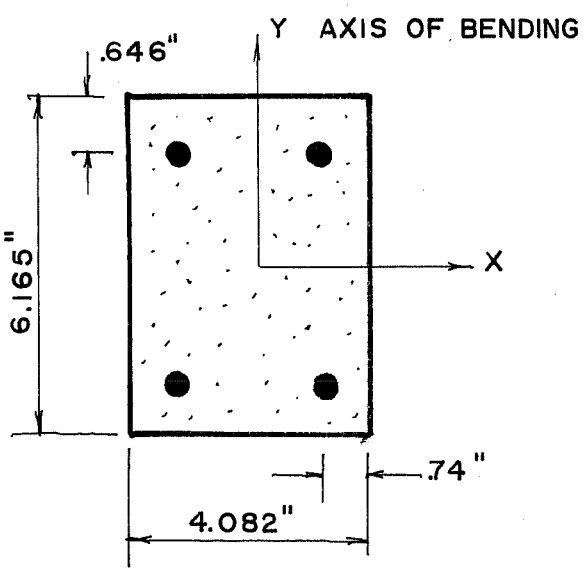

f'_c = 3670 psi

f_y = 51800 psi

E_s = 29×10^6 psi

A_{st} = $4 \times 0.11 = 0.44$ in.^{2}

P/P_o = 0.146

BREEN COLUMN SECTION C7

Fig. 2.5 Sections and properties of Breen's columns analyzed

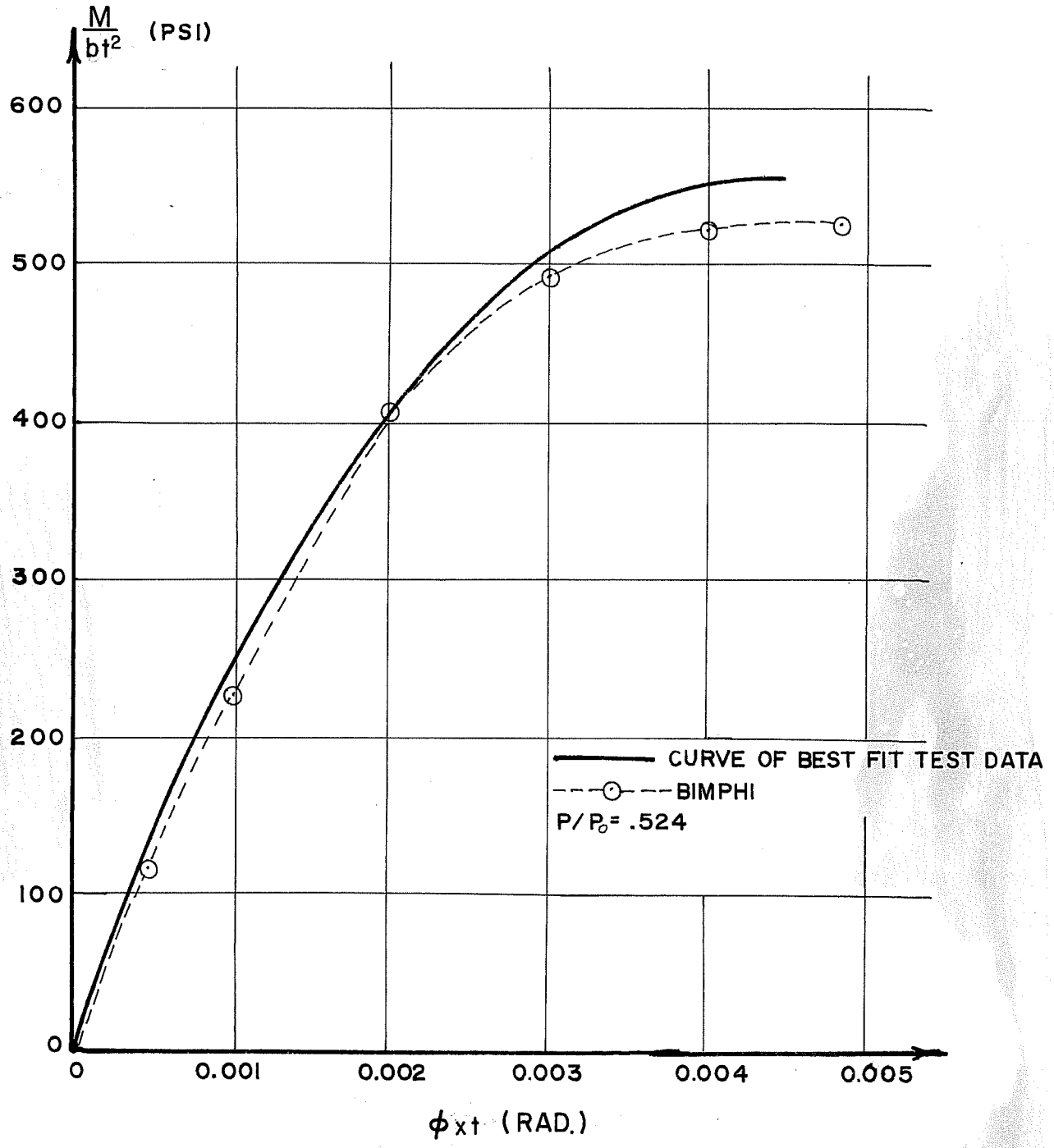

Fig. 2.6 Breen Column C5--moment-curvature curves

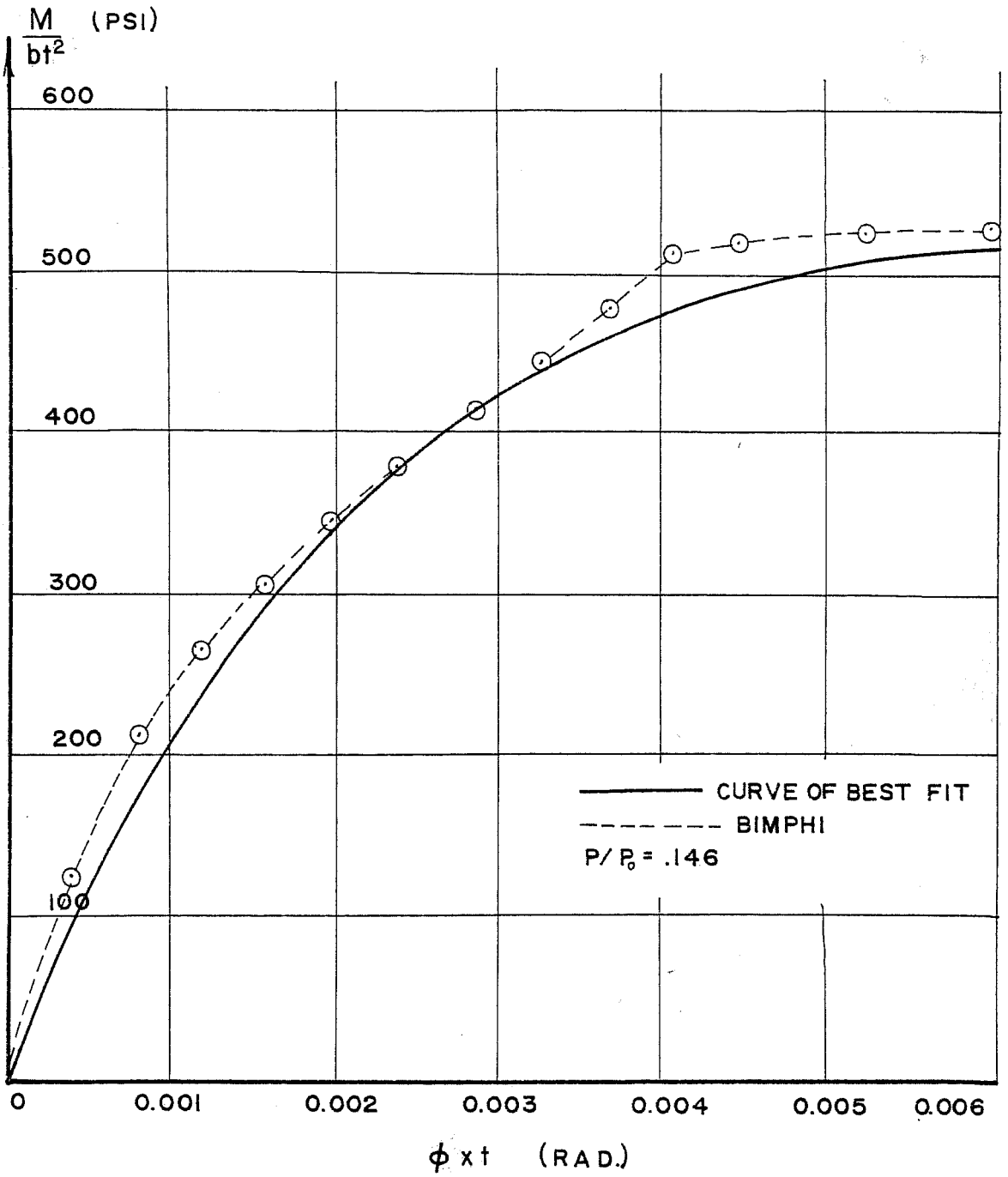

Fig. 2.7 Breen Column C7--moment-curvature curves

is really two cantilever columns loaded at the tip. This loading provided for a moment gradient along the member, thus confinement of the concrete. This effect should be included in the analysis when checking test results. It can be conservatively neglected in design. Pertinent information for the column sections analyzed is shown in Fig. 2.8.

Since the concrete is assumed confined, an ultimate strain must be estimated for the concrete. This was done using

$$\epsilon_u = 0.003 + 0.02 \frac{b}{z} + \left(\frac{\rho''_h f_y}{14.5}\right)^2 \text{ in./in.} \qquad (2.1)$$

where ϵ_u = ultimate strain

b = width of compression face

z = shear span

ρ''_h = volumetric ratio of hoop reinforcement to confined concrete

f_y = yield point of steel

For these columns b/z equals approximately 0.3 and ρ''_h equals approximately 0.003. Given these values, an ultimate strain of 1% was determined from Eq. 2.1. A maximum compressive stress of 0.95 f'_c was used as Ford suggested for the horizontally cast columns.

Ford used the controlled deformation method, thus was able to obtain the descending branch of the P-M-ϕ curve. Ford measured curvature at two points along his column. The station close to the base exhibited a much higher curvature than the curves shown in Figs. 2.9 and 2.10. The P-M-ϕ curve plotted represents the center of compression crushing. BIMPHI closely predicted the experimental curves obtained in Columns SC-6 and SC-9. Also shown in Figs. 2.9 and 2.10 are the P-M-ϕ curves obtained using the unconfined concrete stress-strain curve (Hognestad). This stress-strain relationship underestimates the strength and ductility of the column sections. The use of $f''_c = 0.95\ f'_c$ in the Ford stress-strain relationship seems correct for the horizontally cast columns.

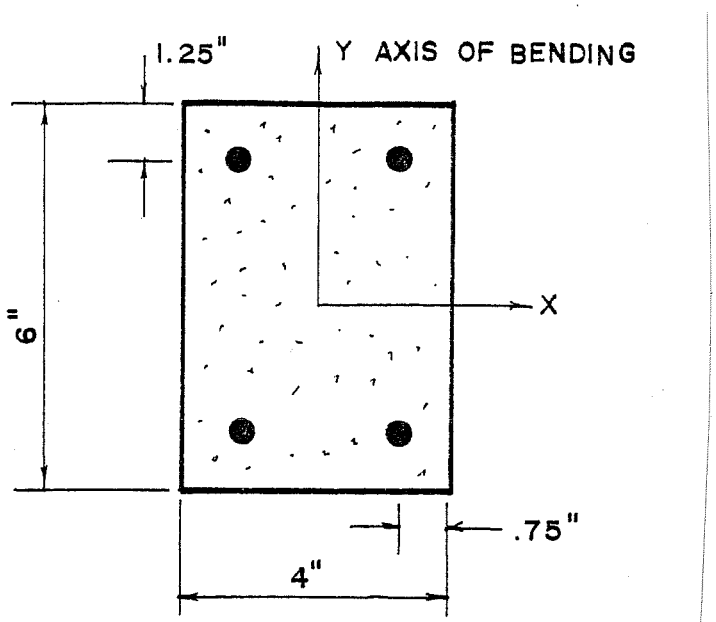

COLUMN CROSS SECTIONS

f'_c = 5590 psi	f'_c = 5285 psi
f_y = 58200 psi	f_y = 73300 psi
E_s = 29×10^6 psi	E_s = 29×10^6 psi
ρ''_h = 0.00345	ρ''_h = 0.00294
A_{st} = $4 \times 0.11 = 0.44$ in.^{2}	A_{st} = $4 \times 0.11 = 0.44$ in.^{2}
P/P_o = 0.62	P/P_o = 0.65
Ford Column SC-6	Ford Column SC-9

Fig. 2.8 Section and properties of Ford's columns analyzed

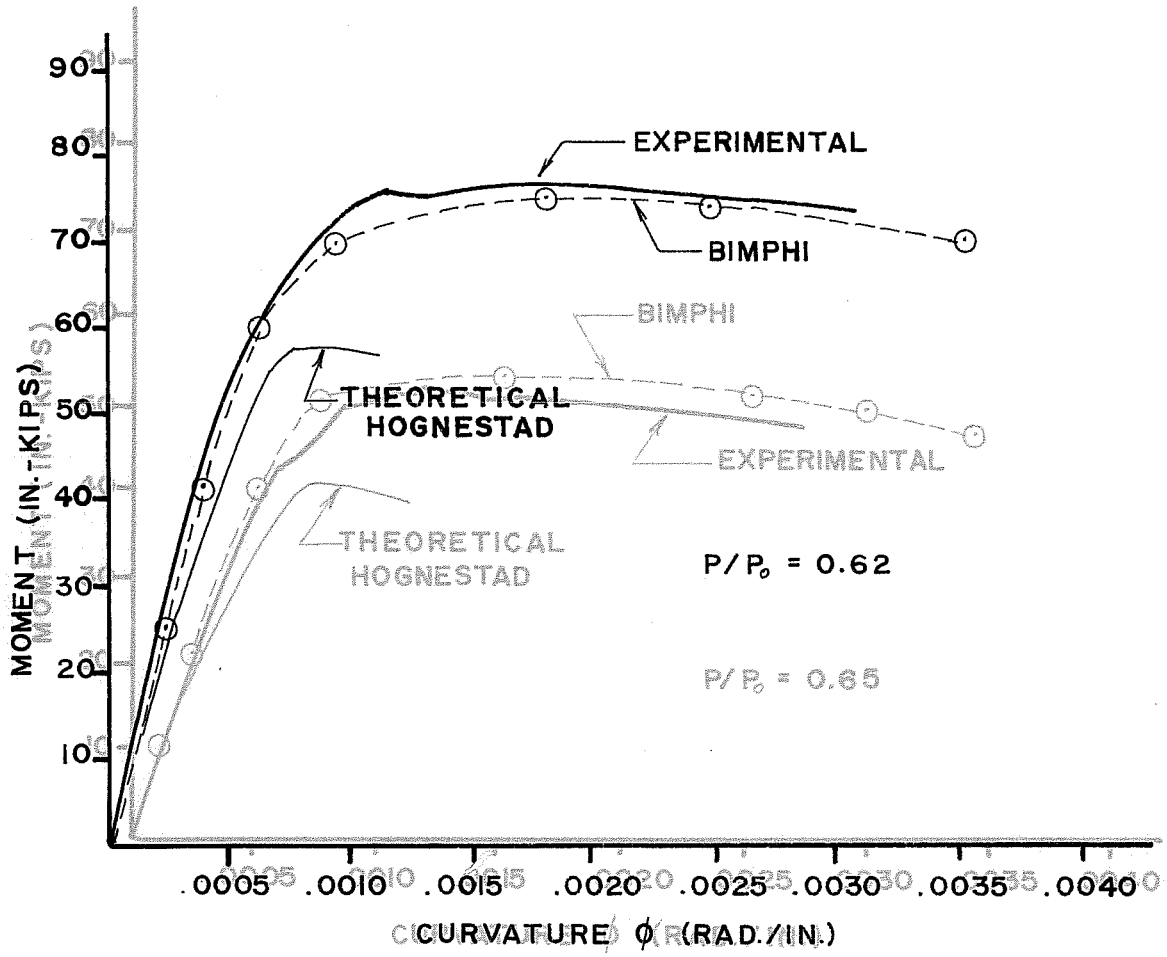

Fig. 2.10 Load-moment-curvature (P-M-ϕ) relationship

Fig. 2.9 Load-moment-curvature (P-M-ϕ) relationship for Ford Column SC-6

2.3.1.3 Mavichak. BIMPHI was used to investigate the moment-curvature relationship of column sections subject to a constant axial load and biaxial bending. The first column section analyzed was from a column analyzed and tested by Mavichak [13]. The column cross section and pertinent material properties are shown in Fig. 2.11.

Mavichak, in his column tests, presented biaxial moment-curvature data, but due to the secondary deflections occurring along the column in the controlled load tests, the ratio of biaxial moments changes. In the incremental curvature mode, BIMPHI works only for a constant ratio of incremental biaxial moments or curvatures. This is the reason why the results presented in Fig. 2.12 do not show good agreement at all levels. The results are excellent for the first few data points where the ratio of incremental biaxial moments is constant and the data correlation for strong axis bending is very good over the entire range since secondary deflections are small. Greatly improved results for this test will be shown in Sec. 2.3.2.2, where secondary deflections are treated by combining the cross section routine BIMPHI with the pier length program PIER.

The Mavichak pier series contained both rectangular and oval cross sections. In order to examine the general applicability of BIMPHI with other cross section types, one of Mavichak's oval pier tests was selected for comparison. The details of this model bridge pier are shown in Fig. 2.13. Figure 2.14 compares Mavichak's oval pier test results with BIMPHI's predictions. While there is some discrepancy between the values due to the changing ratio of biaxial moment, the general agreement is very good.

2.3.1.4 Proctor's Study of Hollow Columns. The first known investigation of hollow columns was in the late 1800's by Considére [14]. He conducted three tests on hollow cylindrical concrete columns. One specimen was unreinforced, while the other two contained longitudinal and spiral reinforcement. His conclusion was that hooped columns should

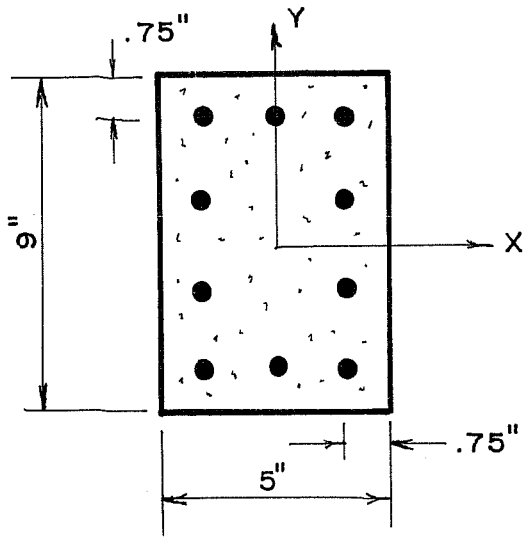

f'_c = 4871 psi

f_y = 66500 psi

E_s = 30×10^6 psi

A_{st} = $10 \times 0.044 = 0.44$ in.^{2}

P/P_o = 0.478

ΔM_x = 1000 lb.-in.

ΔM_y = 1000 lb.-in.

L = 72 in.

Fig. 2.11 Mavichak Column RC-2

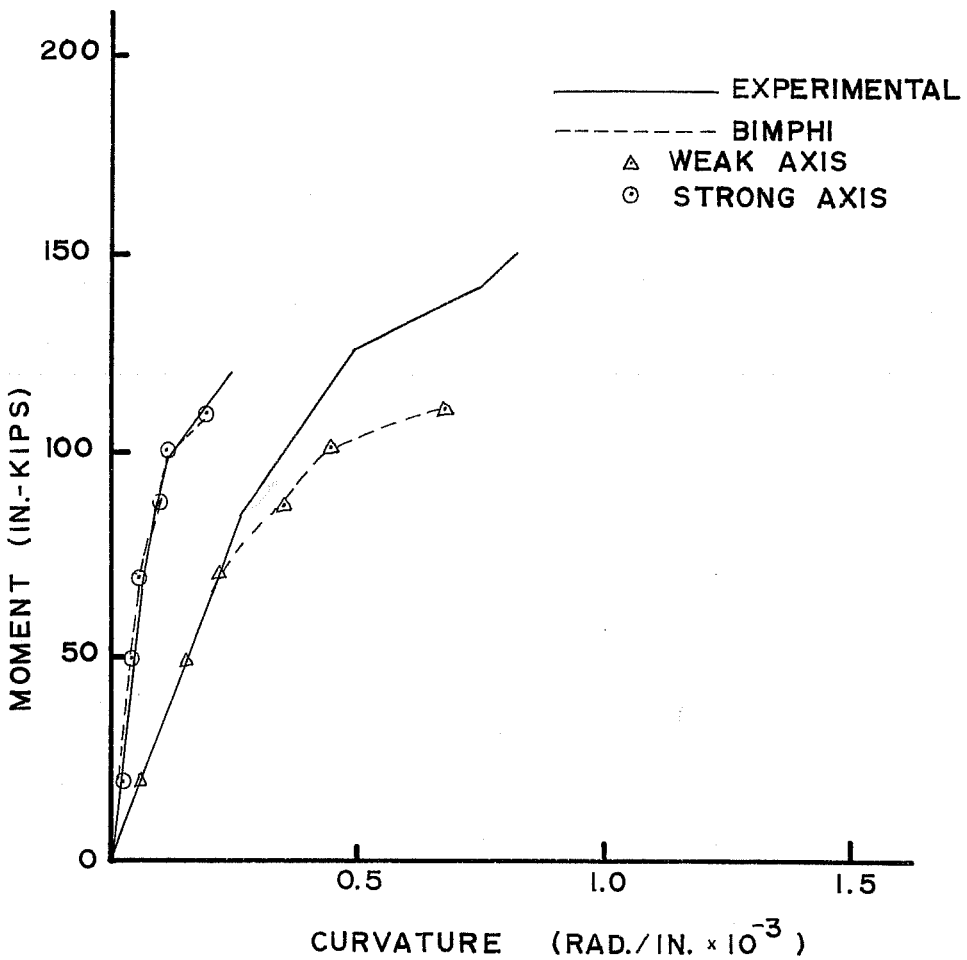

Fig. 2.12 Load-moment-curvature (P-M-ϕ) relationship for Mavichak Column RC-2

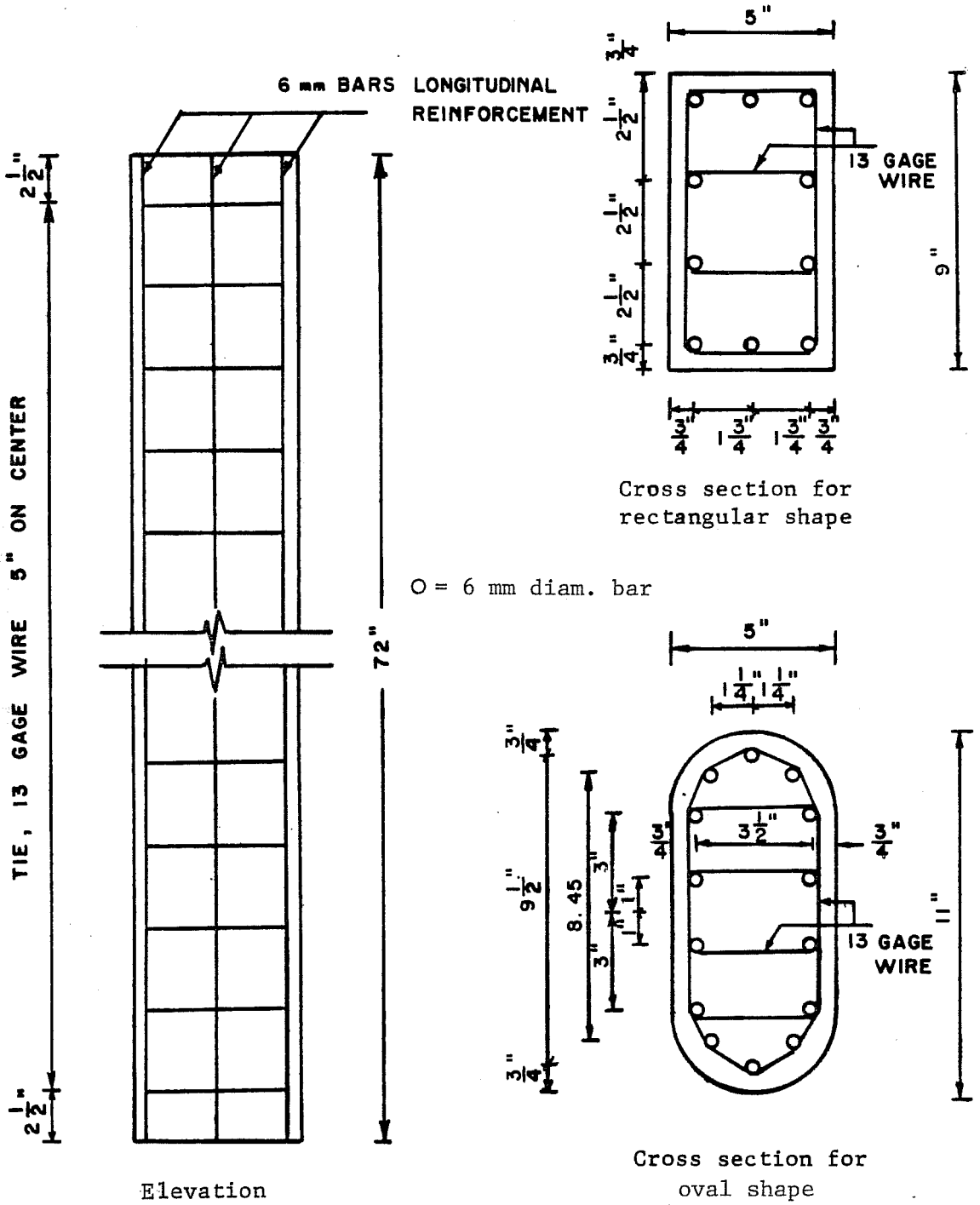

Fig. 2.13 Details of Mavichak's model bridge pier specimens

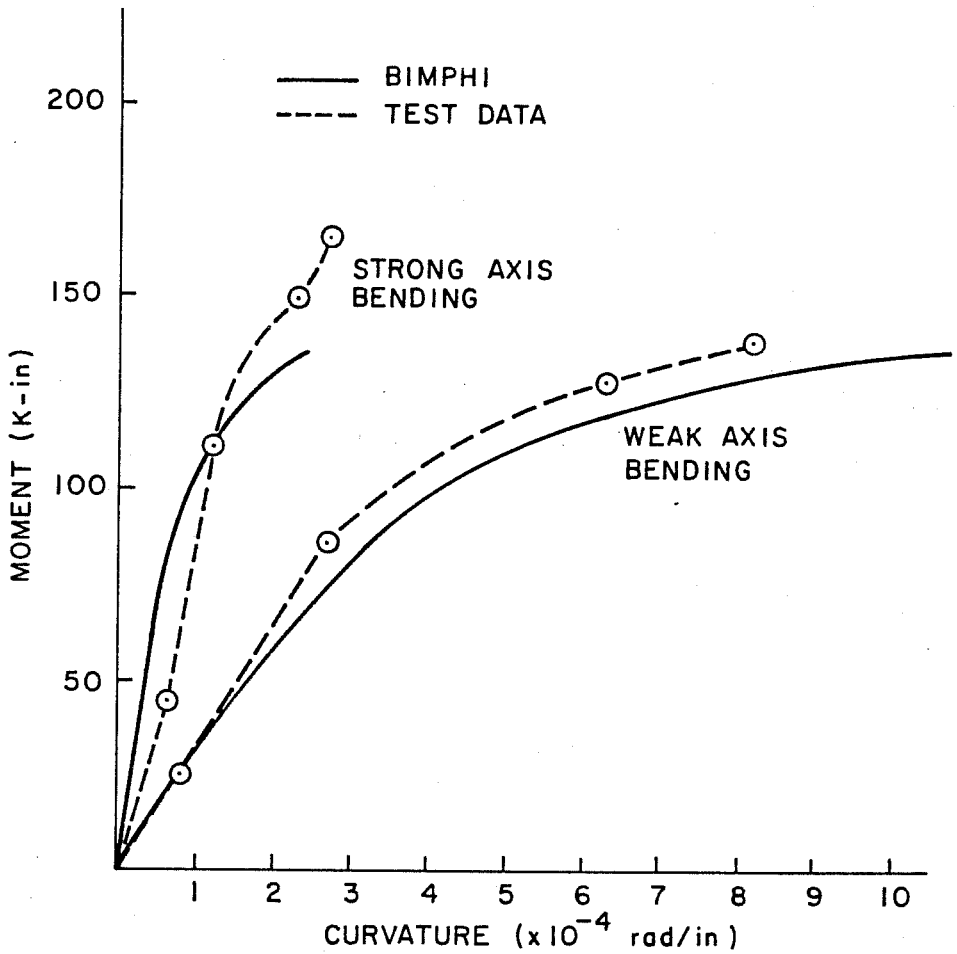

Fig. 2.14 Comparison of Mavichak's C-6 oval pier test data with BIMPHI's predictions ($P = 0.35P_o$, $M_{STR}/M_{WK} = 1.0$)

be solid or have small hollow cores due to a problem of concrete failing on the inward face. In much more recent tests, Procter [15,16] found this to not be a problem.

Procter carried out a series of investigations involving hollow cylindrical stub columns, hollow rectangular stub columns, and hollow rectangular slender columns. In the first series of tests of hollow cylindrical stub columns [15], concrete compressive strengths were high, ranging from 5300 to 9600 psi. In these tests, added reinforcement was found to increase the strength of the column by 12 to 15%. Procter found that there was no tendency for the inward buckling of bars as suggested by Considére. Instead he observed normal compressive failures such as axial cracking due to circumferential tension or diagonal shearing of the concrete. Based on this, Procter felt strongly that the ability of columns to resist compressive axial load is dependent on the tensile and shear strength of the concrete.

Procter next investigated hollow rectangular cross sections [16]. The reinforcement percentages in these specimens ranged from 1 to 2%. First, seven stub columns were tested. Details of the stub column specimens are given in Table 2.1. Again, it was found that there was no problem of inward buckling of the steel reinforcement. Failure was caused by diagonal shear cracking, axial cracking, or shearing off of the concrete cover, all of which are normal compressive failure modes. All specimens essentially developed the normally calculated axial load capacity except for the one with the largest core, and hence thinnest wall. This will be discussed further in Section 4.7.

In the second phase of this program, Procter tested slender hollow rectangular columns with concentric and eccentric loadings. The details of these tests are given in Table 2.2, and the axial load-curvature behavior of the columns at a constant end eccentricity is shown in Fig. 2.15.

TABLE 2.1 DETAILS OF PROCTER'S HOLLOW RECTANGULAR STUB COLUMN TESTS

Core Size (in. × in.)	Wall Thickness (in.)	$\frac{X_u}{t}$	Concrete Area ($in.^2$)	Steel Area ($in.^2$)	Calculated Load (kips)	Test Load (kips)	$\frac{\text{Test}}{\text{Calculated}}$	Remarks
6.22 × 2.28	0.83	7.50	16.59	0.32	104	91	0.88	Concrete cover sheared around perimeter
5.83 × 1.89	1.02	5.70	19.69	0.32	120	125	1.04	Diagonal shear failure from top to midheight
5.39 × 1.46	1.24	4.35	22.79	0.32	136	139	1.02	Bar buckled at one end and pushed out concrete
5.04 × 1.10	1.42	3.55	25.11	0.32	146	162	1.11	Bar buckled at one end
4.69 × 0.75	1.63	2.85	26.97	0.32	155	163	1.05	Corners split from top
4.29 × 0.35	1.79	2.40	29.45	0.32	167	166	0.99	Concrete cracked all around the sides
Solid	Prism	0	30.69	0.32	173	187	1.08	Diagonal crack from top to bottom
							$\bar{x} = 1.02$	
							$\sigma = 0.07$	

Typical of all Specimens:

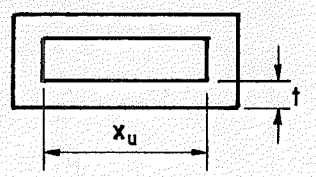

Outside dimensions = 7.87 in. × 3.94 in.

Height = 9.84 in.

Concrete: Cube strength = 7250 psi

Steel: 4 longitudinal rods (f_y = 75 ksi) with mild steel links at 3.9 in. spacing

TABLE 2.2 DETAILS OF PROCTER'S SLENDER HOLLOW RECTANGULAR COLUMN TESTS

(All tabulated curvatures, eccentricities, and moments represent the midheight cross section)

Applied Load (kips)	Curvature about y-axis ($\times 10^{-5}$ rad/in.)	Curvature about x-axis ($\times 10^{-5}$ rad/in.)	e_y, weak axis eccentr. (in.)	e_x, str. axis eccentr. (in.)	M_y, mom. about weak axis (k-in.)	M_x, mom. about strong axis (k-in.)
End eccentricity, e_y = 0.39 in.						
11.2	3.0	-	0.55	-	6.2	-
22.5	8.6	-	0.67	-	15.1	-
33.7	16.2	-	0.82	-	27.6	-
43.7	24.1	-	1.05	-	45.9	-
End eccentricity, e_y = 0.79 in.						
5.6	3.0	-	0.95	-	5.3	-
11.2	6.3	-	1.12	-	12.5	-
16.9	11.9	-	1.39	-	23.5	-
21.6	16.0	-	1.57	-	33.9	-
End eccentricity, e_x = 0.79 in.						
11.2	-	1.7	-	0.82	-	9.2
22.5	-	3.3	-	0.84	-	18.9
33.7	-	5.0	-	0.89	-	30.0
45.0	-	6.6	-	0.94	-	42.3
56.2	-	9.8	-	1.00	-	56.2

Typical details:

Column length = 113.3 in.

Concrete: $f'_c \approx 3200$ psi

Longitudinal steel: $A_{bar} = 0.081$ in.^{2}

$f_y = 75$ ksi

Transverse steel: Mild steel ties at 3.9 in. c.c.

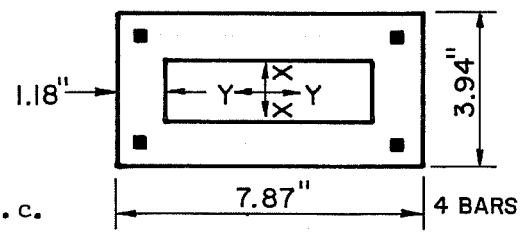

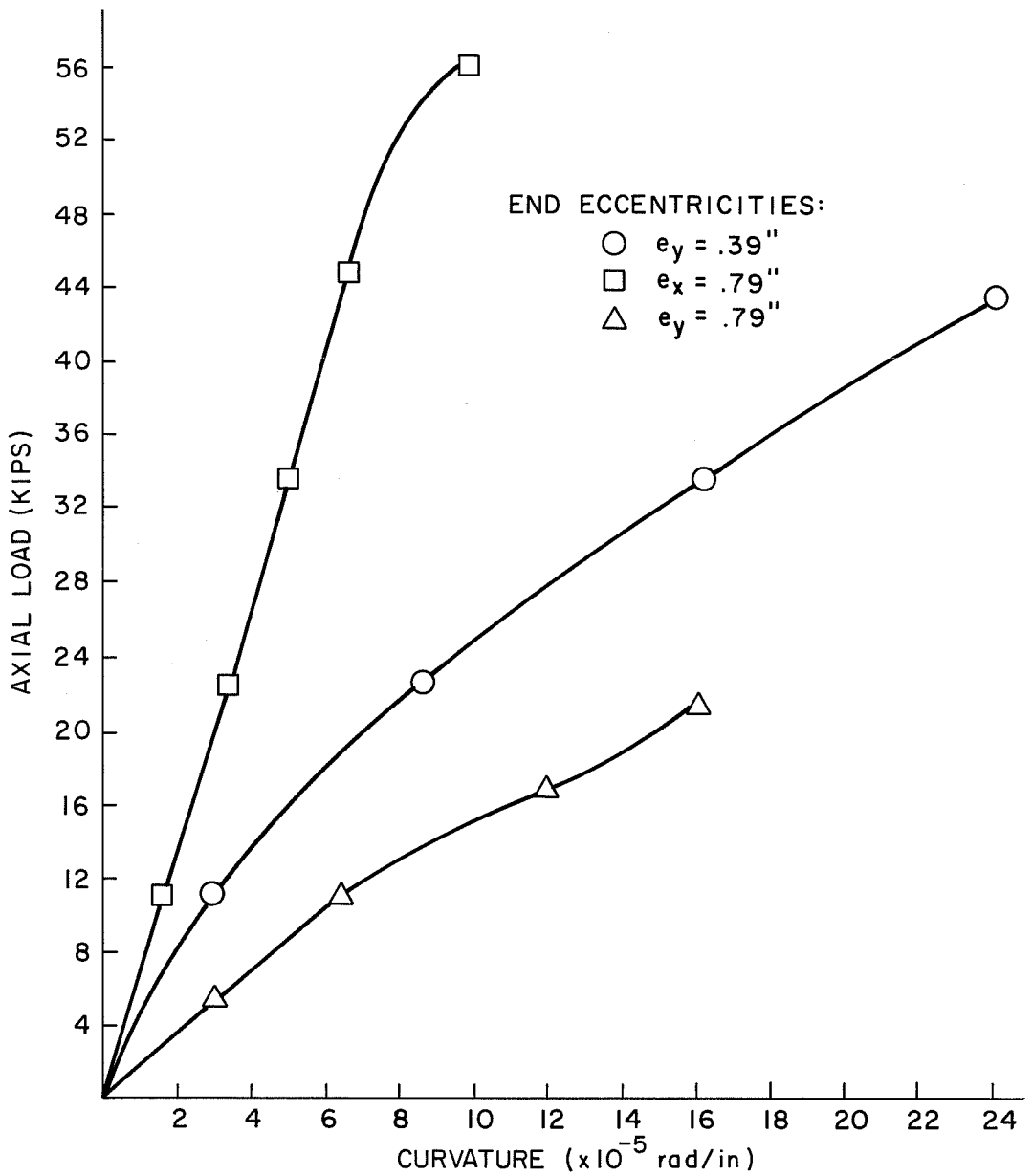

Fig. 2.15 Axial load-curvature behavior of Procter's hollow rectangular slender columns for constant end eccentricities

BIMPHI was compared with Procter's test results for slender hollow rectangular columns. The method of loading used by Procter was different than the method used by the other investigators mentioned in this section. Rather than incrementally applying moments at a constant axial load, Procter chose to incrementally apply axial load at a constant end eccentricity. In the first method, a constant axial load is maintained even though lateral deflections increase the applied moment along the column length. However, the method which Procter utilized has a linearly increasing axial load and an associated increasing lateral deflection which produces substantial nonlinear increase in moment. This arrangement makes it more difficult to present axial load-moment-curvature relationships. The secondary deflection effects on moment cannot be predicted by BIMPHI, although program PIER does treat such behavior.

An envelope of values corresponding to the extreme ranges of eccentricity was calculated by BIMPHI for comparison with Procter's test results. Two separate runs were made and axial loads were incremented at constant eccentricity in each run. The first eccentricity used for each case was the initial end eccentricity. The second eccentricity was the measured midheight eccentricity at failure. This was the sum of the initial end eccentricity and the measured lateral deflection of the instrumented midheight section. In the actual test the eccentricity initially corresponds to the smaller eccentricity case and gradually shifts to the larger eccentricity case. Comparisons of measured data with the analytical envelopes are shown in Figs. 2.16, 2.17, and 2.18. There is generally good agreement in the curvature values. The test results are expected to be closer to the end eccentricity value of the envelope since final failure is very localized. In one case the hollow section appeared stiffer than the prediction.

2.3.1.5 General. Overall, BIMPHI calculations agreed well with actual test results. In the comparisons with Breen's and Ford's columns, BIMPHI's predictions were very close to the actual test values. In the Mavichak comparisons there was overall good agreement at low values of

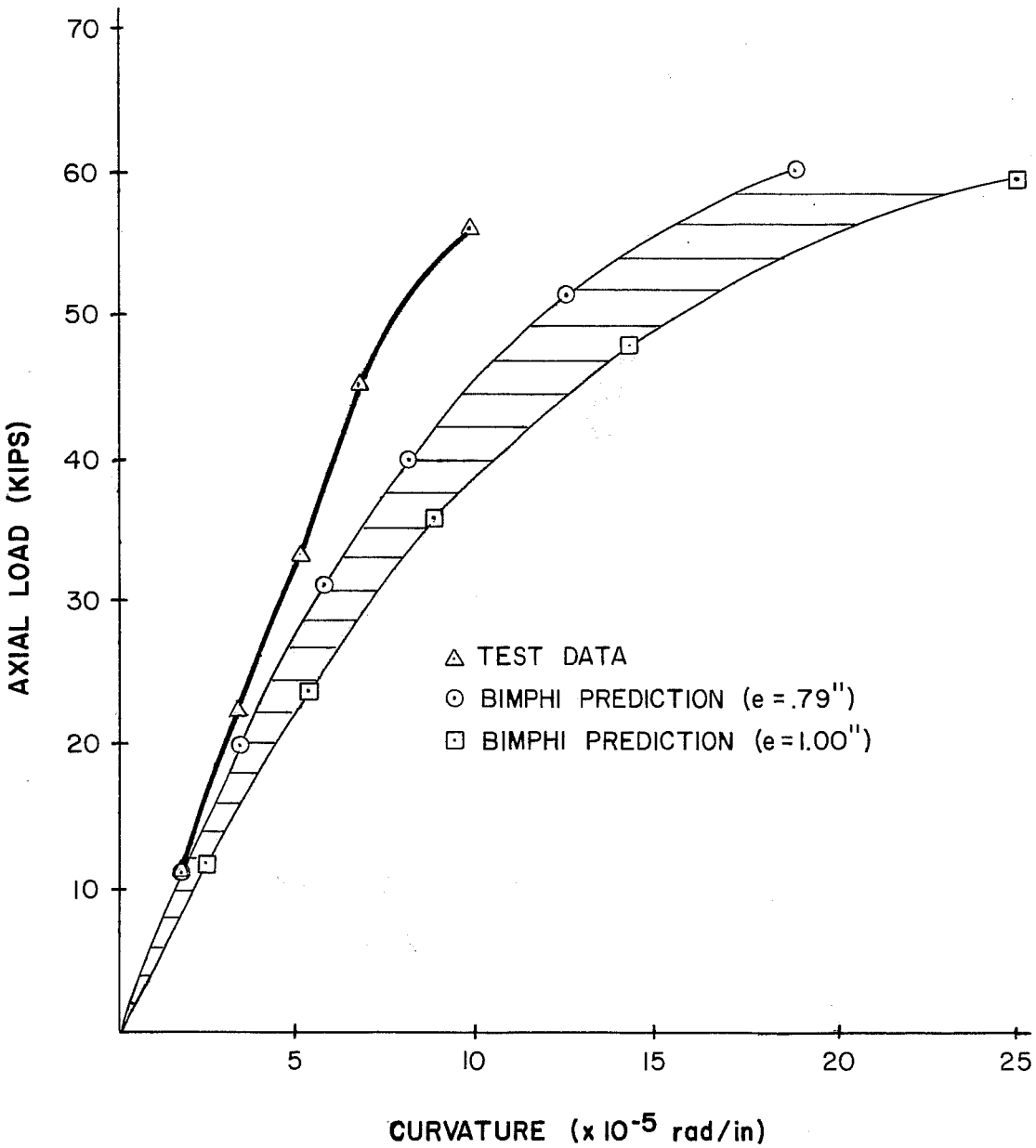

Fig. 2.16 Comparison of BIMPHI predictions with Procter's test results for a 0.79" eccentricity from the strong axis

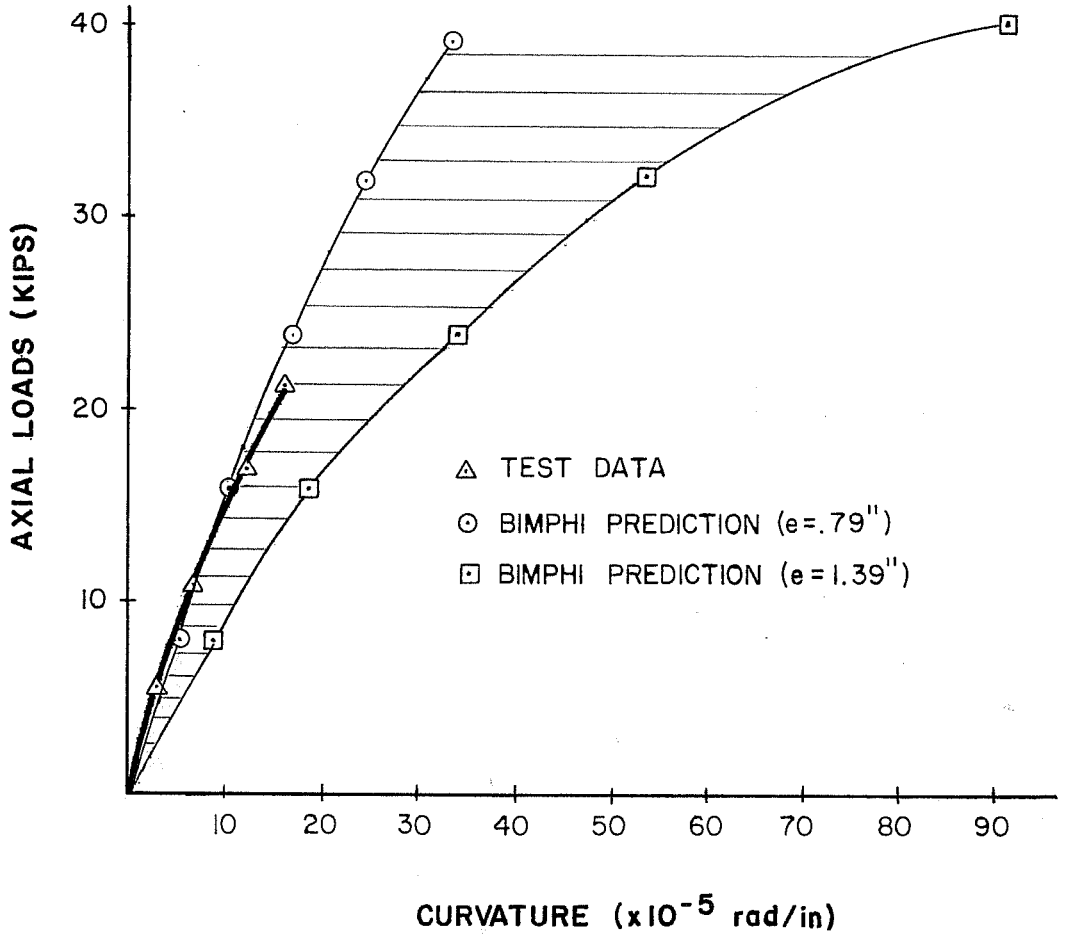

Fig. 2.17 Comparison of BIMPHI predictions with Procter's test results for a 0.79" eccentricity from the weak axis

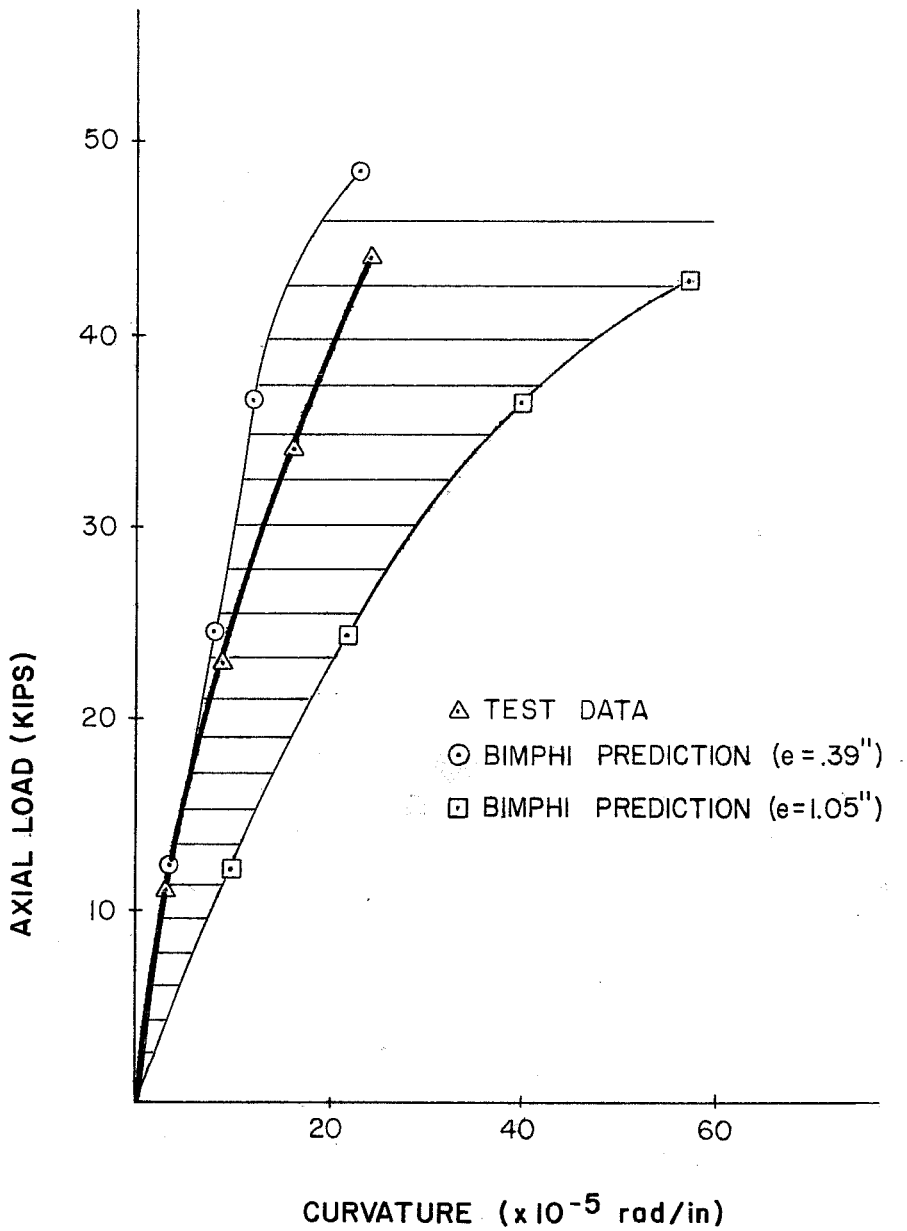

Fig. 2.18 Comparison of BIMPHI predictions with Procter's test results for a 0.39" eccentricity from the weak axis

secondary deflections where the actual biaxial moment ratio was equal to the incremental moment ratio input to BIMPHI. BIMPHI results were in fair agreement with Procter's test results tending to underpredict the axial load, and thus the moment, for each of the columns.

BIMPHI is clearly an excellent predictor of the P-M-ϕ behavior of rectangular solid sections. Good agreement was also found for the behavior of oval sections. BIMPHI results for the hollow rectangular sections seemed to indicate slightly less stiffness than shown by the actual behavior. This indication reinforced the plan to run further physical tests to verify the accuracy of BIMPHI for calculation of the P-M-ϕ behavior of hollow rectangular sections.

2.3.2 Check of Program PIER. PIER is a comprehensive analysis program which needs no peripheral computer devices for a solution. PIER analyzes a reinforced concrete beam-column subjected to static monotonic biaxial loading. Program details are given in Ref. 7. The pier can have a wide range of cross sections and any vertical configuration. The concrete and steel fiber generator subroutines in PIER are the same as in BIMPHI. Input data to describe the pier depend on the vertical configuration.

The pier is divided into a number of individual members or segments as specified. Each segment is divided into ten equal sections for purposes of computing the stiffness matrix of the segment. Each section of a segment has the same fiber properties as the middle section. Incremental loading is specified at the free joints as forces and moments. There can be as many load cases and load increments for each case as desired to predict the pier behavior. The incremental loading is applied in the number of increments specified for that load case. The total load at the end of the load case equals the number of increments multiplied by the incremental load. Translation springs and rotational springs may be specified at joints for the degrees of freedom desired. The output from PIER gives for each load increment the displacements and rotations at each joint, and the forces and moments at the end of each member.

The analysis is finished either when all load cases and all load increments are completed with no failure, or when an assumed material failure occurs. A concrete compression failure is assumed if any concrete fiber strain exceeds the specified ultimate strain of concrete. A tensile failure is assumed if any steel fiber strain exceeds 1%. If the pier undergoes an assumed material failure, the displacements and forces for the last increment before failure will be printed. In some cases with restrained members, a "hinge" may form when maximum moment capacity is attained. This may be before a material limit is reached. In such cases a negative stiffness results with the next displacement increment. This is usually signalled by the displacements becoming opposite in sign from previous increments, or the displacements decreasing from previous increments. In some very slender cases the displacements rapidly increase under very, very small load increments. This signals a stability failure.

2.3.2.1 Breen and Ferguson. PIER was used to analyze a tall pier model subject to uniaxial bending, previously tested by Breen and Ferguson [17]. The column loading and pertinent cross section properties are shown in Fig. 2.19. The analysis by PIER of the column was performed in two load increment stages. In the first twenty load increments, the axial load increment was 480 lbs. and the lateral load increment was 14.4 lbs. Above this level the column was loaded with axial load increments of 120 lbs. and lateral load increments of 3.6 lbs. until failure. The reduced load increments were used to improve sensitivity near the ultimate load. The ratio of H/P was maintained at 0.03 as in the physical test. Ten pier length segments were used in the analysis by PIER. Since the moment gradient was small, the Hognestad stress-strain curve for unconfined concrete was used. The maximum compressive stress was assumed $0.95f'_c$ because the column was horizontally cast.

Comparison of the measured and calculated axial load versus tip deflection relationship are shown in Fig. 2.20. Figure 2.21 shows the axial load and bending moments relative to the interaction diagram for a

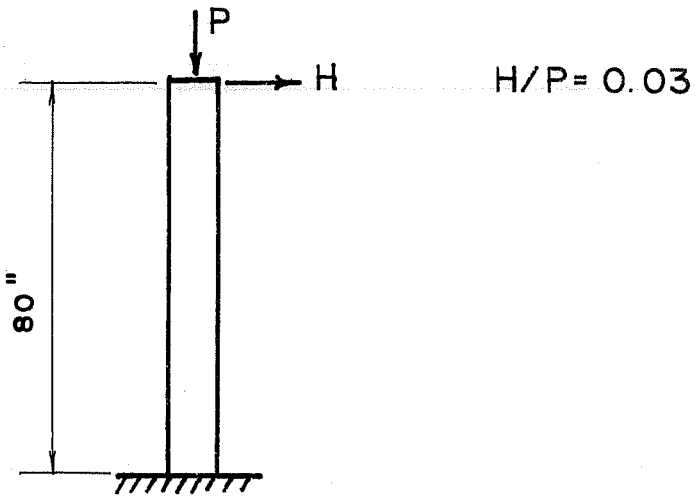

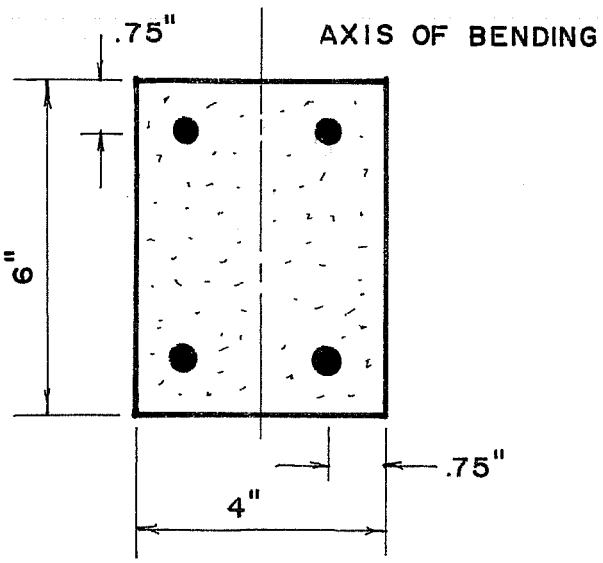

f'_c = 3660 psi

f_y = 58800 psi

E_s = 29×10^6 psi

A_{st} = $4 \times .11 = .44$ in.^{2}

Fig. 2.19 Column G-2 from Breen and Ferguson

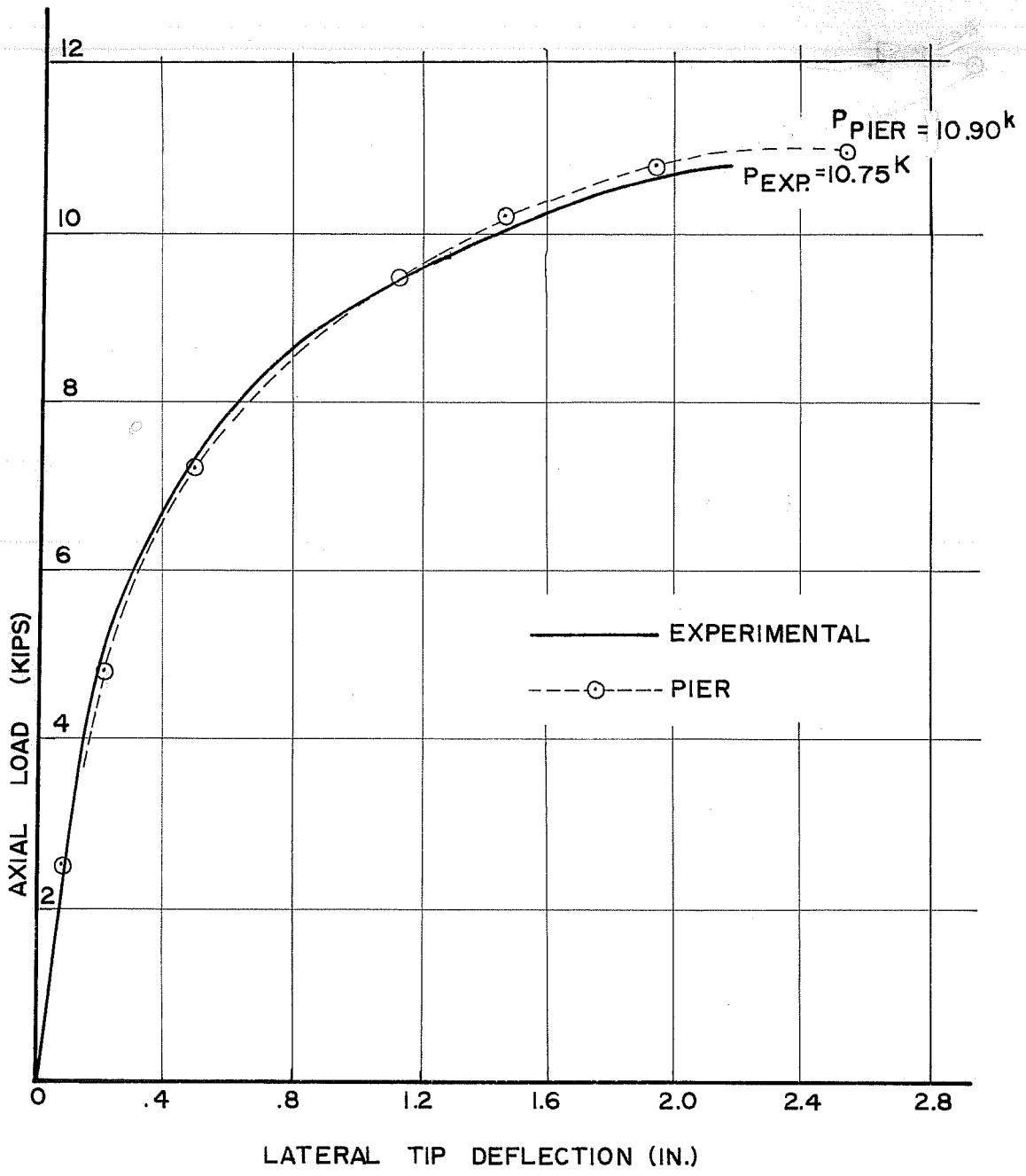

Fig. 2.20 Axial load versus tip deflection of G-2

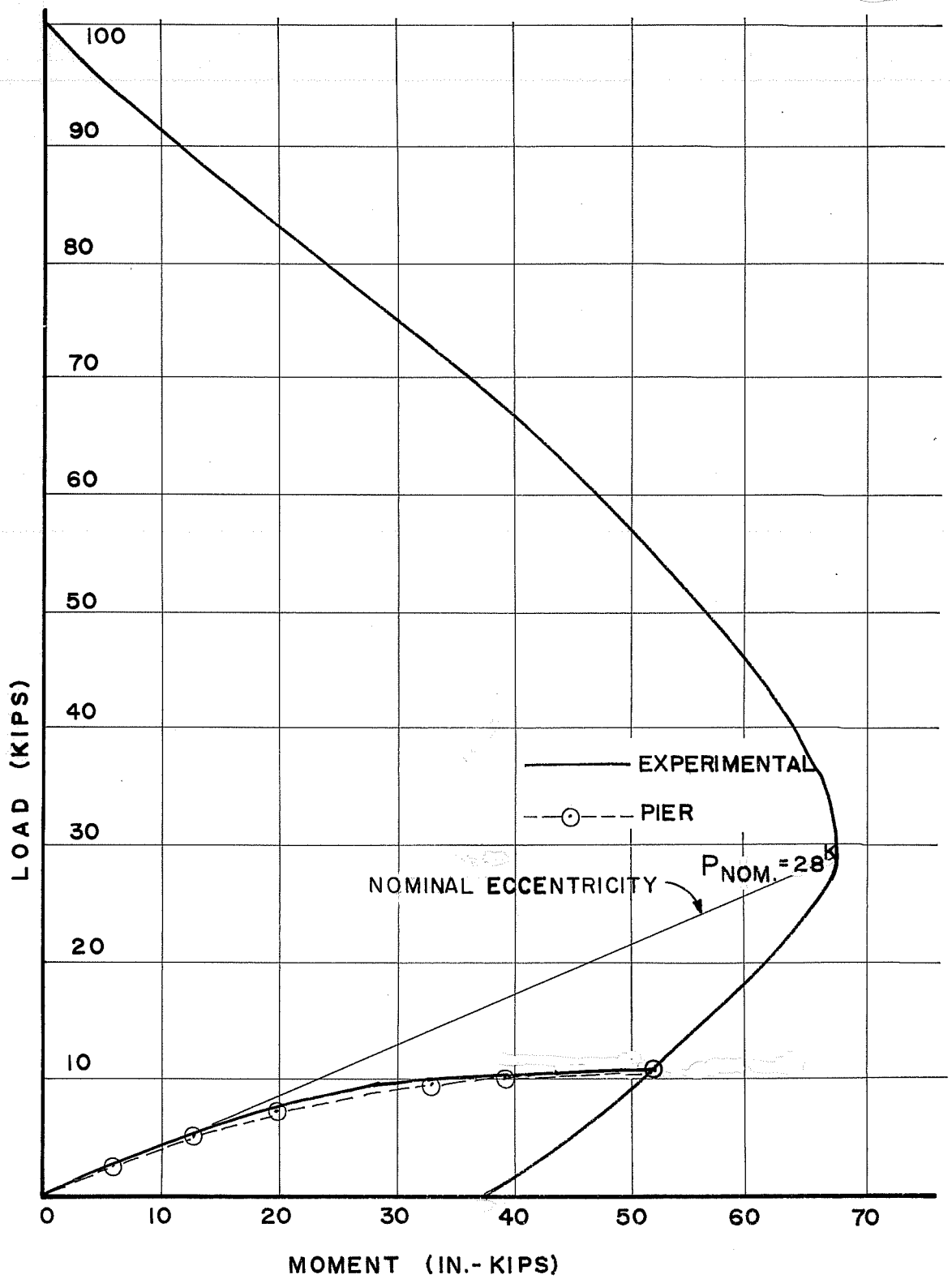

Fig. 2.21 Axial load and bending moments relative to interaction diagram, G-2

point near the base on Column G-2. The curves presented in the figures are so close it is difficult to differentiate between the experimental and analytical curves. The results for this case are excellent. PIER predicted a slightly higher ultimate axial load than the actual test value. Figure 2.21 also shows a straight-line nominal eccentricity line which intersects the interaction diagram. The level of axial load at this point (P_{NOM}) would be the expected failure load if there was no P-Δ effect. Second order effects are very significant in this slender pier.

2.3.2.2 Mavichak. PIER was used to investigate the same Mavichak column analyzed by BIMPHI and illustrated in Fig. 2.12. PIER is a member analysis and includes P-Δ effect. Second order effects incremental biaxial moments do not have to remain in the same ratio which was a requirement with BIMPHI. Mavichak measured the curvature at the center of the column. Curvatures are a function of the second derivative of deflections. Curvature values were obtained from the deflection values computed by using finite difference equations.

Figure 2.22 presents the comparison of the experimental results with PIER. This is the P-M-ϕ relationship for the middle section of the column. The results from PIER are in very good agreement with the observed results. The arrows on the curves denote a negative stiffness occurrence signalling failure. The PIER values show decreasing deflections along the column in the final load increments. The ultimate moments and curvatures predicted by PIER were slightly less than the observed. The greatly improved accuracy when compared to Fig. 2.12 further indicates the ability of PIER to correctly integrate curvatures over the pier length.

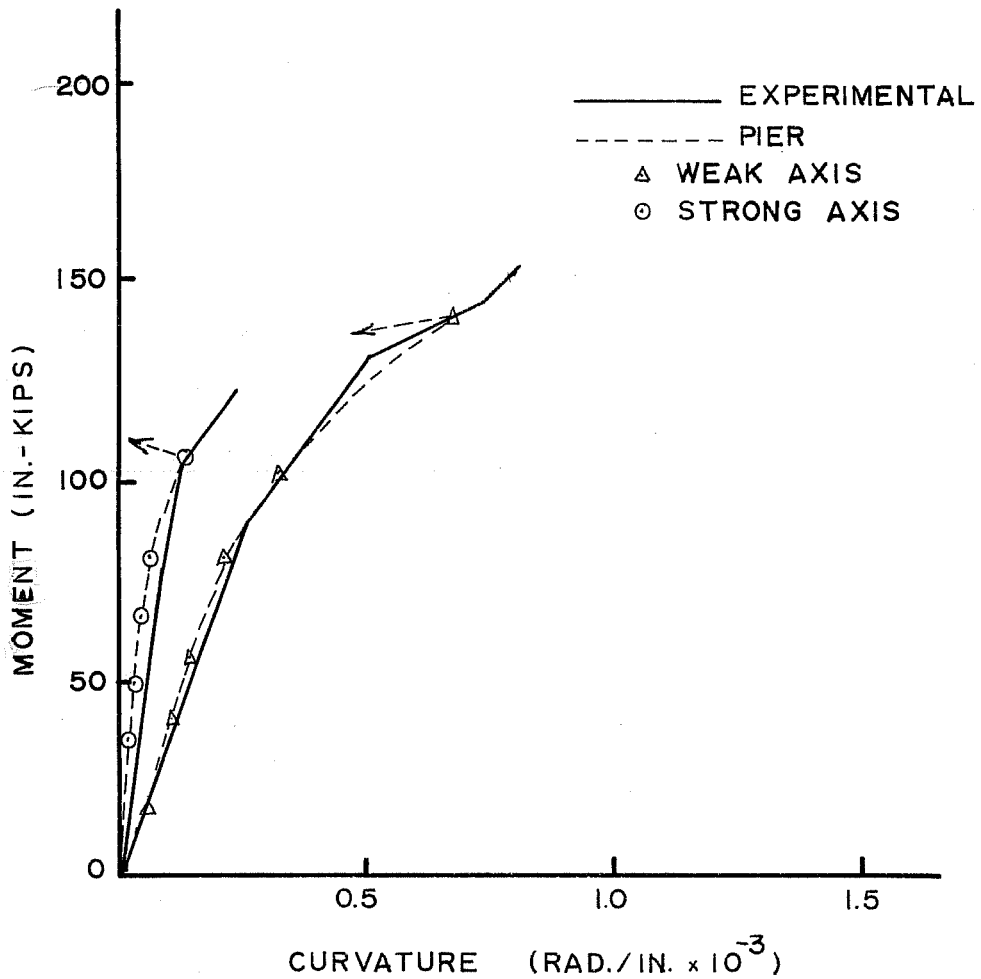

Fig. 2.22 Moment-curvature relationship for Mavichak Column RC-2 as determined from PIER computed deflections.

2.3.2.3 Farah and Huggins [18]. The physical test reported by Farah and Huggins was performed on a column with cross section and material properties shown in Fig. 2.23. The column was pinned at the ends with axial loads applied eccentrically. Since the column had constant moment along its length, the Hognestad stress-strain function was used to model the concrete. The maximum compressive stress was taken as $0.85f'_c$.

In Fig. 2.24 deflections measured along the diagonal are shown together with the analytical predictions from PIER. PIER yields deflections in the component directions. Assuming no nonplanar behavior [19] the resultant deflections are found using the Pythagorean theorem. The deflections measured in the physical test were given for the loads P = 30k and P = 45k only. The results from PIER are in excellent agreement with the test results. PIER predicted an ultimate axial load (P_u) of 52k, slightly higher than the test result of 48k.

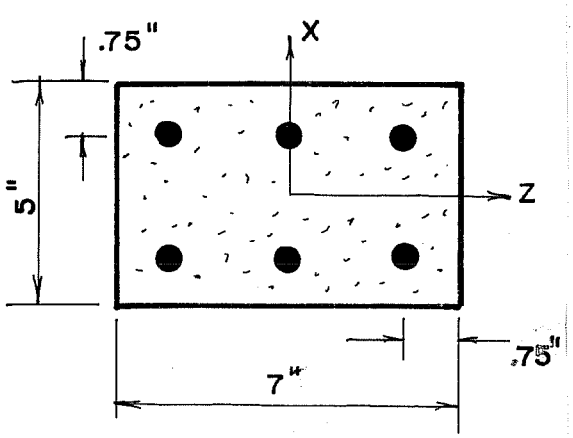

f'_c = 4100 psi
f_y = 55670 psi
E_s = 28.75×10^6 psi
A_{st} = $6 \times .187 = 1.124$ in.^{2}
L = 153 in.
e_z = 1 in.
e_x = 1 in.

Fig. 2.23 Farah and Huggins column-section and properties

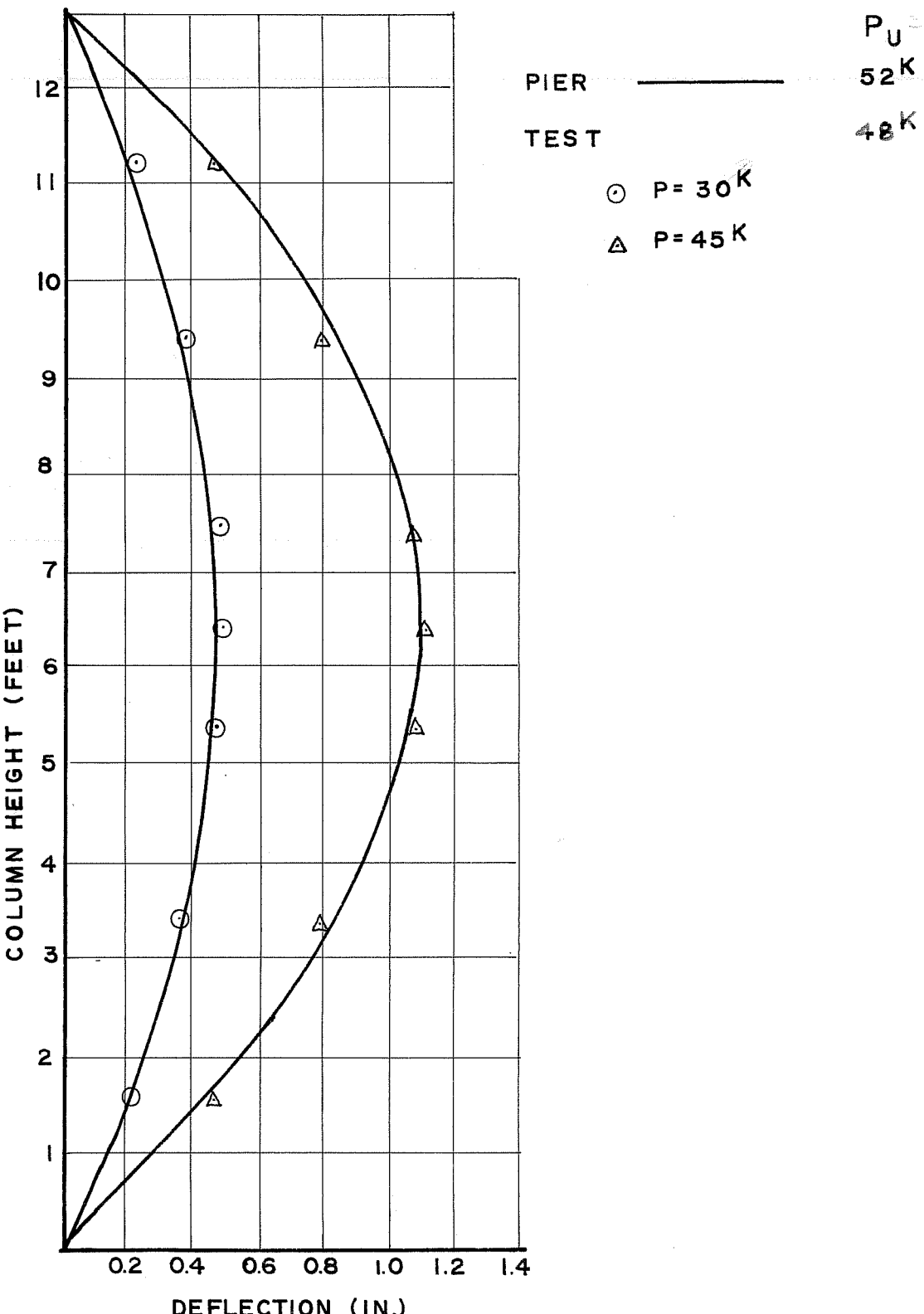

Fig. 2.24 Farah and Huggins column deflections

2.3.2.4 Drysdale. In Drysdale's work on sustained loads [20], several columns were tested in short term biaxial loading to failure. The column section and material properties used in the tests are shown in Fig. 2.25. The column was pinned at the ends with axial loads applied eccentrically. The column had no moment gradient, thus the concrete was modeled as unconfined.

The results predicted by PIER for P = 22.5k and P = 30k are shown with the physical test measurements in Fig. 2.26. For P = 22.5k, the prediction from PIER is very close to the measured. PIER overpredicts the deflections at P = 30k. One possible reason is that in the analytical treatment of the column, the actual built-up section near the column ends was not accounted for. The built-up column ends would increase stiffness, thus decrease column deflections. The ultimate axial load predicted by PIER was 4.5% lower than the actual ultimate load.

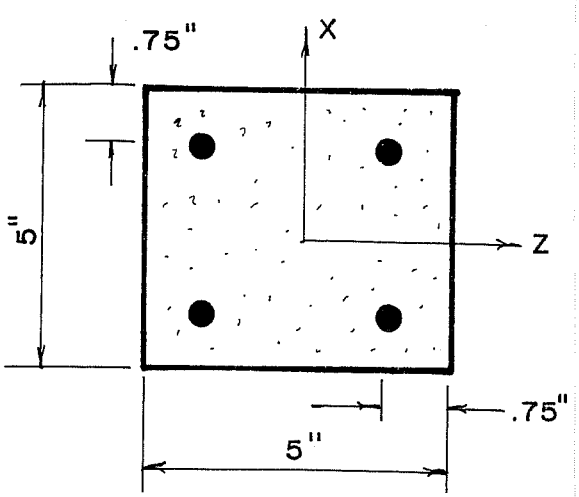

f'_c = 3670 psi
f_y = 56000 psi
E_s = 29×10^6 psi
A_{st} = $4 \times .197 = .788$ in.^{2}
L = 156 in.
e_z = .707 in.
e_x = .707 in.

Fig. 2.25 Drysdale's Column B2C--section and properties

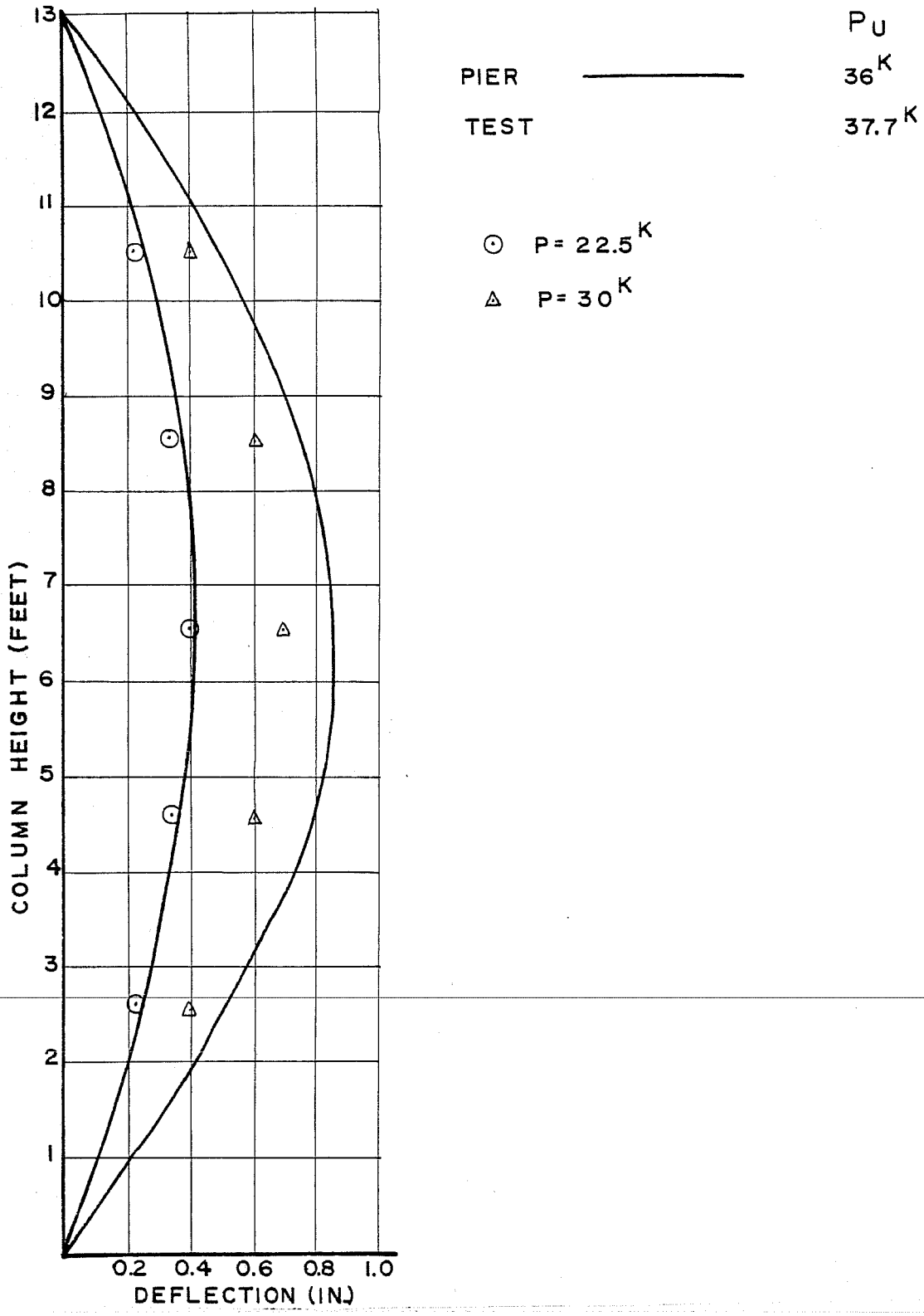

Fig. 2.26 Drysdale's Column B2C--deflections

2.3.2.5 Wu. The physical test reported by Wu [19] was performed on a column with cross section and material properties as shown in Fig. 2.27. Column 27 was eccentrically loaded at a skew angle of 30° (arctan e_z/e_x = 30°). Wu assumed the neutral axis to always be oriented orthogonally with respect to the skew angle. Wu realized deflections would be nonplanar in some instances, but assumed any nonplanar deflections would be negligible. The results of the comparison with the results of program PIER are shown in Fig. 2.28. Predictions from PIER are very close to the experimentally observed deflections at all load levels. The prediction of PIER of the deflections at P = 25k is slightly higher than the experimentally observed. This is probably because the actual reinforcing steel had no well-defined yield plateau as assumed in PIER. The prediction of the ultimate load shows excellent agreement.

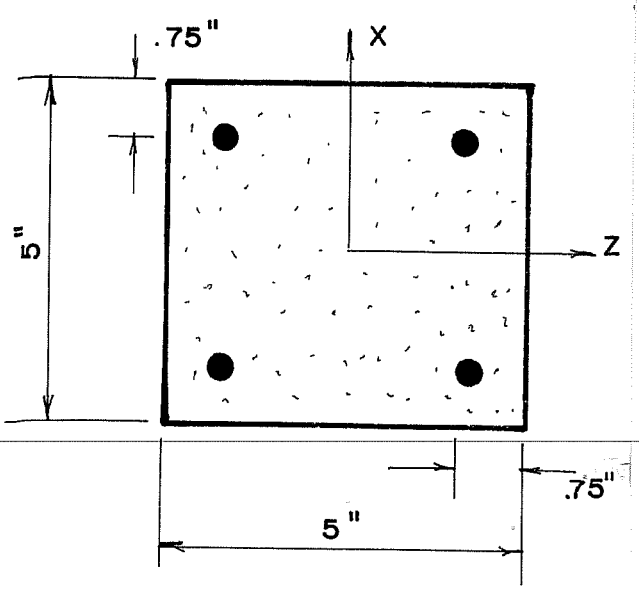

f'_c = 5515 psi
f_y = 97600 psi
E_s = 29×10^6 psi
A_{st} = $4 \times .186 = .744$ in.^{2}
L = 156 in.
e_z = .75 in.
e_x = 1.3 in.

Fig. 2.27 Wu's Column 27--section and properties

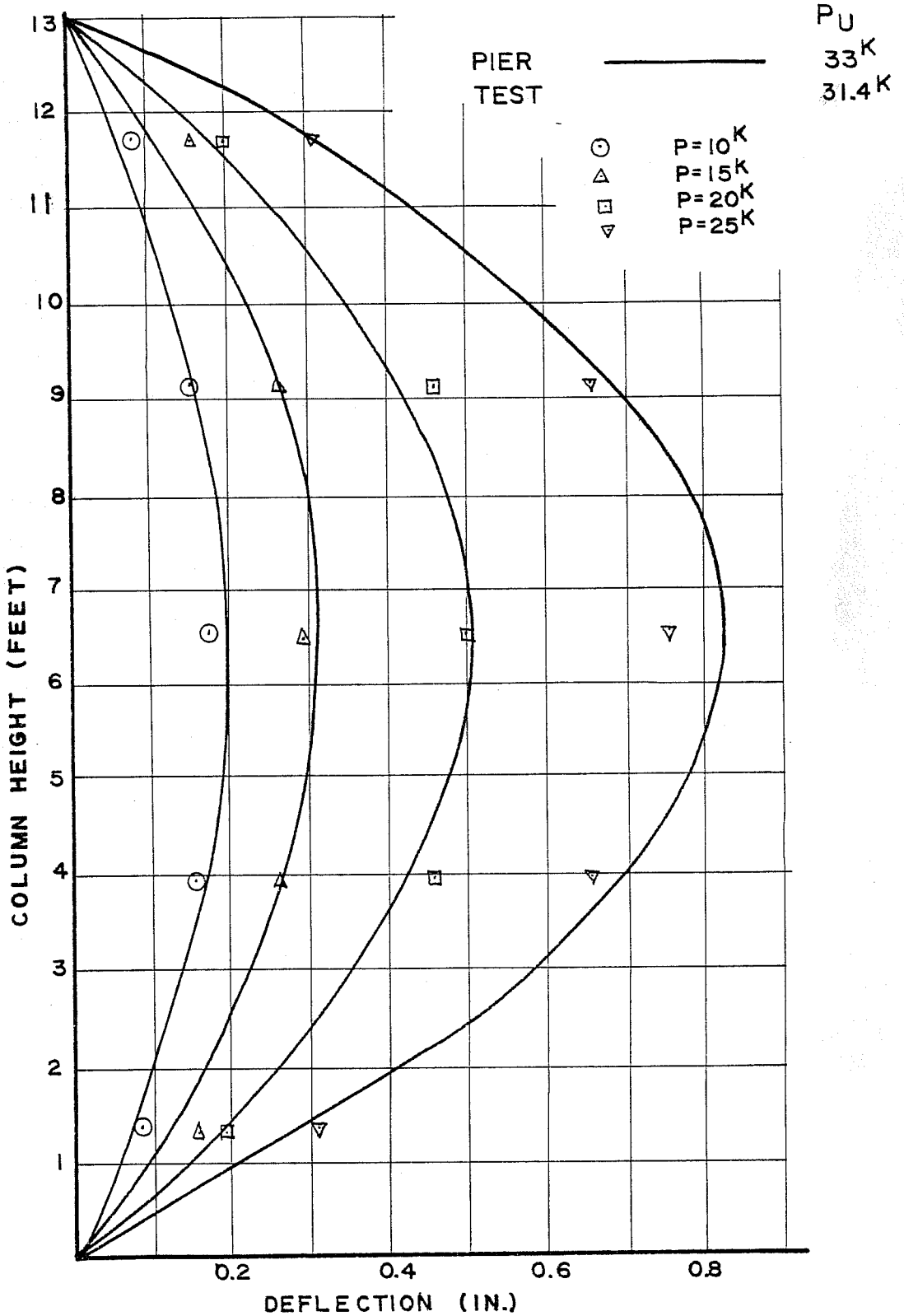

Fig. 2.28 Wu's Column 27--deflections

2.3.2.6 Green. Green experimentally investigated the sustained load response of 10 eccentrically loaded unrestrained reinforced concrete columns. Typical details are shown in Fig. 2.29 [22,23]. Two of these columns, S1 and S3, were analyzed with the creep analysis feature in PIER. The columns were pinned at the ends with the axial load applied eccentrically in one direction. The large end blocks on the physical specimens were not considered in the analytical model. Additionally, the concrete was assumed to be unconfined. The principal difference between Columns S1 and S3 was the level of axial load. Additional details of the specimens can be found in Ref. 23.

The creep analysis feature in PIER follows a method outlined by Chovichien, et al. in Ref. 24. The behavior of a column under sustained load is predicted by modifying the short-term stress-strain relationship for concrete. The concrete strain corresponding to maximum stress is larger for sustained load than for short-term load, and the concrete modulus at a given strain is reduced.

Figures 2.30 and 2.31 present the results of the creep analysis. Figure 2.30 shows the ratio of the centerline moment to the applied end moment versus the time of loading. It clearly shows that PIER accurately predicts the second-order moment at the column midheight for short-term loading ($t = 0$ days) as has been the case for the other verifications. In addition, PIER, using its creep analysis, also very accurately predicts the second-order moment for the center of the column for Column S3. Agreement is less accurate but still is reasonable for Column S1 at a time of 500 days, which was the last experimentally recorded value. Some of the variance for Column S1 at 500 days can be explained by the fact that the column was on the verge of stability failure. Figure 2.31 shows the midheight deflection versus time for the two columns. Again, the results from PIER show very good agreement with the experimentally observed results.

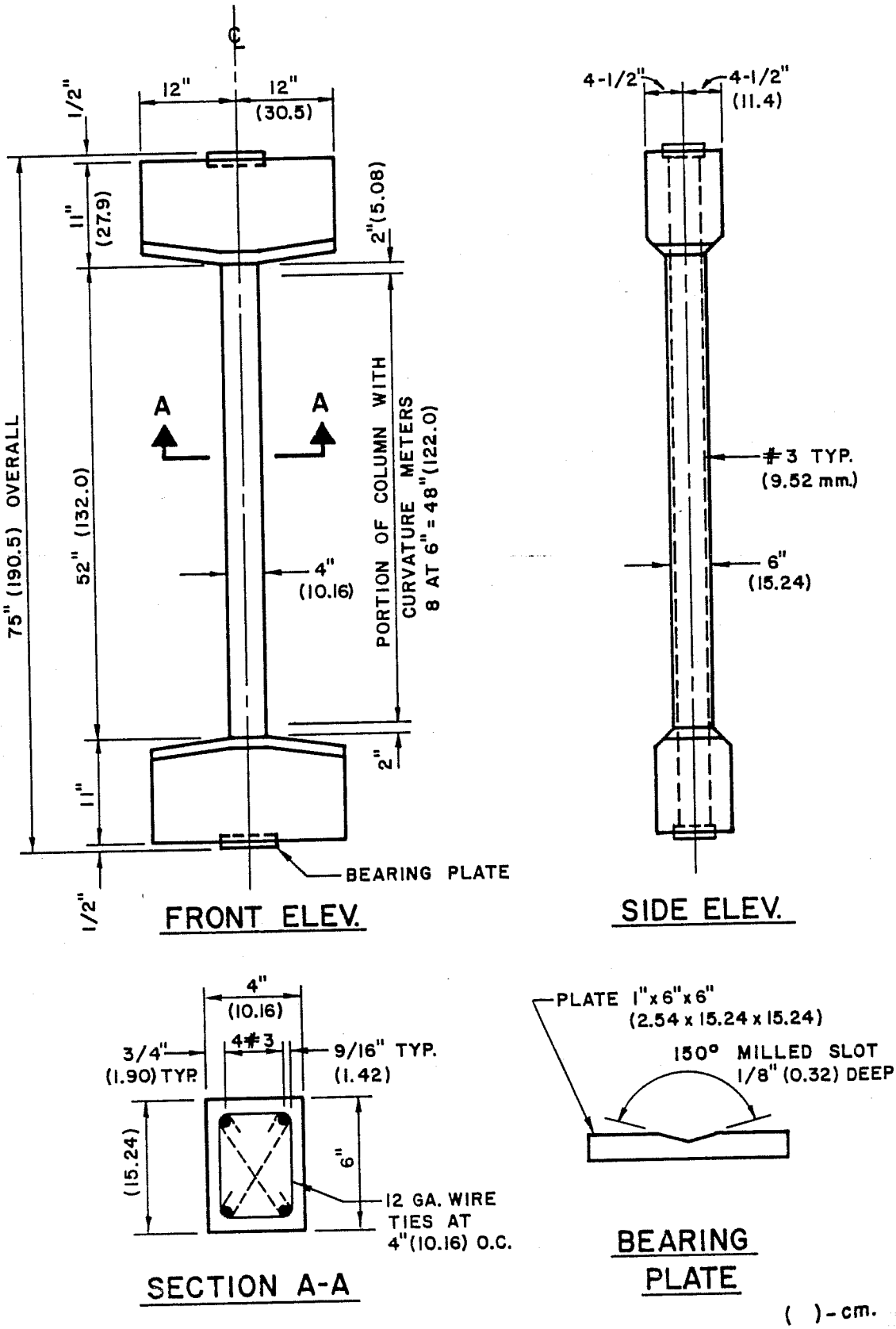

Fig. 2.29 Typical details of Green's columns

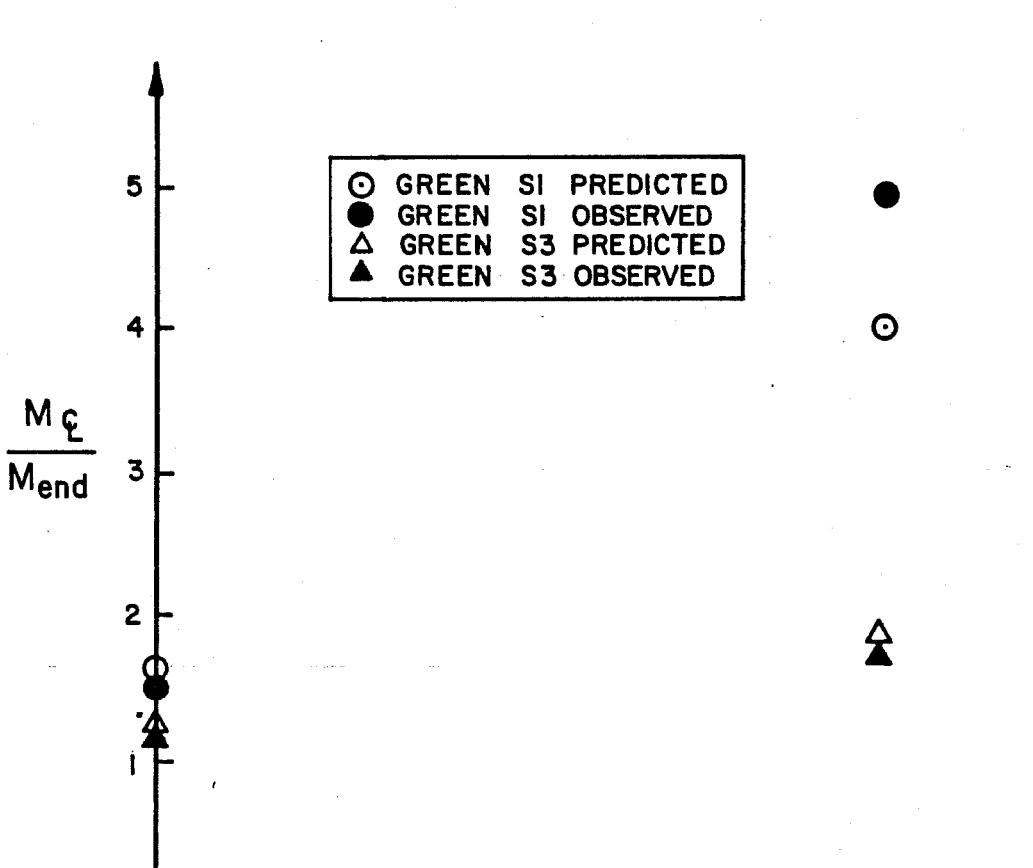

Fig. 2.30 Creep comparison of moments in columns tested by Green

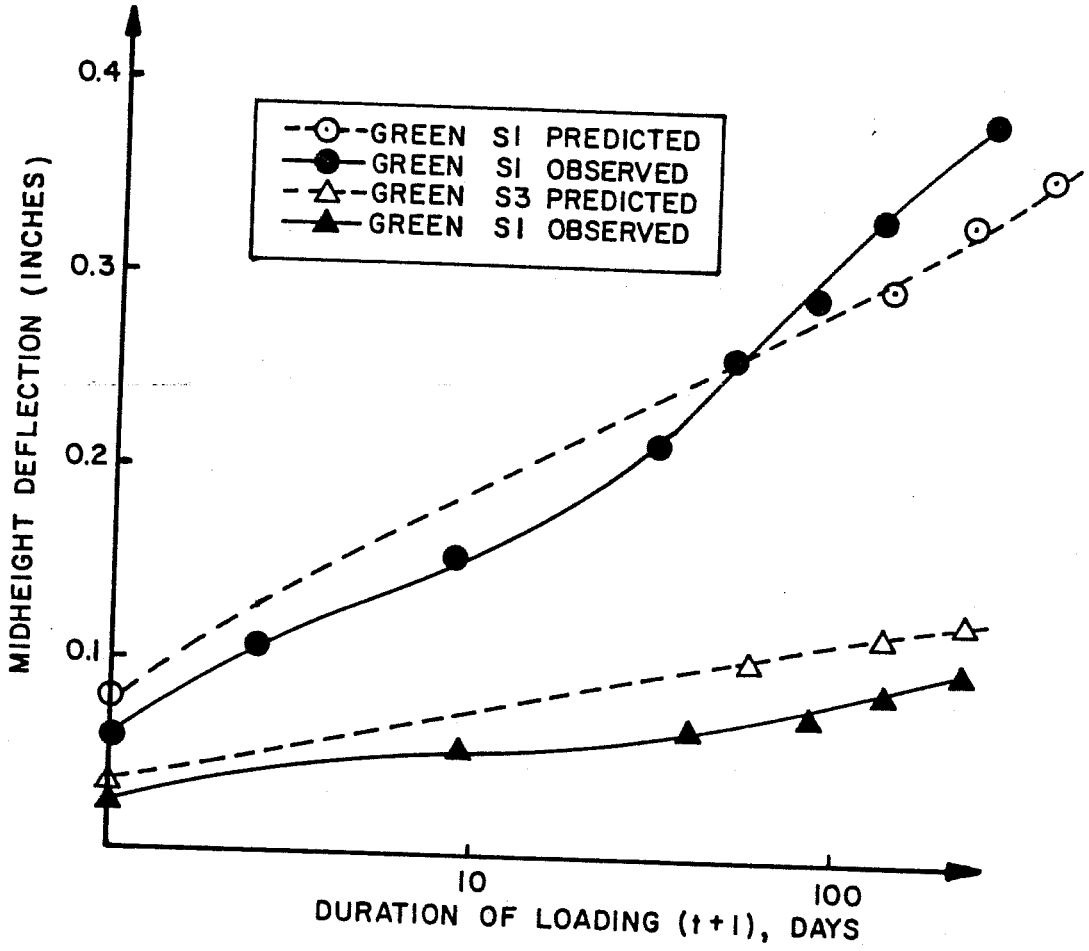

Fig. 2.31 Creep comparison of midheight deflections in columns tested by Green

2.3.2.7 Summary. In all cases, the analytical predictions of PIER were close to the experimentally observed behavior of the columns. The Hognestad stress-strain curve appears accurate for unconfined concrete. For the two confined column sections analyzed by BIMPHI, the Ford stress-strain curve was appropriate. PIER gave excellent results compared to the experimentally observed ultimate load and deflections at various load levels. Checks with data from slender columns under sustained load indicated that the creep analysis feature in PIER gave good agreement with experimental results. While all cases checked worked well, it should be noted that for the biaxial bending case, only 45° and 30° nominal eccentricity angles were investigated. The columns analyzed were either cantilevered or pinned. Other eccentricity angles and end conditions may need examining in the future.

2.3.3 Check of Program FPIER. FPIER is a comprehensive analysis program which does not require peripheral computer devices for a solution. The primary objective of the program is the structural analysis of reinforced concrete pier bents. It handles symmetrical frame configurations of up to two bays and three stories. The program can also handle the analysis of a reinforced concrete beam-column (zero bay, one story). The loading is assumed static and monotonic. Loads can be applied in plane and/or perpendicular to the pier bent plane. The members of the pier bent can have any of the cross sections available in program PIER. FPIER uses the same concrete and steel fiber generator subroutines as PIER. It has been programmed to treat all AASHTO load factor combinations.

Each member of the pier bent is divided into longitudinal segments as specified. Each segment is divided into a number of equal sections for purposes of computing the stiffness matrix of the segment. The number of sections will depend on the number of total segments into which the pier bent has been subdivided. The maximum total number of sections is 150. Once the number of sections per segment has been determined, each section is then divided into fibers. The desired load for the

structure is applied in increments. For each increment of load applied, the incremental displacements and forces are found. New stiffness parameters are obtained and the procedure repeated for each increment load. The stiffness of each segment is placed in a stiffness matrix for the member. The member stiffnesses are assembled to get a total stiffness for the pier bent, and the resulting equilibrium equations are solved.

The incremental loadings are specified at the free joints as forces and moments. FPIER differs from PIER in that FPIER has two types of loading systems. These are frame forces which are forces specified at frame joints, and member forces which are forces specified at segment joints. The sign convention for forces and displacements is the same as PIER. As in PIER there are six degrees of freedom for each joint (frame joints or segment joints). All degrees of freedom of a frame joint are assumed free unless the joint is specified as a support. The release code for a support is the same as that used in PIER and it works identically. Frame joints accept translational springs and rotational springs.

Like PIER there can be as many load cases and load increments for each case as desired to predict the pier bent behavior. The first load cases should be the weight of the members. The incremental loading is applied in the number of increments specified for that load case. If another load case is desired, the new loading and number of increments are specified. The new incremental displacements and incremental forces are added algebraically to the displacements and forces of the previous loading for other load cases. This procedure is identical to the one used in PIER.

The output from FPIER at the end of each load increment (or specified load increments) includes displacements and rotations at each joint, and the forces and moments at the end of each segment for each member. Like PIER the analysis is finished either when all load cases and all load increments are completed with no failure, when there has been an assumed material failure, when a negative stiffness occurs

signalling a plastic hinge formation or when there has been a stability failure. A concrete compression failure is assumed if any concrete fiber strain exceeds the specified ultimate strain of concrete. A tensile failure is assumed if any steel fiber strain exceeds 1%. A negative stiffness failure is assumed when the displacement increments have reversed in sign from previous increments. If the pier bent undergoes any of these types of failures, the displacements and forces for the last increment before failure will be printed. PIER and FPIER are virtually identical when treating a single beam-column. FPIER was used to check those examples checked by PIER and identical results were obtained. The primary checking of FPIER was for frame behavior. Since the beams or girders in the frames may differ from the checks made on columns with PIER, the checks using FPIER focused on beam and frame behavior.

2.3.3.1 Program FPIER Limitations and Extensions. All the limitations associated with program PIER also apply to program FPIER. In addition three other limitations apply. First the number of total sections is limited to 150 which implicitly imposes a limit on the total number of segments which can be used to model the pier bent. Second the pier bent must be symmetric in geometry. Finally the bent cannot have more than two bays and three stories.

Presently, like PIER, the program treats the concrete as either all confined or unconfined. It would be relatively easy to change the program to treat individual concrete fibers in the same member of the pier bent as either confined or unconfined. Another possible extension would be the inclusion of prestressing forces in the analysis. While it would be possible to generalize the program to include nonsymmetrical structures, the input required would then be very extensive.

2.3.3.2 Breen and Pauw. PIER was used to analyze a beam under two concentrated loads previously reported by Breen and Pauw [25]. Loading material properties and dimensions are shown in Fig. 2.32 along with the experimental results and those predicted by FPIER. As expected, some

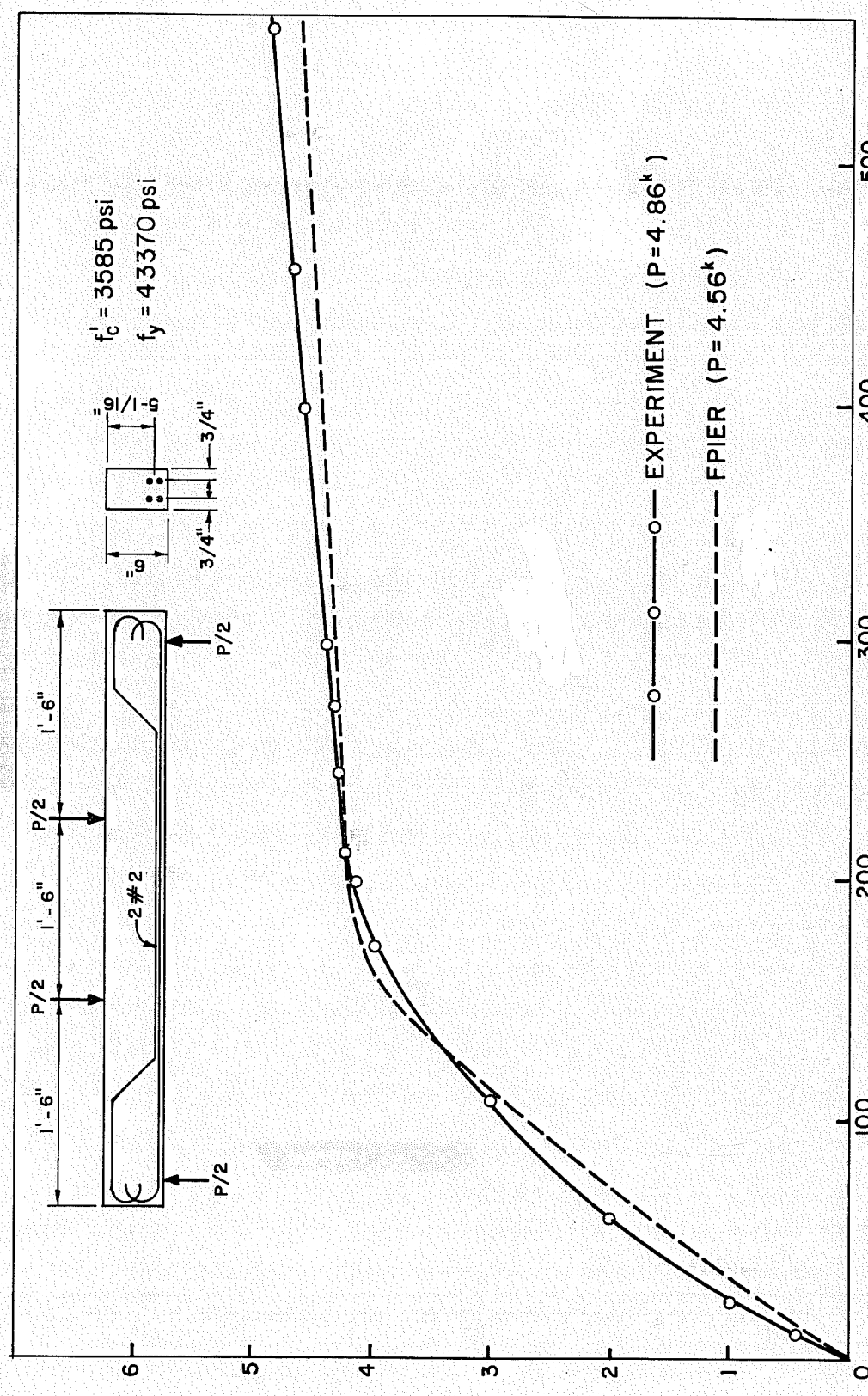

Fig. 2.32 Beam 2C, from Breen and Pauw (25)

differences are evident before cracking. After yielding the differences tend to diminish. The predicted ultimate load was 4.56 kips. The ultimate load from the experiment was 4.86k which differs from the predicted values by 6%. The overall agreement is quite acceptable for this typical flexural failure.

2.3.3.3 Baron and Siess. The physical test reported by Baron and Siess [26] was performed on a beam with cross section and material properties as shown in Fig. 2.33. A concentrated load was applied through an integrally cast column stub at midspan. This beam was reported to have a shear-compression failure with an ultimate load P_u = 33.0k. In this case FPIER predicts the ultimate load with a 2% error. The load deflection agreement is very good for approximately 60% of the load range. However, in this shear type failure the deflections at ultimate differed appreciably from the experimental results. Thus the program is not as accurate when joint slip or large shear deflection contributions are present.

2.3.3.4 Ernst, Smith, Riveland and Pierce. From the fifteen frame tests reported [27] three were chosen at random to check program FPIER.

Frame A40: Geometric characteristics and material properties are shown in Fig. 2.34. Columns and beams had the same cross section. The tension steel was equal to the compression steel. An ultimate load of P_u = 16.1k was predicted by FPIER. This differs only 5% from the ultimate load of P_u = 15.9k measured in the test. The midspan deflection versus total load is also shown in Fig. 2.34. At low load levels there is very good agreement between computed and measured values. FPIER predicts a stiffer structure in the higher load ranges but does soften and indicates both ultimate loads and deflections very close to those observed.

Frame 2D12: This frame was also loaded with concentrated loads at the third points. The cross section of the beam and columns were not

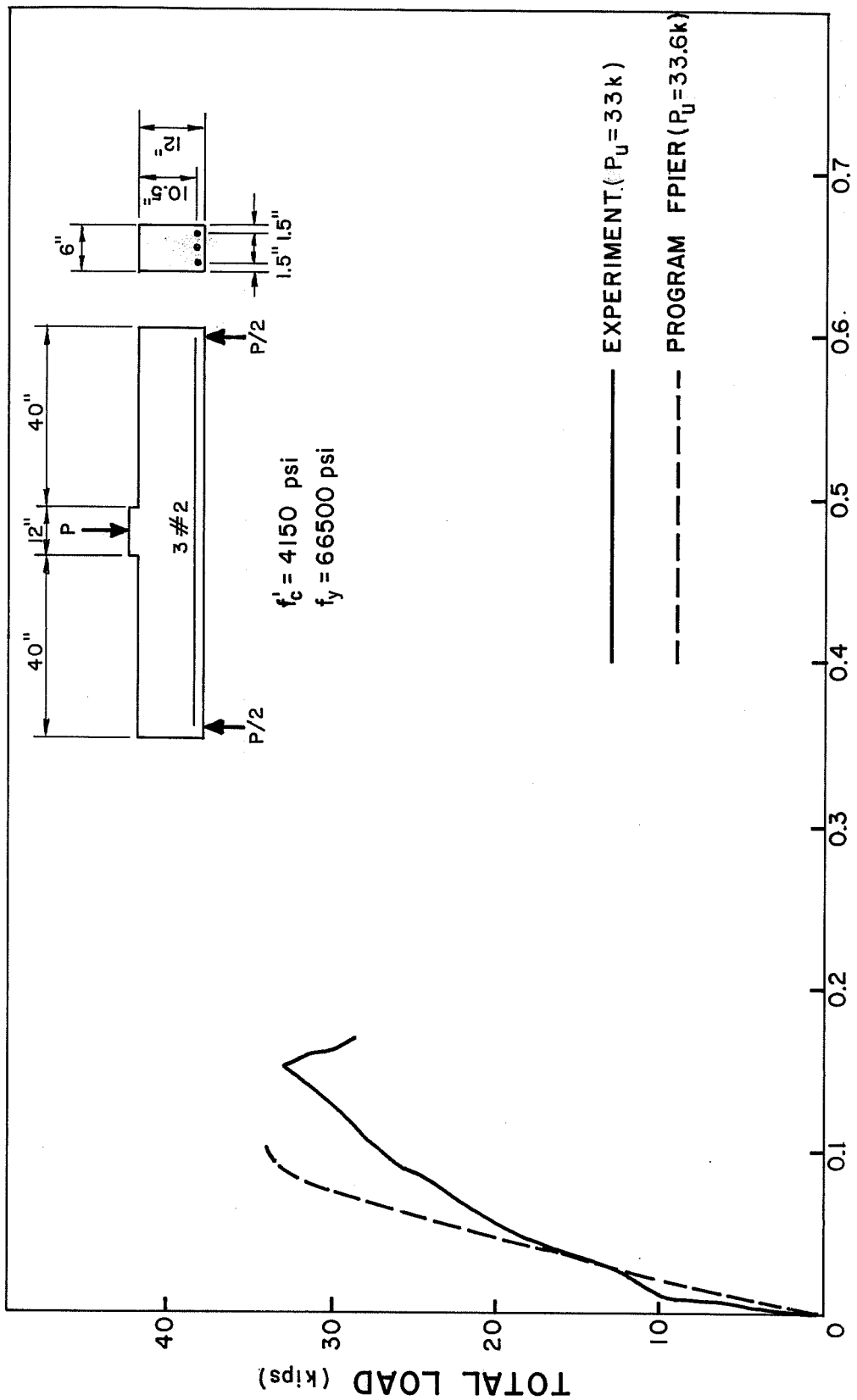

Fig. 2.33 Beam A-1, from Baron and Siess (26)

2.33

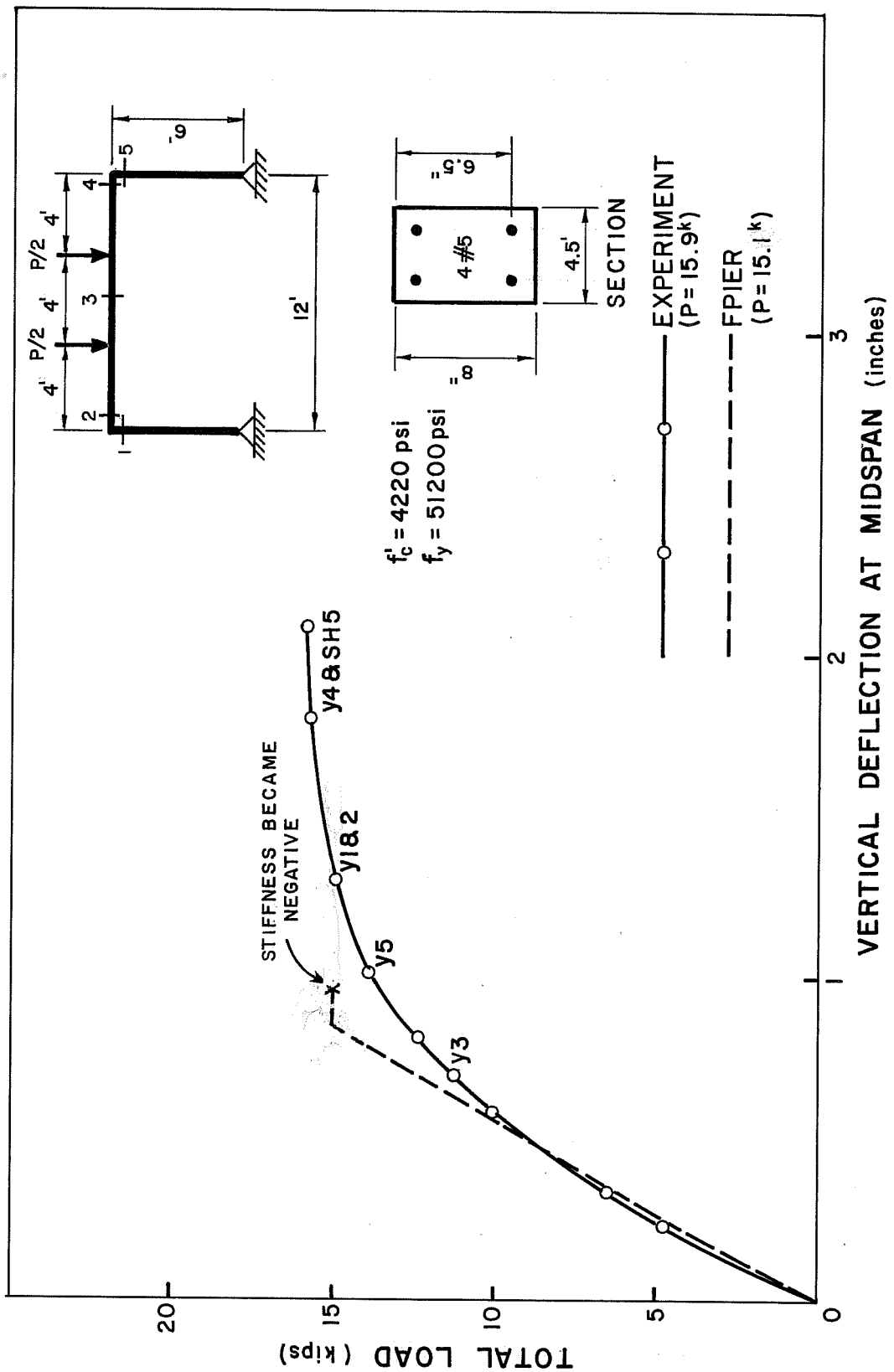

Fig. 2.34 Frame A-40, from Ernst, et al.

equal. Cross sections and material properties are shown in Fig. 2.35 along with the midspan deflection versus total load. There is excellent agreement between measured and predicted values until major redistribution occurred. The ultimate load predicted is 13.50k while the measured value was 14.88k. Lack of agreement for deflections above 1.5 in. is not serious since this is beyond the range of plastic hinge formation in the test.

Frame 2D12H: This frame had the same general properties as Frame 2D12 except for lower concrete strength. However it had a horizontal load applied at the east knee of the frame in addition to the vertical load. This is an important test of the program. The lateral displacement versus lateral load is shown in Fig. 2.36. The predicted ultimate horizontal load was 3.00k which was 3% lower than that measured in the experiment. The vertical load was kept constant at 7.88k. Except for the initial stages where tension in the concrete plays a major role, the agreement between predicted and measured behavior was very good. For the very high load levels the general agreement was very good and the basic shape of the curves is identical up to the point where the load capacity began to diminish with very large deflections.

2.3.3.3 Repa. The results of a test of a very detailed small-scale reinforced concrete model of a typical highway support bent carried out by Repa [28] was used to check FPIER. The structure was a two-bay one story frame. The prototype frame for the model is a typical supporting substructure for the CG series of pan-formed slab and girder bridge systems developed by the Texas Highway Department. The properties of the prototype are specified in the Texas Highway Department Standard Plan Sheet BCG-0-33-40 (26° - 34'). Section properties of the reinforced concrete model are shown in Fig. 2.37. In order to model the bent using FPIER, the columns and beams were all divided into ten segments. The columns were modeled assuming two types of cross sections. The first two segments included the overlapping footing reinforcement while the remaining eight segments had the column reinforcement only. In order to model the distribution of flexural

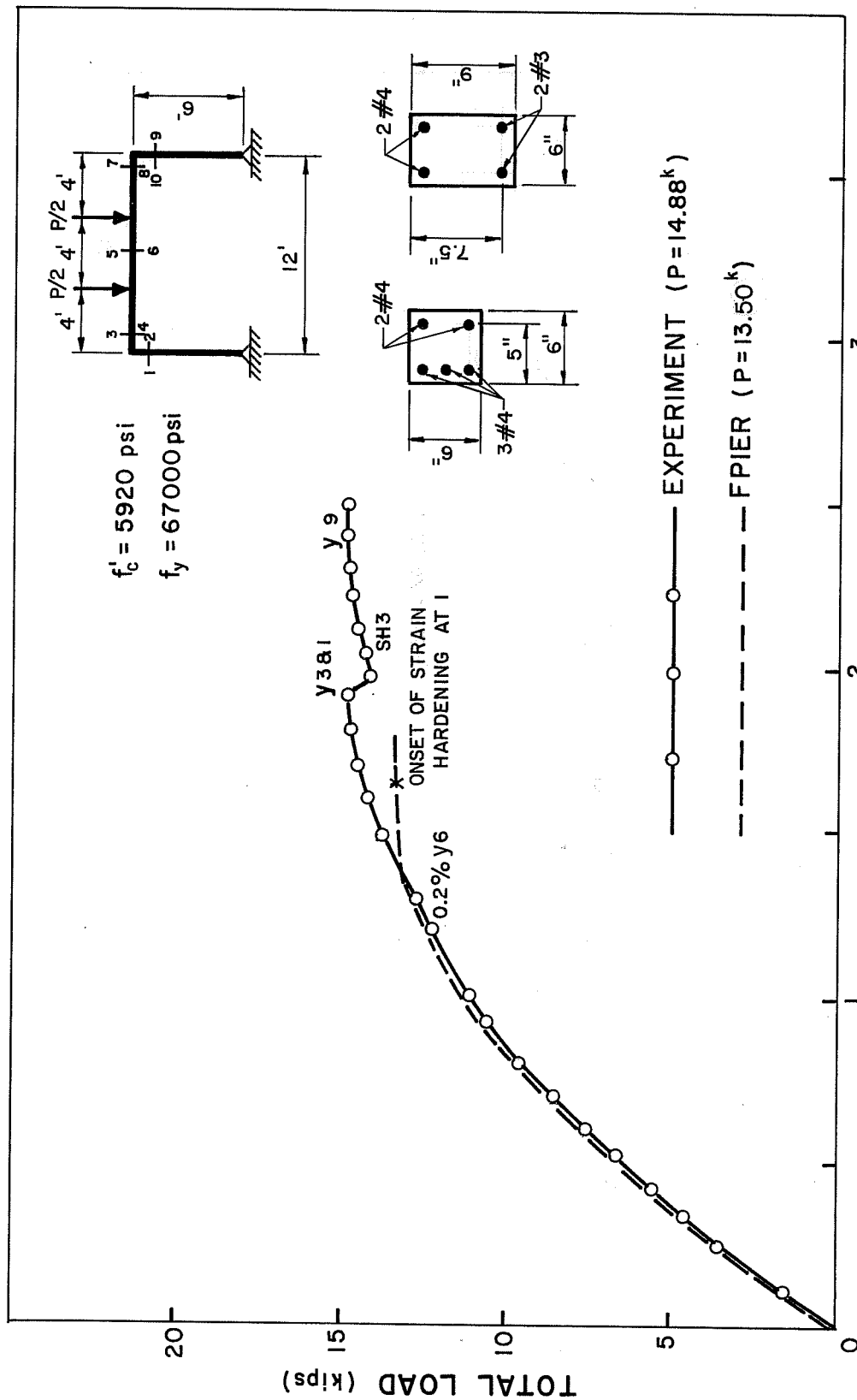

Fig. 2.35 Frame 2D12, from Ernst, et al.

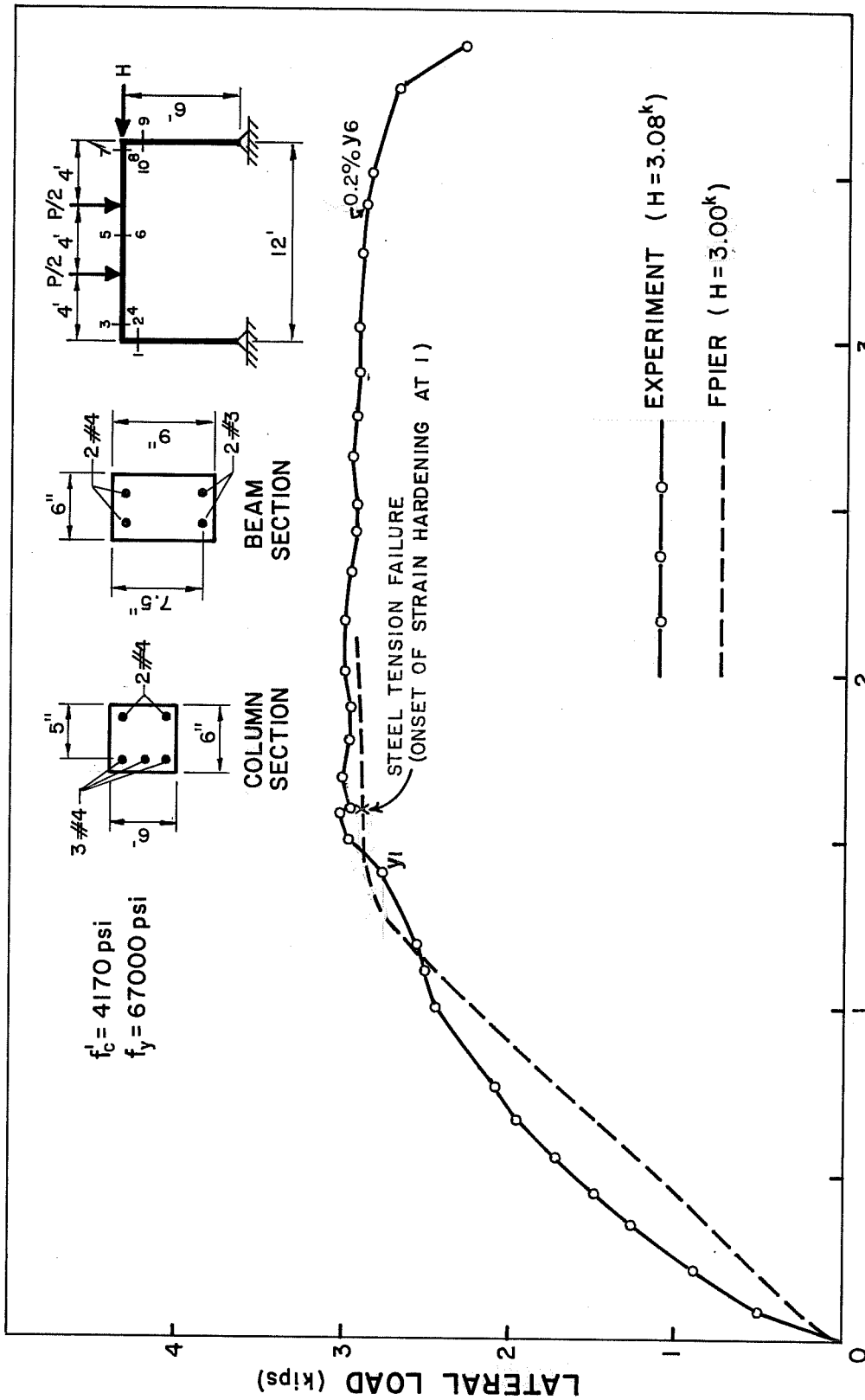

Fig. 2.36 Lateral displacements for Frame 2D12H, from Ernst, et al.

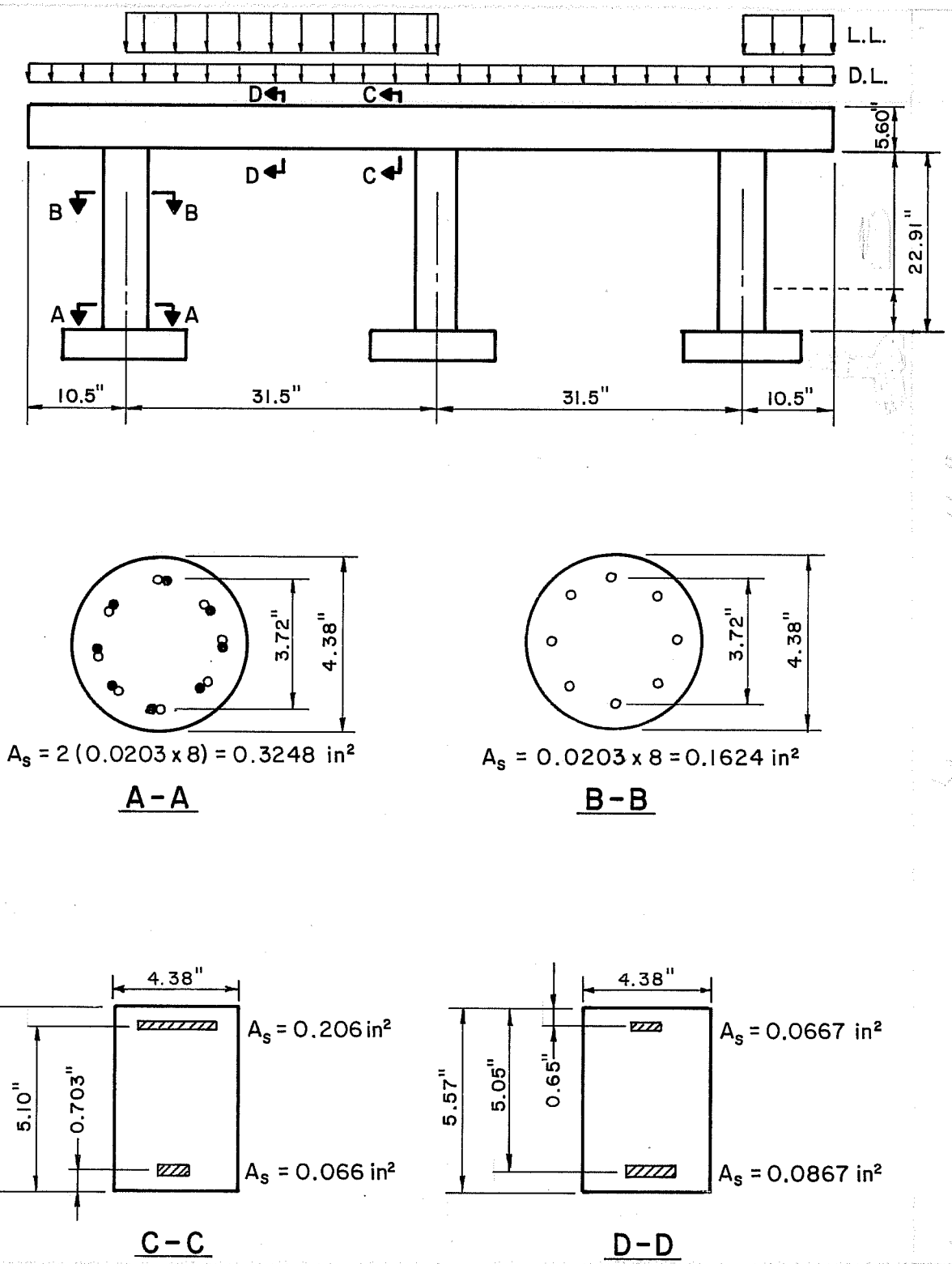

Fig. 2.37 Multiple column bent from Repa

reinforcement in the beams five types of cross sections were required. In the physical test program two frames (BC-1 and BC-3) with identical material properties were tested. The predicted and measured beam deflections are shown in Fig. 2.38. There is good agreement through service load levels. FPIER can only predict the behavior up to the first hinge formation. This first hinge was observed to form in both specimens at the middle of beam BC, at load levels of about 4.4k/ft. The frames continued to take substantial load through development of second and then third plastic hinges. In this highly redundant unsymmetrically loaded structure, development of three hinges were required before collapse ensued.

Program FPIER is primarily intended for use in design under AASHTO rules which do not recognize or allow load capacity to rely on moment redistribution. Thus the effective limit on FPIER is the formation of first hinging. For this case the program prediction is 4.18k which is about 93% of the general load at which first hinging occurred. The deflection predicted is quite high at that level but again is believed to be affected by the fact that the program does not count on deformation restraint when hinging is taking place.

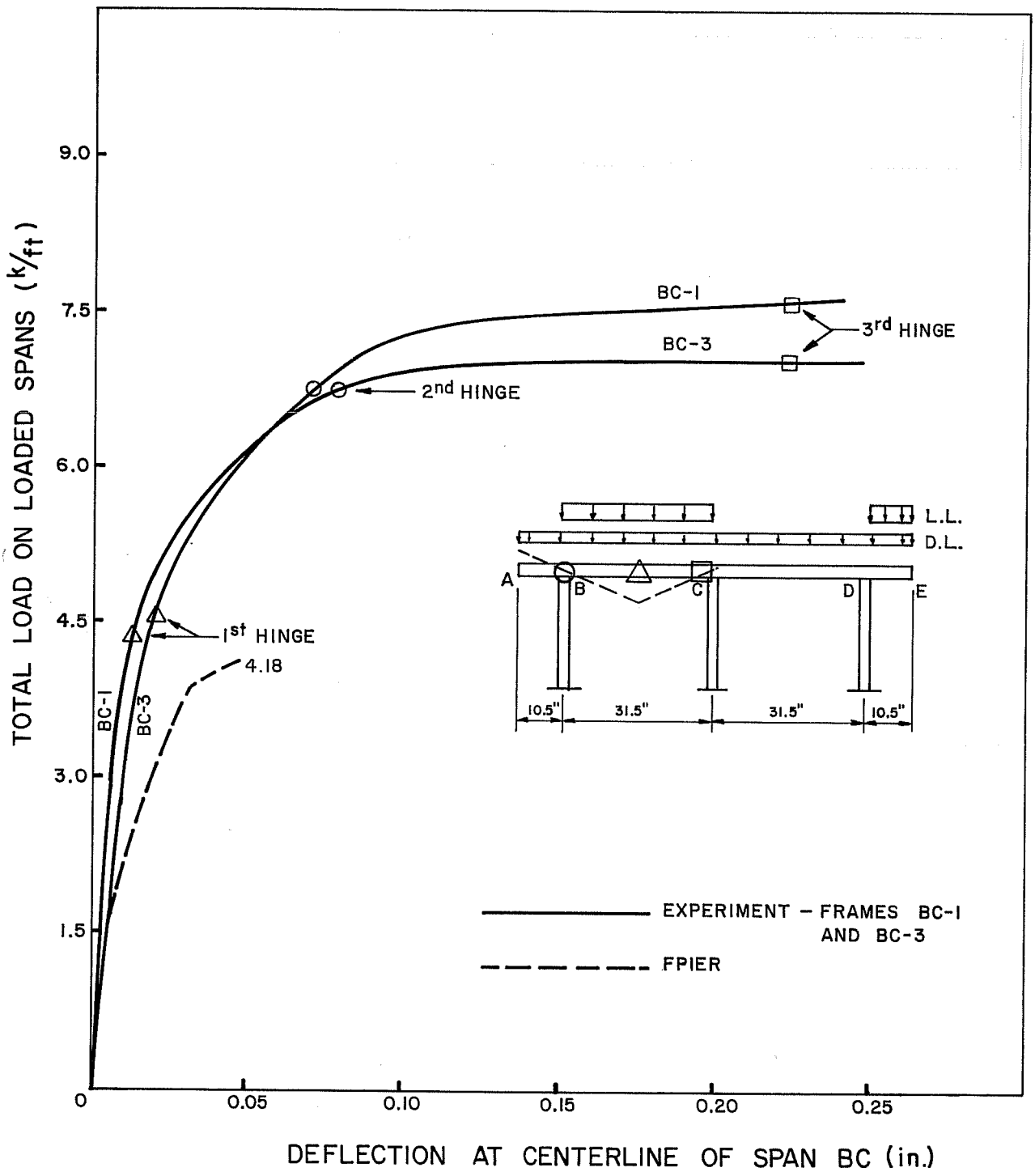

Fig. 2.38 Displacements for multiple column bents from Repa

CHAPTER 3

PHYSICAL TEST PROGRAM

3.1 Modeling

After studying many plans of typical bridge piers obtained from a state-of-the-art survey, prototype piers were selected and the cross sections were modeled on a scale of 1 to 6. The outside dimensions of the prototypes were 4 ft by 12 ft; therefore, the models had outside dimensions of 8 in. by 24 in. The hollow prototypes had wall thicknesses of 15 in., thus the hollow models had 2-1/2 in. wall thicknesses. The clear cover over the reinforcing steel was 3 in. in the prototypes, dictating 1/2 in. clear cover in the models.

Careful consideration was given to modeling of the reinforcing steel. The longitudinal reinforcing steel in the prototypes consisted of #11 bars, which were modeled by 6 mm. deformed bars. For the transverse reinforcement, smooth SWG 13 wires were used. These wires were heat treated to ensure a flat topped yield plateau typical of intermediate grade reinforcement. It is believed that the lack of deformations did not affect the present study because the transverse reinforcement was slightly rusted to improve bond and was well anchored by bending around the longitudinal bars. The AASHTO Specification [1] requires adherence to certain dimensional limits concerning bar spacing and instructions for placement of ties in a column. These limiting values were also multiplied by the 1:6 scale factor, and these requirements were satisfied in the fabrication of the models.

A reasonable model concrete was used. The normal maximum aggregate size of 1-1/2 in. would have required 1/4 in. size maximum

aggregate in the model. However, since 3/8 in. was the smallest maximum aggregate available at local ready-mix plants, it was used.

3.2 Specimen Details

Four specimens were tested in this study. One was a solid pier, one was a single cell hollow pier, while the others were two and three cell hollow piers, respectively. The behavior of each pier was compared with the results generated by program BIMPHI. All four piers had identical exterior dimensions. Each had a prismatic shaft which was 72 in. in height and each had larger end zones. The shaft cross section had exterior dimensions of 8 × 24 in. The cross sections and the reinforcement patterns are shown in Figs. 3.1 through 3.4. Painstaking care was exercised in the fabrication of the steel cages since the scaling factor also applies to the dimensional tolerances. Careful measurement after casting indicated all dimensions were within the 1/32 in. tolerances. The longitudinal bars were well anchored into the 28 in. deep loading heads shown at each end of the specimen in Fig. 3.5.

3.3 Materials

3.3.1 Concrete. The concrete used for the solid and the single cell hollow specimens contained entrained air plus an ASTM C494 cement dispersing and set-retarding admixture. The concrete mixture was designed to produce a 28-day strength of 4000 psi. The concrete for the solid and the single cell hollow specimen was obtained from a ready-mix plant. The concrete for the two cell and three cell specimens was mixed in the laboratory. The concrete mix design for the solid pier is presented in Fig. 3.6 along with information concerning the gain in concrete strength with time. Similar information for the concrete used in the hollow piers is presented in Figs. 3.7 through 3.9. Each point on the concrete strength curves is the average strength obtained from two to five cylinder tests. The cylinders were cured in the same manner as the model pier specimens.

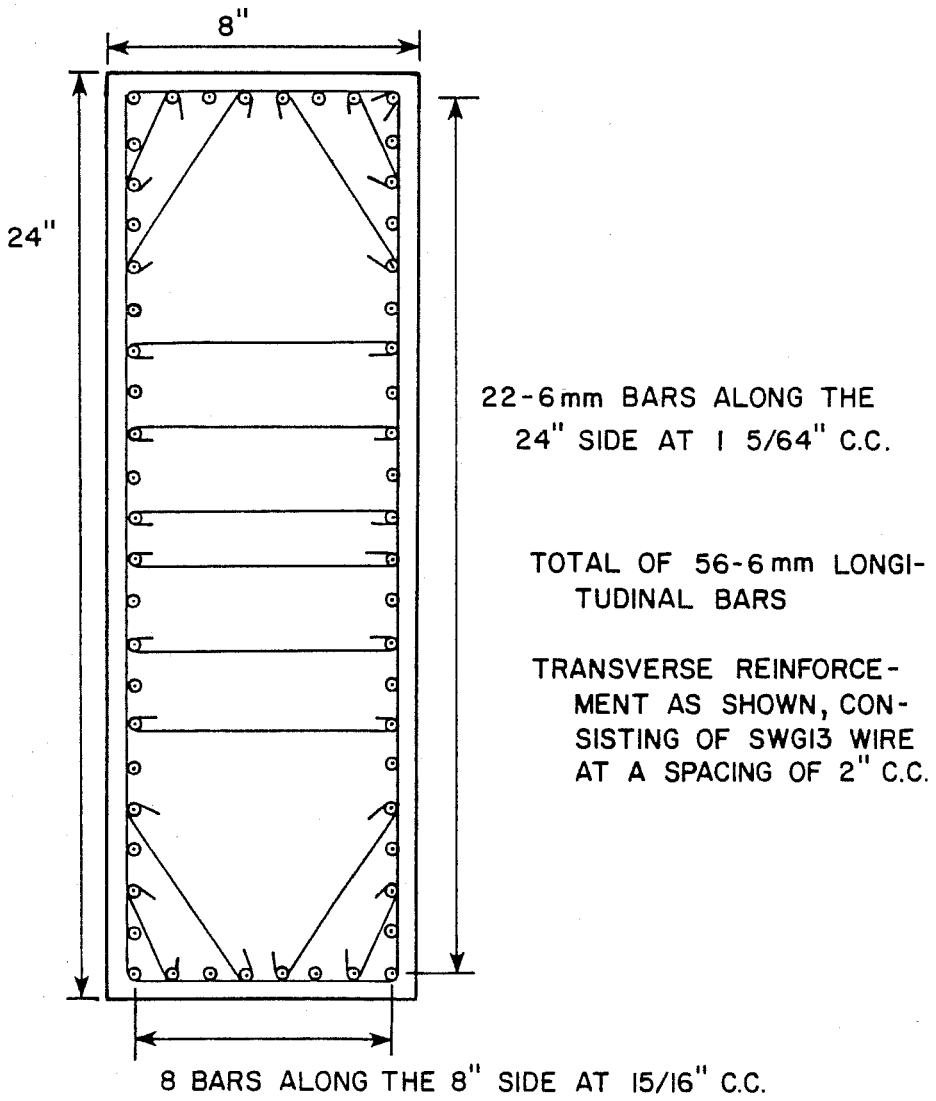

Fig. 3.1 Details of the solid model pier cross section

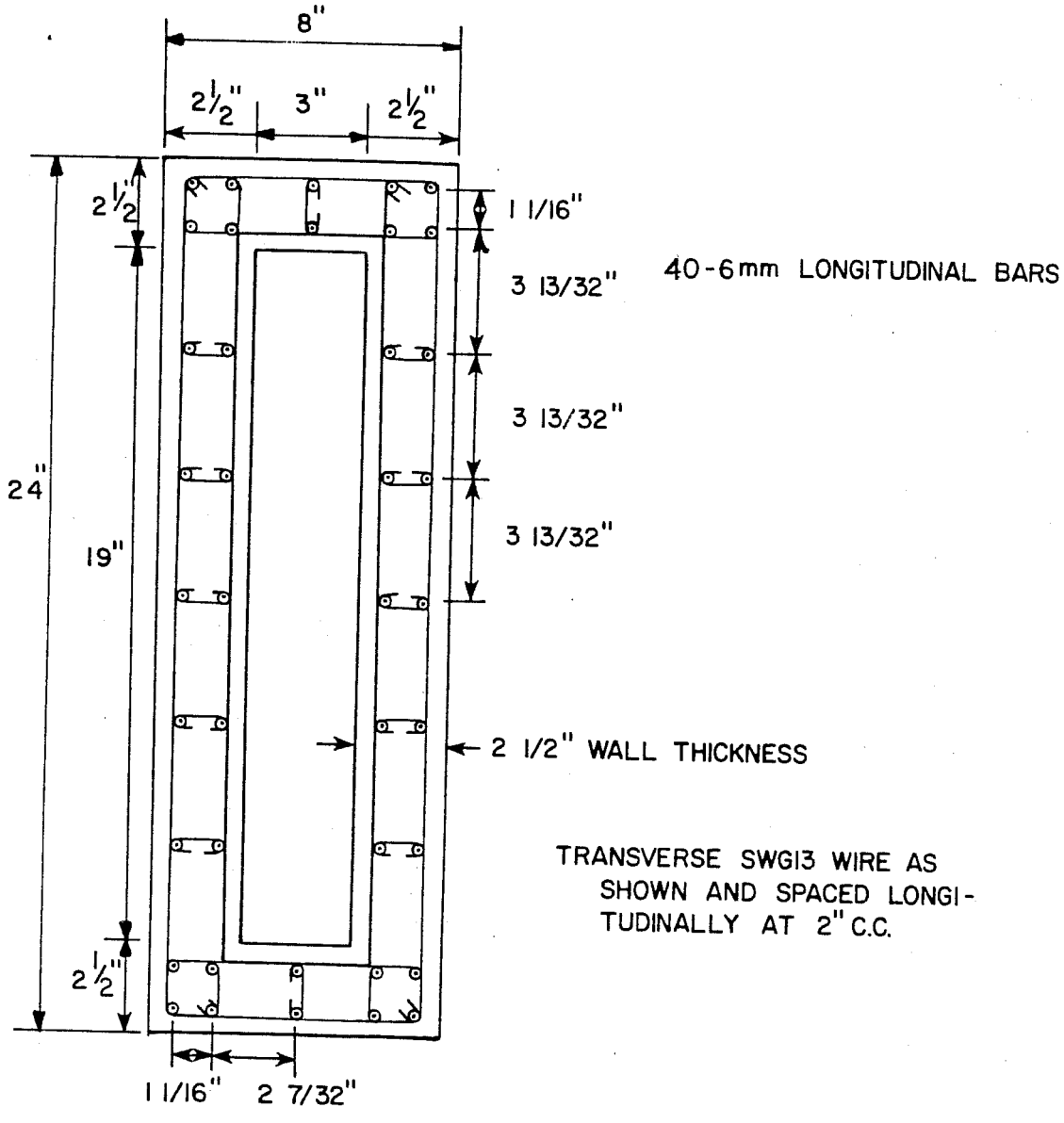

Fig. 3.2 Details of the single cell model pier cross section

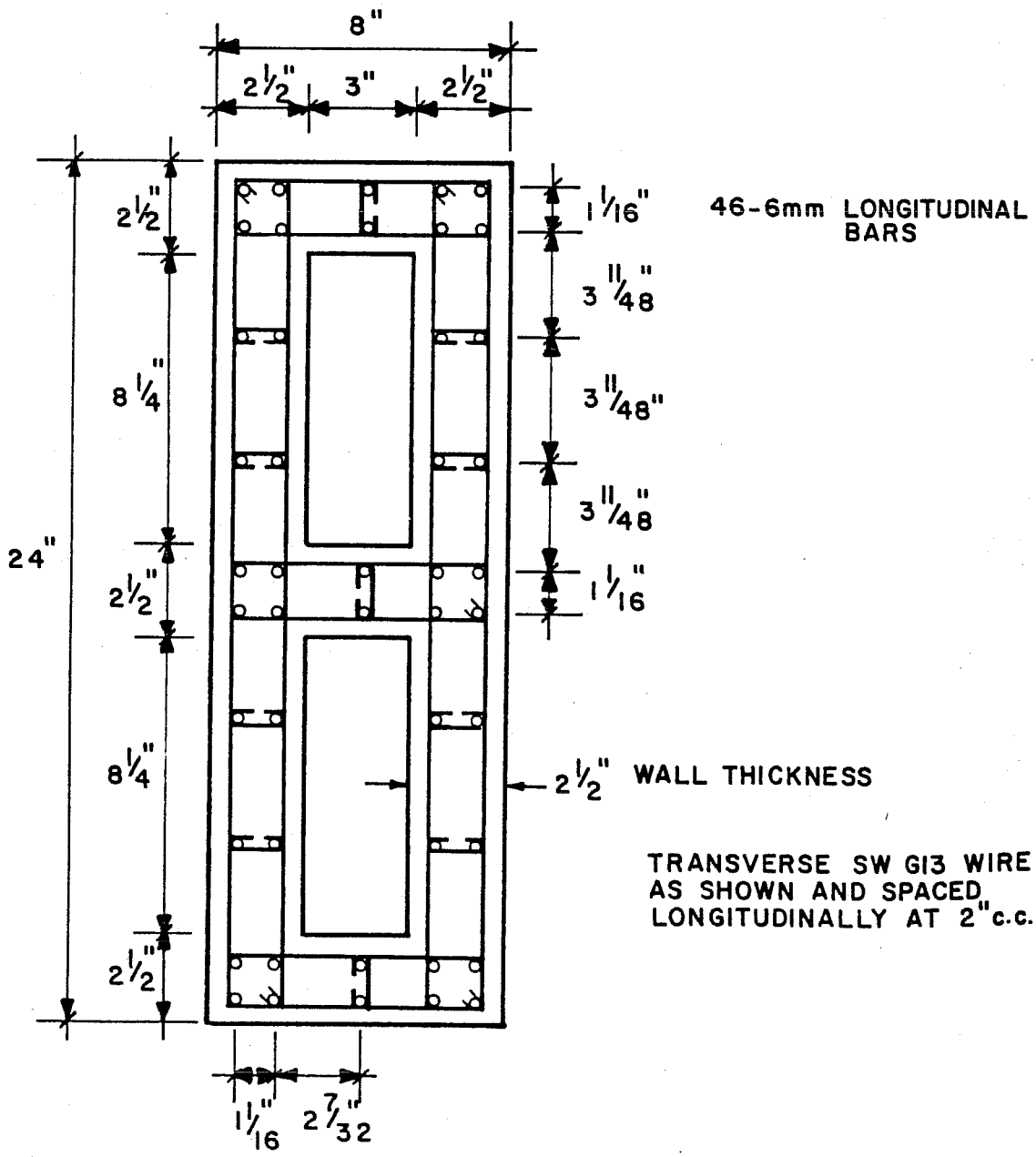

Fig. 3.3 Details of the two cell model pier cross section

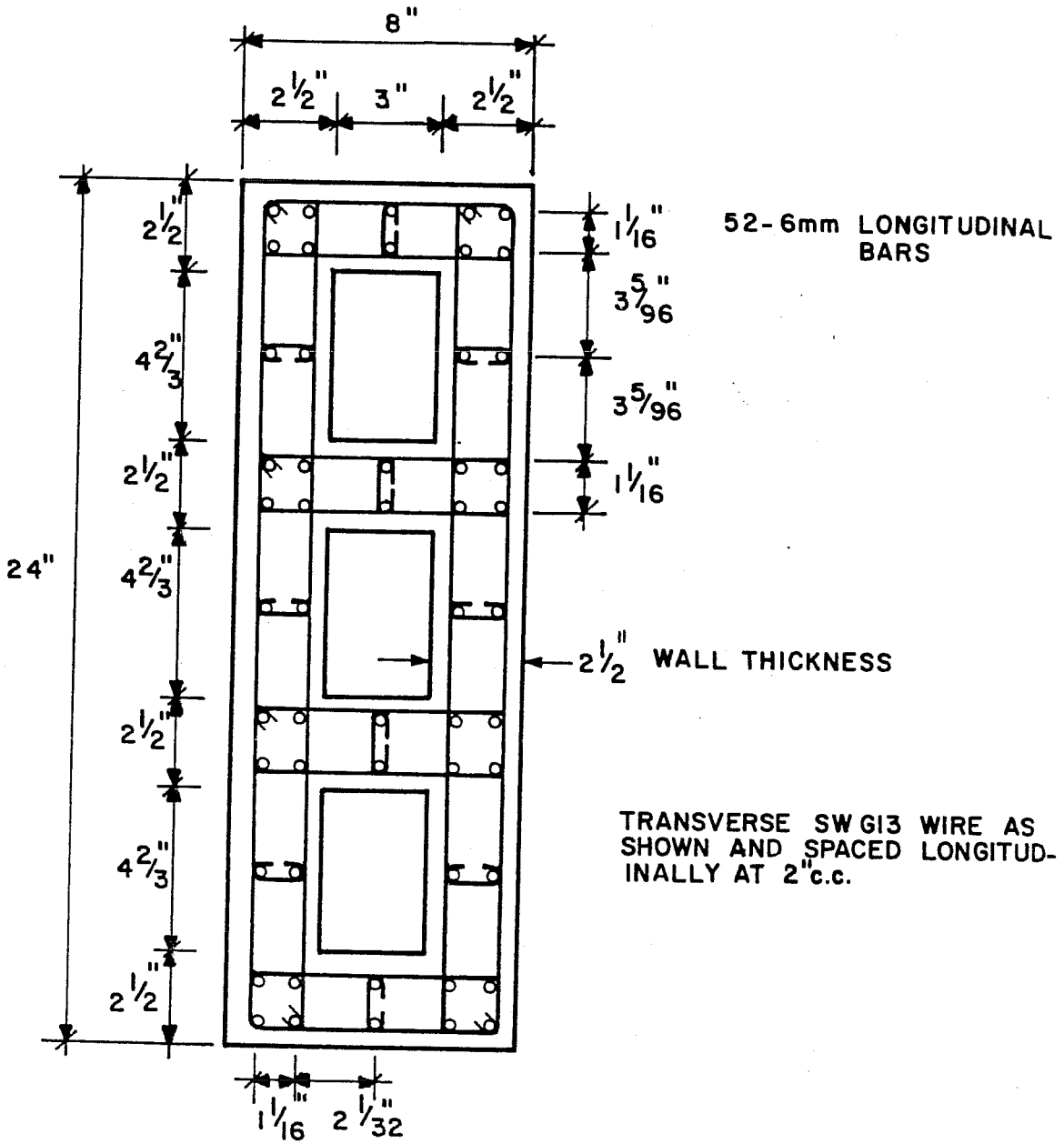

Fig. 3.4 Details of the three cell model pier cross section

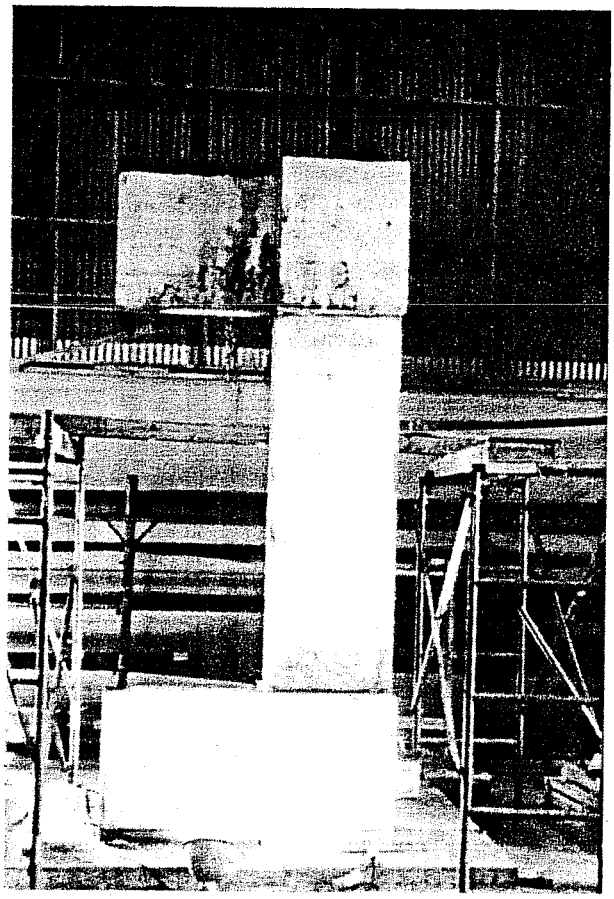

Fig. 3.5 Hollow pier specimen

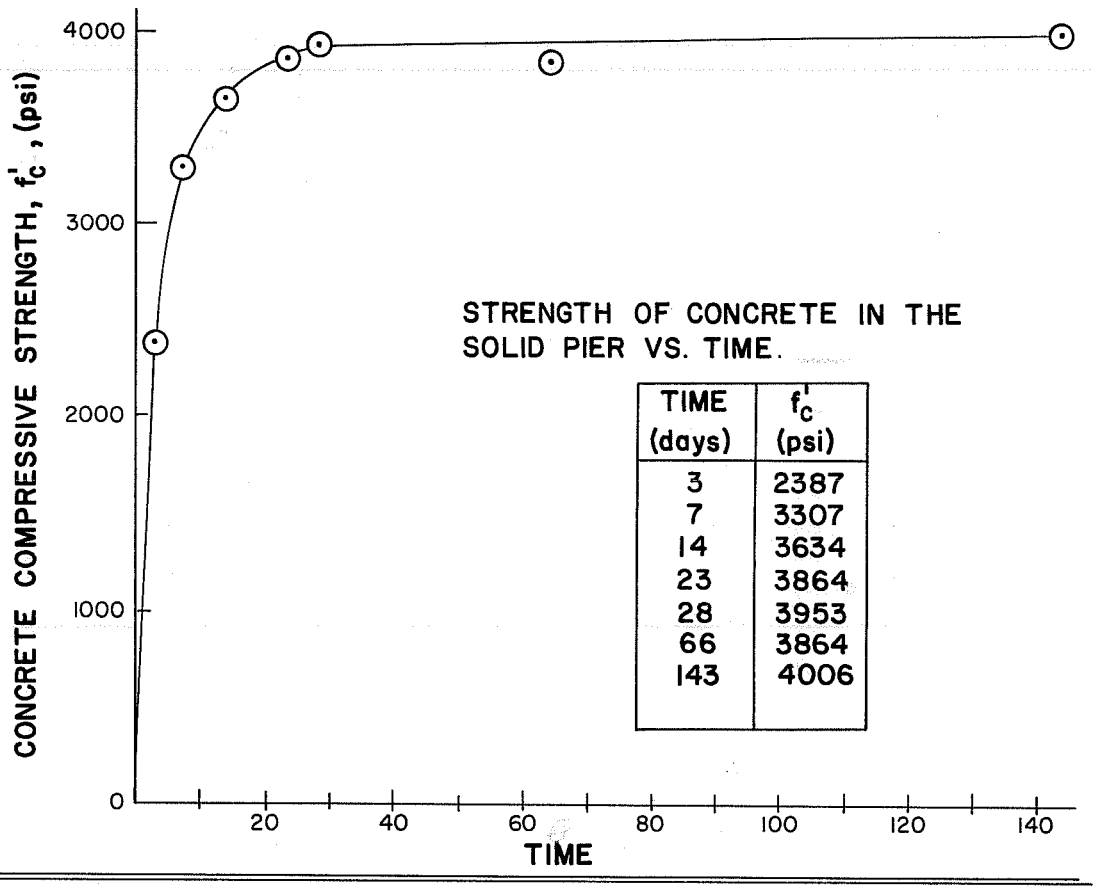

TIME (days)	f'_c (psi)
3	2387
7	3307
14	3634
23	3864
28	3953
66	3864
143	4006

CONCRETE MIX DESIGN FOR THE SOLID PIER

MATERIAL	% ABSOLUTE VOLUME	BATCH WEIGHTS (lb/cu.yd.)
CEMENT	9.5	501
WATER	21.0	274
FINE AGG.	29.4	1352
COARSE AGG.	33.1	1467
AIR	7.0	0
ADDITIVES: SEPTAIR		2.7 oz/cu.yd.
TRISENE R		21.8 oz/cu.yd.
WATER/CEMENT RATIO = .55 lb/lb = 6.2 gal./sk		
SLUMP = 7 1/2"		

Fig. 3.6 Mix design and strength of concrete for the solid pier

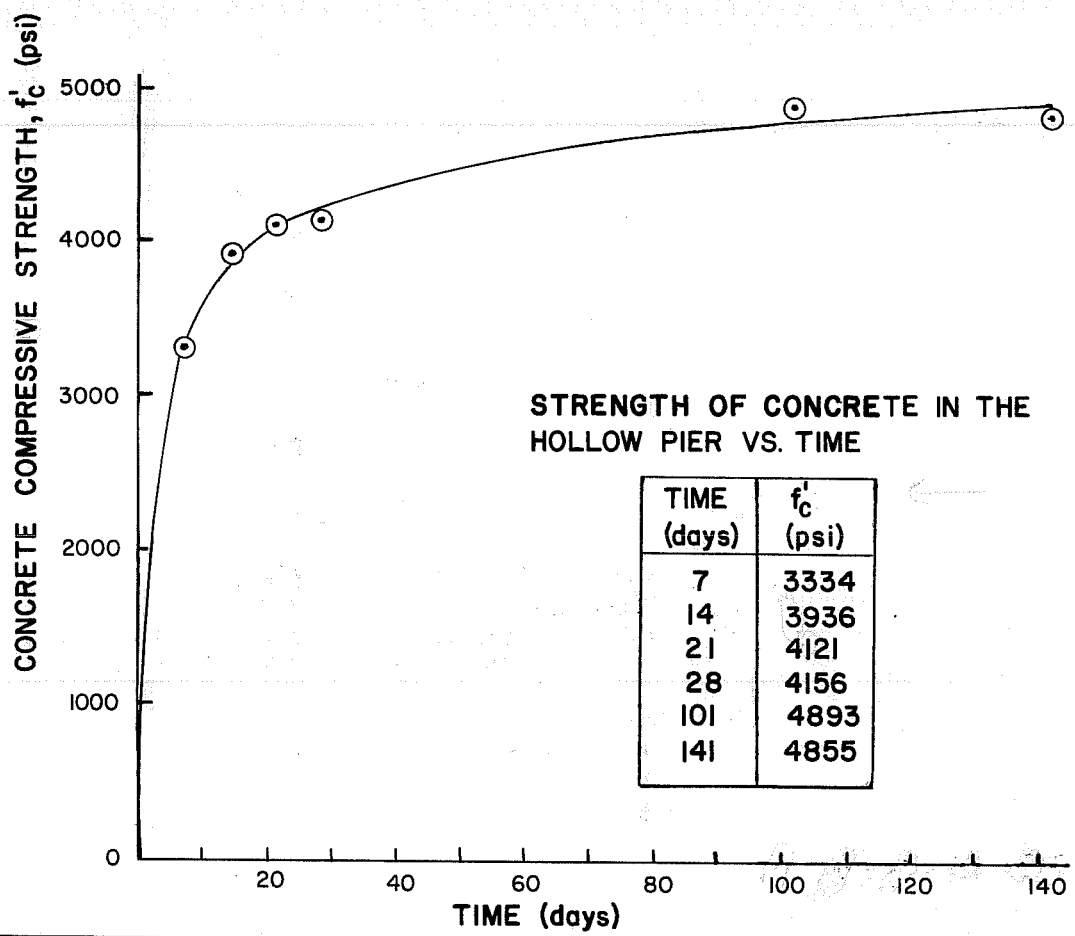

TIME (days)	f'_c (psi)
7	3334
14	3936
21	4121
28	4156
101	4893
141	4855

CONCRETE MIX DESIGN FOR THE HOLLOW PIER

MATERIAL	% ABSOLUTE VOLUME	BATCH WEIGHTS (lb./cu.yd.)
CEMENT	6.8	364
WATER	18.6	246
FINE AGG.	21.4	982
COARSE AGG.	46.2	2047
AIR	7.0	0
ADDITIVES: SEPTAIR 1.8 oz./cu.yd. TRISENE R 15.5 oz./cu.yd.		
WATER/CEMENT RATIO = .68 lb./lb. = 7.7 gal./sk SLUMP = 6 1/2"		

Fig. 3.7 Mix design and strength of concrete for the single cell pier

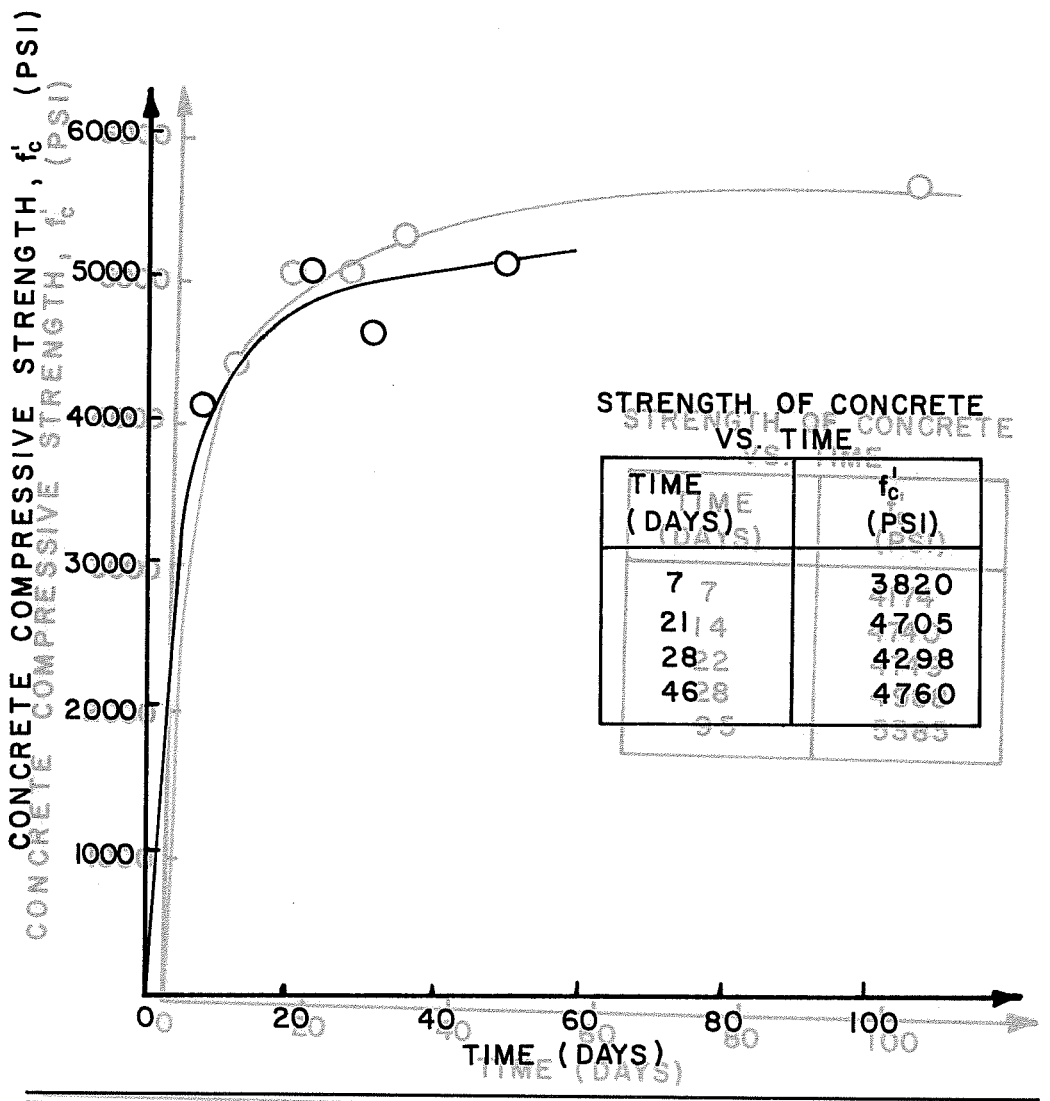

STRENGTH OF CONCRETE VS. TIME

TIME (DAYS)	f'_c (PSI)
7	3820
21	4705
28	4298
46	4760

CONCRETE MIX DESIGN

MATERIAL	BATCH WEIGHT (lb/cu. yd.)
CEMENT	599
WATER	433
FINE AGG.	1472
COARSE AGG.	1238
WATER/CEMENT RATIO = .72 lb/lb	
SLUMP = 8 1/2 "	

Fig. 3.8 Mix design and strength of concrete for the two cell pier

For the concrete in the single cell hollow pier, measurement of the modulus of elasticity was made in order to check the assumptions made concerning this value. Tests revealed an average secant modulus of 3,800,000 psi and an average tangent modulus of 4,100,000 psi. The value assumed for the analytical calculations was 3,990,000 psi based on the ACI 318-77 formula which gives the concrete modulus as $57{,}000\sqrt{f'_c}$. The Hognestad stress-strain curve was used to describe the behavior of the concrete, and it is based upon using a tangent modulus of elasticity [8]. Since the assumed value for analysis is within 3% of the experimentally found tangent modulus, it is considered quite acceptable.

3.3.2 Steel. Two types of reinforcing steel were used in the model piers. For the longitudinal steel, 6 mm. deformed bars were used. The bars had a cross-sectional area of 0.052 square in.

Three bars were tested to determine the strength and Young's modulus of the bars. They had an average yield strength of 61.1 ksi, an average ultimate strength of 84.3 ksi, and an average modulus of elasticity of 30,500 ksi.

The transverse reinforcement consisted of smooth SWG 13 wires. They had an average yield strength of 36.6 ksi and an average ultimate strength of 48 ksi. The average area of these wires was 0.0064 sq. in.

3.4 Forming and Casting

The specimens were cast in a vertical position just as prototype piers would be cast in the field. This was necessary to properly model actual bridge piers since the position of casting affects the strength and behavior of a specimen.

3.4.1 Forms. The forms used for the model pier portion of the specimen were very stiff in order to prevent any bowing of the forms. Structural steel angles were used to carry much of the gravity load in order to prevent unwanted deflections in the forms, especially in the overhanging loading heads.

3.4.2 Concrete Placement. The concrete for the solid pier was all placed in a single casting operation. Shores were used between the heads to support the gravity loads from the concrete. The concrete was placed in three layers in the central shaft, and the concrete was vibrated between the placement of each layer. External form vibrators were used as well as conventional vibrators inside of the forms. Cylinders were made simultaneously. Placement was fairly easy with the desired concrete slump of 7-1/2 in.

The placement of the concrete for the hollow piers was accomplished in three separate casting stages at different times. This was mandatory in order to create the voids in the pier. The voids were created by placing cores in the specimen which were subsequently removed. This task required great care in order to ensure removal of the cores. Wooden cores were made with a 1/16 in. taper obtained by using tapers of 1/32 in. on each side along the 72 in. length. Then these cores were covered with a low shear strength material (DuPont 3/32 in. Microfoam) which was selected from several materials tested for this purpose. These cores had to be positioned carefully to ensure that the proper dimensions were obtained. Also the cores were anchored to resist the buoyant forces.

The concrete was first placed in the lower head. Then the central shaft portion of the specimen was cast with the cores in the center. After approximately 8 to 24 hours, the cores were successfully removed. Then the voids were covered and sealed and the concrete for the top loading head was placed. Again the placement of the concrete was simplified due to obtaining a high slump comcrete and due to the use of extensive vibration.

3.4.3 Curing. All pier specimens and all cylinders were cured in the same manner. They were covered with large plastic sheets for several days in order to prevent evaporation of moisture. Then the forms were removed after 3 days for the solid pier and after 7 days for the hollow piers.

3.5 Instrumentation

There were four primary measurements which needed to be recorded accurately in this study. These included measurement of the strains in the reinforcement, strains on the surface of the pier concrete, deflections of the potentiometers in the curvature meters, and the amount of load being applied through each of the three loading rams.

3.5.1 Strain Gages. Strain gages were applied to reinforcing bars at three different levels in each of the pier tests. A total of 18 strain gages was applied to bars in the solid model pier, and their distribution is shown in Fig. 3.10. Hollow piers were more heavily instrumented and contained approximately 28 strain gages. The distribution of gages is shown in Figs. 3.11 through 3.13. These gage readings were used in computing the curvature at various sections and for checking the assumption that plane sections before bending remain plane after bending. No strain gages were damaged in the solid pier, but five gages were lost in the single cell pier, and one gage was lost in both the two and three cell piers during placement of the concrete.

3.5.2 Demec Strain Gage. A Demec mechanical strain gage which had a gage length of 8 in. was used to measure the average strain within the gage length on the surface of the pier concrete. Demec readings were used to check the Bernoulli's plane section assumption. The use of the Demec strain gage was found to be much better for checking this assumption, since strains measured by strain gages on reinforcement can be greatly influenced by the presence of the cracks in the concrete. In addition, the Demec gage averages the strain over a longer length and is thus less sensitive to local cracking. The Demec strain gage was not used in the earlier tests of the solid pier or the single cell pier. After reduction of the strain gage data in those tests it was used in the remaining tests of the two cell pier and the three cell pier. The layout of the Demec measuring points is shown in Figs. 3.14 and 3.15. Because of a change

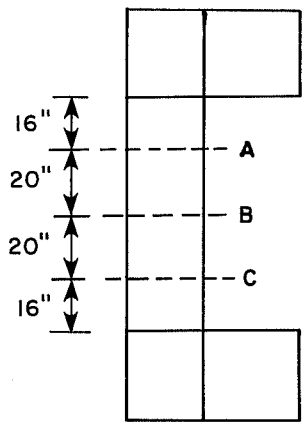

GAGE LAYOUT AT SECTIONS A AND C

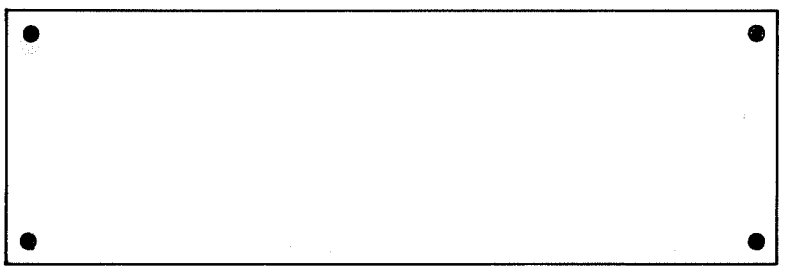

GAGE LAYOUT AT SECTION B

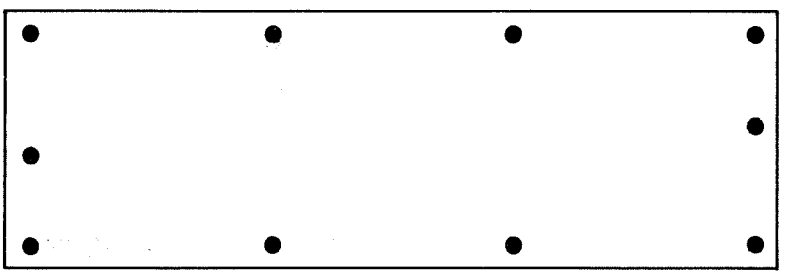

Fig. 3.10 Strain gage layout for the solid pier

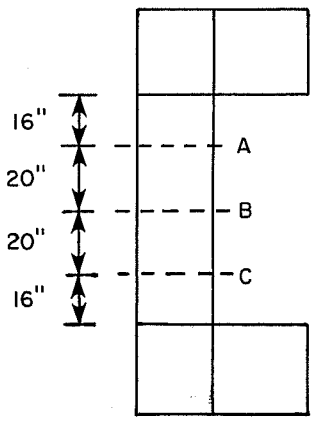

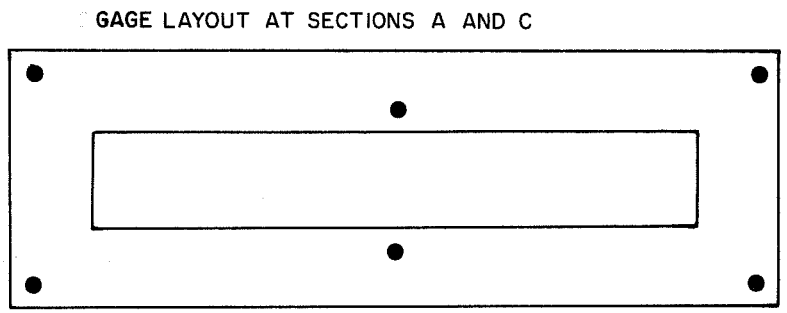

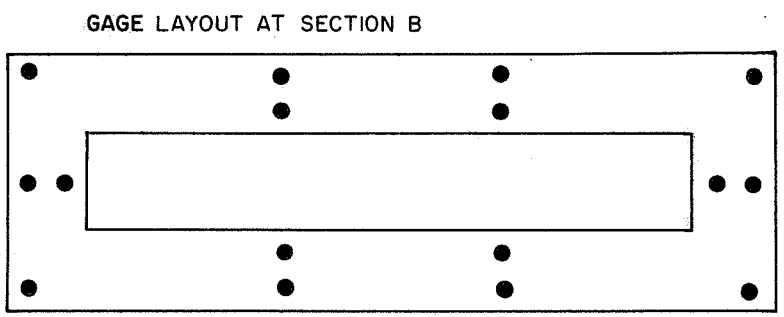

Fig. 3.11 Strain gage layout for the single cell pier

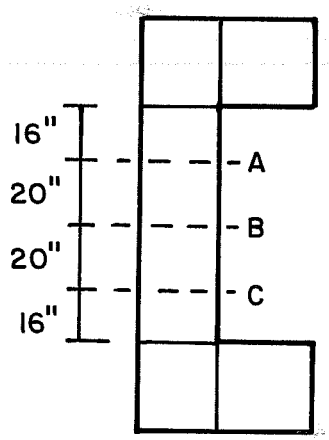

GAGE LAYOUT AT SECTION B

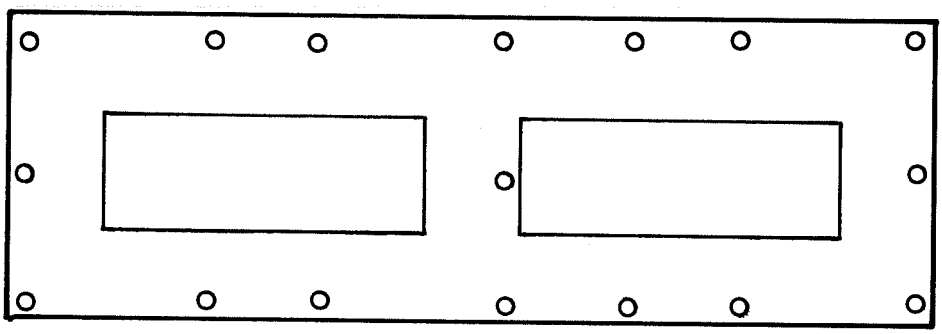

GAGE LAYOUT AT SECTIONS A AND C

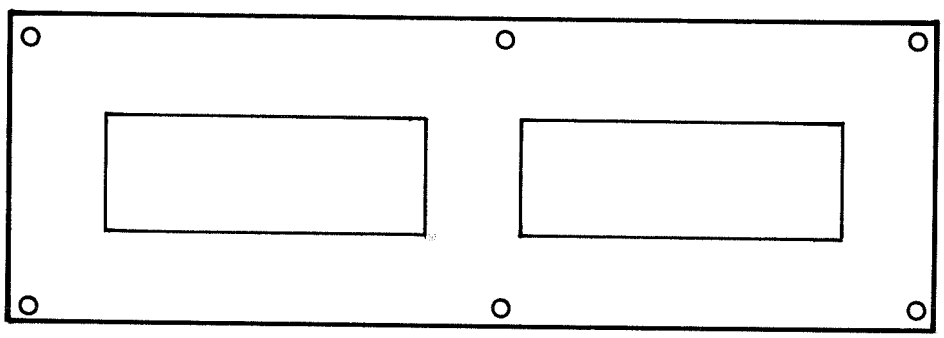

Fig. 3.12 Strain gage layout for the two cell pier

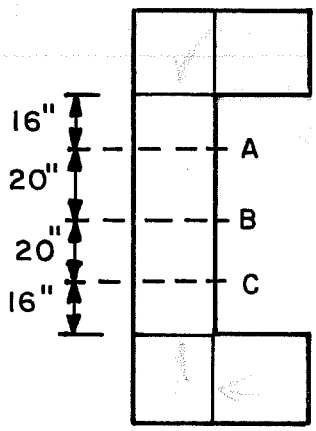

GAGE LAYOUT AT SECTION B

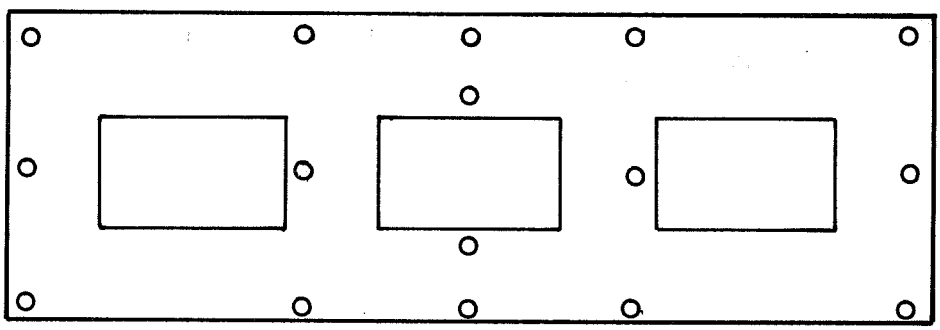

GAGE LAYOUT AT SECTIONS A AND C

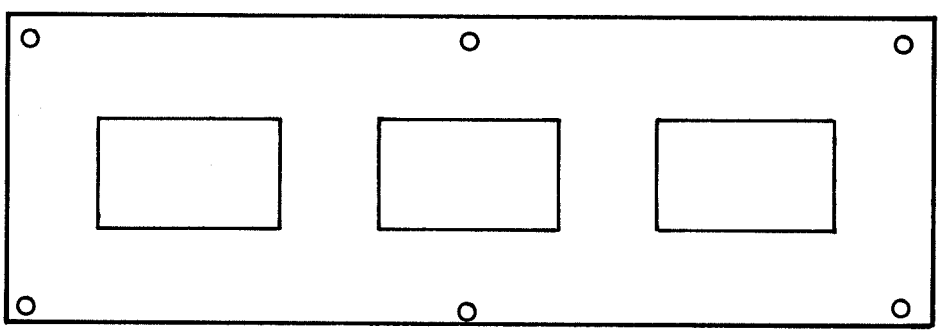

Fig. 3.13 Strain gage layout for the three cell pier

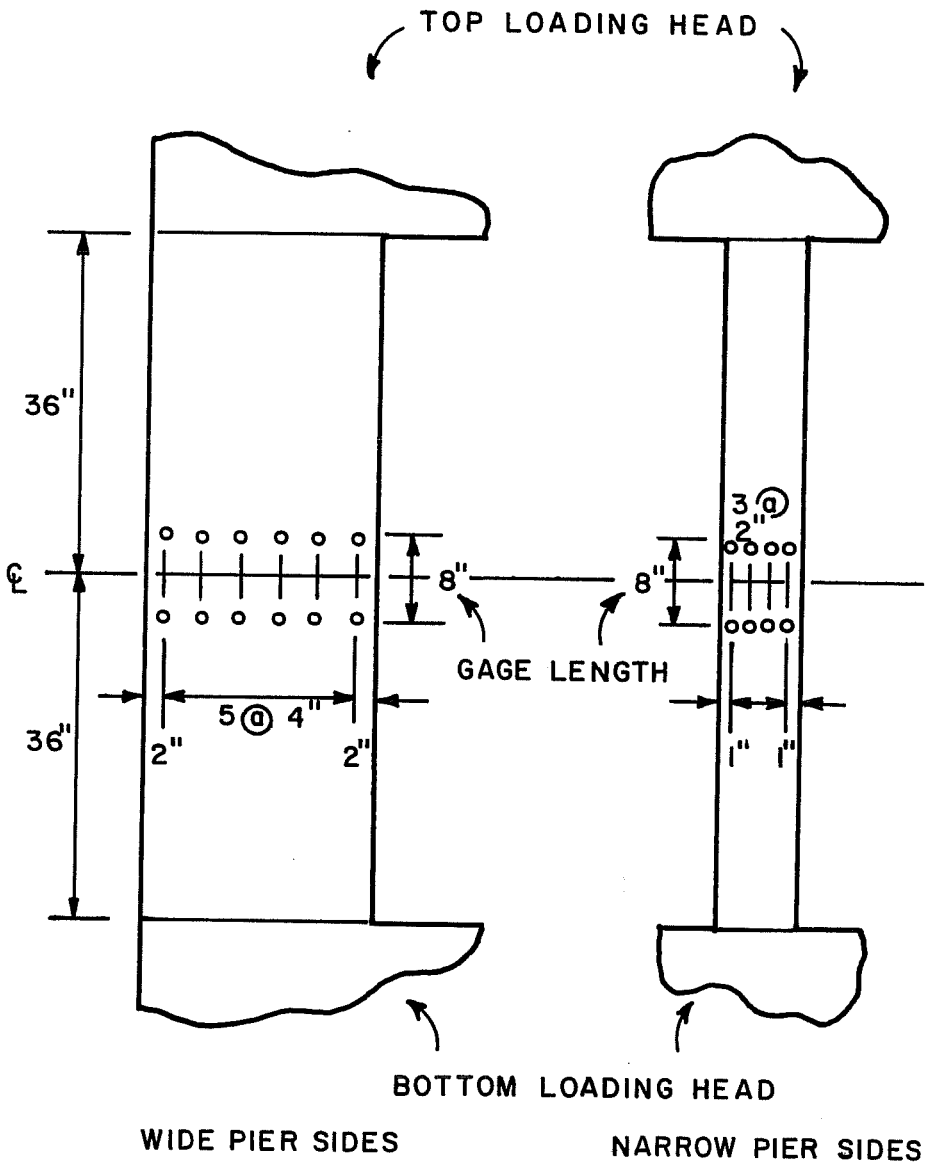

Fig. 3.14 Layout of Demec strain gage measuring points on the two cell pier

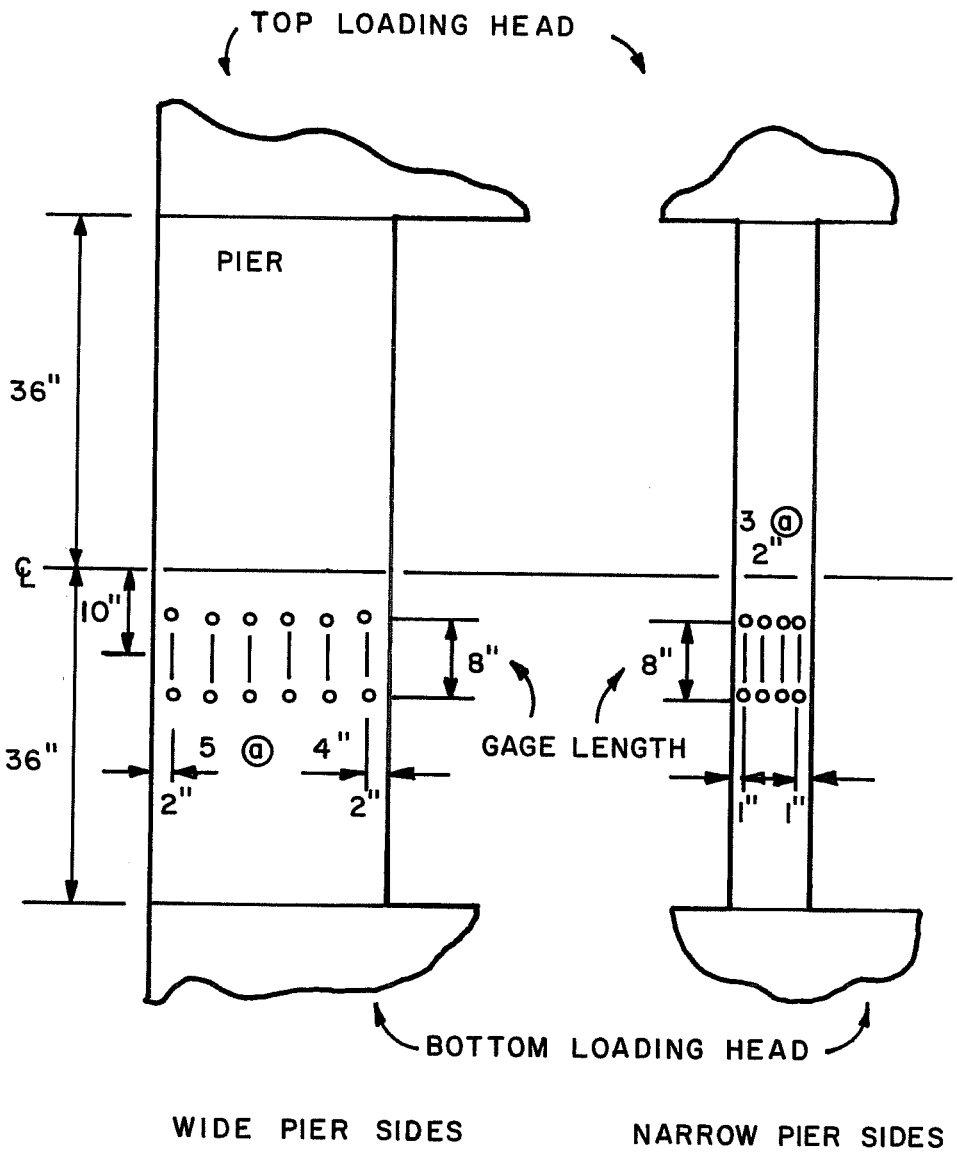

Fig. 3.15 Layout of Demec strain gage measuring points on the three cell pier

of the position of the curvature meter frames on these two specimens, the stations for Demec measurement differed slightly on the two specimens. The total number of Demec gage lengths on each specimen was twenty. The gage length of 8 in. was chosen so that at least three cracks would be covered with the gage lengths. The average strain within a gage length is influenced less as the number of cracks increases. In the earlier tests (solid and single cell pier specimens), it had been observed that the cracks generally developed along the horizontal reinforcement which had a spacing of 2 in. Thus a gage length of 8 in. was chosen to minimize local cracking effects.

3.5.3 Curvature Meters. Many methods for measuring curvatures were investigated. The meter configuration decided upon was an extension of various types used by Breen [11], Ford [12], Mavichak [13], and others. The meters were steel frames with potentiometers mounted between them, as shown in Fig. 3.16, to measure relative deflections. They were attached to the pier at six locations along its height. Pointed bolts were used for attachment, so the exact location of contact could be controlled. They were tightened against small steel bearing plates which were glued onto the pier at the appropriate locations. Potentiometers were mounted on the ends of the extending steel angles in order to measure the change in the vertical distance between adjacent frames. From these measurements and geometrical measurements of the frames, the average curvatures at various points along the height were calculated.

3.5.4 Pressure Transducers. Pressure transducers were used to measure the loads applied by the three hydraulic loading rams. A 400 ton Simplex ram was used to apply the major concentric load on the piers, while the minor eccentric loads on each axis were applied through two 100 ton Simplex rams. These loads were measured by multiplying the effective area of each ram times its recorded pressure. The ram pressures were measured by pressure transducers. These transducers will record an accuracy of $\pm.07$ percent.

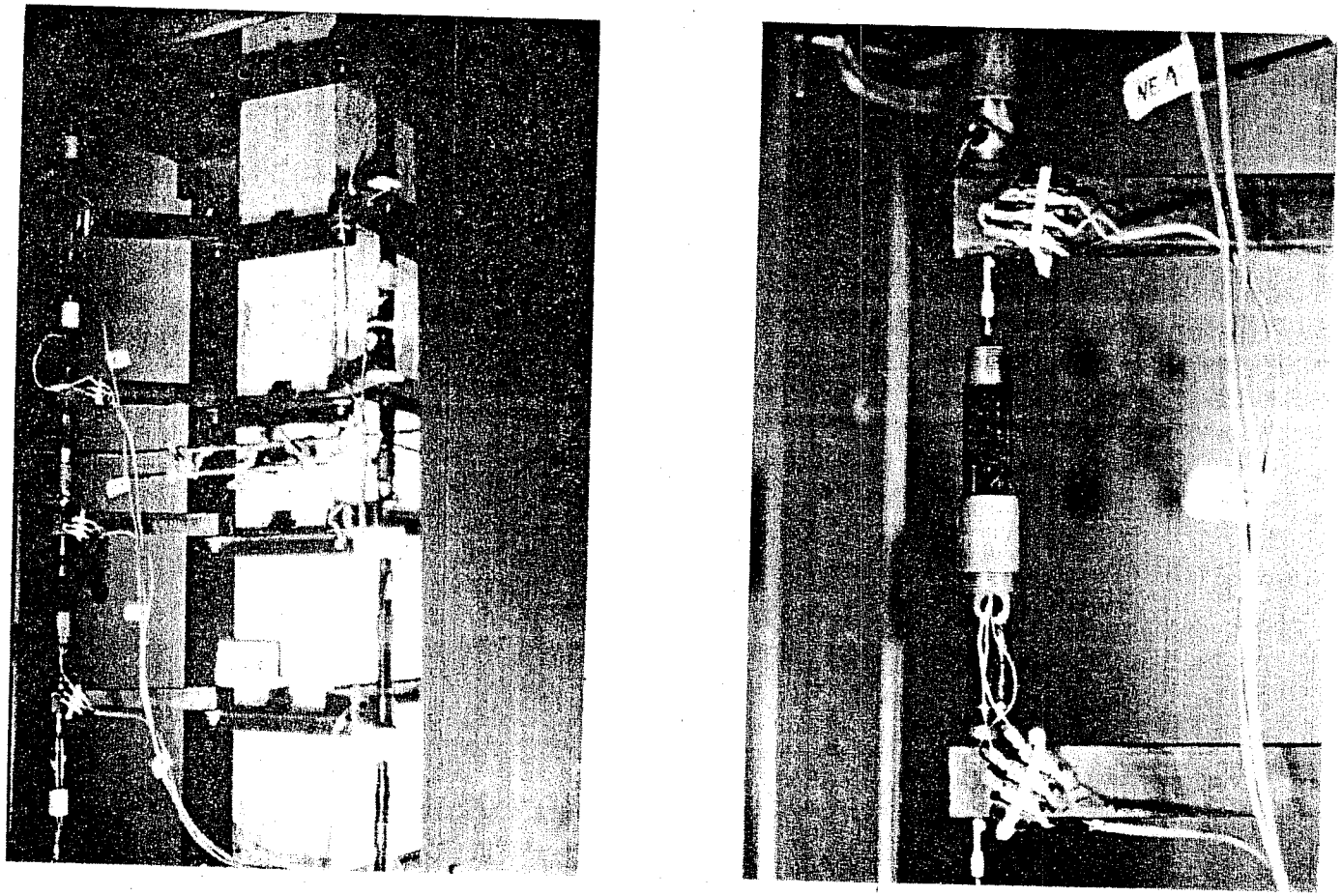

Fig. 3.16 Curvature meters

3.6 Test Set-up

3.6.1 Testing Position. The model piers were loaded in a structural steel loading frame as shown in Fig. 3.17. The ends of the specimens were supported by spherical loading platens. This allowed rotation at the ends of the specimen, which would be idealized as a pinned-pinned support condition.

3.6.2 Method of Loading. There were three points of load application on each of the piers as shown in Fig. 3.18. A concentric axial load was applied through the 400 ton ram (P_1). It was desired to maintain the total axial load at a constant value as moments about both axes were applied. Therefore, the eccentric loads on the two axes (P_2, P_3) were increased using the two 100 ton rams. Figure 3.19 shows a simplified uniaxial bending case to illustrate the method of loading. An initial axial load was applied. The total axial load level was then held constant while eccentric loads were added. For each specimen many loading cases were carried out before loading the pier to failure. In the solid and single cell tests, after each case all the loads were decreased to zero and then the axial load was reapplied. However, in the tests of the two and three cell piers, the concentrated axial load was not decreased to zero after each case but was increased for the next loading case. Prior to the final loading case in which the specimens were taken to failure, the load was decreased to zero.

As previously discussed, the P_1 load applied through the concentric 400 ton ram was increased to the total axial load ($P_1 = K$) and then decreased as the moments were applied to maintain the total load constant ($\Sigma[P_1 + P_2 + P_3] = K$). Breen [11] has shown that when the direction of travel of a Simplex-type ram is reversed, the pressure readings are not always reliable. This is due to certain frictional characteristics associated with reversing the travel direction of a ram. In order to check the magnitude of such an error, the ram was carefully calibrated on a Satec 600 kip testing machine. It was found that the maximum error induced due to frictional problems would be 2.5%. This was considered to be acceptable.

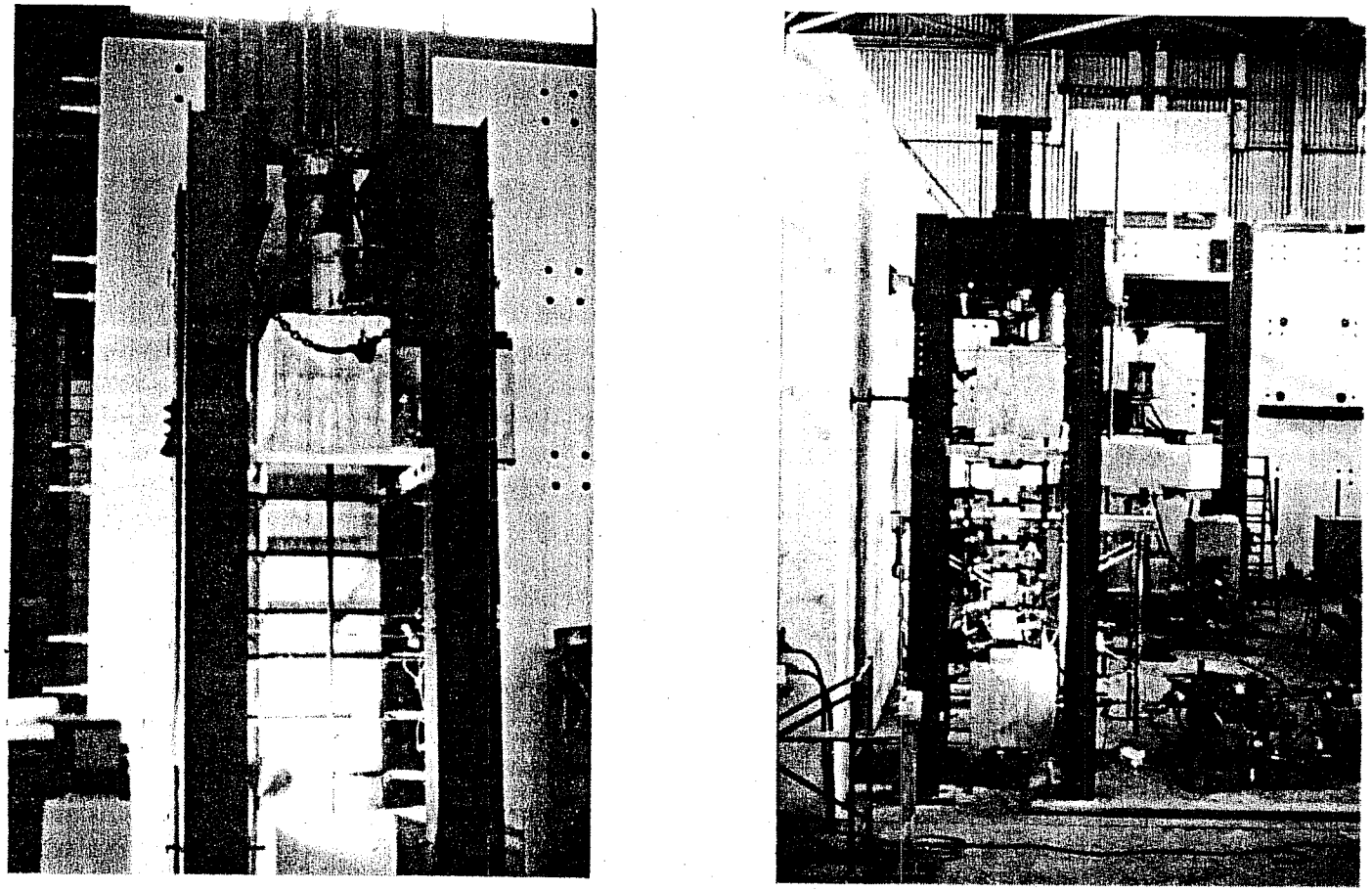

Fig. 3.17 Pier specimen within structural steel loading frame

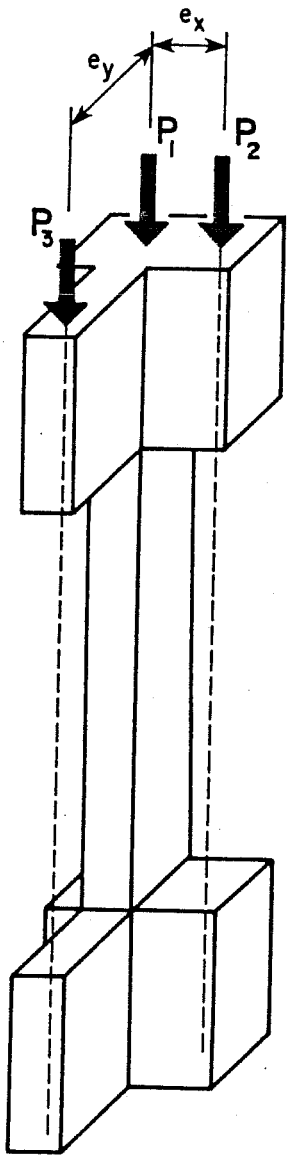

Fig. 3.18 Method of load application

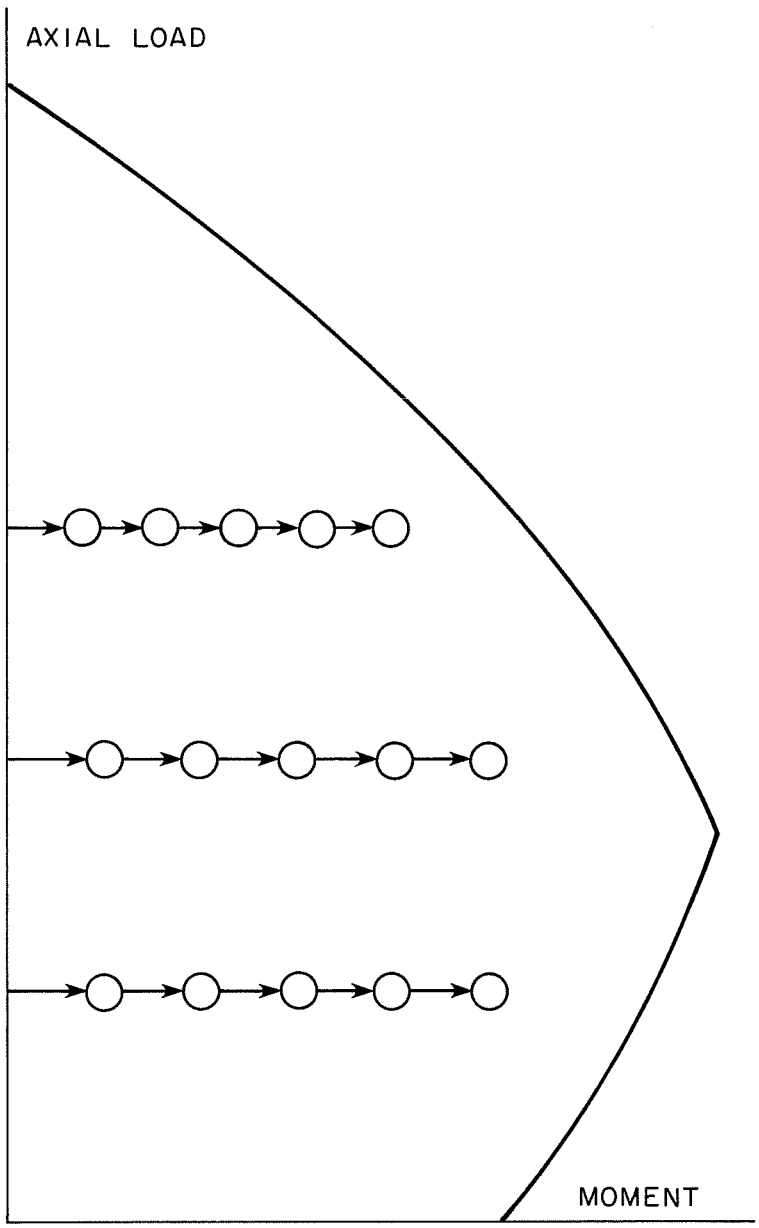

Fig. 3.19 Simplified uniaxial bending case to illustrate method of loading

3.6.3 Alignment. The alignment of the specimen and the loading system was thoroughly checked with a transit. Several adjustments had to be made before the alignment was acceptable. Then an axial load was applied and deflections were recorded to see if the pier was deflecting laterally. The actual amount of load eccentricity was calculated and components were realigned until an acceptable lateral deflection was recorded. Similarly, the actual eccentricities of the moment-producing ram rams were checked to guarantee that they were properly positioned.

3.7 Data Acquisition

All strain gage and potentiometer readings were recorded onto magnetic tape by a VIDAR data acquisition system. This system also provided a means of recording a large number of readings in a small amount of time. Demec readings were hand-recorded.

The predetermined ram loads were applied using ram pressure as the basic method of control. These pressures were indicated by manually read strain readings from pressure transducers. The desired ram pressures were maintained until all other readings were recorded.

3.8 Data Reduction

There were primarily three sets of data to be reduced for each test. These included the load data, the curvature data, and the data to check the validity of the plane sections assumption.

3.8.1 Loads. The actual ram loads on the specimens were known but any variation in alignment had to be checked. Before loading, the axial load alignment was checked and realigned to an acceptable level. However, any residual variation was corrected in the data reduction. This was accomplished by first determining the curvature at the midsection. Then, based on this curvature, the corresponding moment at the midsection was determined with the aid of program BIMPHI. From this moment the apparent accidental eccentricity of the axial load was found. All subsequent moment values included this correction. The average eccentricity

of the concentric ram from the strong axis was 0.305 in. with a standard deviation of 0.200 in. The average weak axis eccentricity of the concentric ram was 0.157 in. with a standard deviation of 0.090 in.

3.8.2 Curvatures. All of the initial data readings recorded by the VIDAR data acquisition system were reduced on a Data General Nova computer. Standard computer programs written for the VIDAR system adjusted for gage factors and voltage variations. Further data reduction was done on The University of Texas at Austin CDC Cyber 170/750 computer.

The strain readings were first investigated at various loads to see which gage combination produced a plane that best represented the average plane of all the strain readings. The method used for this determination is discussed in Section 3.8.3. After the most representative combinations were determined, curvatures were found from the slopes of these planes. Additionally, the curvatures were determined from the curvature meters. Therefore, the curvature measurements are presented for both the curvature meter readings as well as the strain readings. In the tests of the two and three cell pier specimens, however, the curvatures were determined from both the curvature meters and the Demec strain readings. The curvatures determined from the Demec strain readings do not give local strains but give average strains over a realistic gage length (8 in. in this case). In addition, they are not influenced by the electrical drift which is inevitable when potentiometers are used. To calculate the curvatures for these specimens the Demec readings obtained at the four corner stations points on the wider sides were used.

3.8.3 Plane Sections Check. For the solid and single cell pier specimens, the strain readings were used to check the validity of the assumption that plane sections before bending remain plane after bending. The most consistently representative combination of three gages was selected to define the most representative plane. The deviation of all other gage readings from this plane was computed. Examples of these comparisons are seen in Figs. 4.1 and 4.2. The deviations from the

computed planar strain values were used to judge the adequacy of the plane sections assumption. The slopes of the most representative planes determined the curvatures of the section as measured by the strain gages. For the two cell and three cell pier specimens, both the Demec readings and the strain readings were used to check the Bernoulli's plane section assumption. The plane of strains in a section was determined only by using the Demec readings, because quite accurate planes of strains could be determined without any large deviations of the measured strains from the determined plane as shown in Figs. 4.3 and 4.4. Then the strains obtained from strain gages were compared to see the overall distribution of the strains.

CHAPTER 4

TEST RESULTS

4.1 Verification of Plane Sections Assumption

One of the principal assumptions made in the fiber model, on which BIMPHI, PIER, and FPIER are based, is that plane sections before bending remain plane after bending. This assumption has been widely verified for solid sections. Determination of the validity of this assumption for hollow sections was a major purpose of this study. Mavichak [13] found this assumption acceptable for biaxial bending of oval and rectangular bridge piers. He found that over a 30 in. gage length some strains deviated from being in a plane by 10%, with the average deviation being 3%. Over a 6 in. gage length he found greater deviations of up to 54%, with an approximate average deviation of 9%. The plane sections check presented for the first two specimens in this study were based on a 0.32 in. strain gage length mounted on reinforcement at the midheight cross section; therefore, deviations greater than 10% might be expected. The other two specimens were equipped with 8 in. gage length mechanical gaging points and showed much better agreement where longer gage lengths were used.

The purpose of this section is to compare the planes of strains for the solid and hollow piers under various levels of biaxial loading.

First, a comparison will be made of the solid section and the single cell section. Both of these relied on the short length electrical strain gages. For the solid section, the most representative planes of strains are compared to the actual strain readings in Fig. 4.1. The heavy bars represent differences between individual gage readings and the planar value at that point. Comparatively, planes of strains for the

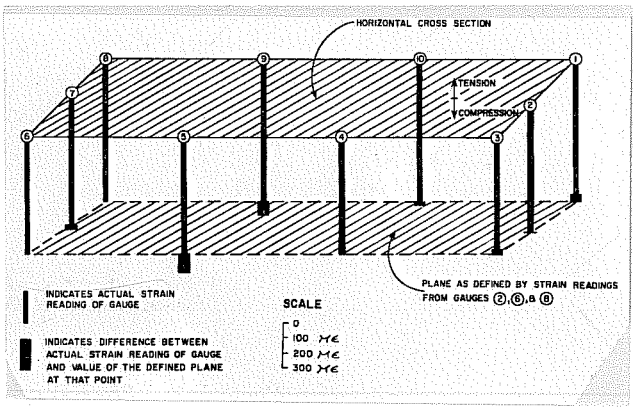

(a) At initial load stage

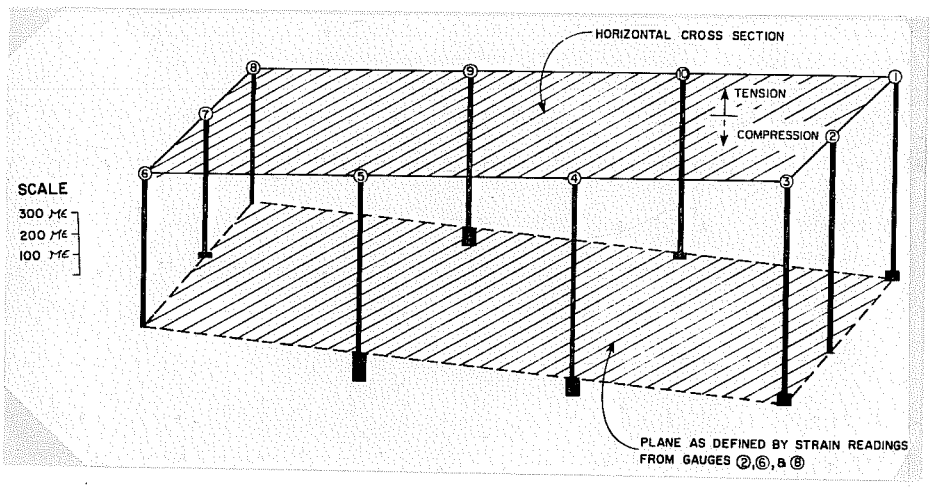

(b) At intermediate load stage

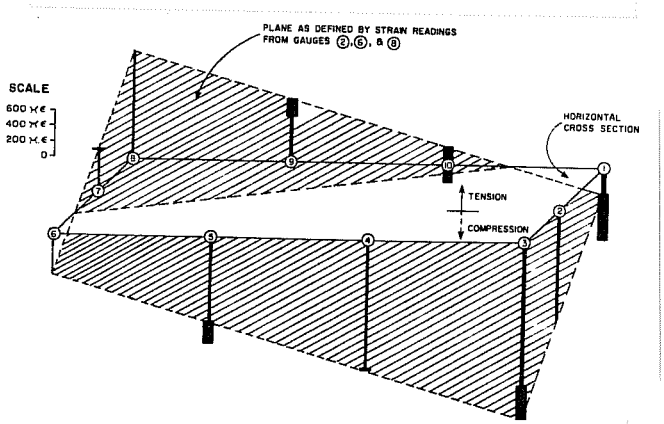

(c) At final load stage

Fig. 4.1 Plane of strains compared to actual strain readings for the solid pier

hollow section are shown in Fig. 4.2. The single cell section has somewhat more variation from the plane than does the solid section. However, there are more gages in the single cell section, so the number of significant variations cannot be directly compared. Only for the final load stage shown in Fig. 4.2(c) does the single cell section have large abnormal variations and that is only for two gages (No. 10 and 12).

Overall, the single cell and solid sections seem to exhibit about the same levels of deviation from the planes of strains for various load stages. For the solid section, the average deviation of all the values, shown in Fig. 4.1(a-c), was 5.2%. The average deviation of all the values for the single cell section, shown in Fig. 4.2(a-c), was 3.8%. The greatest deviations occurred at the ultimate load stages where the average deviation of all the gages was 10.4% in the solid section and 12.9% in the single cell section. Considering that an extremely short gage length was used (3/8 in. strain gages at a specified section), the values shown in Figs. 4.1 and 4.2 seem to have about the same scatter as experienced by Mavichak.

Interpretation of the data from the first two pier specimens indicated that the experimental verification of the assumption of planar sections needed further refinement. In the solid and single cell pier tests the accuracy of the plane sections assumption was found to be similar to that found by Mavichak. The tests did show the apparent deviation of the strains from the most representative plane to be approximately the same for the solid and single cell sections. Therefore, it could be concluded that if the plane sections assumption is valid for solid sections then it is also a valid assumption to use in predicting the behavior of hollow sections under biaxial bending.

To completely validate the assumption, the longer gage length Demec gage points were also used on the next two specimens. It was hoped that the use of longer averaging gage lengths would reduce scatter. For the two cell and three cell pier specimens, the most representative

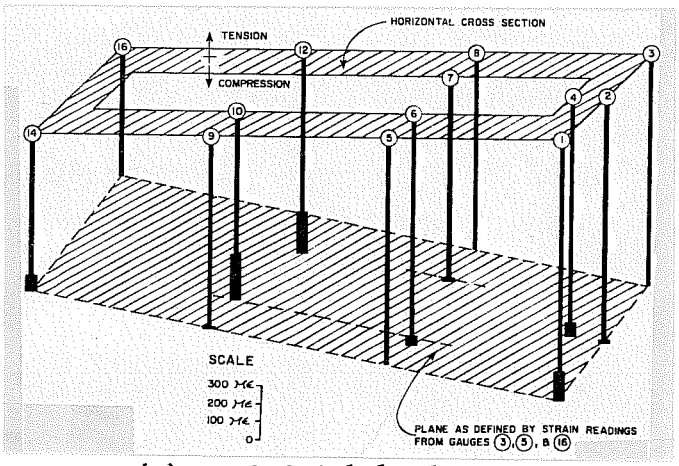

(a) At initial load stage

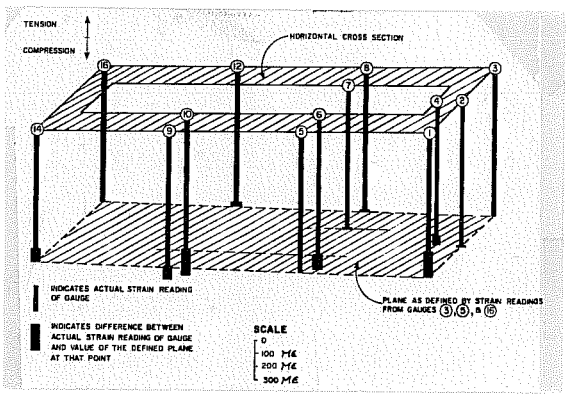

(b) At intermediate load stage

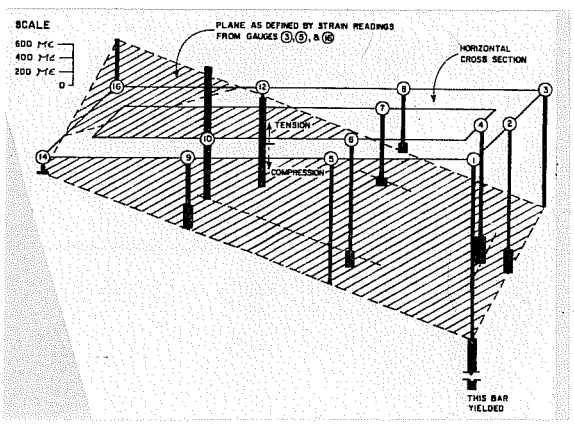

(c) At final load stage

Fig. 4.2 Plane of strains compared to actual strain readings for the single cell pier

planes of strains were determined using the Demec strain readings. All Demec gage points were on the exterior surfaces. In the presentation of data for these two specimens, first the agreement between the external gages and the averaged plane will be illustrated. Then the readings of the individual 3/8 in. electric strain gages mounted on the reinforcement will be compared to the planar profiles.

The planes of strains were determined by using Demec readings as described in Section 3.8.3. The planes of strains are shown in Fig. 4.3 for the two cell section and in Fig. 4.4 for the three cell section.

For the two cell section, the first two loading modes and the last or failure loading mode were chosen to check the plane section assumption. Figure 4.3(a) shows results for the first loading mode which had uniaxial bending around the strong axis. The magnitude of bending moment applied is about 73% of the calculated ultimate bending moment. At this loading stage, substantial cracking developed on the tension side of the specimen. General agreement with planar behavior is extremely good with only small variations at the two corner points on the tension face.

Figure 4.3(b) shows the result for uniaxial bending about the weak axis. The bending moment applied is about 70% of the calculated ultimate bending moment. At this loading stage, new cracks developed on the tension side of the specimen. Except for final loading, little additional cracking occurred. Again, in this case the strains at each point are in a plane excluding one corner point on the tension face.

Figures 4.3(c), (d), and (e) show the results for the final biaxial loading case where the specimen was taken to failure. These figures are shown in ascending order of loading stage. The axial force applied was 40% of the concentric axial strength of the specimen. Bending moments were applied about both axes and the ratio of the bending moment around the strong axis to the bending moment around the weak axis was kept constant at 3. In Figs. 4.3(c), (d), and (e), the levels of bending

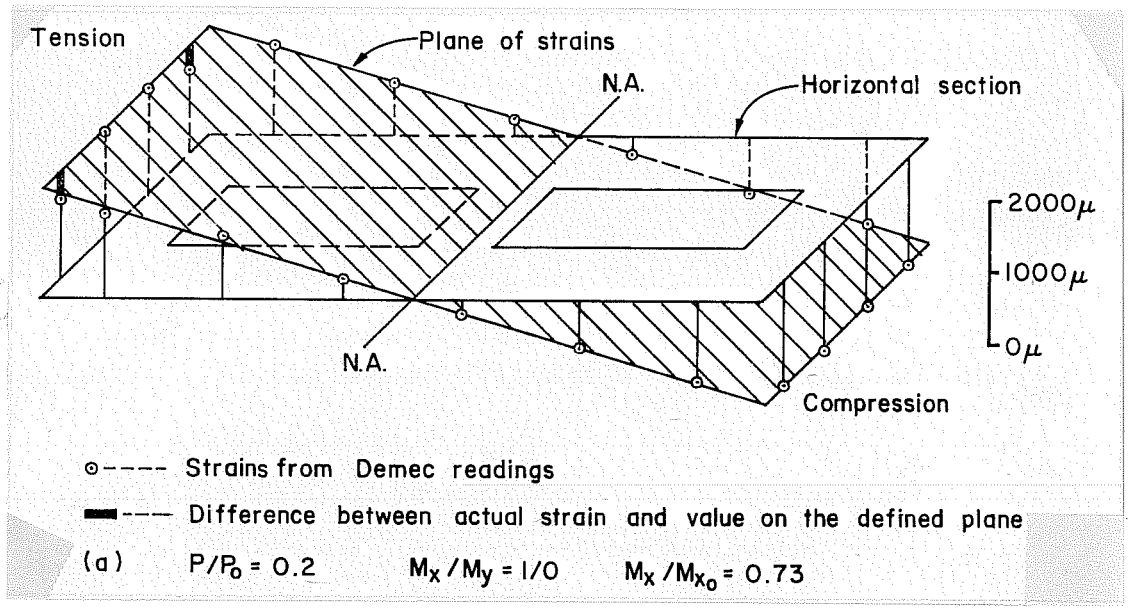

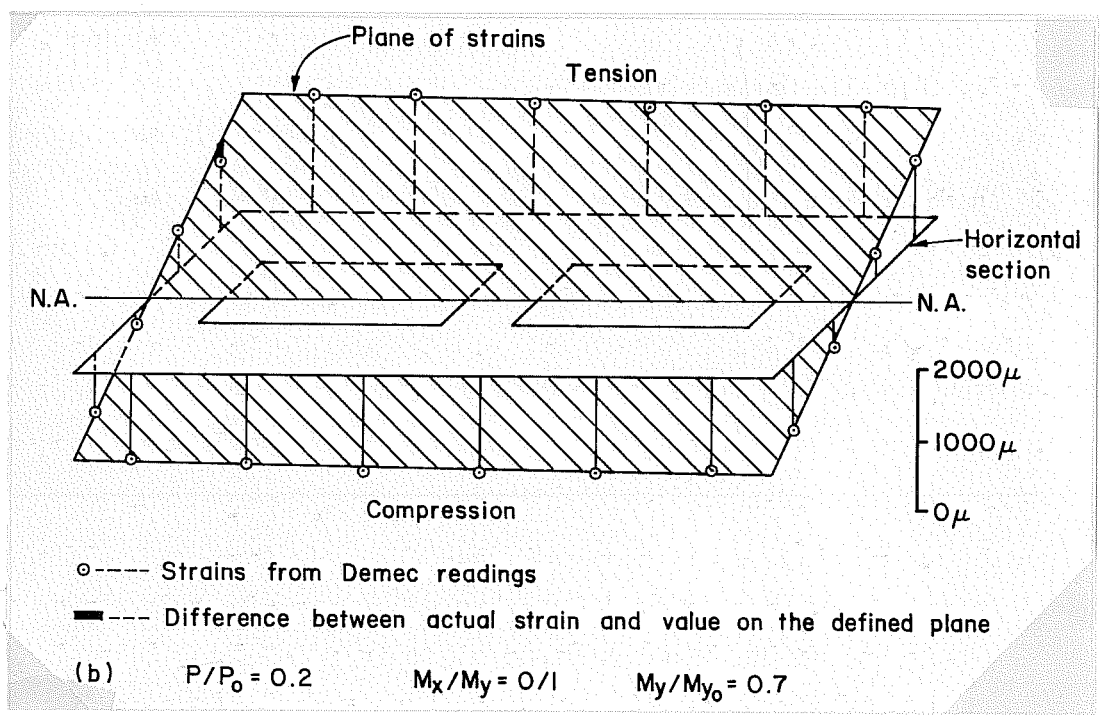

Fig. 4.3 Plane of strains from Demec readings (two cell pier)

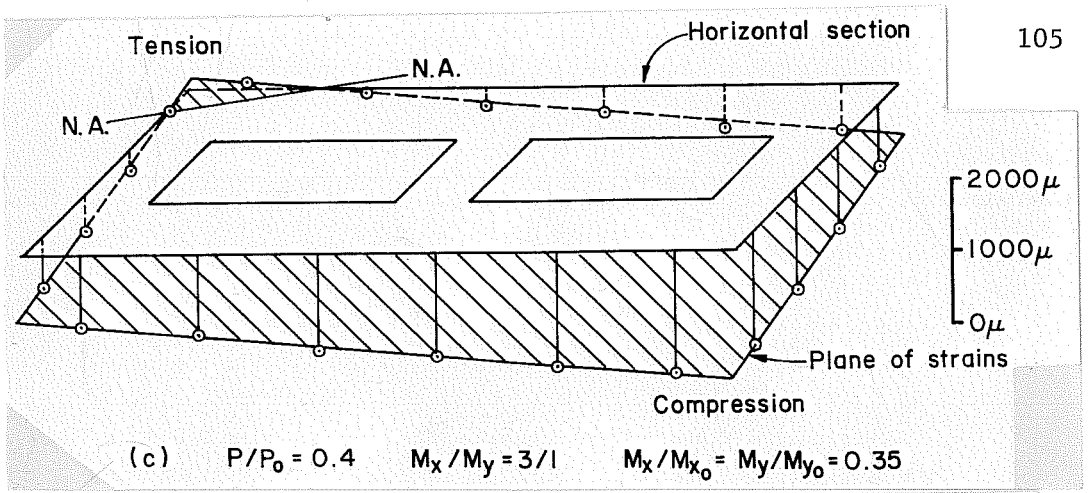

(c) $P/P_o = 0.4$ $M_x/M_y = 3/1$ $M_x/M_{x_o} = M_y/M_{y_o} = 0.35$

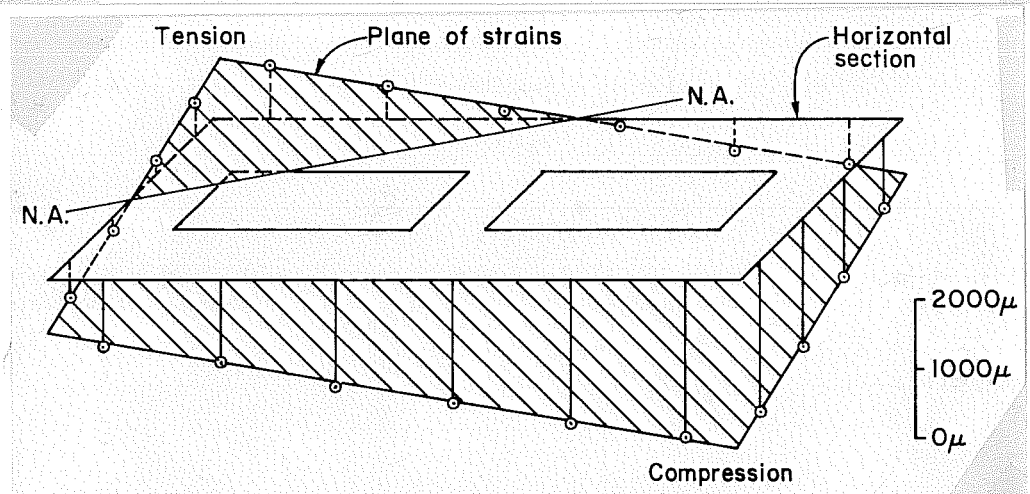

(d) $P/P_o = 0.4$ $M_x/M_y = 3/1$ $M_x/M_{x_o} = M_y/M_{y_o} = 0.69$

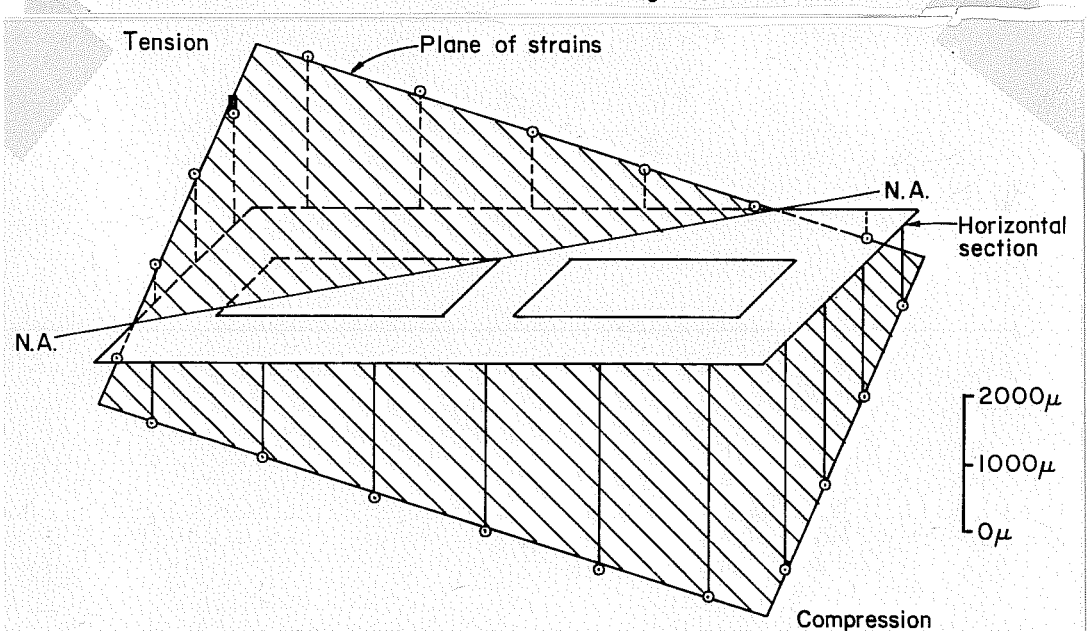

(e) $P/P_o = 0.4$ $M_x/M_y = 3/1$ $M_x/M_{x_o} = M_y/M_{y_o} = 0.97$

⊙---- Strains from Demec readings

▬--- Difference between actual strain and value on the defined plane

Fig. 4.3 (Continued)

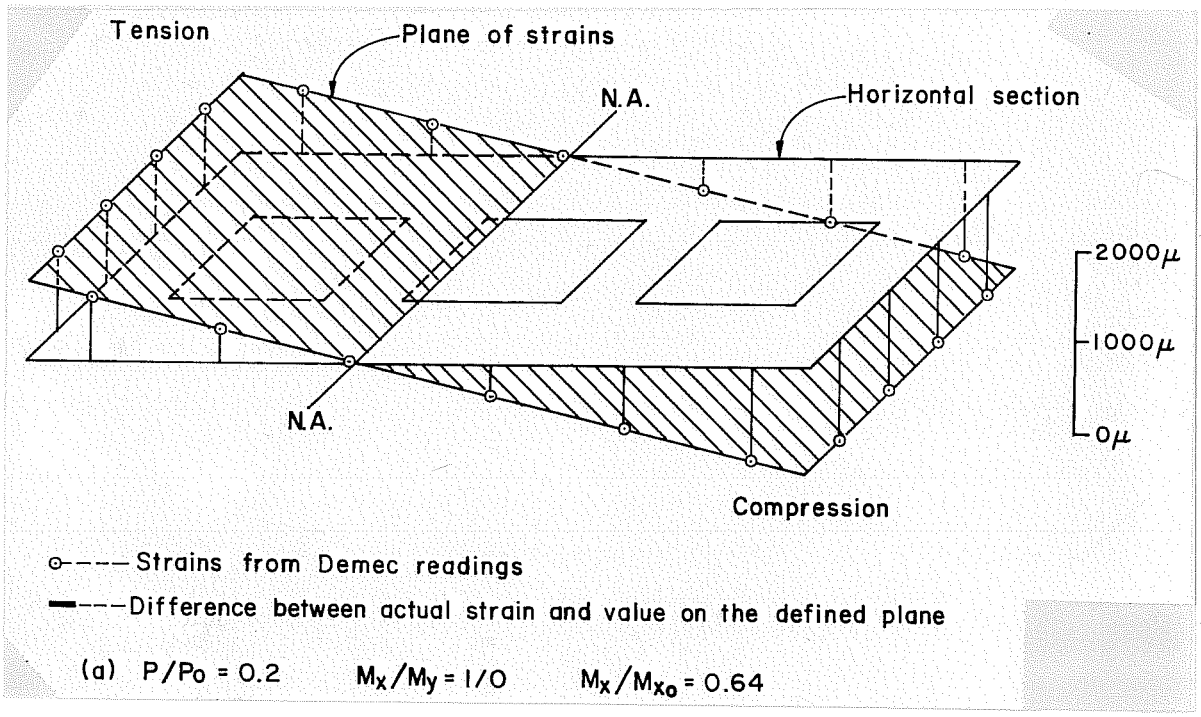

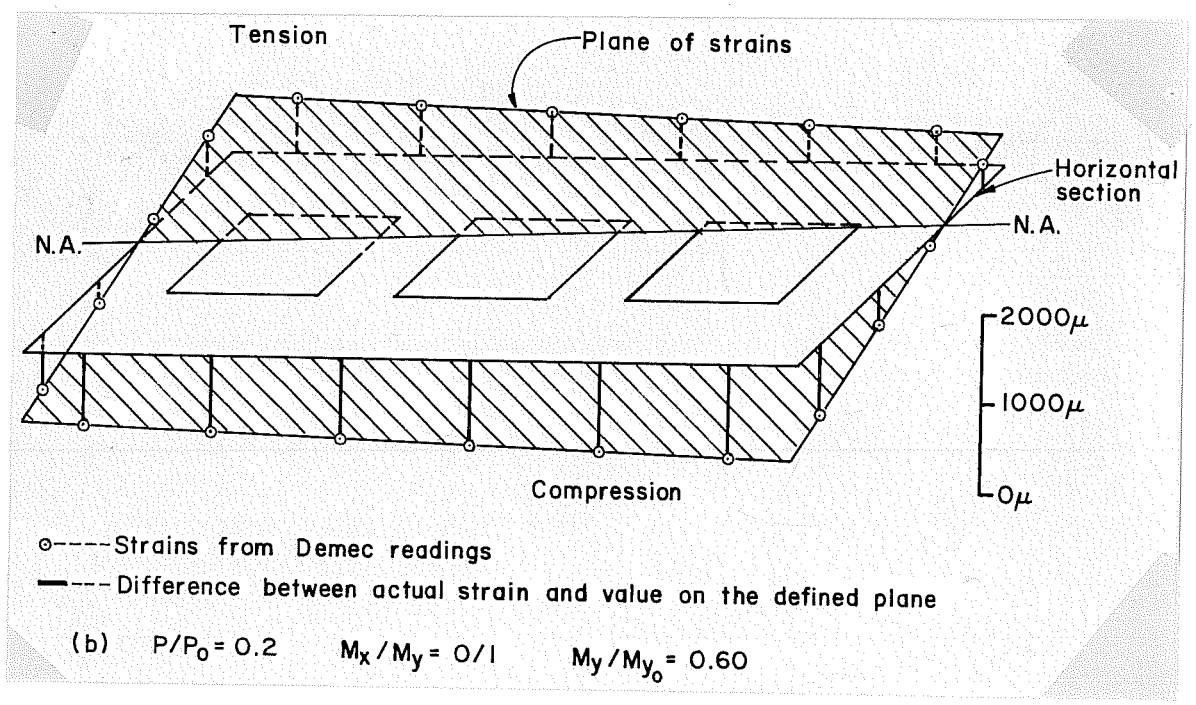

Fig. 4.4 Plane of strains from Demec readings (three cell pier)

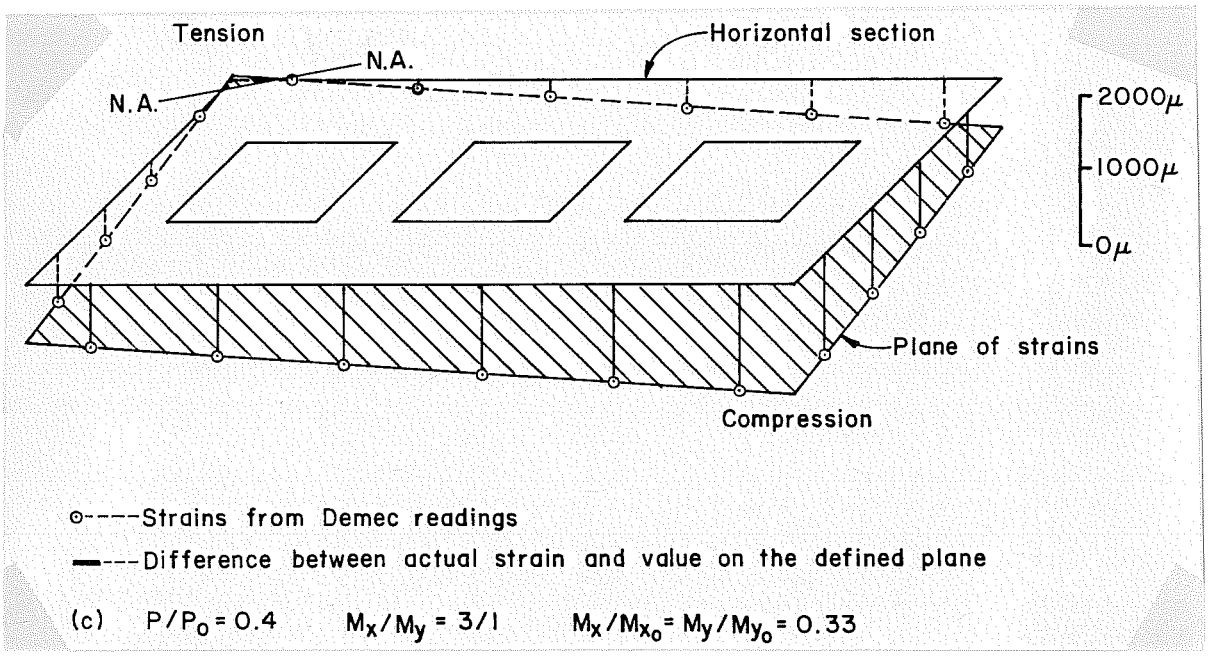

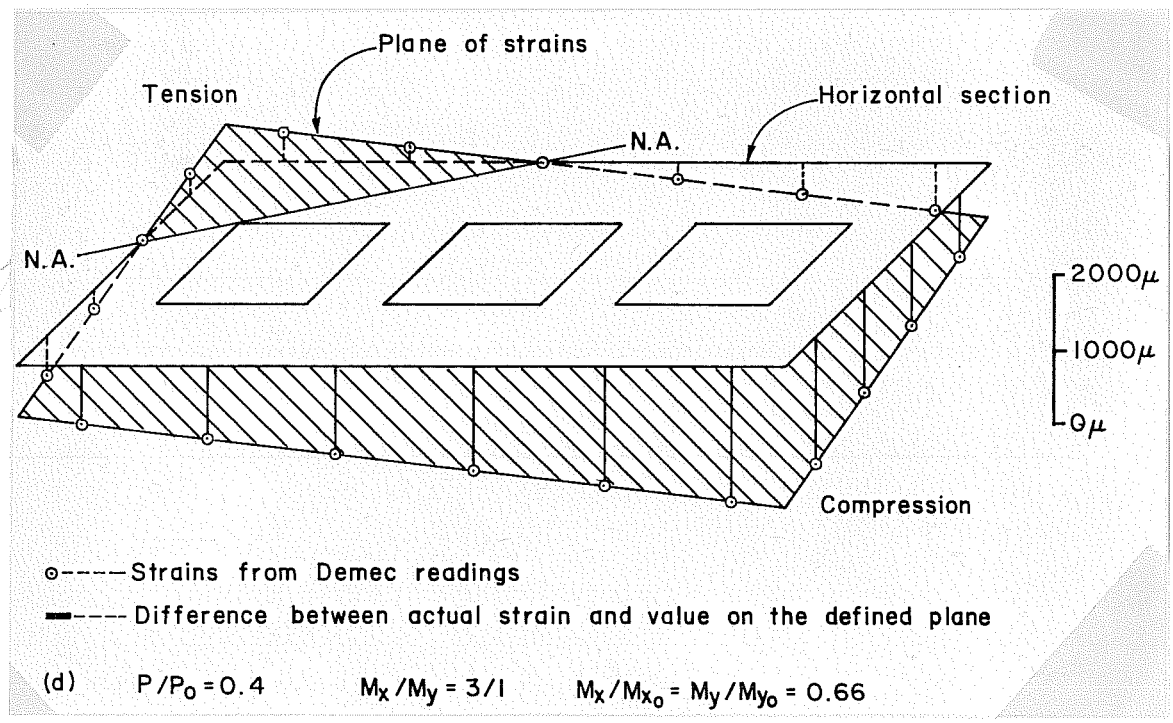

Fig. 4.4 (Continued)

moments to the ultimate bending moments are about 35%, 69%, and 97%, respectively. At the loading stage following the one shown in Fig. 4.3(e), the specimen suffered a compression failure at the highest stressed corner of the compression side. As shown in these figures, the plane of strains determined from Demec readings gives excellent results with all external gages for the ultimate biaxial loading stage. The plane section assumption is completely valid.

For the three call pier, the same kind of results are shown in Fig. 4.4. Figure 4.4(a) shows the result for uniaxial bending around the strong axis. In this case, the bending moment was about 64% of the ultimate bending capacity of the pier and no major cracking was observed. There is no noticeable variation of strains from the plane of strains. Figure 4.4(b) shows the result for uniaxial bending about the weak axis. The maximum bending moment applied in this case was about 60% of the ultimate bending moment. No major cracking was observed. The variation of strains from the plane of strains was very small. In this case, however, a small accidental eccentricity of loading around the strong axis can be seen. Figures 4.4(c) and (d) show the results for a biaxial loading combination. The ratio of the bending moment around the strong axis to the bending moment around the weak axis is 3. No major cracking occurred in this case since the specimen is largely in compression. Figure 4.4(c) shows the plane of strains when the level of bending moments applied was about 33% of the ultimate bending moments. In Fig. 4.4(d), the level has been increased to 66% of the ultimate loading level. These figures also clearly show that the plane section assumption is completely valid in the test of the three cell pier. Unfortunately, the Demec gage was not available at the time of the ultimate testing of this specimen. Figures 4.3 and 4.4 clearly show that the assumption of a plane section remaining plane is valid for hollow sections under uniaxial and biaxial bending with axial compression. They indicate that this assumption can be used with assurance in the computer routines.

Figures 4.5 and 4.6 show the comparison between the plane of strains determined from the external Demec gages in Figs. 4.3 and 4.4 and the short gage length strains measured on the embedded longitudinal bars. Readings are for the gages at the midheight of the pier specimens. Each figure corresponds to a loading stage in Figs. 4.3 and 4.4. These figures clearly indicate that while external long gage lengths indicated average strains in virtual complete agreement with the planar strain assumption, individual local gages frequently vary from the plane. This may be due to localized cracking, local transverse bending, or other local effects. The variation of strains seems to be almost of the same order as that found in the cases of the solid and single cell pier specimens. The analysis programs further integrate local curvatures so that there is continued smoothing and averaging. Thus it is concluded that the plane strain assumption is valid for use with P-M-ϕ subroutines. Since the behavior of all four specimens was similar when similar measurements were made, it is felt that the assumption is valid for all piers of this general configuration.

4.2 Solid Pier Curvatures

The primary goal of the physical testing phase was to compare the P-M-ϕ behavior of the model piers with the values generated by program BIMPHI. Therefore, obtaining the P-M-ϕ behavior of the four piers and comparing the measured behavior with the analytical program predictions was a most important task. The utilization of subprogram BIMPHI in program PIER is such that the P-M-ϕ relationship predictions must be fairly accurate if program PIER is to be accurate. As long as the P-M-ϕ prediction is accurate PIER should give good results even if the plane sections assumption is not rigorously correct.

Figures 4.7 through 4.15 compare the experimental axial load-moment-curvature observations (symbols indicate data measured) with the analytically calculated (BIMPHI) relationships shown by the solid lines. These figures show the behavior of the solid pier for various load

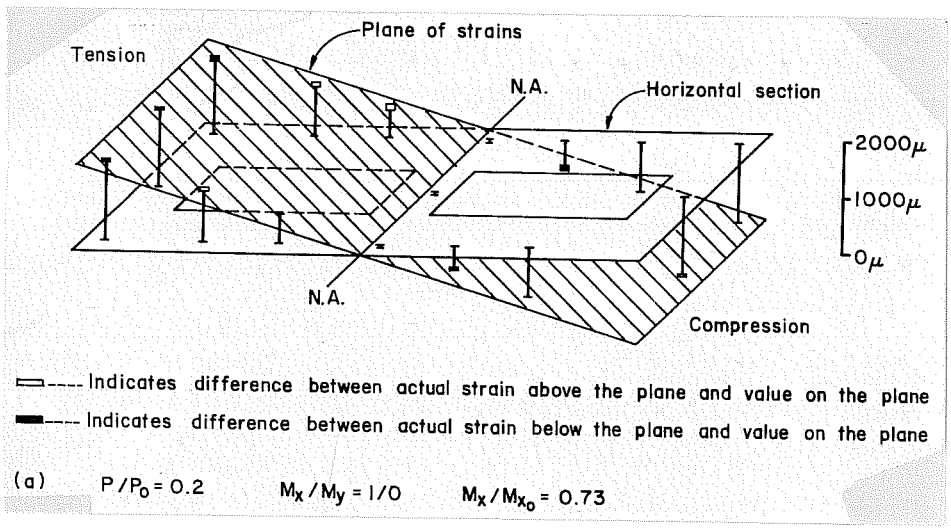

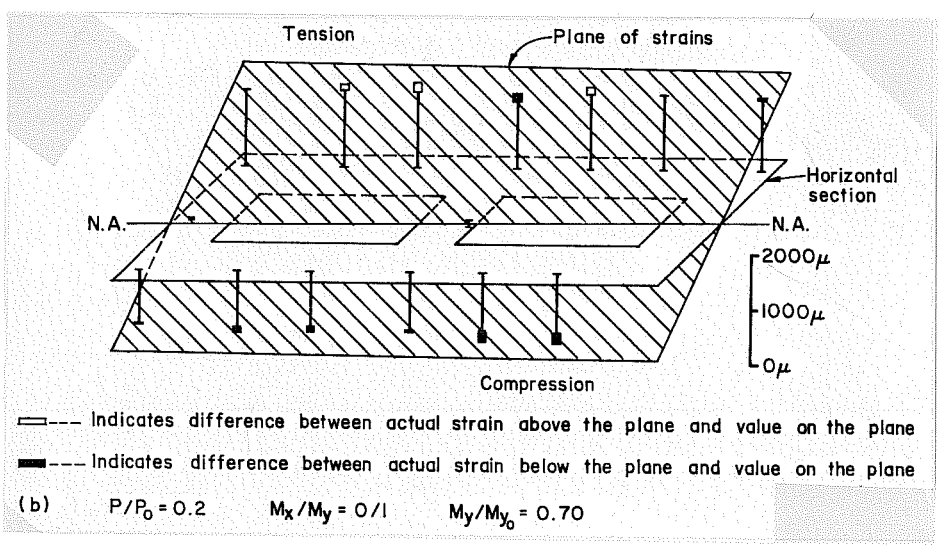

Fig. 4.5 Comparison between strain gages and the defined plane of strains for two cell piers

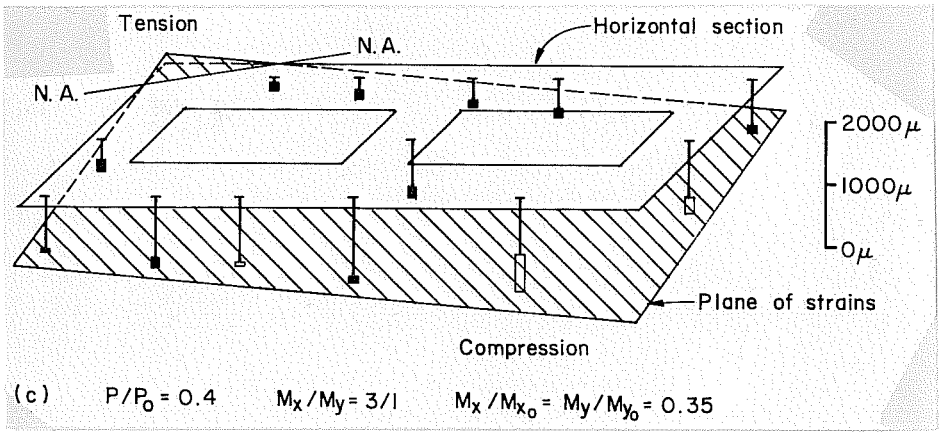

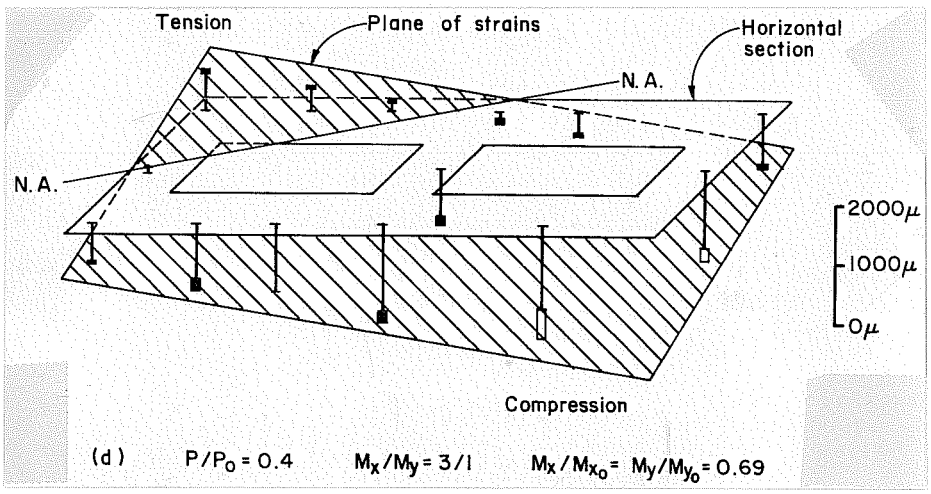

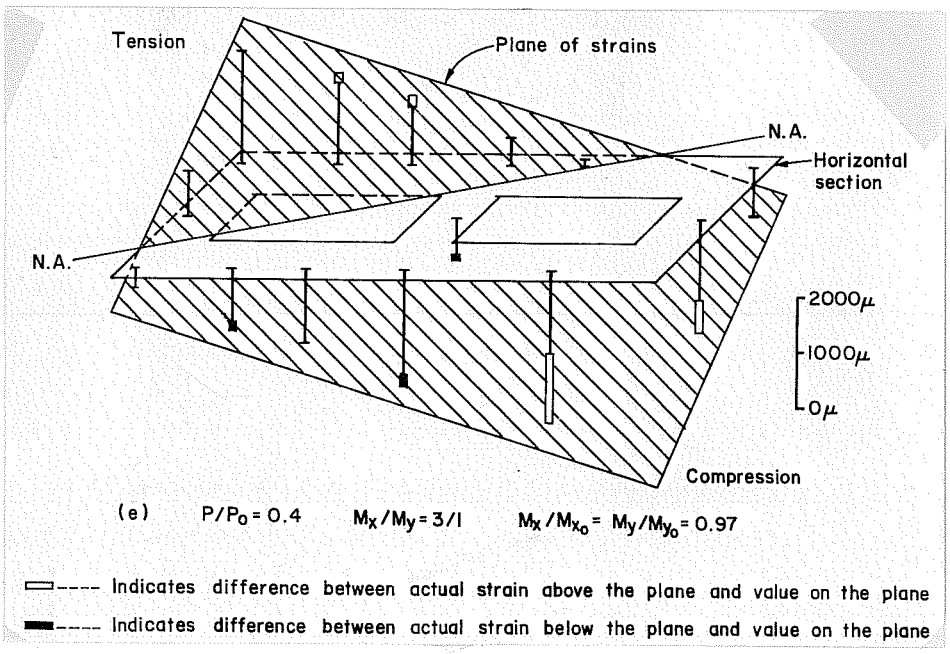

Fig. 4.5 (Continued)

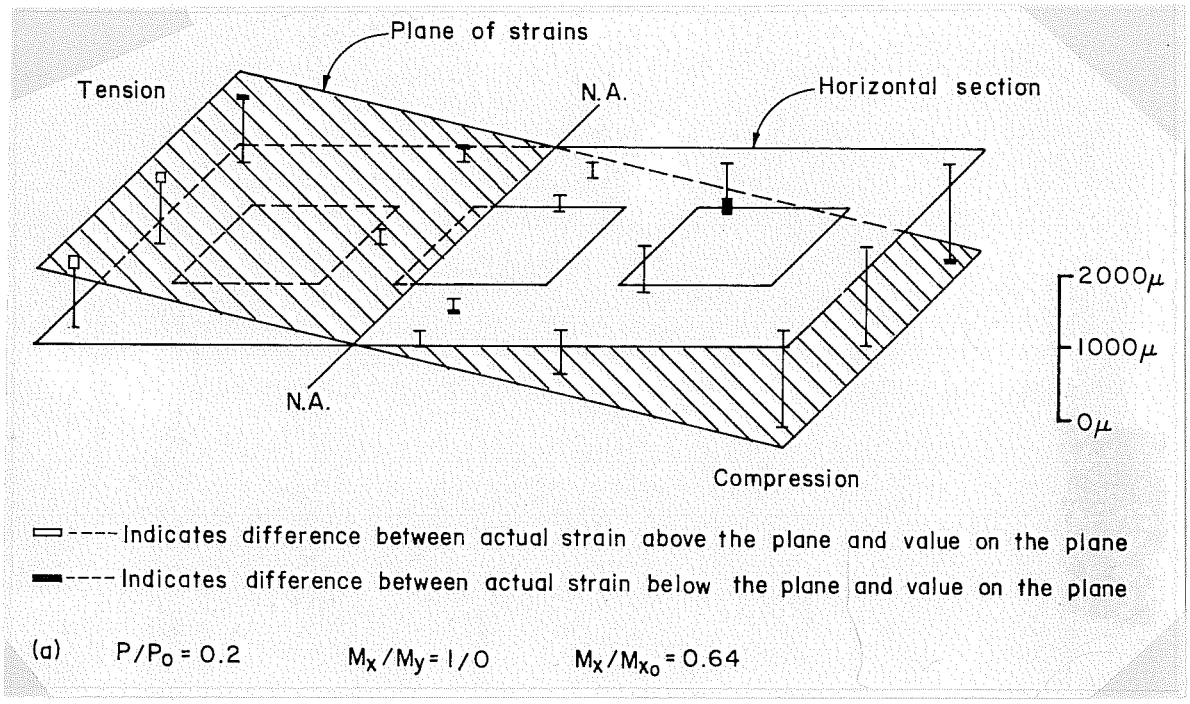

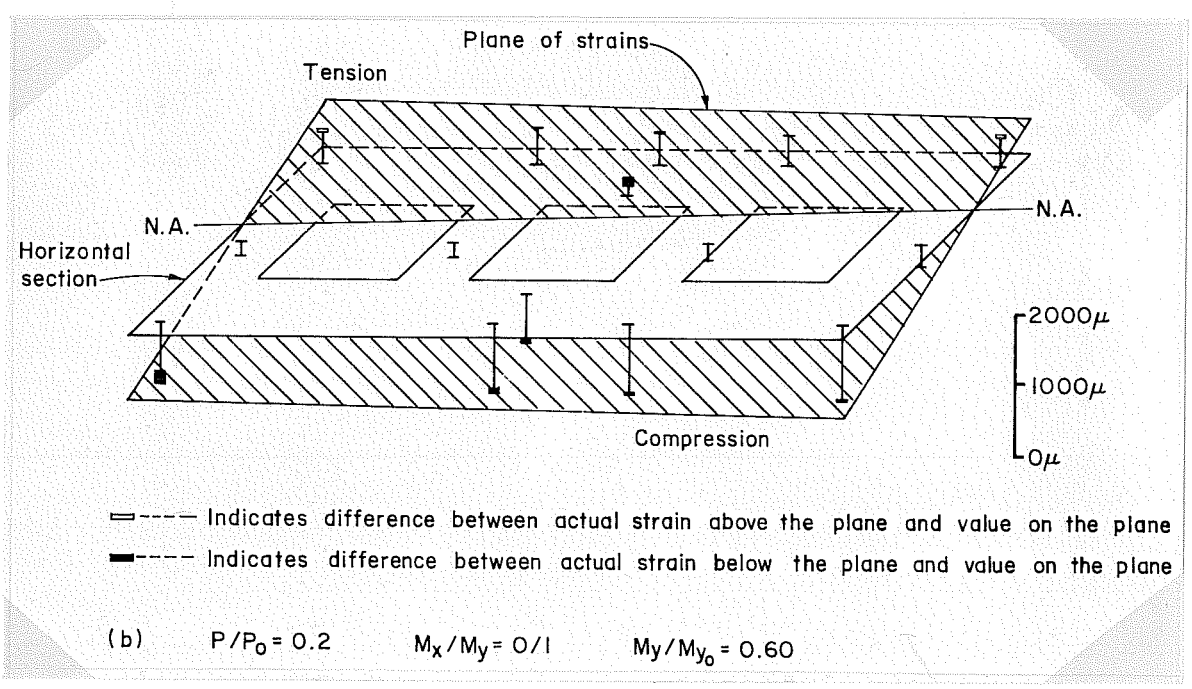

Fig. 4.6 Comparison between strain gages and the defined plane of strains for three cell piers

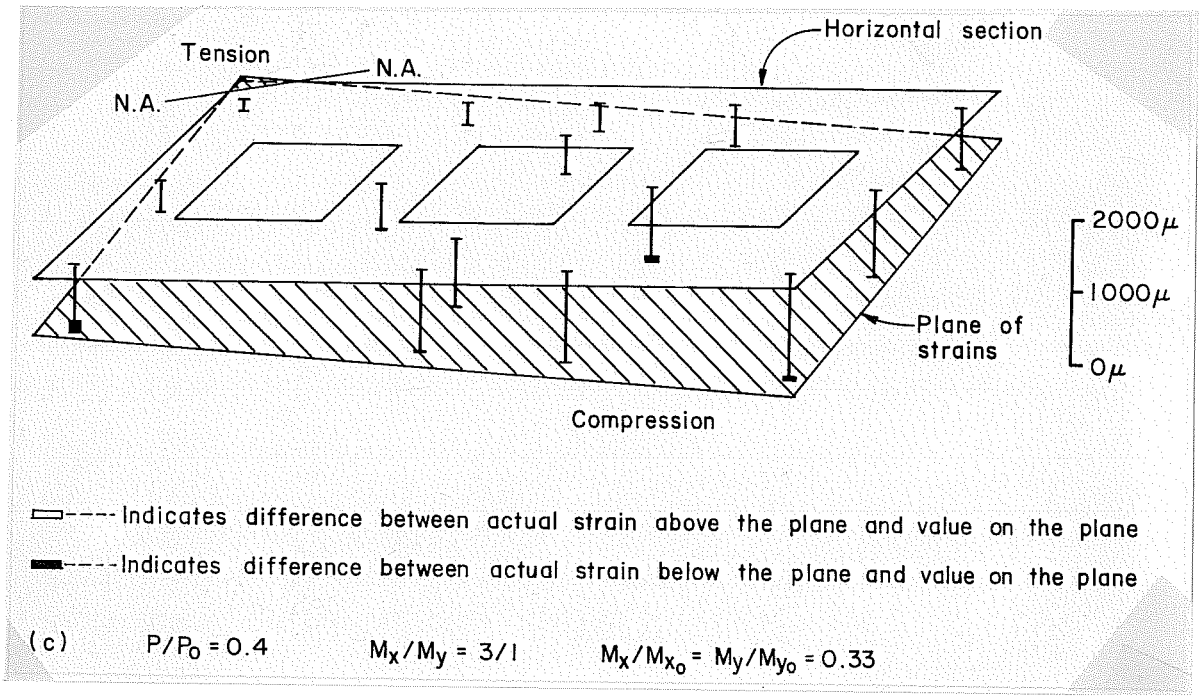

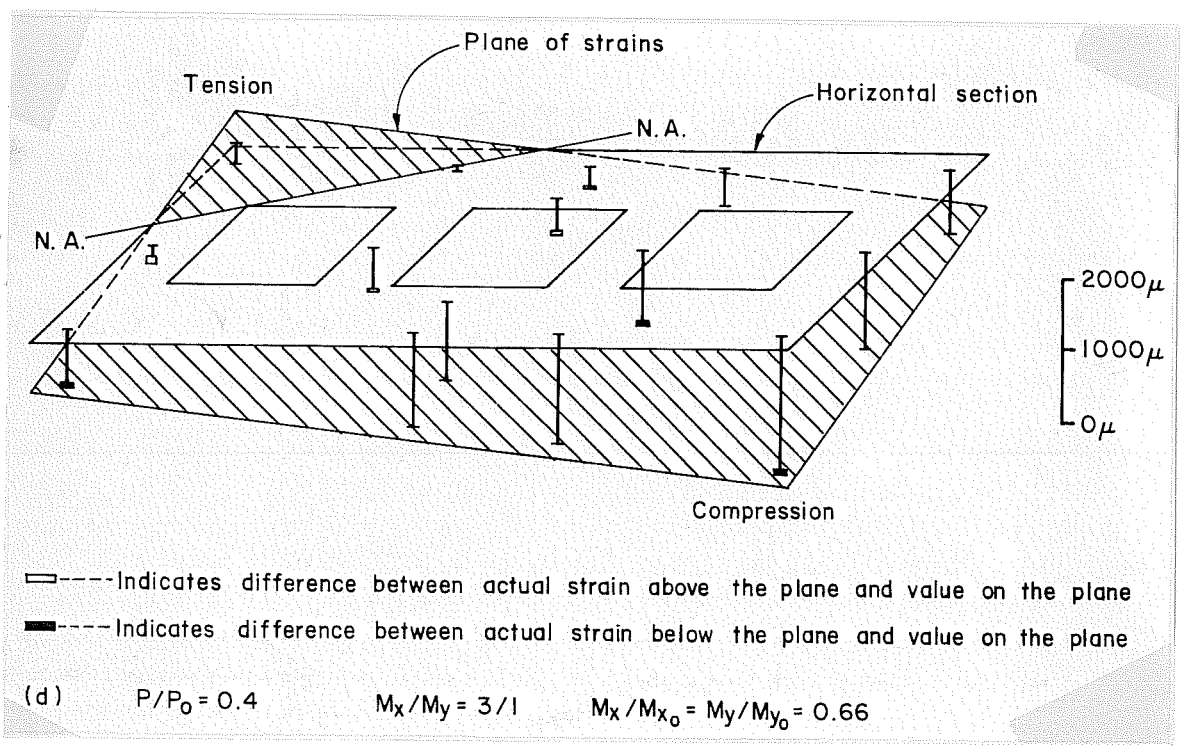

Fig. 4.6 (Continued)

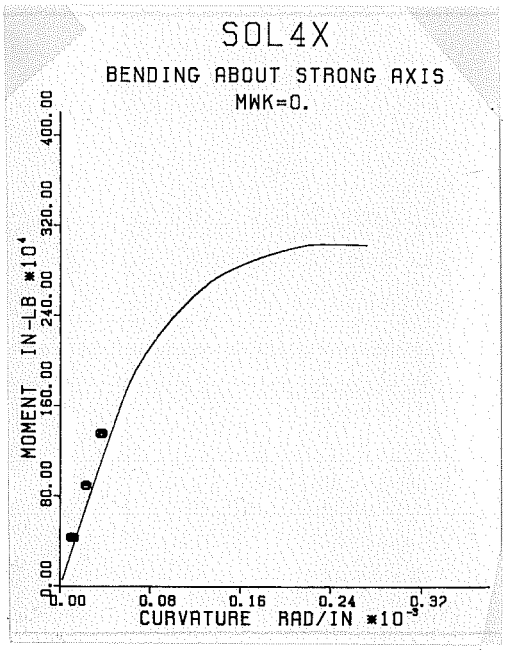

Fig. 4.7 P-M-ϕ behavior of solid pier for $P = 0.4P_o$ and $M_{WK} = 0$

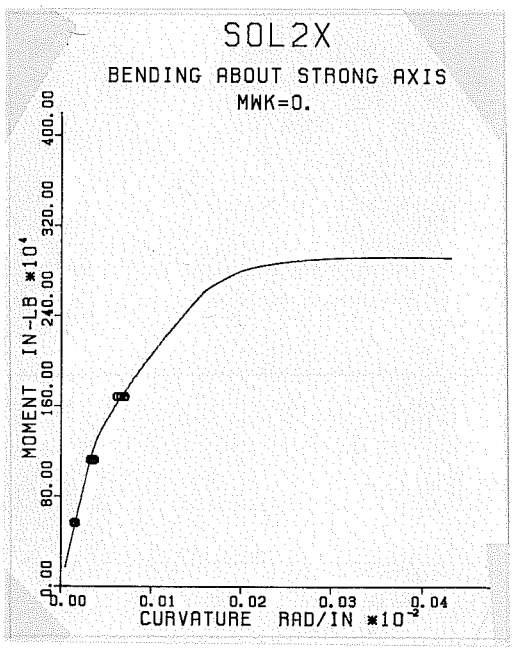

Fig. 4.8 P-M-ϕ behavior of solid pier for $P = 0.2P_o$ and $M_{WK} = 0$

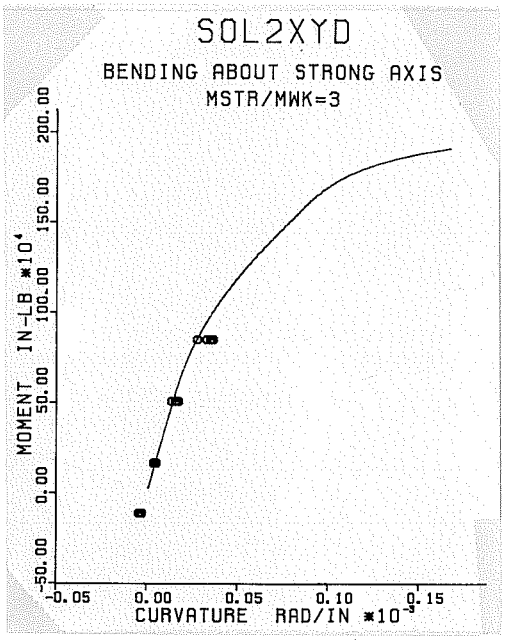

Fig. 4.9 P-M-ϕ behavior of solid pier for $P = 0.2P_o$ and $M_{STR}/M_{WK} = 3$

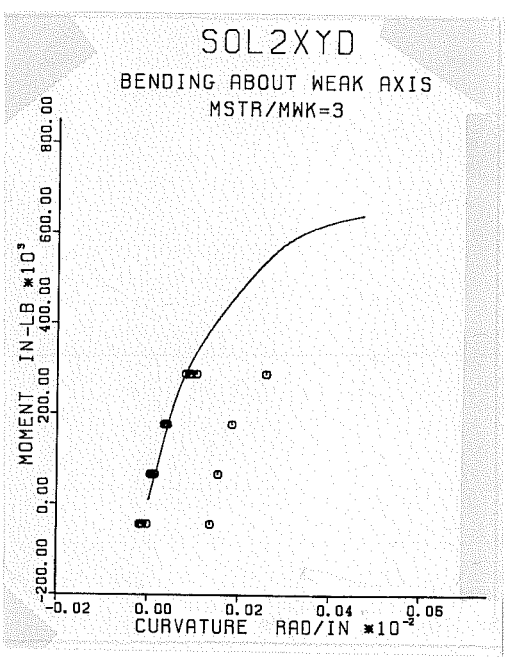

Fig. 4.10 P-M-ϕ behavior of solid pier for $P = 0.2P_o$ and $M_{STR}/M_{WK} = 3$

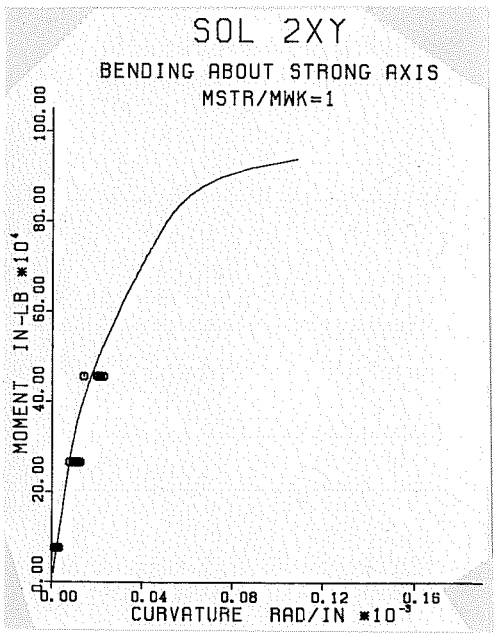

Fig. 4.11 P-M-ϕ behavior of solid pier for $P = 0.2P_o$ and $M_{STR}/M_{WK} = 1$

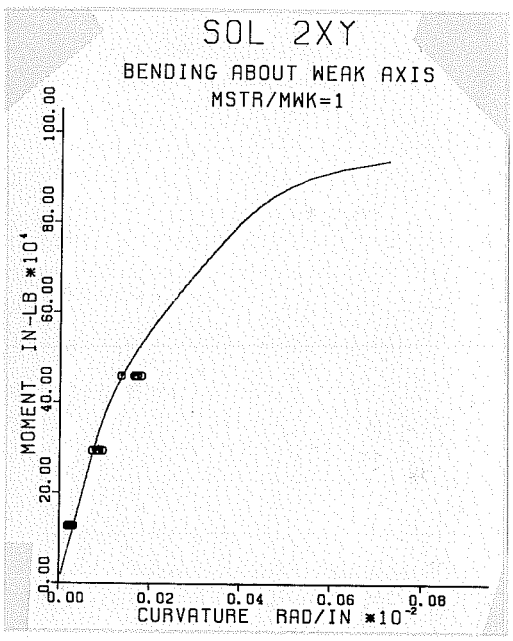

Fig. 4.12 P-M-ϕ behavior of solid pier for $P = 0.2P_o$ and $M_{STR}/M_{WK} = 1$

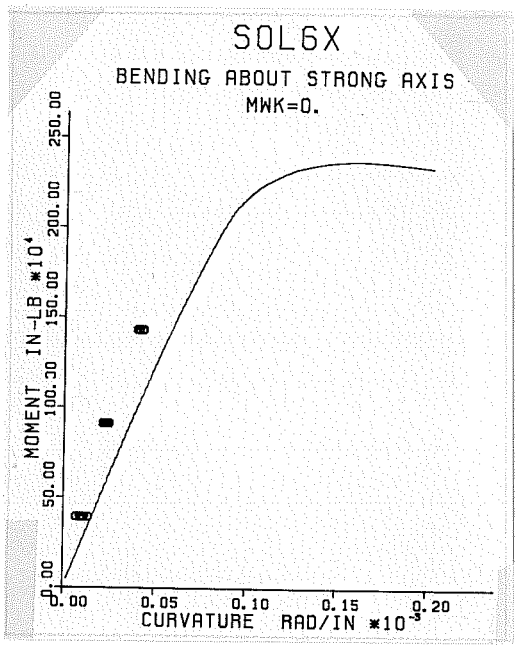

Fig. 4.13 P-M-ϕ behavior of solid pier for $P = 0.6P_o$ and $M_{WK} = 0$

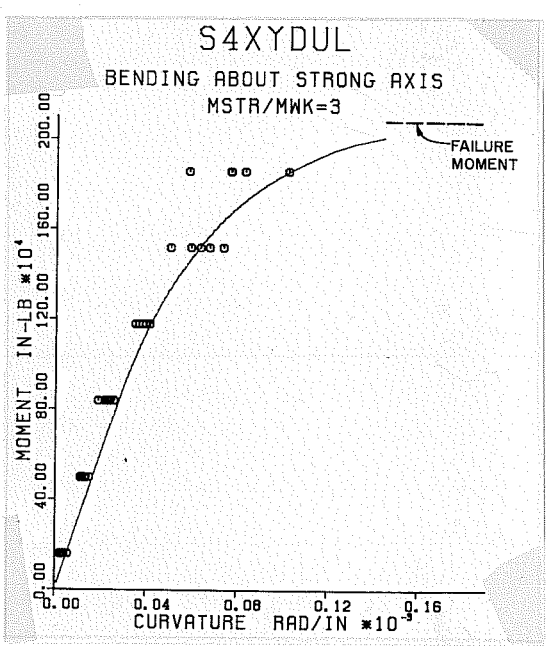

Fig. 4.14 P-M-ϕ behavior of solid pier for $P = 0.4P_o$ and $M_{STR}/M_{WK} = 3$

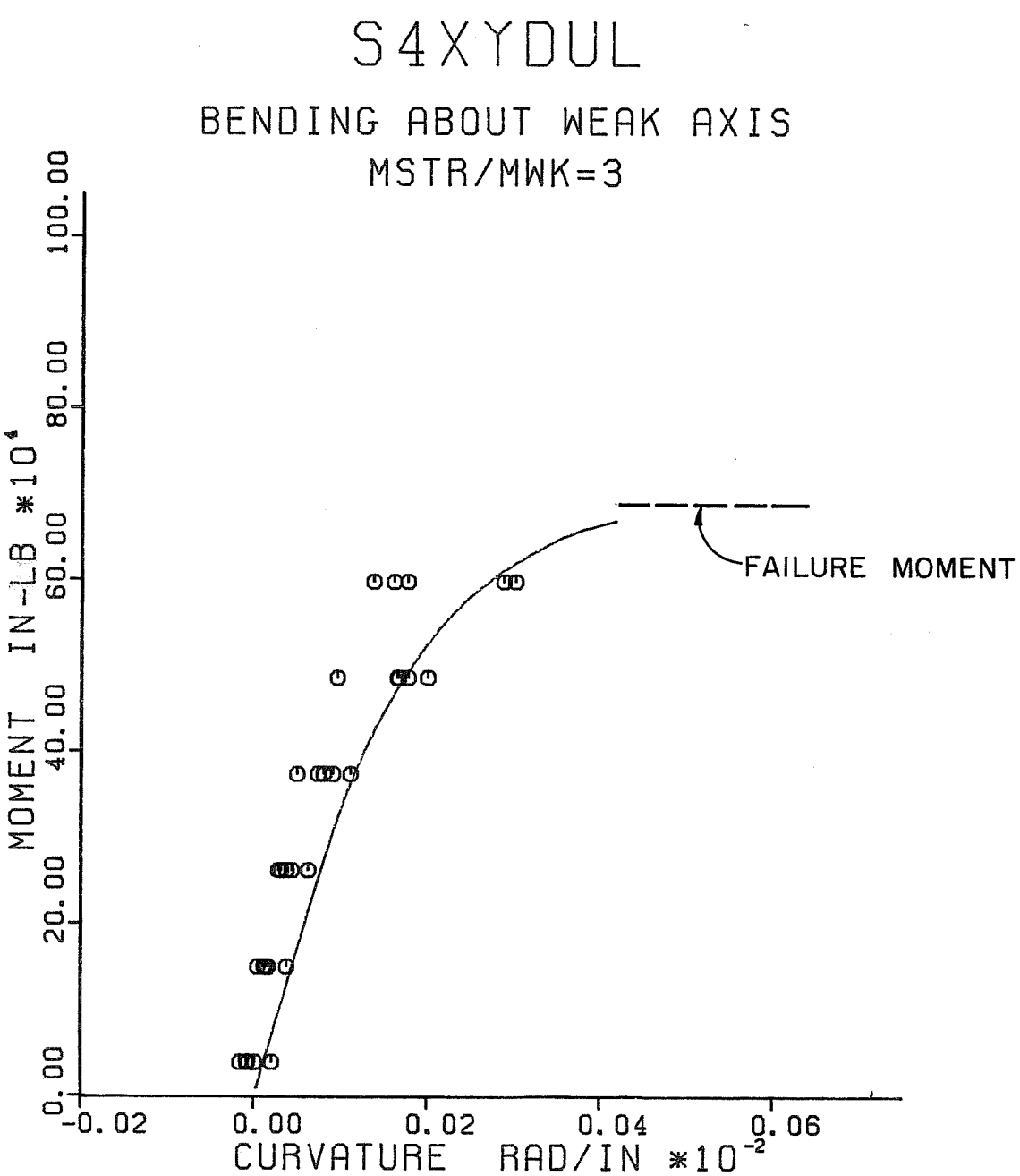

Fig. 4.15 P-M-ϕ behavior of solid pier for P = $0.4P_o$ and M_{STR}/M_{WK} = 3

combinations. The order of the figures reflects the sequence of testing. Therefore, the section upon which the final loading was applied was somewhat degraded by widespread cracking from previous loadings. At each moment level there are five curvature station values. In general very good agreement is seen between the calculated and actual behavior. These comparisons will be discussed in Chapter 5.

Each pier was subjected to a wide variety of load levels and loading paths. The axial load levels applied included $0.2P_o$, $0.4P_o$, and $0.6P_o$ (where P_o is the concentric axial load capacity of the section). The calculated concentric axial load capacity was 821 kips for the solid section. The loading paths included uniaxial bending cases as well as cases where the biaxial bending moment ratios equaled 1 and 3. Many combinations of the various axial load levels and loading paths were applied with loading limited to about 67% of the ultimate. After these combinations were applied, an axial load of $0.4P_o$ and a ratio of strong to weak axis moments equal to 3 (diagonal loading) was reapplied and increased until failure occurred. As shown in Figs. 4.14 and 4.15 failure occurred during applications of a loading increment and before a new set of curvature data could be taken.

About half the curvature values were obtained from the curvature meter readings while the other half of the curvature values were computed from selected sets of electrical resistance strain gages which best represented the average plane of strains most consistently throughout all the load combinations. Since the selections were based upon the consistency of the set of gages for all the load cases, there were individual load cases where one set of gages may not have been the most representative. An example of such a case is shown in Fig. 4.10, where all the curvature values are in close agreement except for one at each moment level.

4.3 Single Cell Pier Curvatures

The observed and computed axial load-moment-curvature relationships for the single cell pier are shown in Figs. 4.16 through 4.24 for various

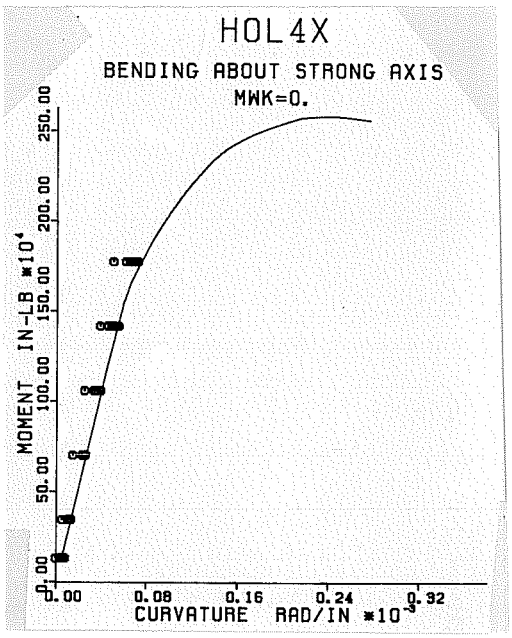

Fig. 4.16 P-M-ϕ behavior of single cell pier for $P = 0.4P_o$ and $M_{WK} = 0$

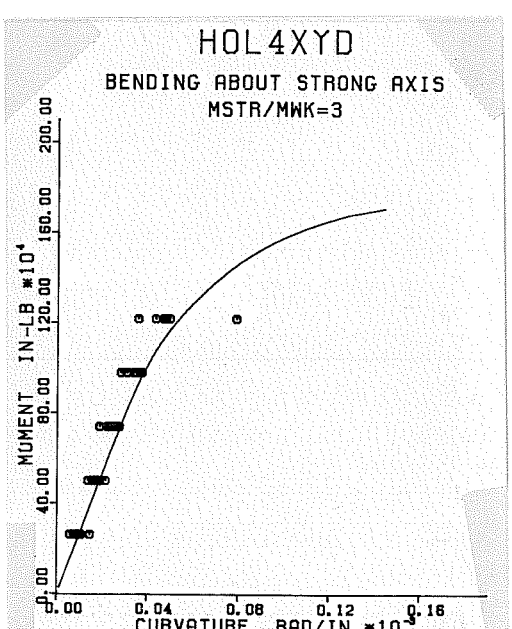

Fig. 4.17 P-M-ϕ behavior of single cell pier for $P = 0.4P_o$ and $M_{STR}/M_{WK} = 3$

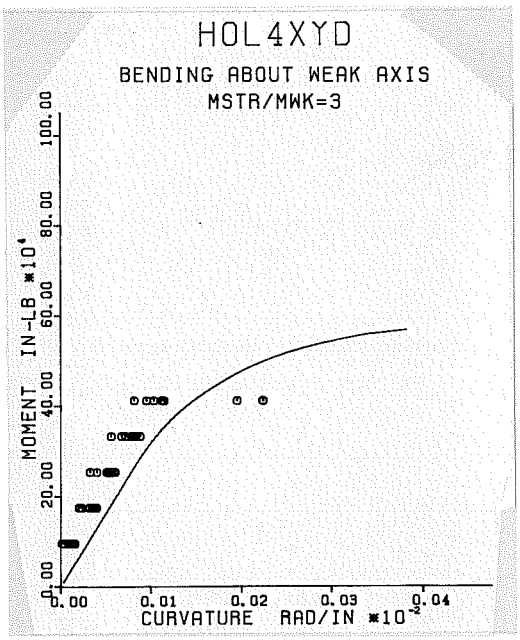

Fig. 4.18 P-M-ϕ behavior of single cell pier for $P = 0.4P_o$ and $M_{STR}/M_{WK} = 3$

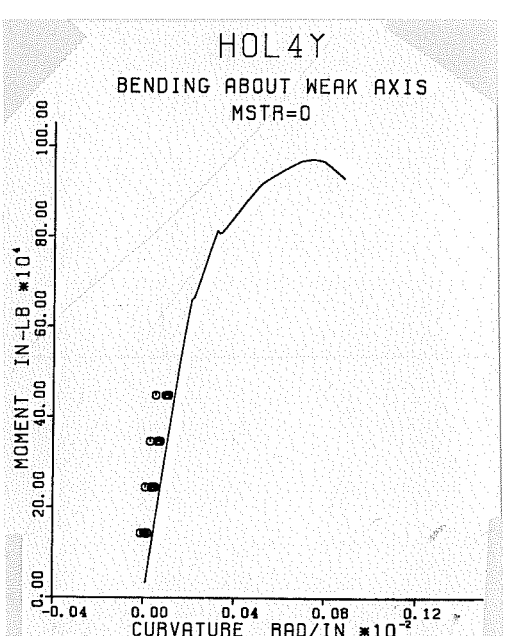

Fig. 4.19 P-M-ϕ behavior of single cell pier for $P = 0.4P_o$ and $M_{STR} = 0$

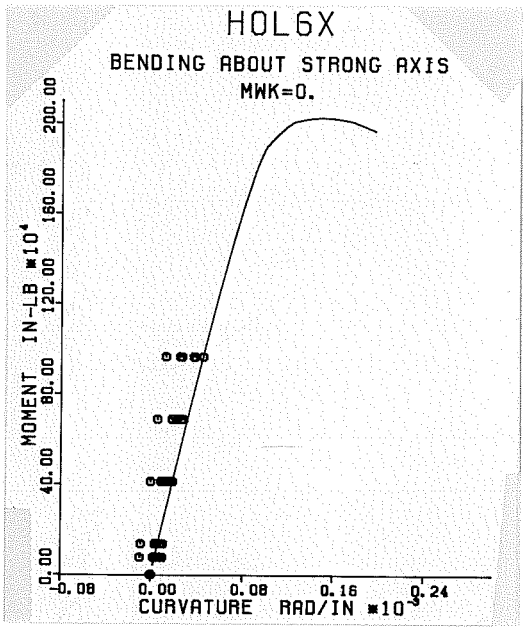

Fig. 4.20 P-M-ϕ behavior of single cell pier for $P = 0.6P_o$ and $M_{WK} = 0$

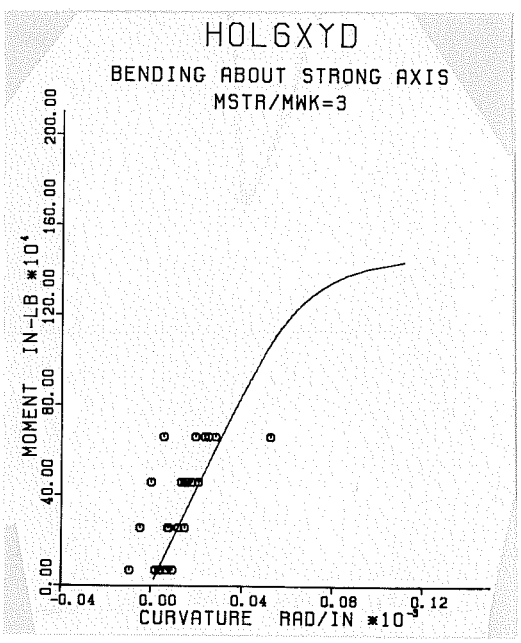

Fig. 4.21 P-M-ϕ behavior of single cell pier for $P = 0.6P_o$ and $M_{STR}/M_{WK} = 3$

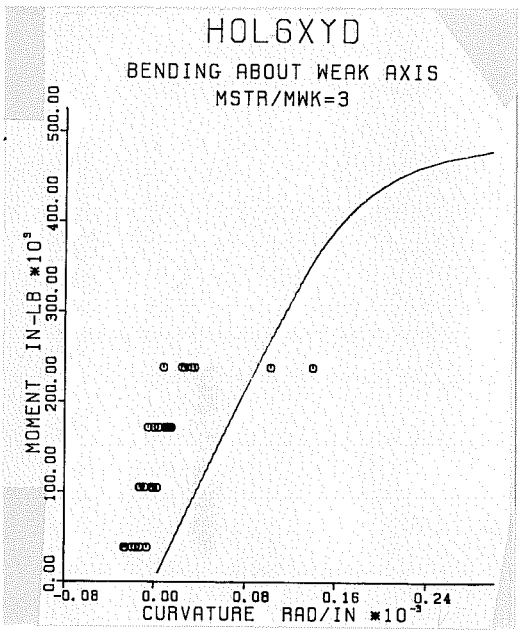

Fig. 4.22 P-M-ϕ behavior of single cell pier for P = 0.6P_o and M_{STR}/M_{WK} = 3

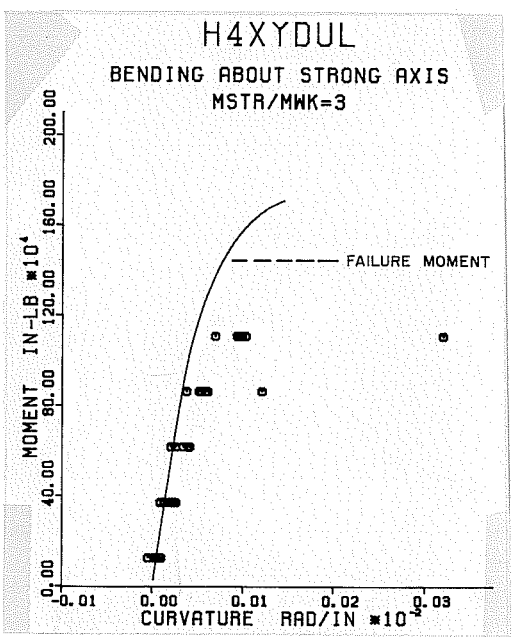

Fig. 4.23 P-M-ϕ behavior of single cell pier for P = 0.4P_o and M_{STR}/M_{WK} = 3

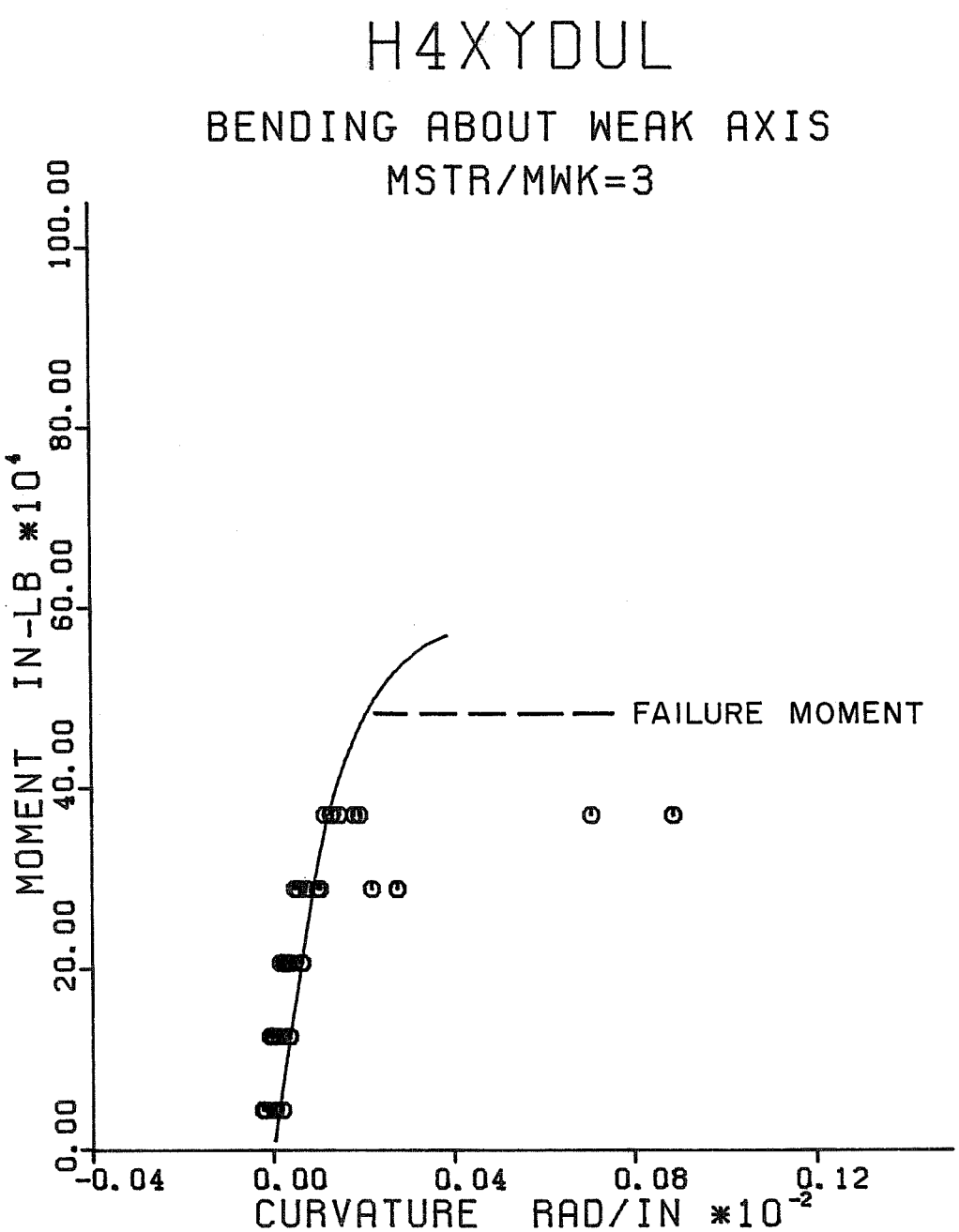

Fig. 4.24 P-M-ϕ behavior of single cell pier for $P = 0.4P_o$ and $M_{STR}/M_{WK} = 3$

load combinations. As with the solid pier, the order of the figures reflects the order of testing and the solid line represents the behavior predicted by BIMPHI while the symbols represent the measured experimental data. At each moment level these are seven curvature station values for the single cell pier. In general good agreement is seen between the calculated and actual behavior. These comparisons will be further discussed in Chapter 5.

The single cell pier was loaded in the same manner as the solid pier. It was subjected to axial loads of $0.2P_o$, $0.4P_o$, and $0.6P_o$ (P_o = 681 kips) and loading paths which included uniaxial bending as well as biaxial bending. The failure load combination was along the diagonal just as for the solid pier. It consisted of an axial load of $0.4P_o$ and the ratio of strong to weak axis moments equaled 3. The failure mode was again a concrete compressive failure occurring about 10 in. above midheight and destroying the highly stressed corner. As shown in Figs. 4.23 and 4.24, failure occurred just as the sixth increment of moment loading was essentially attained but before any curvature meters or strain instrumentation was read. Failure levels are indicated on these figures. The moments applied at time of failure were approximately 85% of the computed moment capacities. The significance and possible cause of this reduction are discussed in Section 4.7.

Even though there is a good general agreement between the calculated and observed behavior, two cases seem to deviate more than the others. These deviations are shown in Figs. 4.18 and 4.22 and are most probably due to an eccentricity which was not accounted for by the method used for correction of accidental eccentricities. All of the load cases have some scatter. Most of this is normal scatter associated with such measurements. However, in Figs. 4.23 and 4.24 the points which fall far to the right are most probably due to yielding of the reinforcement which causes the embedded strain gages to no longer record accurately. The curvature meters did not show such values. This load case was the last load case for which data were obtained. Loading was increased to the level shown and the load dropped off sharply before data readings were made.

4.4 Two Cell Pier Curvatures

The two cell pier was loaded in almost the same manner as the solid and the single cell pier. The loading modes and their sequence were exactly the same as the order of the figures shown in Figs. 4.25 through 4.36. All test results are covered in these figures. The two cell pier was subjected to axial loads of $0.2P_o$, $0.4P_o$, and $0.6P_o$ where P_o = 725k. The loading paths included uniaxial bending as well as biaxial bending just as the solid and the single cell pier. The loading mode used in the ultimate load test of the two cell pier was along the diagonal just as used for the solid and the single cell piers. An axial load of $0.4P_o$ and bending moments around both axes were applied. The ratio of strong to weak axis bending moments was 3. The final mode of the failure was compressive failure of concrete at the highest compressed corner of the pier at its midheight. Before the final failure, local compressive spalling of concrete appeared along the highly compressed corner of the pier. The ultimate bending capacity of the pier was only slightly above the capacity predicted by BIMPHI (4%).

The observed and computed P-M-ϕ relationships for the two cell pier are shown in Fig. 4.25 through 4.36 for various load combinations. As with the solid and single cell piers, the order of the figures corresponds to the order of testing. In these figures, the solid line represents the moment-curvature relationship predicted by the computer program BIMPHI while open and closed symbols represent the measured data. The closed symbols represent the curvatures determined from Demec readings and the open symbols represent the curvature determined from curvature meters. To calculate curvatures from Demec readings, the corner Demec measuring stations on both wide pier sides were used. As shown in Figs. 4.3 and 4.4, strains are extremely consistent. Thus the curvatures which were found from strain differences should quite accurately reflect the actual curvatures. In some cases, the curvatures determined from the curvature meter were less reliable because of electrical drift during the long

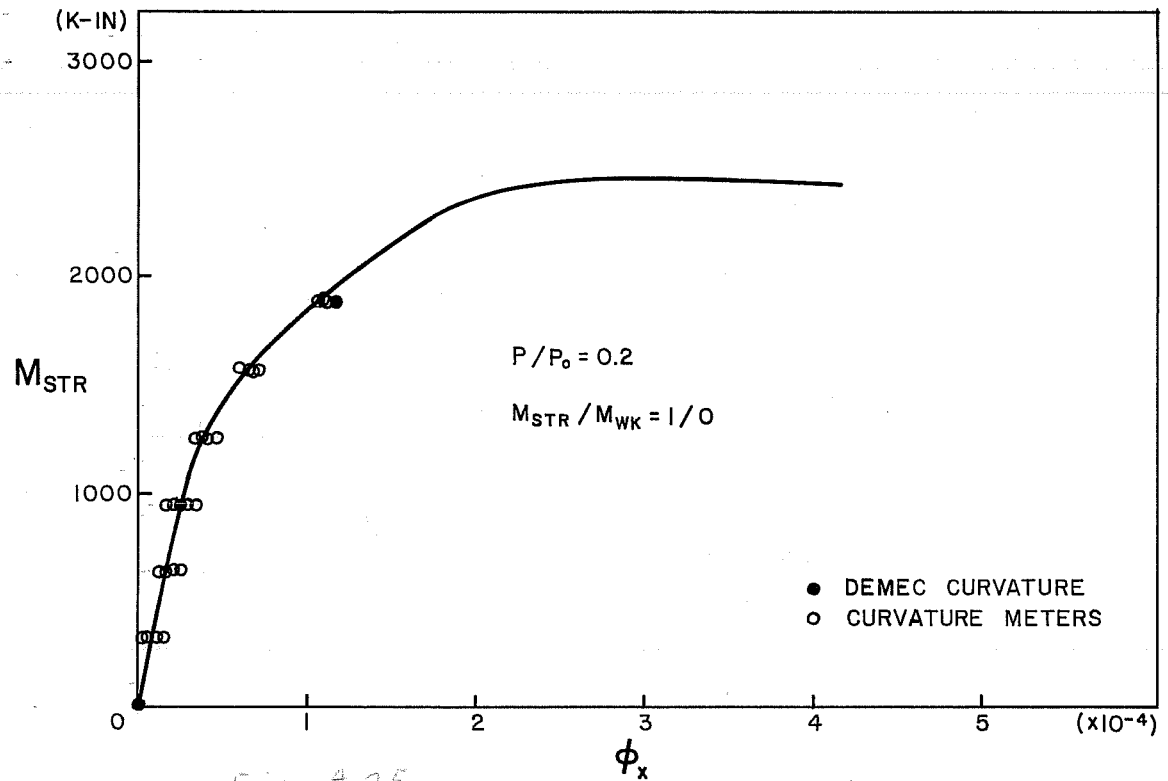

Fig. 4.25 P-M-ϕ behavior of two cell pier for P/P_o = 0.2 and M_{STR}/M_{WK} = 1/0

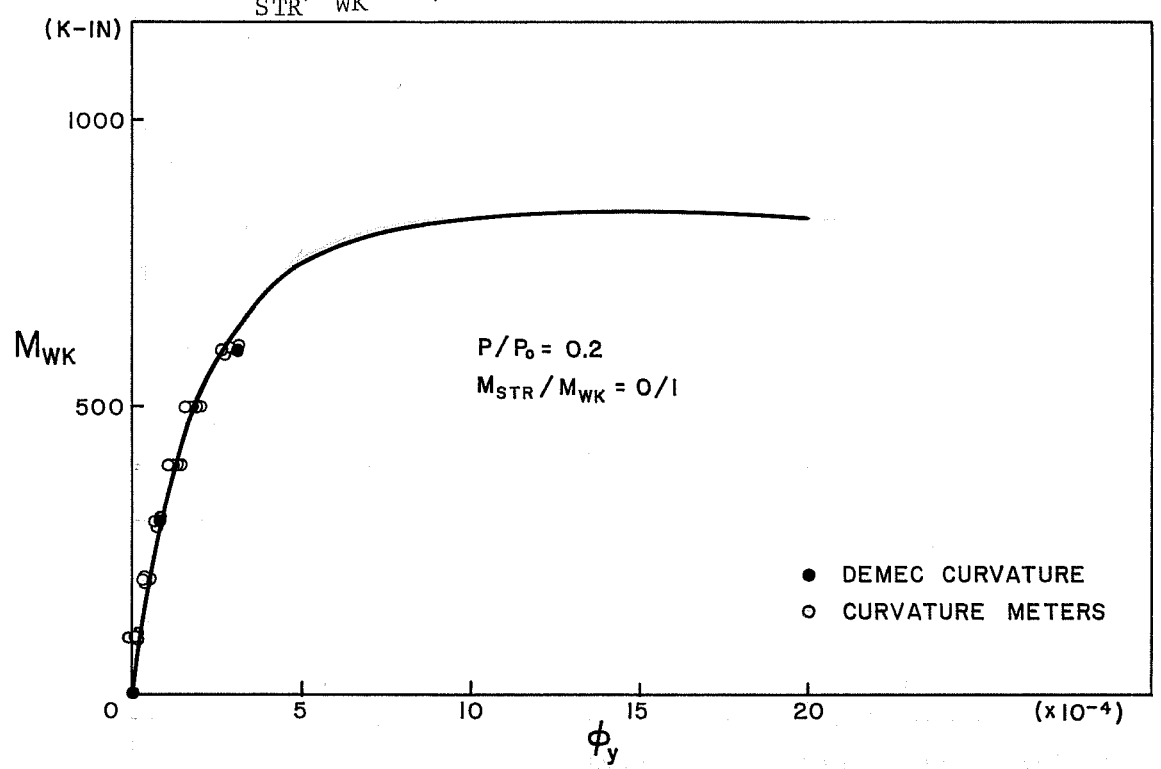

Fig. 4.26 P-M-ϕ behavior of two cell pier for P/P_o = 0.2 and M_{STR}/M_{WK} = 0/1

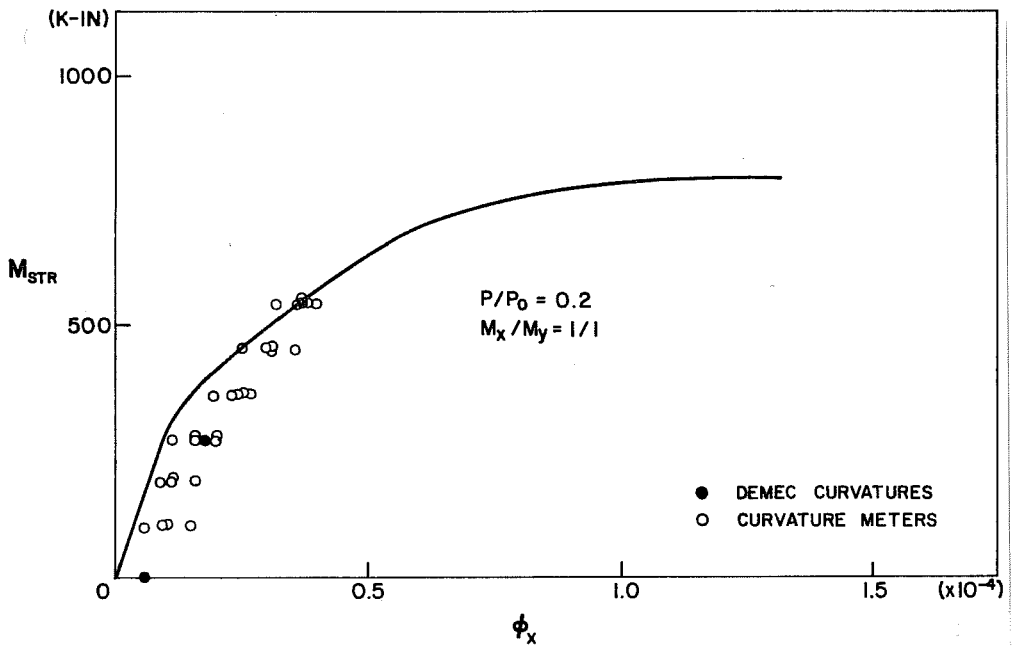

(a) $P/P_o = 0.2$, $M_x/M_y = 1$

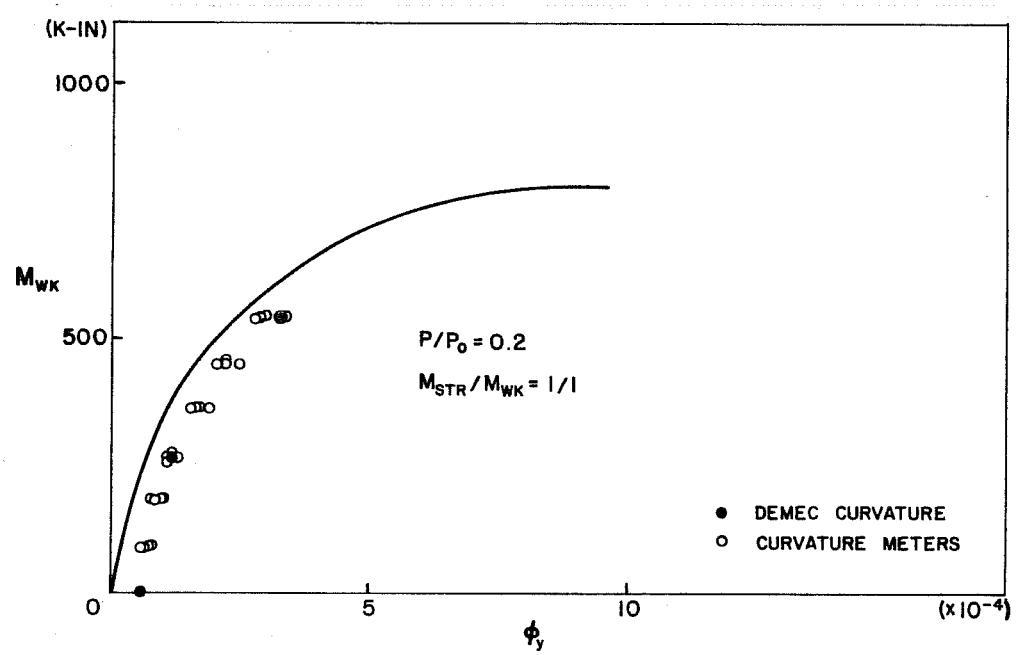

(b) $P/P_o = 0.2$, $M_{STR}/M_{WK} = 1/1$

Fig. 4.27 P-M-ϕ behavior of two cell pier

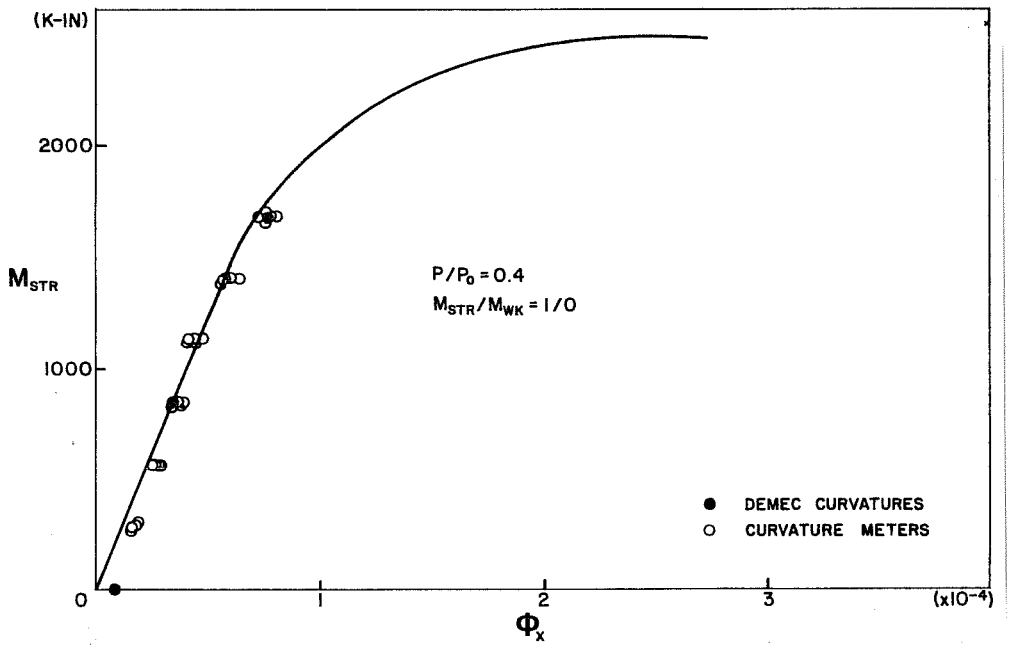

Fig. 4.28 P-M-ϕ behavior of two cell pier, P/P_o = 0.4 and M_{STR}/M_{WK} = 1/0

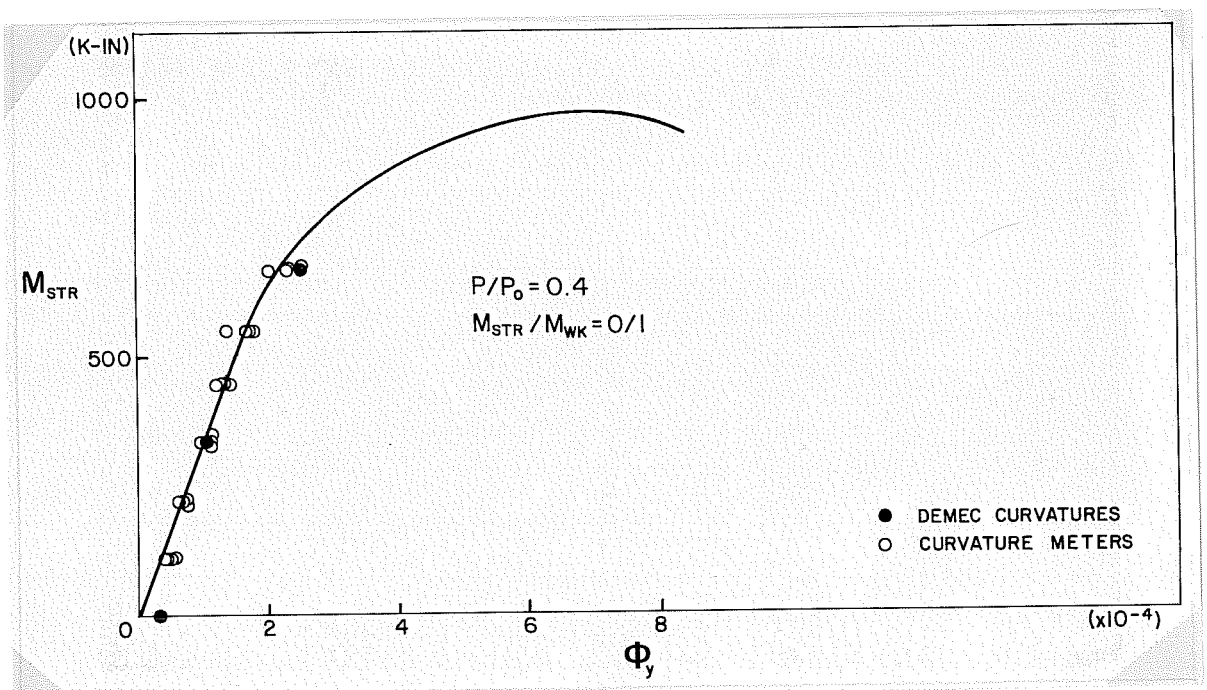

Fig. 4.29 P-M-ϕ behavior of two cell pier, P/P_o = 0.4 and M_{STR}/M_{WK} = 0/1

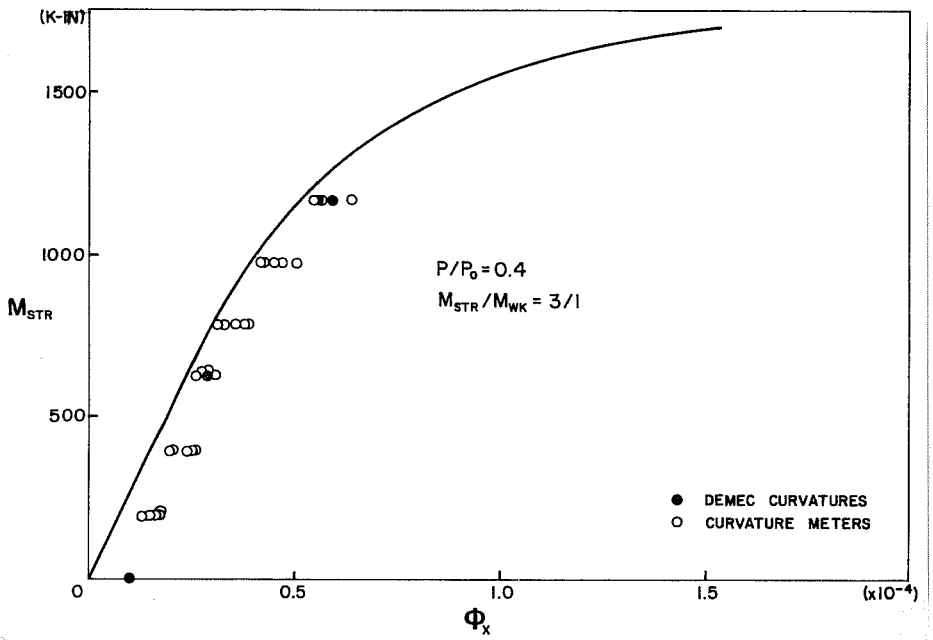

(a)

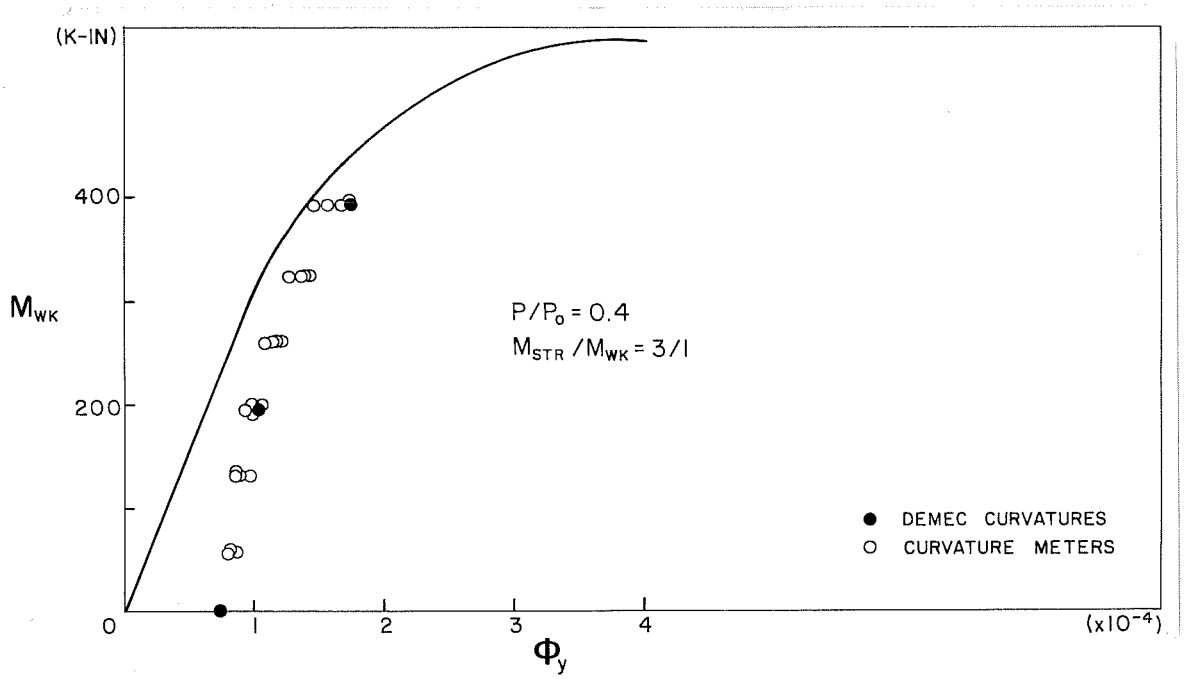

(b)

Fig. 4.30 P-M-ϕ behavior of two cell pier, P/P_o = 0.4 and M_{STR}/M_{WK} = 3/1

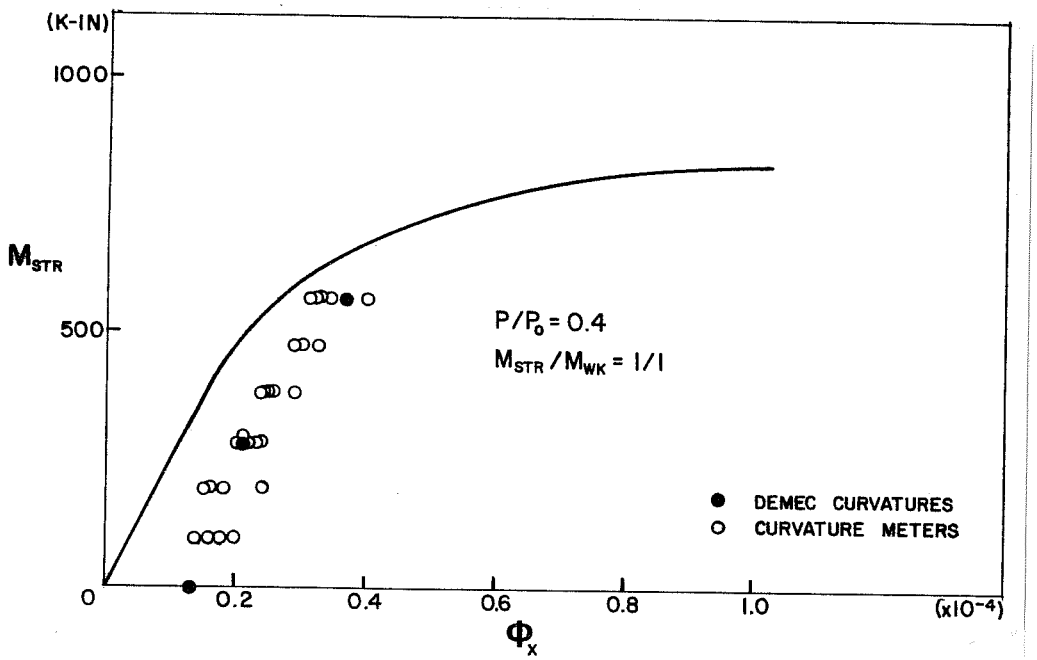

(a)

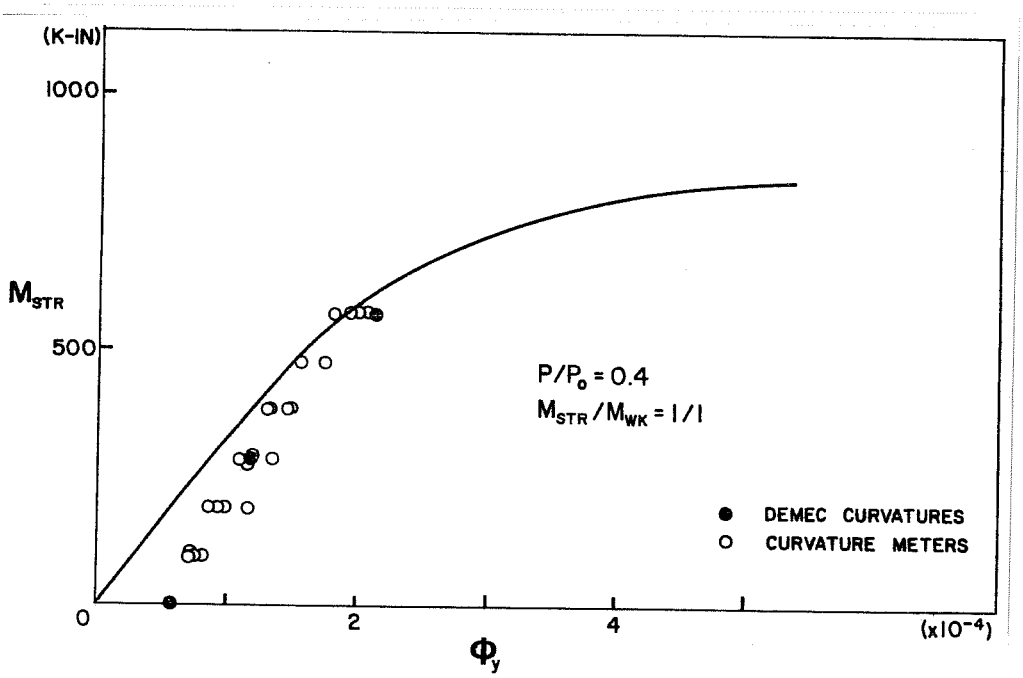

(b)

Fig. 4.31 P-M-ϕ behavior of two cell pier, P/P_o = 0.4 and M_{STR}/M_{WK} = 1/1

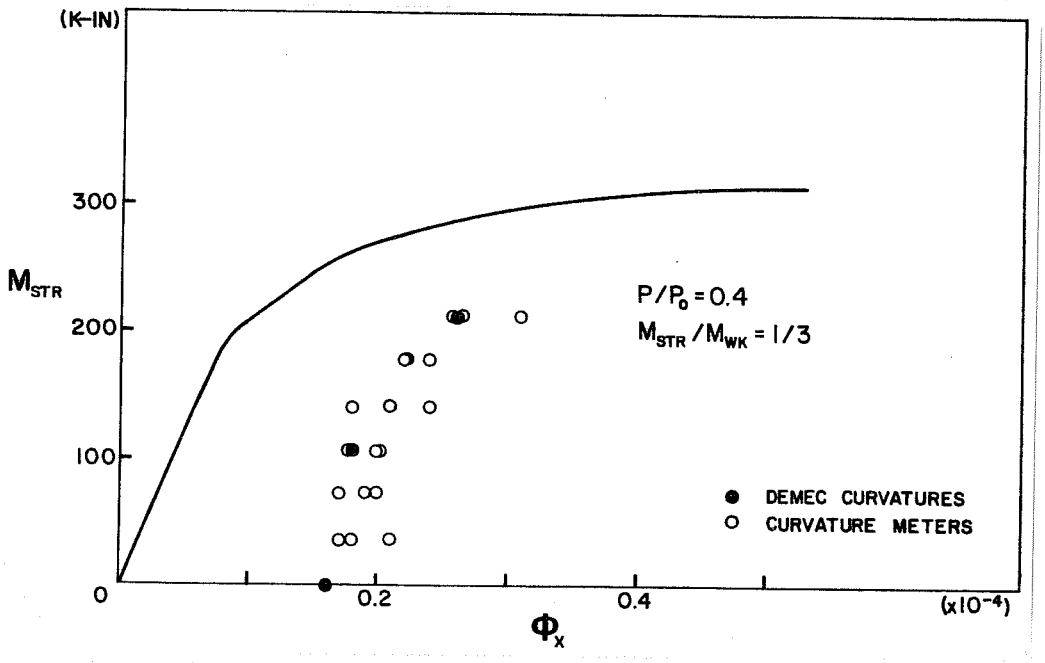

(a)

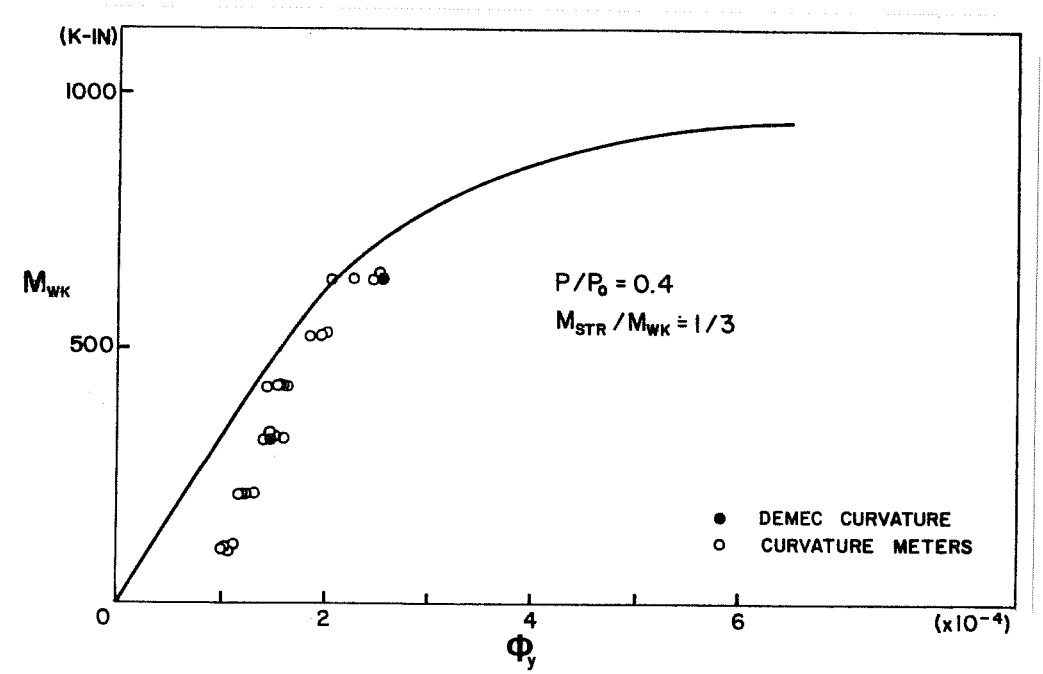

(b)

Fig. 4.32 P-M-ϕ behavior of two cell pier, P/P_o = 0.4 and M_{STR}/M_{WK} = 1/3

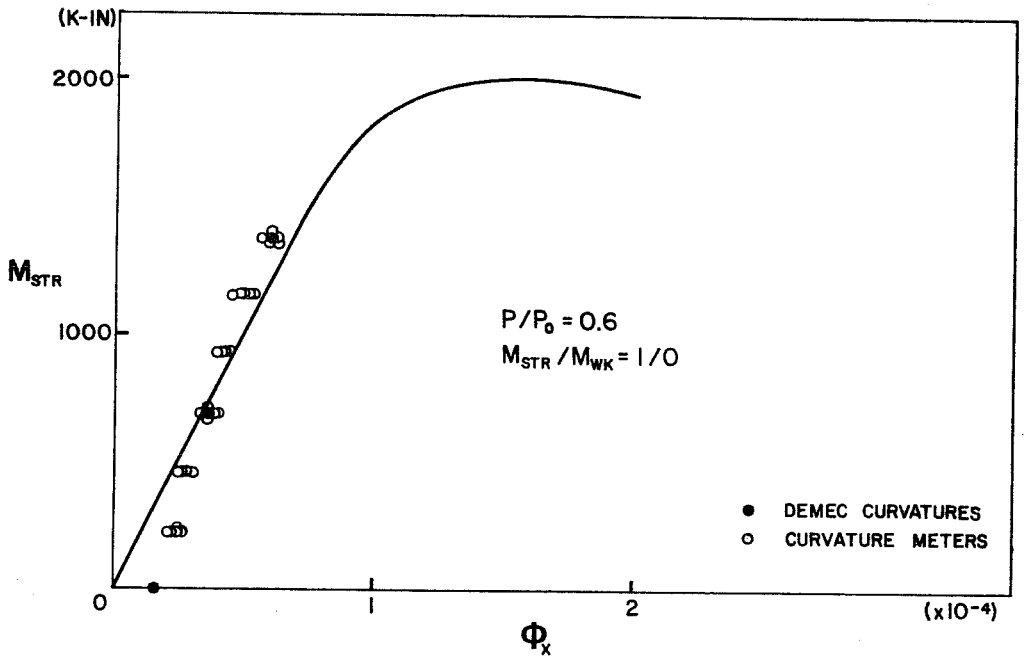

Fig. 4.33 P-M-ϕ behavior of two cell pier, P/P_o = 0.6 and M_{STR}/M_{WK} = 1/0

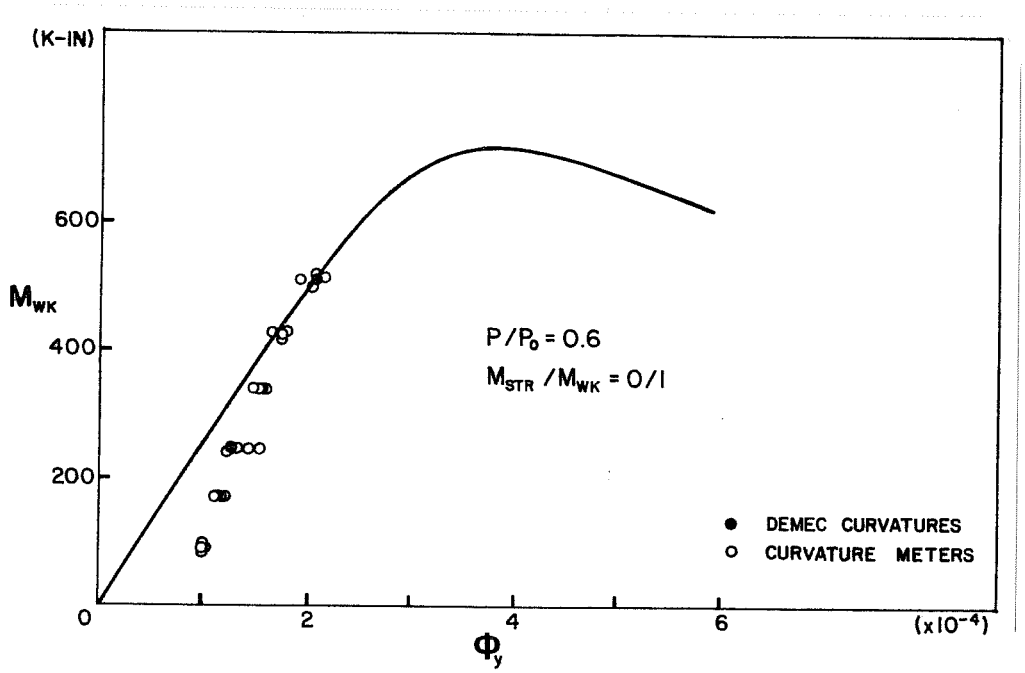

Fig. 4.34 P-M-ϕ behavior of two cell pier, P/P_o = 0.6 and M_{STR}/M_{WK} = 0/1

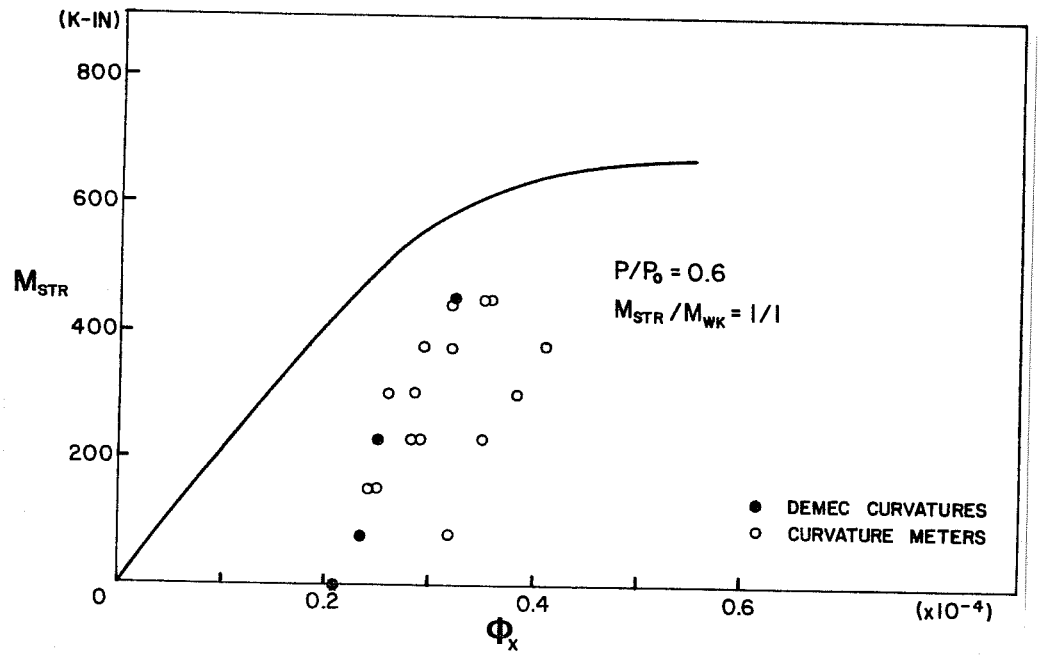

(a)

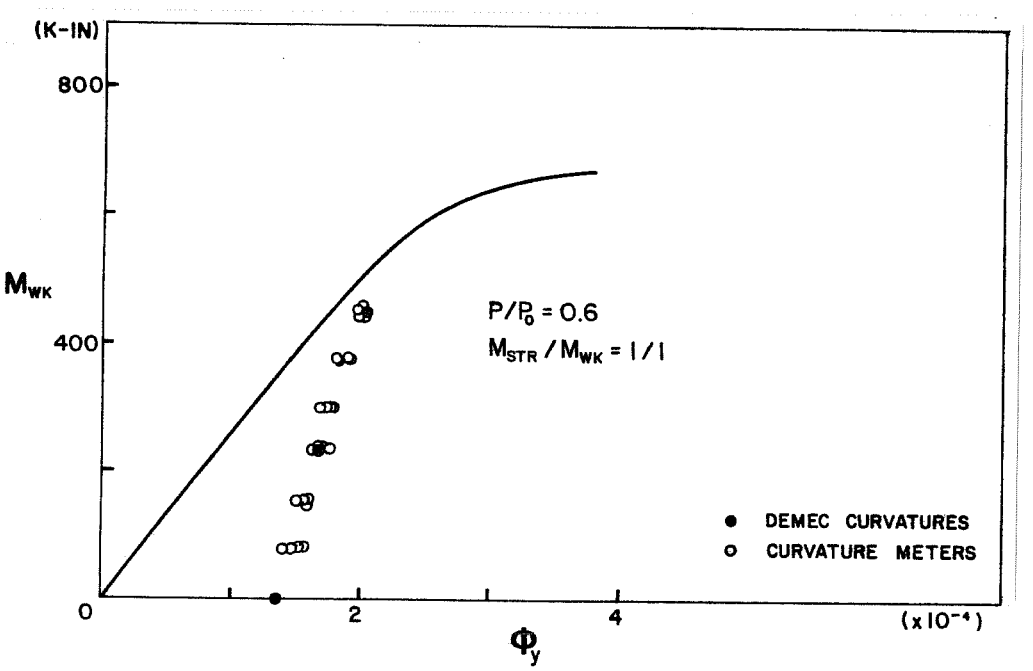

(b)

Fig. 4.35 P-M-ϕ behavior of two cell pier, $P/P_o = 0.6$ and $M_{STR}/M_{WK} = 1/1$

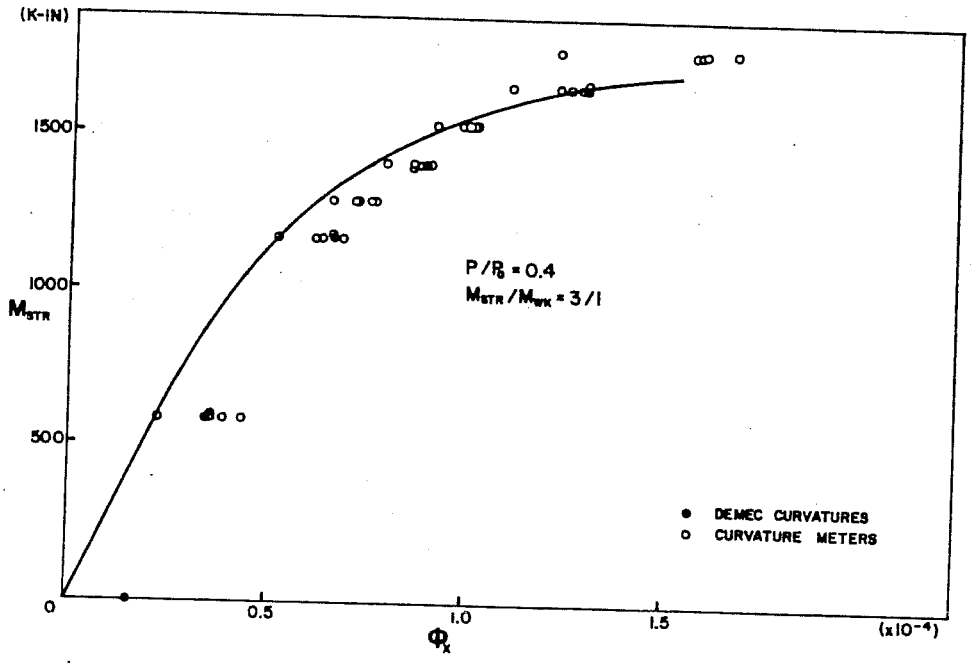

(a)

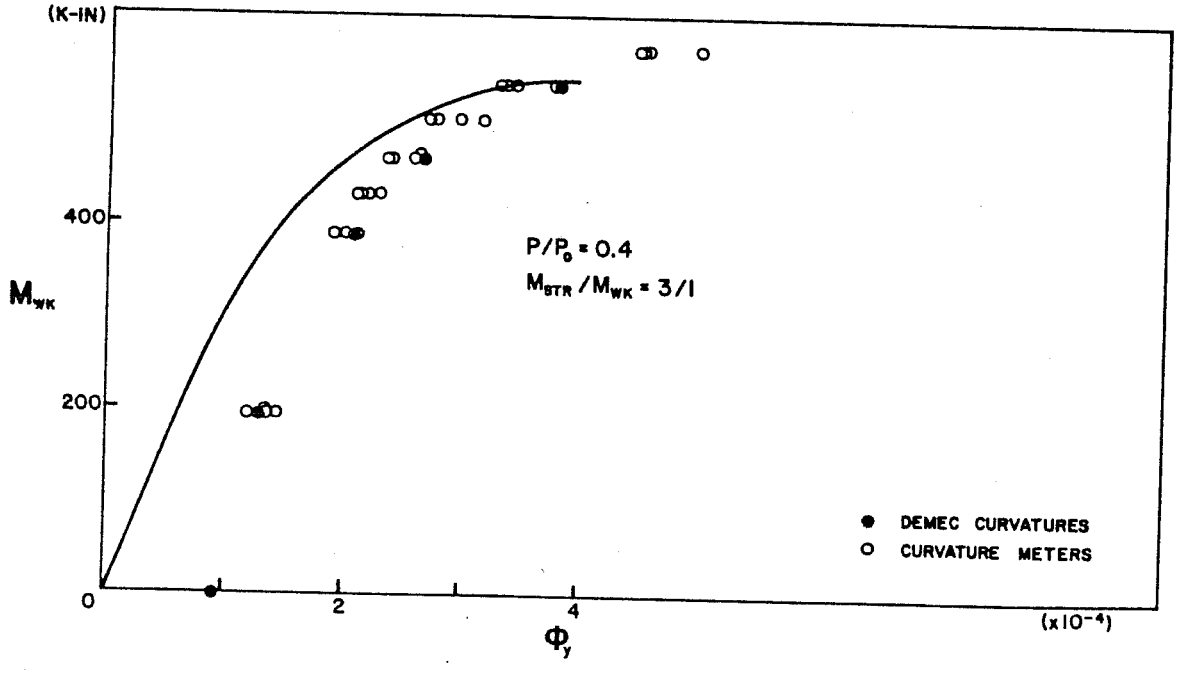

(b)

Fig. 4.36 P-M-ϕ behavior of two cell pier, $P/P_o = 0.4$ and $M_{STR}/M_{WK} = 3/1$

duration test as well as extraneous electrical disturbances from other heavy electrical equipment in the laboratory. In the calculation of curvatures from curvature meter readings, residual curvatures after each loading mode were determined by using Demec readings. The effects of the electrical drift were excluded. The incremental curvatures observed in each loading mode were added to the previous residual curvatures to calculate the curvatures from curvature meters. Each curvature meter reading was carefully examined. Data which showed sudden jumps on drops due to apparent electrical drift or disturbance were excluded from the data plots. In general the agreement between the measured and the calculated moment-curvature relationship is particularly good in the beginning of the series of the loading modes (Figs. 4.25 through 4.30 and Fig. 4.33 for example). In the latter part of the series of the loading modes at $P/P_o = 0.4$ and $P/P_o = 0.6$, the agreement is not as good due to the residual curvature caused by the degradation of the pier (see Figs. 4.32 and 4.35). However, the agreement over the full range in the ultimate loading cycle shown in Fig. 4.36 is extremely good when compared to other such test data [11,12]. Comparisons between measured and computed curvatures will be further discussed in Chapter 5.

4.5 Three Cell Pier Curvatures

The three cell pier was loaded in the same manner as the two cell pier. The loading modes and their sequence were exactly the same as the order of the figures shown in Figs. 4.37 through 4.49. The three cell pier was subjected to axial loads of $0.20P_o$, $0.40P_o$, and $0.6P_o$ where $P_o = 852$k. The loading paths included uniaxial bending as well as biaxial bending. The loading mode used in the ultimate load test of the three cell pier was along the diagonal just as in the other three pier specimens. An axial load of $0.4P_o$ and bending moments around both axes were applied, of which ratio around strong to weak axis bending moments was 3. The final failure mode was compressive failure of the concrete at the highest stressed corner of the compression zone at midheight of the pier. The ultimate bending moments observed were slightly higher than the calculated ones (8%).

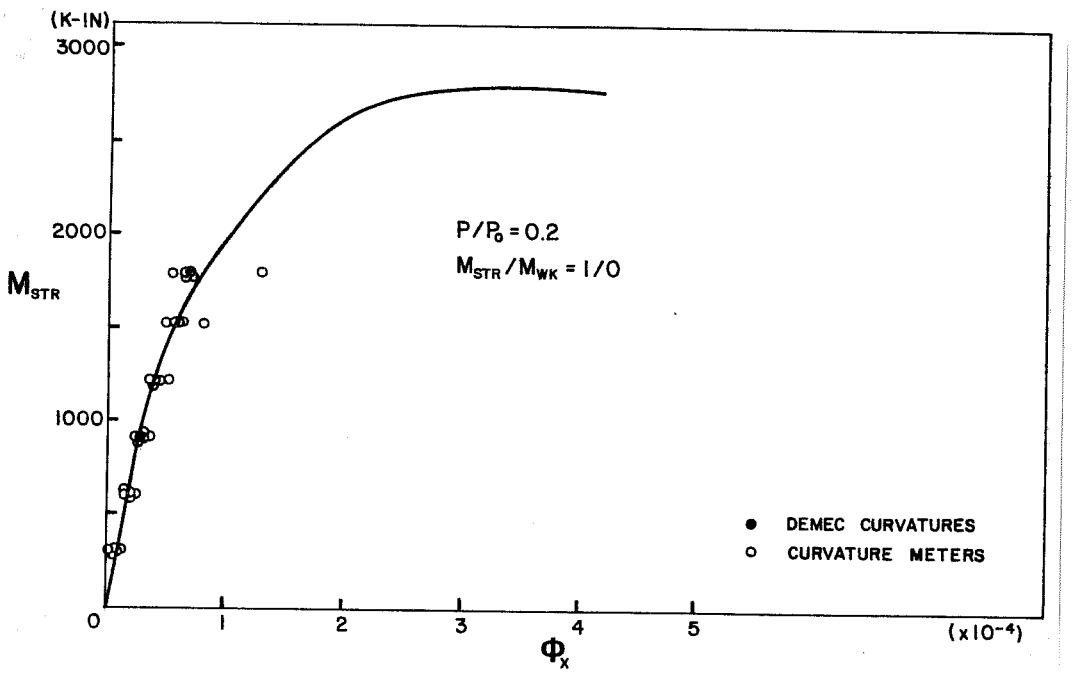

Fig. 4.37 P-M-ϕ behavior of three cell pier for $P/P_o = 0.2$ and $M_{STR}/M_{WK} = 1/0$

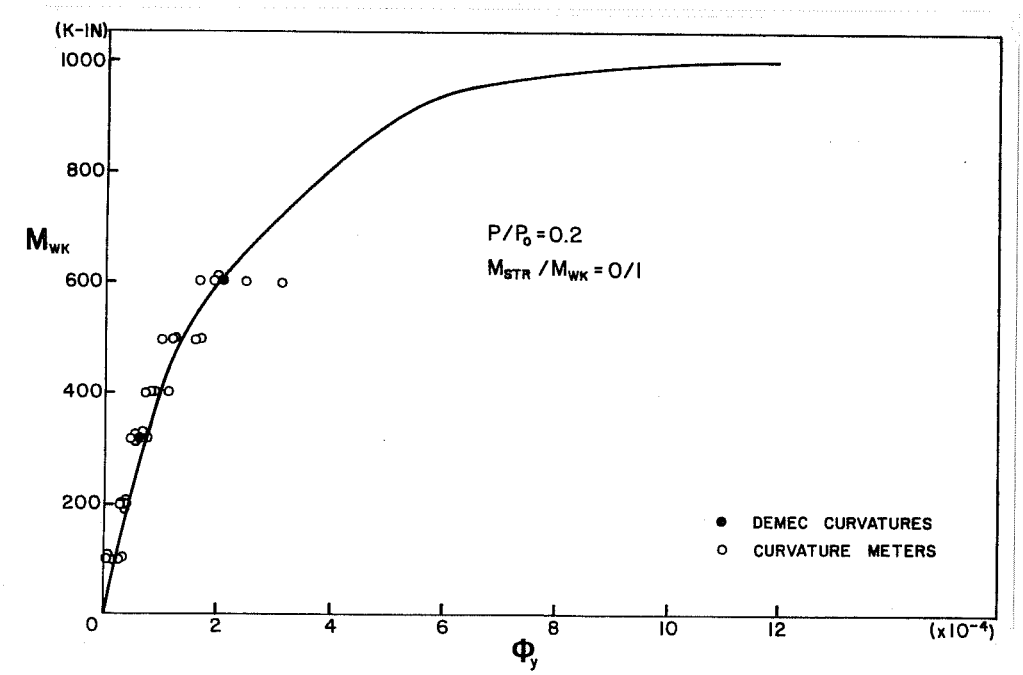

Fig. 4.38 P-M-ϕ behavior of three cell pier for $P/P_o = 0.2$ and $M_{STR}/M_{WK} = 0/1$

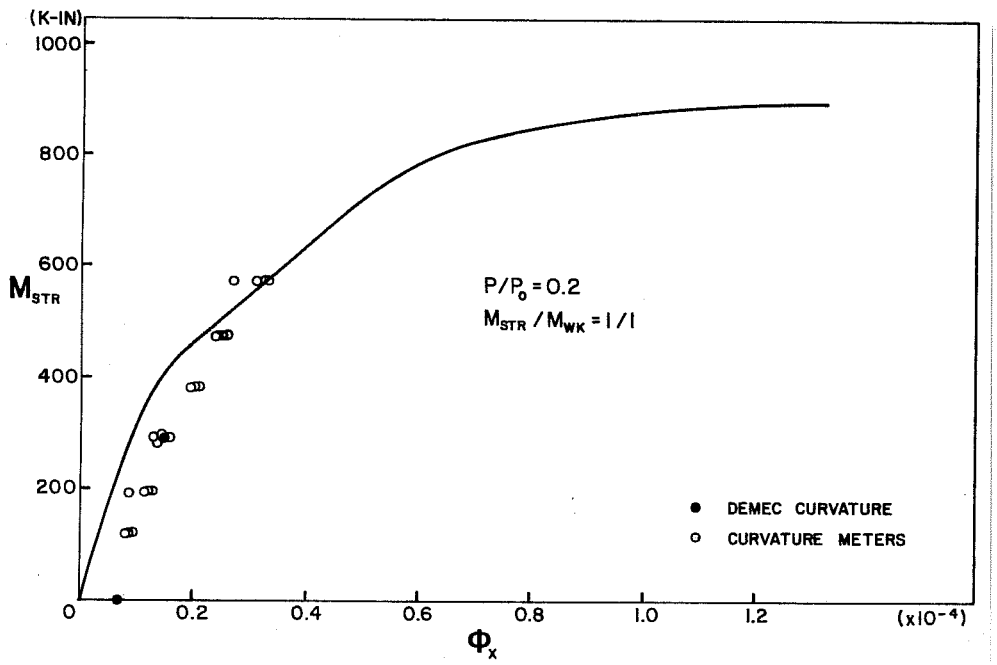

(a)

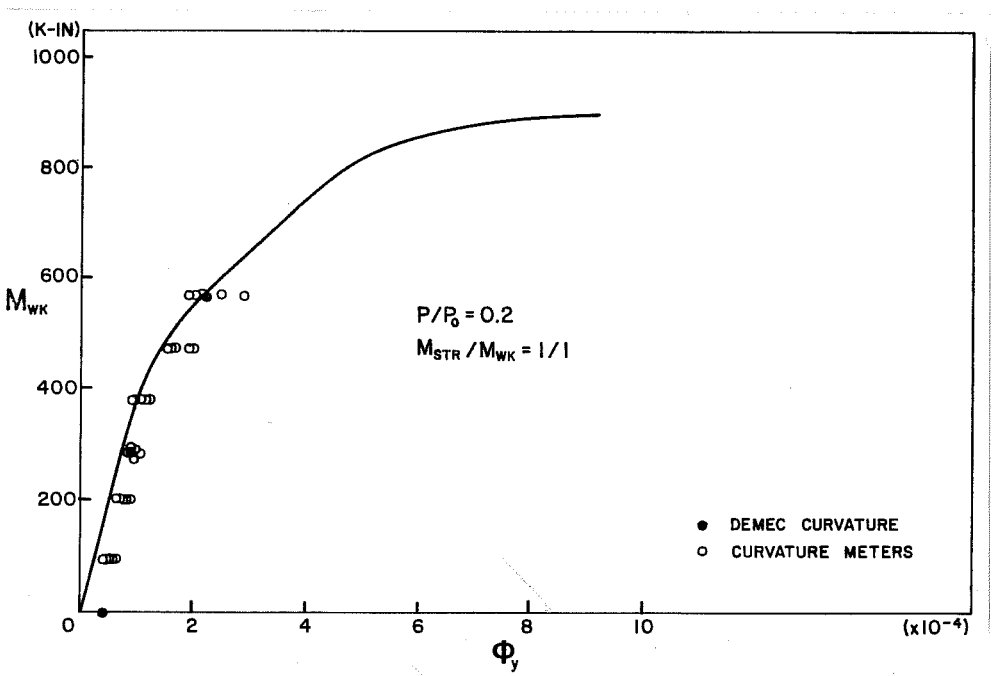

(b)

Fig. 4.39 P-M-ϕ behavior of three cell pier for P/P_o = 0.2 and M_{STR}/M_{WK} = 1/1

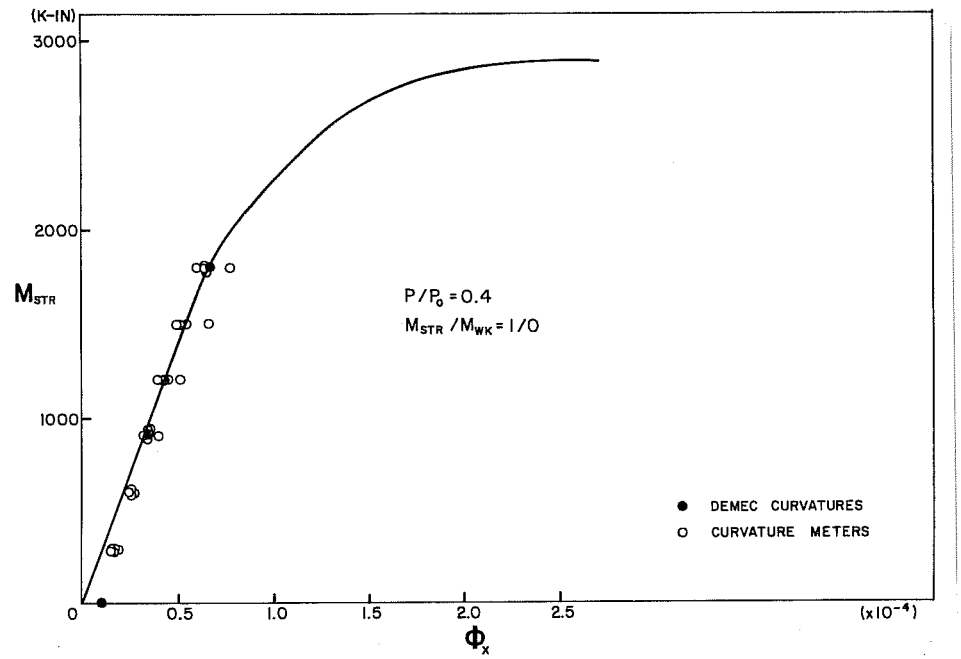

Fig. 4.40 P-M-ϕ behavior of three cell pier for $P/P_o = 0.4$ and $M_{STR}/M_{WK} = 1/0$

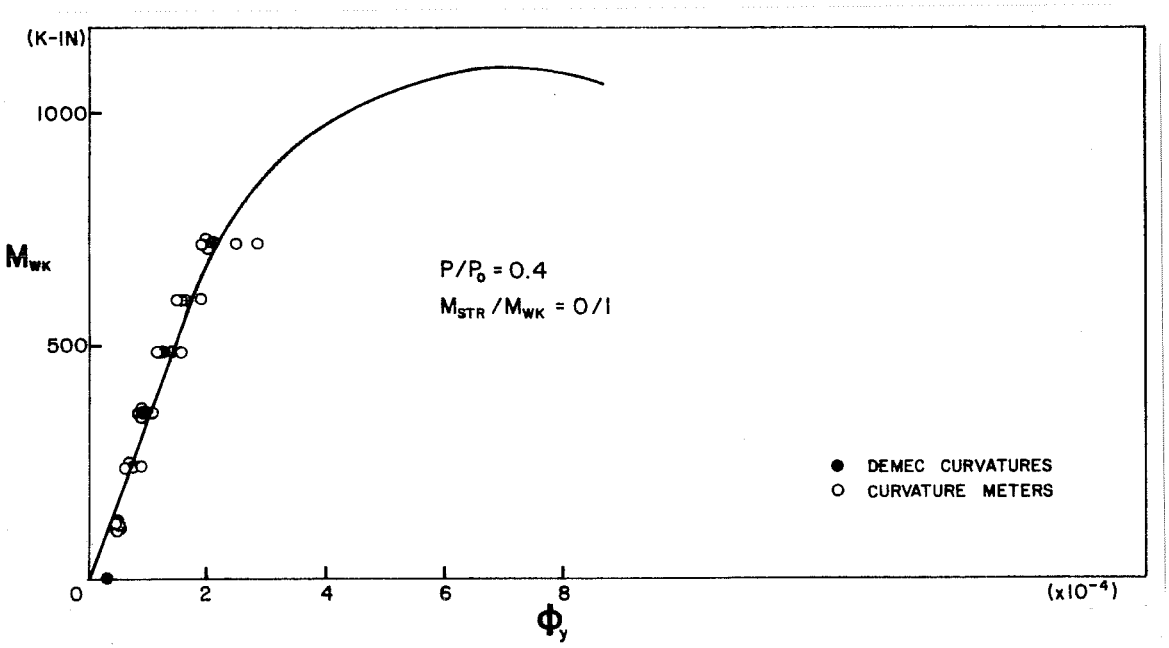

Fig. 4.41 P-M-ϕ behavior of three cell pier for $P/P_o = 0.4$ and $M_{STR}/M_{WK} = 0/1$

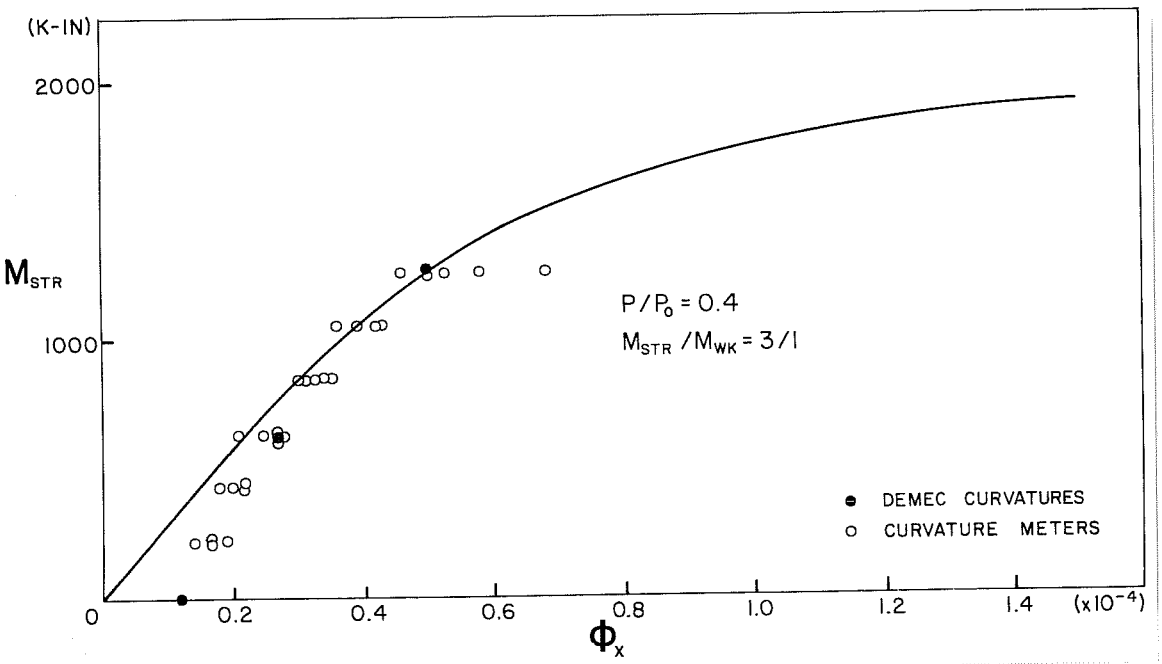

(a)

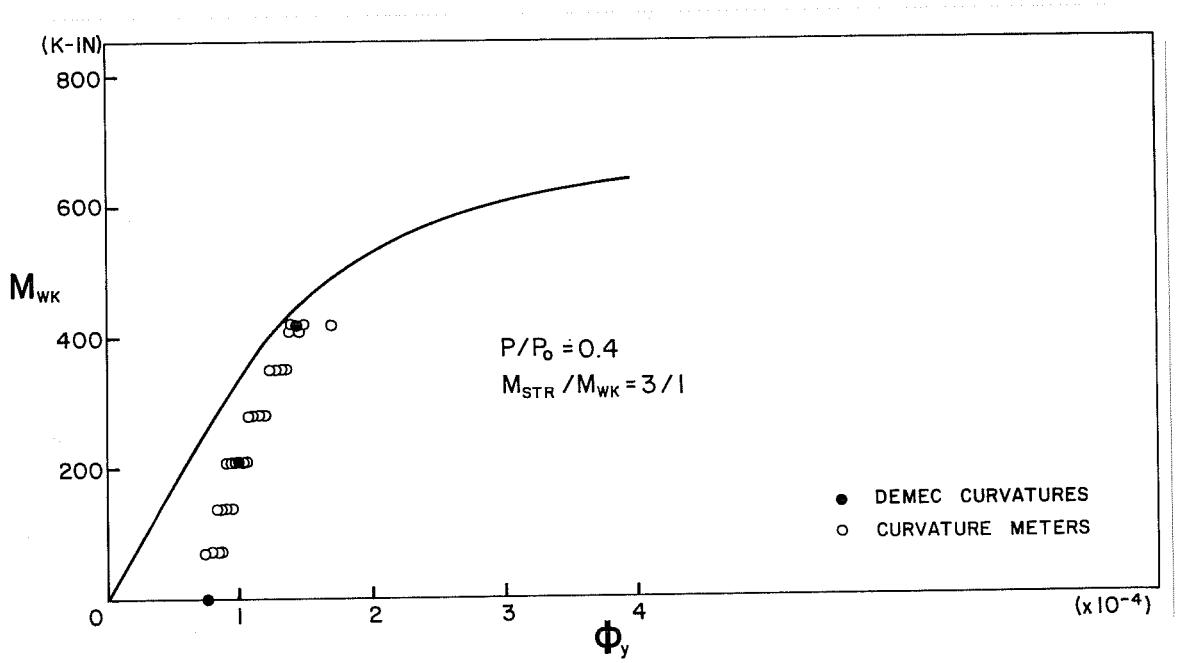

(b)

Fig. 4.42 P-M-ϕ behavior of three cell pier for P/P_o = 0.4 and M_{STR}/M_{WK} = 3/1

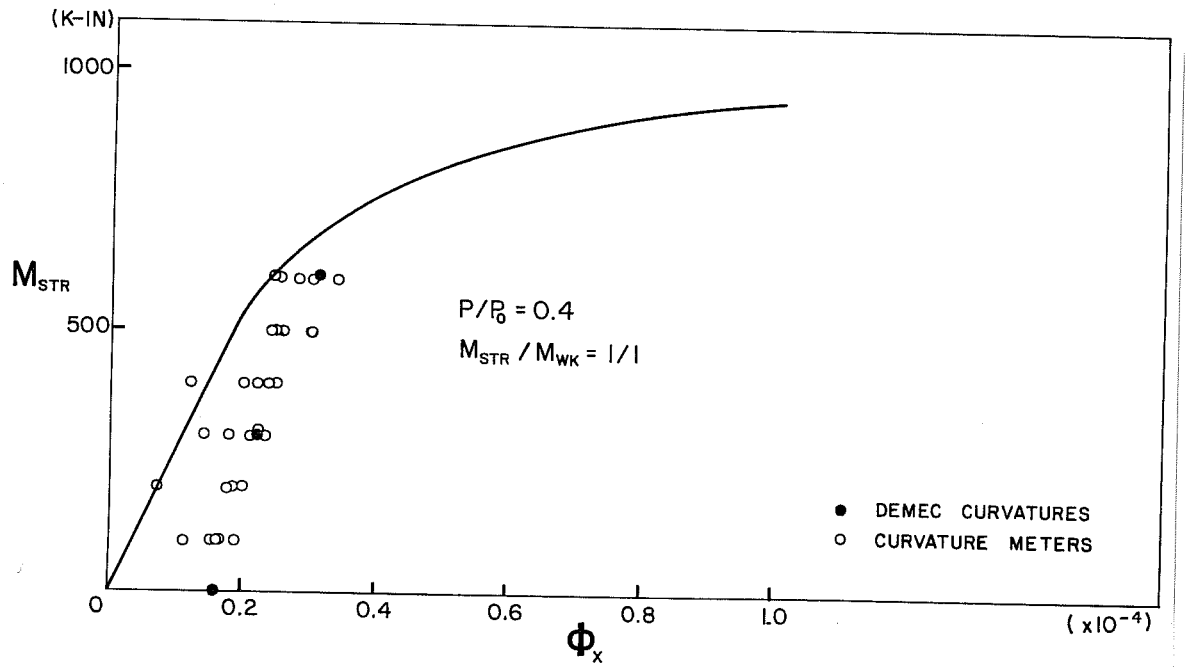

(a)

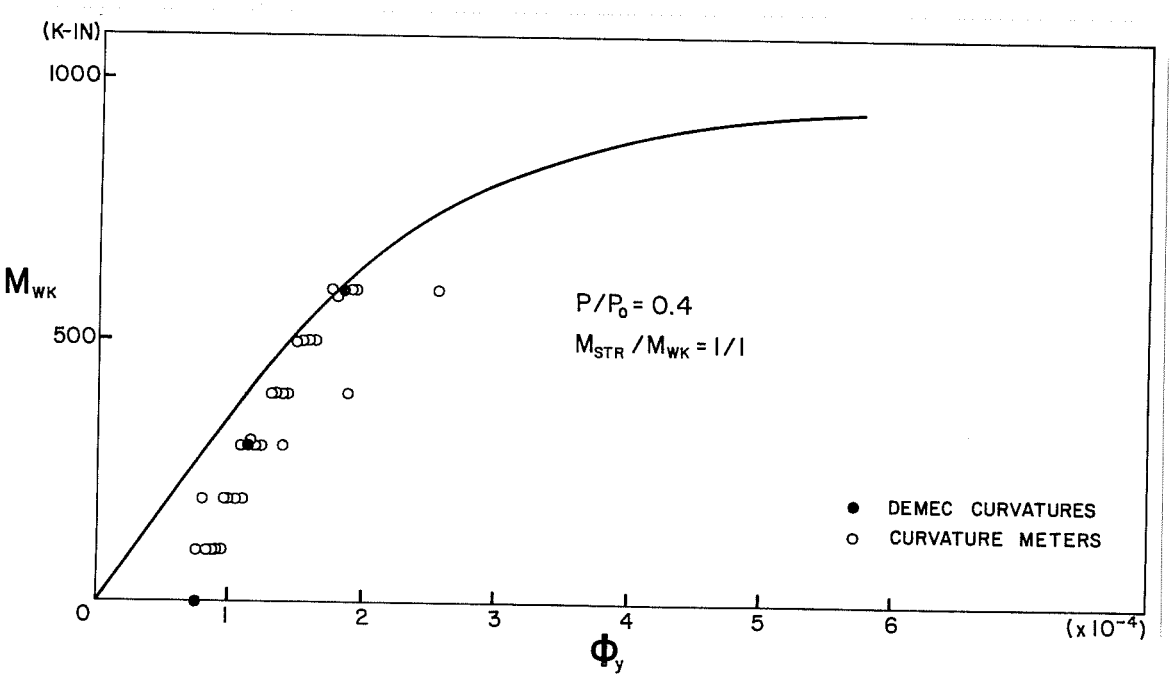

(b)

Fig. 4.43 P-M-ϕ behavior of three cell pier for $P/P_o = 0.4$ and $M_{STR}/M_{WK} = 1/1$

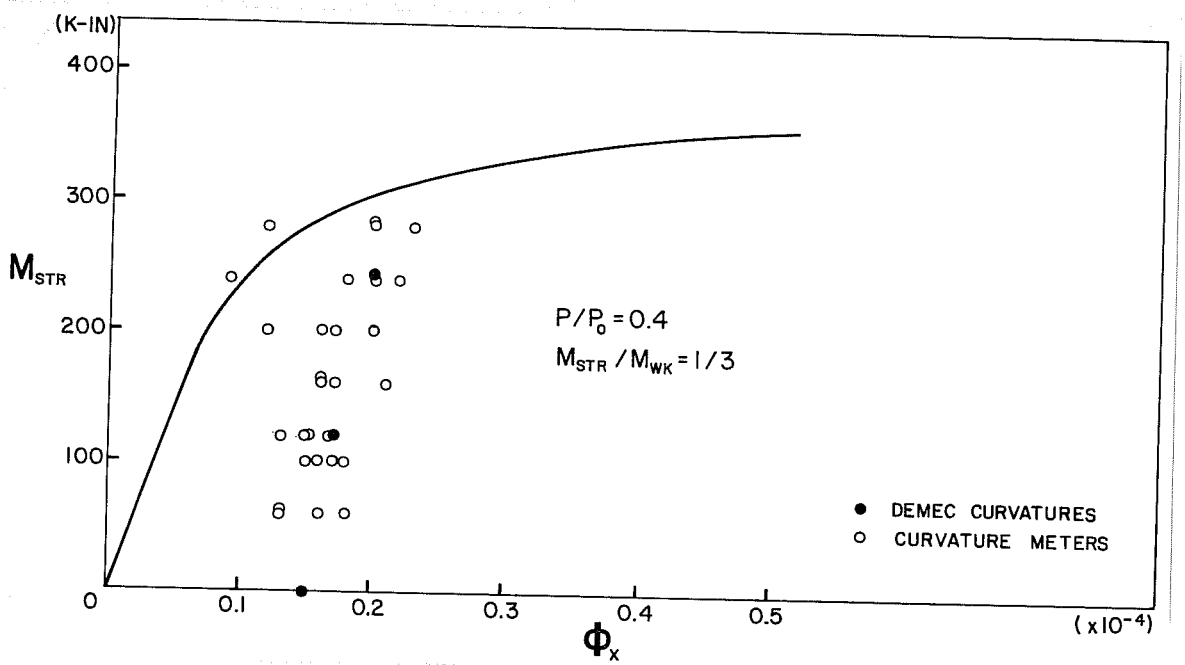

(a)

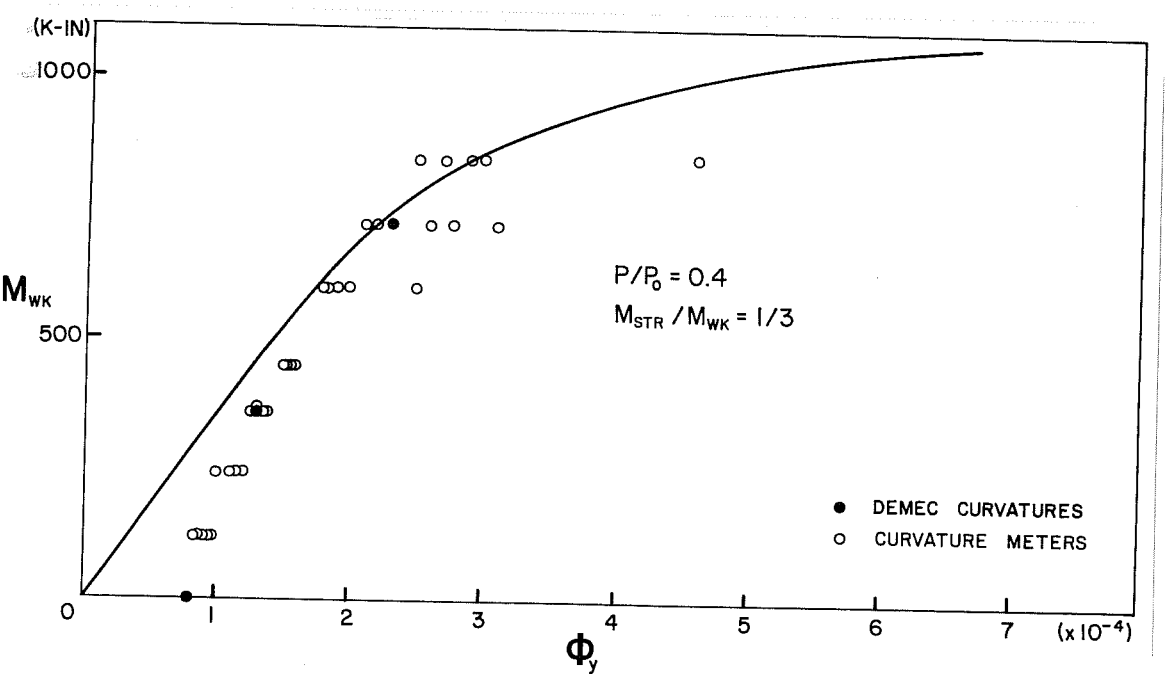

(b)

Fig. 4.44 P-M-ϕ behavior of three cell pier for $P/P_o = 0.4$ and $M_{STR}/M_{WK} = 1/3$

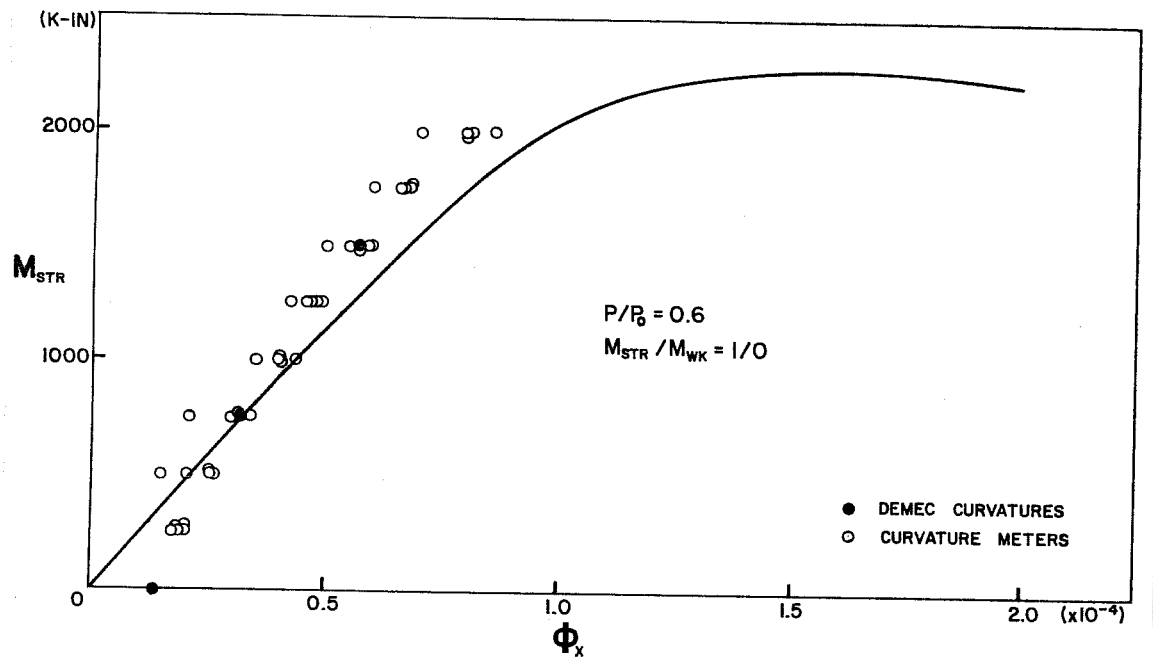

Fig. 4.45 P-M-ϕ behavior of three cell pier for $P/P_o = 0.6$ and $M_{STR}/M_{WK} = 1/0$

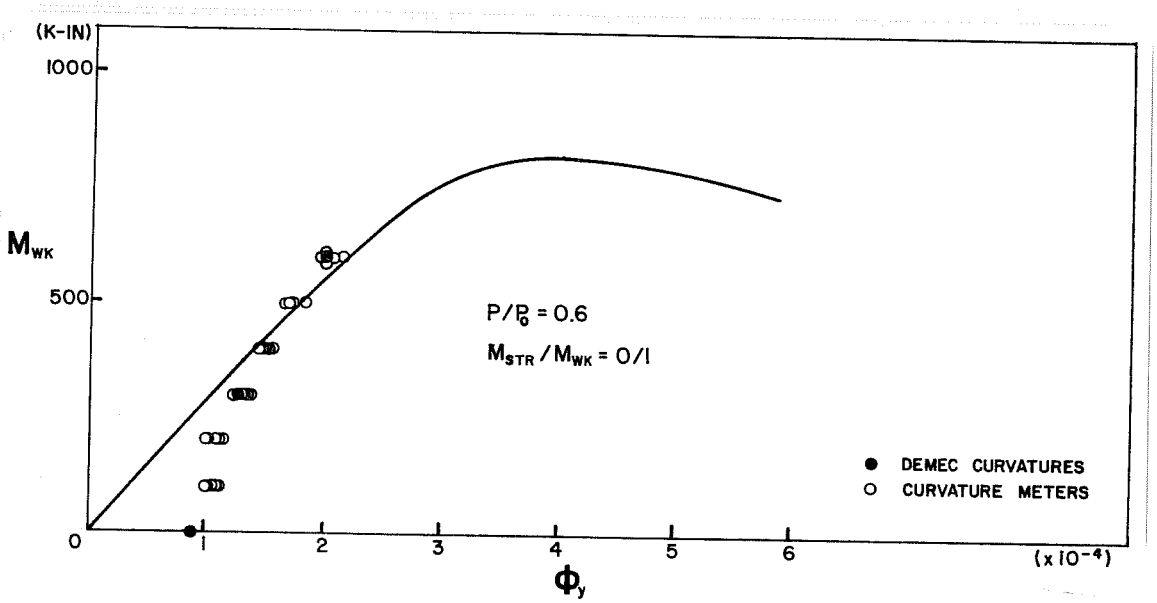

Fig. 4.46 P-M-ϕ behavior of three cell pier for $P/P_o = 0.6$ and $M_{STR}/M_{WK} = 0/1$

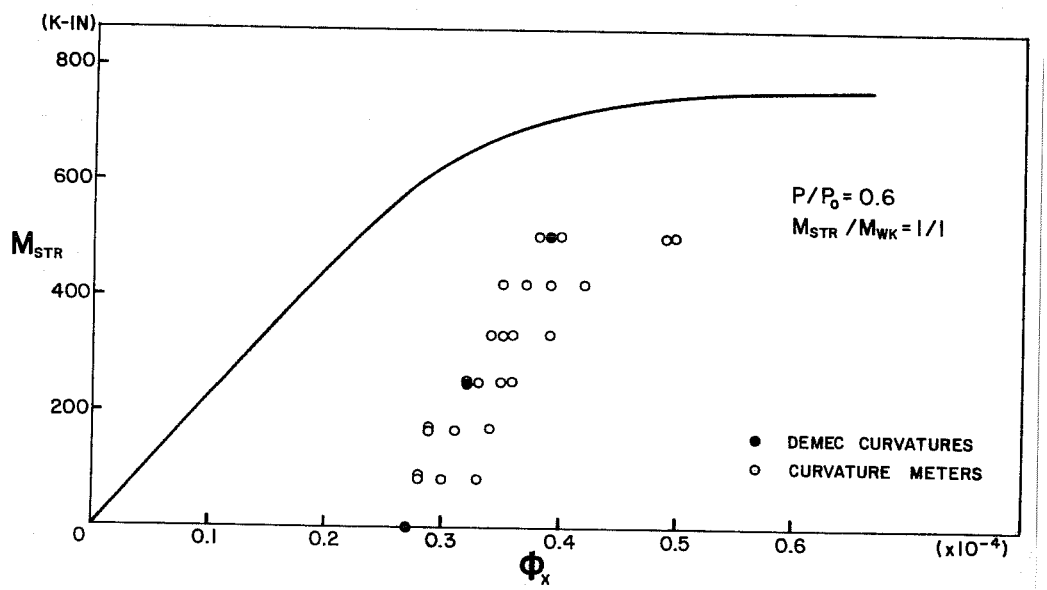

(a)

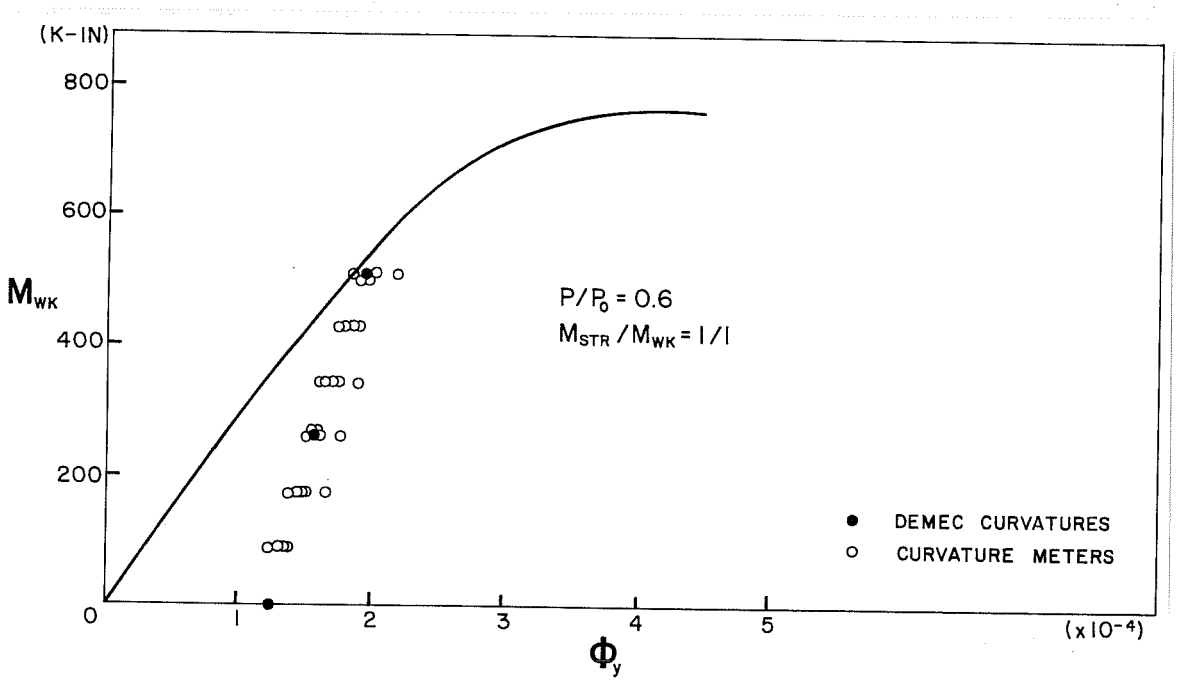

(b)

Fig. 4.47 P-M-ϕ behavior of three cell pier for $P/P_o = 0.6$ and $M_{STR}/M_{WK} = 1/1$

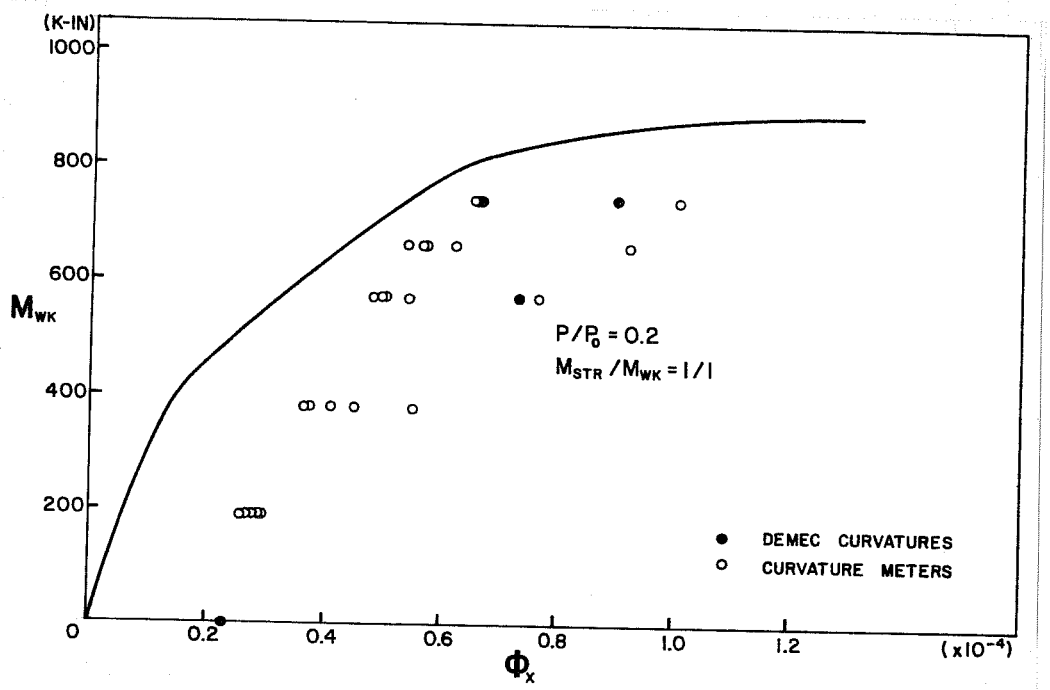

(a)

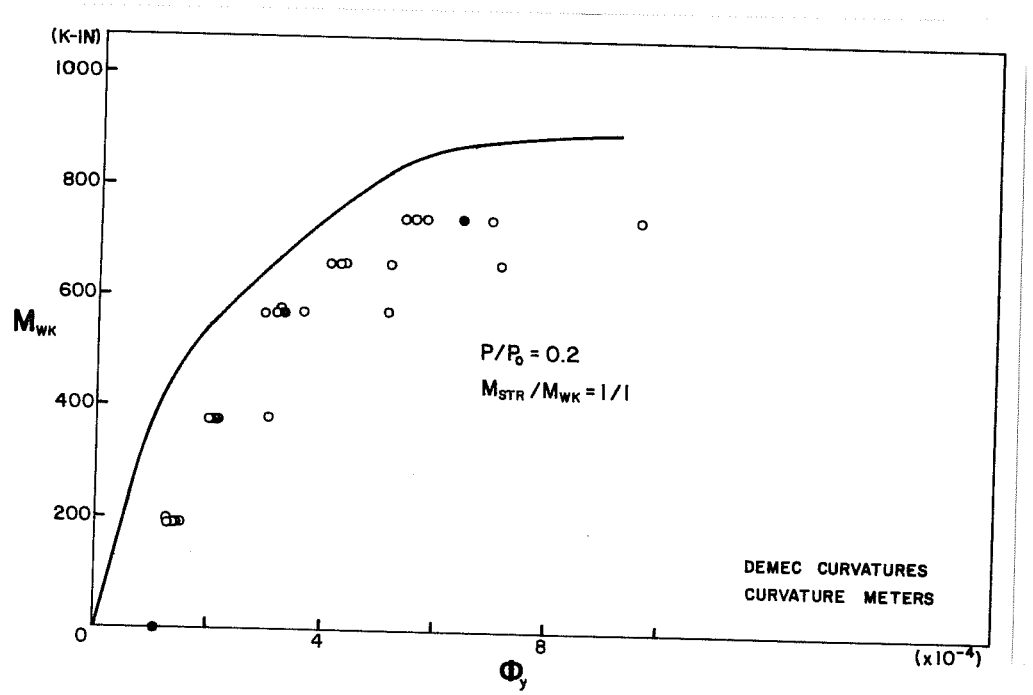

(b)

Fig. 4.48 P-M-ϕ behavior of three cell pier for $P/P_o = 0.2$ and $M_{STR}/M_{WK} = 1/1$

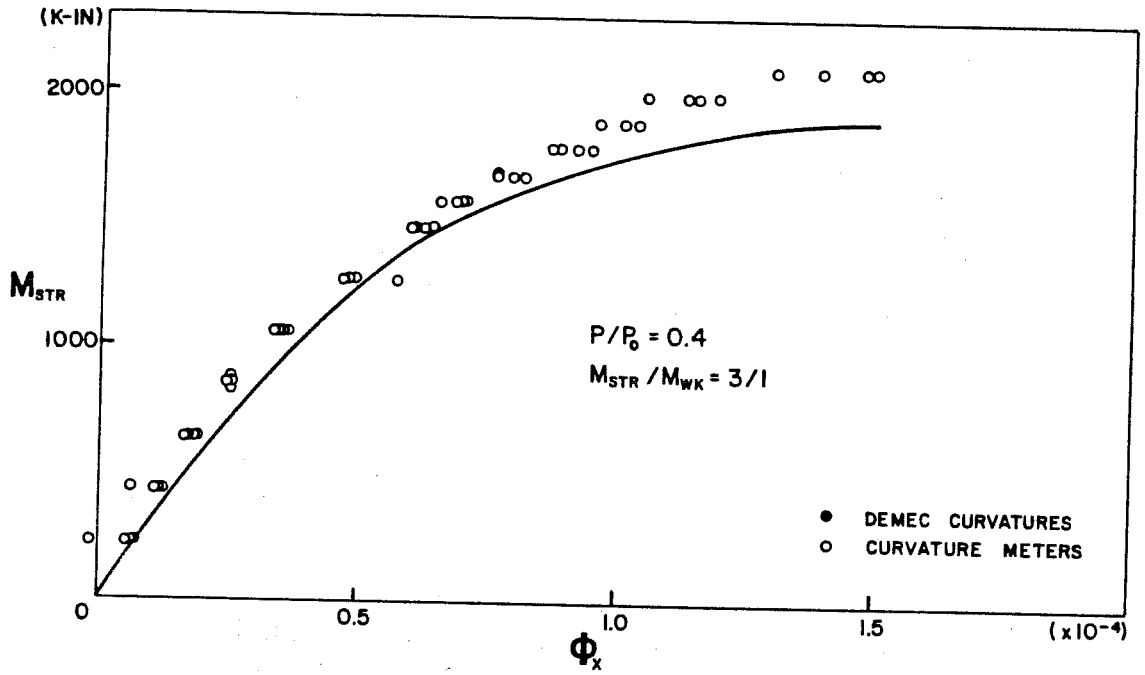

(a)

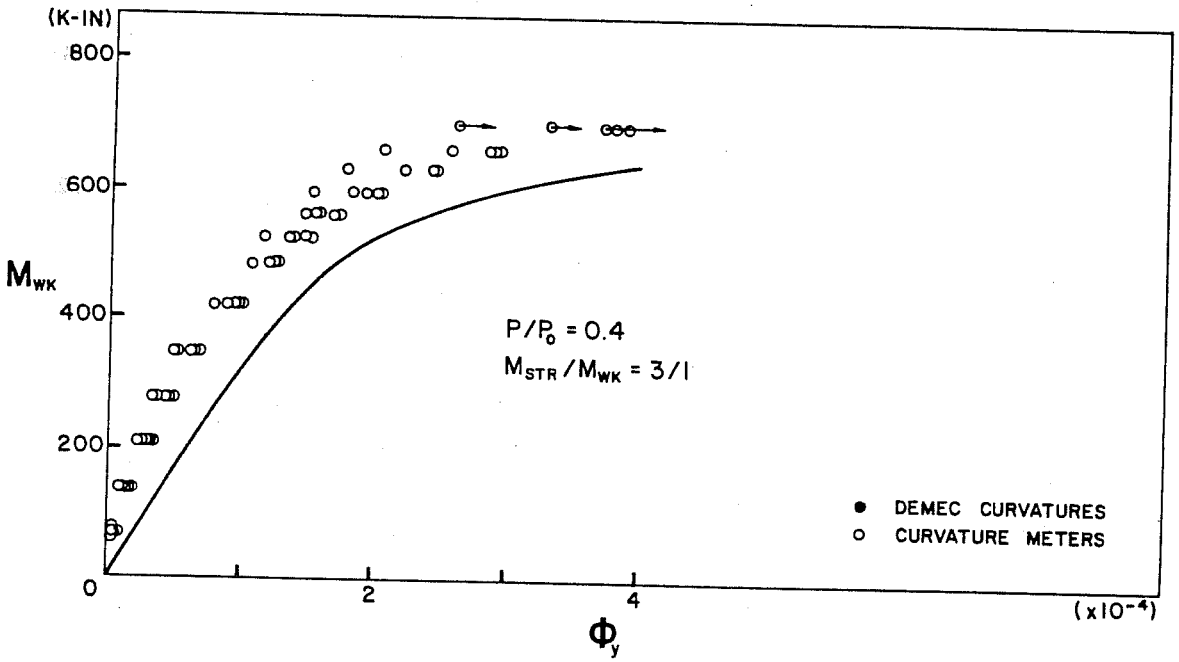

(b)

Fig. 4.49 P-M-ϕ behavior of three cell pier for $P/P_o = 0.4$ and $M_{STR}/M_{WK} = 3/1$

The observed and computed P-M-ϕ relationships for the three cell pier are shown in Figs. 4.37 through 4.49 for various loading modes. As with the other three specimens, the order of the figures corresponds to the order of the loading test. In these figures, the solid line represents the moment-curvature relationship predicted by BIMPHI while open and closed symbols represent the measured data. As with the two cell pier, the closed symbols represent the curvatures determined from Demec readings while open symbols represent the curvatures from the curvature meters. The same modification of the curvatures from curvature meters to take the residual curvatures into account was done using Demec readings as with the two cell pier, except for the ultimate loading case (Fig. 4.49) when the Demec strain gage was not available. Thus, the curvatures shown in Fig. 4.49 do not include residual curvatures which existed before applying bending moments to the specimen.

As shown in Figs. 4.37 through 4.49, the agreement of calculated and observed curvatures is good whenever the initial residual curvatures are small. All of the $P/P_o = 0.2$ loading cases (Figs. 4.37 through 4.39) show very good agreement. Residual curvature does not seem to be a problem at this level. With $P/P_o = 0.4$ and 0.6, the effect of residual curvature becomes more serious as loading progressed and observed curvatures were considerably larger than calculated values because of these residual curvatures. However, Fig. 4.49 indicates that the general relationship during the overall ultimate loading is closely predicted by BIMPHI when residual curvatures are ignored. The agreement in this figure is impressive when one considers the wide range of overload level loading the specimen had previously been subjected to.

4.6 Problems Encountered

The primary problem encountered in the physical test program was one of load alignment. Great effort was put forth to attain a concentric axial load initially. Techniques for alignment continually improved and this was a much reduced problem in the two and three cell pier tests. Effects of accidental eccentricity were corrected for in data reduction as previously discussed in Section 3.8.

Another serious problem involved a premature failure stage during an early loading in the solid pier near the upper head. This failure could have had two causes. First there may have been some unwanted eccentricity in the system which applied an upper end eccentricity much greater than the lower end eccentricity. The actual failure was a slight concrete compressive failure in the upper zone of the pier. It occurred on the first loading path for bending about the weak axis with an applied axial load of $0.6P_o$. Bending about the weak axis would create a long rectangular compression block much like that of a T-beam. This brings up a second possible cause of the failure.

Rüsch [21] showed that the ultimate concrete compressive strain is a function of the cross-sectional shape as shown in Fig. 4.50. He showed that a T-beam-type compression block can only withstand an ultimate concrete strain of about 0.0024 while a triangular-type compression block can withstand ultimate strains of around 0.0048. In the case at hand the ultimate capacity was estimated based on an ultimate concrete strain of 0.0038. This may have been too high for the weak axis bending of this section. Program BIMPHI allows the user to input the ultimate concrete strain, so the solid section's behavior was recalculated using an ultimate concrete compressive strain of 0.0024. Table 4.1 shows how moment and curvature values for weak axis bending are affected when different ultimate concrete strains are input. This resulted in a 7% reduction in the moment capacity, which certainly may have contributed to the premature failure. The designer needs to keep this potential problem of a thin rectangular compression block in mind. Note from Table 4.1 that this effect is less serious in a hollow pier. Similar calculations showed little reduction for the single cell pier.

The failure zone of the pier was patched with an epoxy typically used by the Texas State Department of Highways and Public Transportation for concrete repair. The repair was very successful. The retested solid pier experienced a compressive failure near midheight and well away from the damaged zone. Some of the instrumentation in the upper zone was felt to be unreliable due to the premature failure; therefore, no data from the top zone were used in this report.

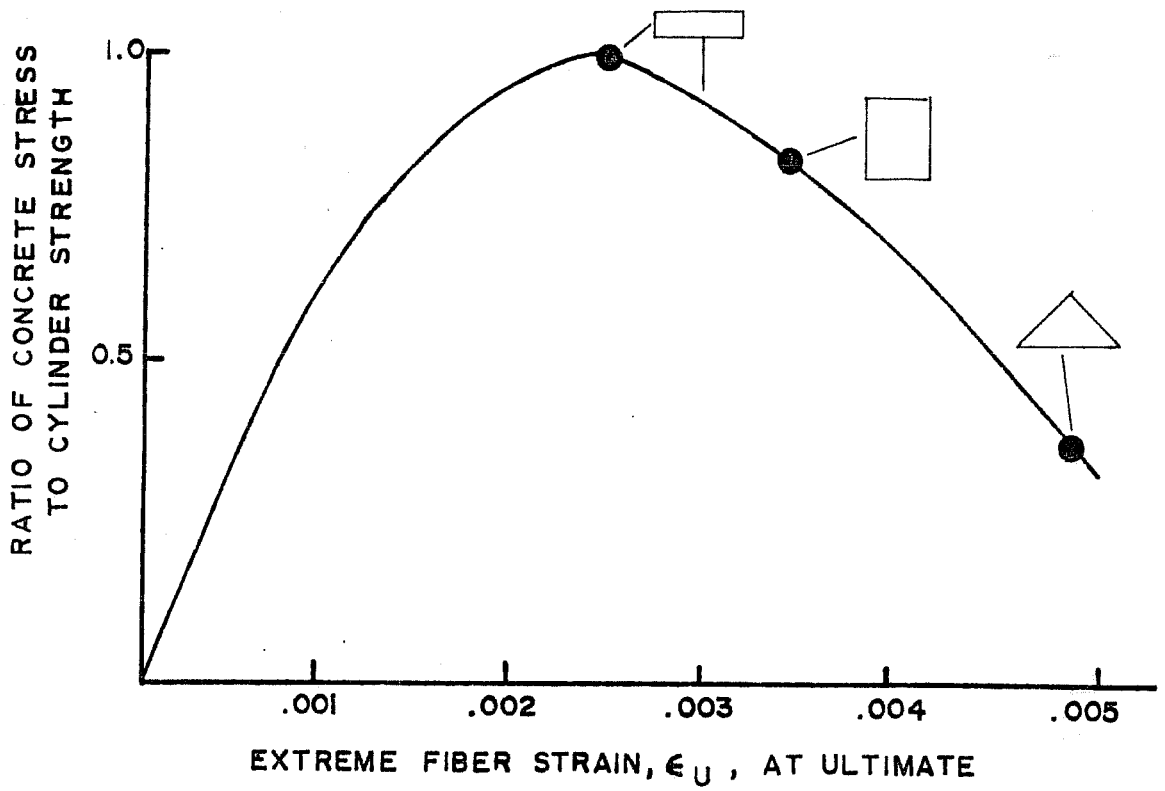

Fig. 4.50 Ultimate strain as a function of cross section

TABLE 4.1 EFFECT OF ULTIMATE COMPRESSIVE CONCRETE STRAIN ON PREDICTIONS FOR WEAK AXIS BENDING UNDER $0.6P_o$ AXIAL LOAD

	Maximum Moment M_{max} (k-in)	$\phi_{M_{max}}$ ($x10^{-4}$ $\frac{rad}{in}$)	Ultimate Moment M_{ult} (k-in)	$\phi_{M_{ult}}$ ($x10^{-4}$ $\frac{rad}{in}$)
Single Cell Pier $E_{ult} = 0.0024$	697	3.05	645	3.45
Single Cell Pier $E_{ult} = 0.0038$	728	3.70	636	5.70
SOLID PIER $E_{ult} = 0.0024$	762	3.15	745	3.70
SOLID PIER $E_{ult} = 0.0038$	813	4.55	791	6.25

Reductions due to using $E_{ult} = 0.0024$ instead of $E_{ult} = 0.0038$

	% Reduction in M_{max}	% Reduction in $\phi_{M_{max}}$	% Reduction in M_{ult}	% Reduction in $\phi_{M_{ult}}$
Single Cell Pier	4	21	-1	65
SOLID PIER	7	44	6	69

4.7 Comparison between Test Results and BIMPHI Predictions

4.7.1 Introduction. The primary purpose of the experimental phase of this study was to determine whether program BIMPHI is valid for predicting the behavior of hollow sections as well as for solid sections. In this section BIMPHI calculations will be compared with test results obtained in this study from both the solid and hollow piers to determine whether BIMPHI is valid for determining the behavior of solid, hollow, and cellular sections.

4.7.2 Data Input to BIMPHI. Program BIMPHI generated comparative P-M-ϕ values for each of the loading cases conducted. The data input based on measured geometrical and material values which was used for the generation of these calculated values is shown in Table 4.2. The computed P-M-ϕ values were shown in graphical form as the solid curves in Figs. 4.7 through 4.49.

4.7.3 Solid Section Comparison. The behavior of the solid pier is shown in Figs. 4.7 through 4.15. The moments are plotted against the curvatures for constant axial load levels. Each moment value is plotted against five curvature measurements to show the scatter of the data. The solid curve in each figure is the behavior predicted by program BIMPHI for that loading case.

The comparisons for the solid pier indicate that BIMPHI provides an excellent calculation of solid section behavior. The slight deviations between test data and BIMPHI calculations are equally divided between high and low moment values for a given curvature. Overall, the BIMPHI analysis was very accurate in the case of the solid section.

The values of calculated ultimate loads and measured ultimate loads for all four piers are shown in Table 4.3. The solid pier failed during application of an additional load increment when approximately 75% of that increment had been applied. Even though no curvature data were obtained at the load level, the value of the failure load was known. The failure load was very close to that predicted by BIMPHI. This shows

TABLE 4.2 INPUT DATA FOR BIMPHI PREDICTIONS

(a) Solid Section

f'_c = 4000 psi

E_c = 3605 ksi

$f_{c,max} = 0.85\ f'_c$

$\varepsilon_{c,max}$ = 0.0038

Hognestad concrete stress-strain curve

f_y = 61.1 ksi

E_s = 30500 ksi

Dimensions: 8.01" × 24.02"

(b) Single Cell Section

f'_c = 4900 psi

E_c = 3990 ksi

$f_{c,max} = 0.85 f'_c$

$\varepsilon_{c,max}$ = 0.0038

Hognestad concrete stress-strain curve

f_y = 61.1 ksi

E_s = 30500 ksi

Dimensions: 8.00" × 24.02"
2.50" wall thickness

(c) Two Cell Section

f'_c = 4760 psi

E_c = 3930 ksi

$f_{c,max} = 0.85\ f'_c$

$\varepsilon_{c,max}$ = 0.0038

Hognestad concrete stress-strain curve

f_y = 61.1 ksi

E_s = 30500 ksi

Dimensions: 8.0" × 24.0"
2.50" wall thickness

(d) Three Cell Section

f'_c = 5385 psi

E_c = 4183 ksi

$f_{c,max} = 0.85\ f'_c$

$\varepsilon_{c,max}$ = 0.0038

Hognestad concrete stress-strain curve

f_y = 61.1 ksi

E_s = 30500 ksi

Dimensions: 8.0" × 24.0"
2.50" wall thickness

TABLE 4.3 COMPARISONS OF OBSERVED ULTIMATE LOADS AND BIMPHI PREDICTIONS

		BIMPHI Prediction	Observed
Solid Section $X_{u/t} = 0$	P_{ult}	329 k	329 k
	$M_{str, ult}$	1955 k-in.	2110 k-in.
	$M_{wk, ult}$	665 k-in.	680 k-in.
Single Cell Section $X_{u/t} = 7.6$	P_{ult}	272 k	272 k
	$M_{str, ult}$	1685 k-in.	1440 k-in.
	$M_{wk, ult}$	560 k-in.	480 k-in.
Two Cell Section $X_{u/t} = 3.3$	P_{ult}	290 k	290 k
	$M_{str, ult}$	1695 k-in.	1770 k-in.
	$M_{wk, ult}$	565 k-in.	590 k-in.
Three Cell Section $X_{u/t} = 1.9$	P_{ult}	340 k	340 k
	$M_{str, ult}$	1920 k-in.	2085 k-in.
	$M_{wk, ult}$	640 k-in.	695 k-in.

that BIMPHI calculations were quite accurate for the solid section from both a behavior standpoint and from a capacity standpoint.

4.7.4 Single Cell Section Comparison. The P-M-ϕ behavior of the single cell section is shown in Figs. 4.16 through 4.24 for constant axial load levels. Seven curvature values are plotted for each moment value in order to show the scatter of the data. The behavior calculated by BIMPHI is shown as a solid curve in each figure.

The calculations by program BIMPHI are in good agreement with the test data shown in these figures. Most deviations seem to somewhat overestimate curvature values for a given moment. This would result in larger computed deflections and hence larger secondary moments and so it would be conservative for use in design. The only load case where calculated curvatures would be seriously unconservative is noted in test H4XYDUL which is shown in Figs. 4.23 and 4.24 and Table 4.3. This was the final loading case in which the section was loaded to failure. This came after a series of other loadings which produced widespread cracking, so the stiffness of the section at that point had severely degraded. This loading case was a repetition of an earlier load case, HOL4XYD, as shown in Figs. 4.17 and 4.18. Comparison of Figs. 4.23 and 4.24 with the earlier loading shown in Figs. 4.17 and 4.18 (note curvature scale change) show that the curvatures at the highest moment levels at which data were obtained were greatly increased (doubled) in the heavily cracked section. The analysis values agreed very well before widespread cracking from all loading cases but significantly underestimated curvatures in the ultimate test cycle. Before this final load case was applied, the pier had experienced cracking over one-half of its depth and one-half of its width. The specimen failed when about 90% of the next load increment had been applied but before data could be recorded. Figures 4.17 and 4.18 clearly show conservative behavior in the earlier application of load case HOL4XYD. However, close examination of Fig. 4.2 also indicates that strain gages 10, 12, and 16 showed abnormally high deviation from plane section behavior near

ultimate. The actual levels of applied moments at failure are shown on Figs. 4.23 and 4.24 and given in Table 4.3. A possible deficiency due to wall thinness is further discussed in Section 4.7.7.

4.7.5 Two Cell Section Comparison. The P-M-ϕ behavior of the two cell section is shown in Figs. 4.25 through 4.36. As previously mentioned, the residual curvatures around both strong and weak axes increase gradually due to the cracking or slight degradation of the concrete. This is clearly seen in these figures. In the first loading case, shown in Fig. 4.25 (uniaxial bending around strong axis), the agreement of the curvature predicted by BIMPHI and observed ones is excellent. In the second loading case, shown in Fig. 4.26 (uniaxial bending around weak axis), predicted and observed curvatures again show excellent agreement. In the third loading case, shown in Figs. 4.27(a) and (b), however, small residual curvatures around both axes are present prior to loading due to the two previous loading cases. This is because the preceding load cases had caused cracks on both tension faces of the specimen over more than half of the specimen height. The cracks do not completely close upon unloading. Up to the 6th loading case, shown in Fig. 4.30, the agreement of the predicted and observed curvature is still very satisfactory. As the number of severe loading cases increases, the residual curvature increase and the deviations of the observed and computed moment-curvature relationships increase. Their effect has been commonly seen in the load-deflection curve of structural members. The effects of the residual curvature are clearly shown in Fig. 4.31 through 4.35. It should be recognized that these reflect the condition of a specimen brought quite near ultimate very many times. Figures 4.36(a) and (b) show the results for the final loading case (12th) where the specimen was taken to failure. The load pattern is exactly the same as shown in Fig. 4.30. Initial residual curvatures around both strong and weak axes are also seen in Fig. 4.36. However, as the bending moments increase above previous load application levels, observed curvatures agree very well with the predicted ones. The ultimate bending capacities observed are slightly higher than the predicted ones as shown in Fig. 4.36

and Table 4.3. From these results, it can be concluded that for this type of pier and/or monotonic loading or major overload following a series of varied service load level loadings, the computer program BIMPHI will give very reasonable moment-curvature relationships and ultimate capacity for a section subjected to axial load and biaxial bending moment.

4.7.6 Three Cell Section Comparison. The P-M-ϕ behavior of the three cell section is shown in Figs. 4.37 through 4.49. As with the two cell section, predicted and observed curvatures agree very well up to the 6th loading case (see Figs. 4.37 to 4.42). As the residual curvatures increase with greater previous loading history, the slopes of the observed moment-curvature relationship are steeper than those of the predicted ones. This is true until they reach the level of the predicted relationship (see Figs. 4.43 to 4.48). This behavior is the same as was observed in the test of the two cell pier.

Figure 4.49 is the result for the final loading case (13th loading case). The load application pattern is the same as used in the 6th loading case, shown in Fig. 4.42, except the specimen was loaded until its failure. No Demec gage data could be obtained in this test. Thus, actual residual curvatures are not known although their possible magnitude could be estimated from the residual curvature of the preceding loading case, shown in Fig. 4.48. The observed curvatures in Fig. 4.49 do not include residual curvatures. However, even in Fig. 4.48 the observed and predicted curvatures had similar shapes. Agreement between observed and computed moment-curvatures is very good all the way to failure. The final failure mode was a compressive failure of the concrete at the compression corner of the specimen. The ultimate capacity observed was quite close to the predicted one as shown in Fig. 4.49 and Table 4.3.

From these results, the same conclusion can be drawn as found with the two cell pier, i.e., for this type pier under monotonic loading or major overloading following a series of varied service load level loadings, the computer program BIMPHI will give very reasonable moment-curvature relationships and ultimate capacity for a section subjected to axial load and biaxial bending moment.

4.7.7 General Comparison. Overall, quite good agreement was found between BIMPHI predictions and the pier test series data. No significant problems were found in either plane section behavior, or computed vs actual curvature and strength relationships for the solid specimen or for the two cell or three cell specimens. At service load levels and earlier loading stages the results for the single cell pier were also in good general agreement with predicted values. However, the ultimate loading test for that specimen indicated that near ultimate the strain distribution deviated substantially from the plane of strains (see Fig. 4.2) and only 85% of the computed ultimate moment capacity was developed (see Table 4.3). Since this was not experienced in the other three specimens which had similar load pattern applications it would not appear that this reduction should be categorically attributed to residual loading damage, unrealistic loading histories, or experimental equipment errors.

Since the major variation between test specimens was the cross-sectional shape, a series of checks was made of the effects of possible variables. Examinations using the data from the present test series as well as the hollow test series of Procter (Section 2.3.1.4) of variables such as the percentage of voids in the cross section or the wall thickness showed no trends. However, the data as shown in Fig. 4.51 did indicate a significant effect of wall cross section slenderness. This was defined as the ratio of unsupported cross-sectional wall length to wall thickness. Using this cross-sectional parameter (X_u/t), no strength reductions of any significance are indicated for specimens in which the wall cross section slenderness ratio was 6% or less. However, in both Procter's and the present study for the thin wall specimens with ratios of approximately 7.5, an approximately 12 to 15% decrease in capacity occurred. Test data for even thinner wall hollow piers are very scarce, although large piers have been built with more slender ratios [7]. A recent report by Jobse [29] describes tests of two square hollow piers made with very thin plates of high strength concrete. Piers 15 ft. long and 5 ft. square

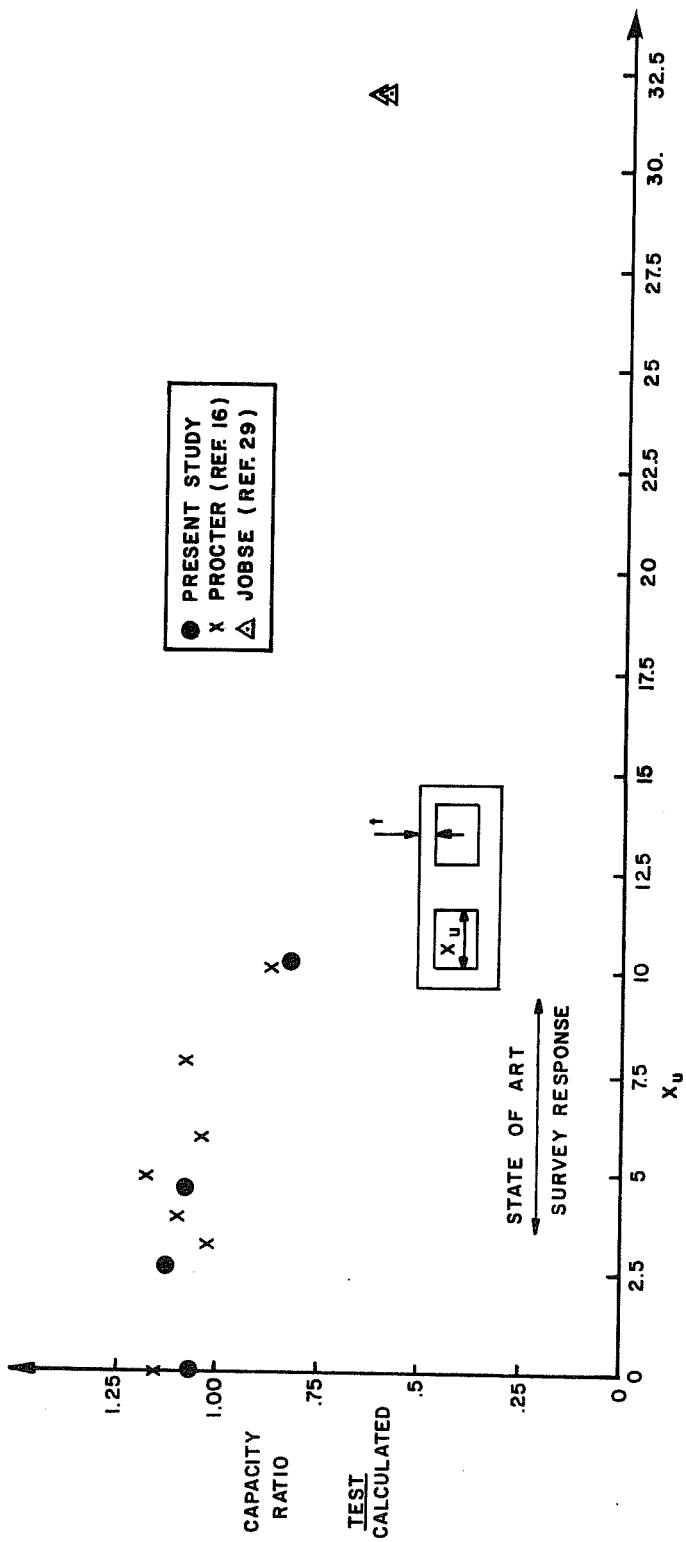

Fig. 4.51 Effect of wall thinness on pier capacity

with 1-1/2 in. thick walls were loaded with varying eccentricities. Failure loads were compared to the conventional interaction diagram predictions. The sections had large fillets at the corner and the unsupported cross-sectional wall length to wall thickness was taken as the ratio $X_u/t = 48/1.5 = 32$. Substantial reduction in the expected column strength based on normal column cross section capacity was found as shown in Fig. 4.51. Approximately half of the reduction in capacity for these two specimens was predicted by the consideration of compression flange buckling as reported by Jobse. Failures were extremely explosive in nature. These interesting tests of a relatively stocky pier overall (height/outside depth = 3) indicate substantial deviation from normal cross section behavior when extremely thin wall members are used. In the state of art survey responses summarized in the other report of this series (Ref. 7), the respondents (representing a wide cross section of states) had indicated a range for this parameter of 3 to 6 had been used and was of major interest. This is why the experimental program only included values up to 7.5. In light of the recent use of thinner wall piers, this effect should be further investigated.

It is important to recognize that the loadings to which these piers were subjected are representative of the smallest eccentricities and highest axial load levels likely in bridge piers. As axial load levels decrease and pier behavior becomes more like a beam in character, this may not be as major a problem. Conventional limits for flange thickness in isolated T-girders in which the T-shape is used to provide a flange for additional compressive area (AASHTO Art. 1.5.23(J)(2)(c)) require the flange width to be not more than four times the width of the girder web. Thus the overhanging flanges could not be more than three times the web thickness. If, as shown in Fig. 4.52, one applied this type limit to a box type cross section (which is not specifically covered under that Article) it could be assumed that the X_u/t ratio should be restricted to a limit of 6 which would be quite safe when checked against

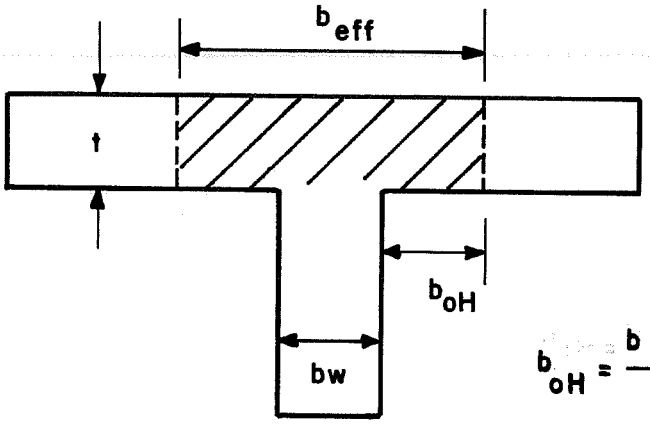

AASHTO Art I.5.23(J)(2)(C)

LIMITS $\begin{cases} t \geq \frac{bw}{2} \\ b_{eff} \leq 4bw \end{cases}$

IF $bw = 2t$ THEN

$b_{oH} \leq 3t$

(a) AASHTO ISOLATED T-GIRDER LIMITS

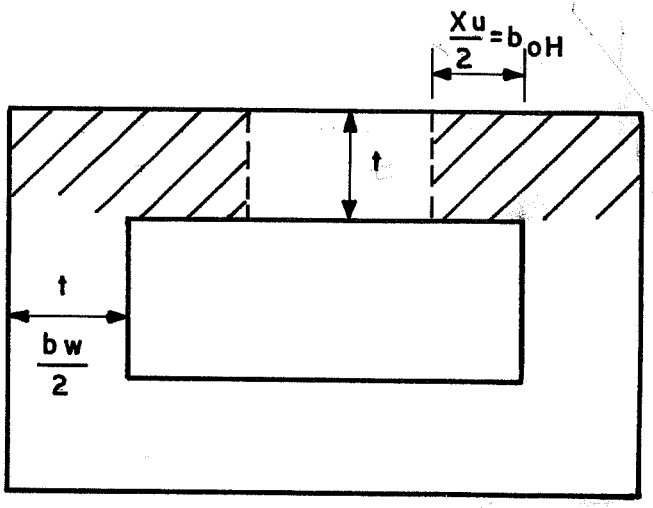

IF $t = \frac{bw}{2}$ AND

$b_{OH} \leq 3t$

$\therefore \frac{Xu}{2} \leq 3t$

$\frac{Xu}{t} \leq 6$

(b) POSSIBLE APPLICATION TO HOLLOW PIERS

Fig. 4.52 AASHTO isolated compression flange limits

Fig. 4.51. The present limit on isolated T-girder flanges was set for those cases where the T-shape is being used to provide additional compression area which is certainly the case in the pier cross sections tested. The origin of the original limit on the effective flange width stems from elastic studies which consider support conditions, moment gradients, and similar parameters which differ from this case. However, the similarity in end result is striking.

Jobse [29] suggests that the development of high quality dense concrete will lead to more use of thin sections. He indicates such use will require the incorporation of criteria for concrete thin plate buckling in codes and standards. As an interim measure he recommended that in the absence of a detailed rational analysis, plate thinness should be limited to $X_u/t \leq 10$. As can be seen from Fig. 4.51, caution is advised whenever the X_u/t ratio enters the 8 to 10 range and very appreciable reductions in capacity occur in comparison to solid members.

CHAPTER 5

SUMMARY, CONCLUSIONS, AND RECOMMENDATIONS

5.1 Summary of the Study

The basic purpose of this portion of the overall study of slender pier design was the verification of the accuracy and applicability of subprogram BIMPHI and programs PIER and FPIER. In most cases the accuracy of these programs over the full nonlinear range was checked against previous studies reported in the engineering literature. In order to provide a verification of the basic moment-curvature routines for hollow sections, a series of physical tests was undertaken of single and multiple cell sections to develop basic data for verifying the key subprogram BIMPHI. The sections chosen represent typical state-of-the-art sections reported in a national survey and were limited to unsupported wall cross section length to thickness ratios of about 7.5.

Comparisons of the analytical results with test results reported in the literature are given in Chapter 2. Verifications reported included nonlinear moment-curvature relationships, effect of creep, second order moments due to axial loads, beam flexural behavior, and multiple member frame behavior. A detailed report on test procedures and results for a series of biaxially loaded pier specimens is given in Chapters 3 and 4. The pier cross sections tested varied from solid through single and multiple cell types. The linearity of strain profile and the axial load-moment-curvature relationships were examined under a wide variety of loading combinations. Ultimate capacities were determined for each section. The program predictions are compared with the experimental results.

5.2 Conclusions

These conclusions are restricted to axial and flexural load combinations. Neither the programs nor the experimental test program

treated significant shear forces. These conclusions are also based on a reasonably stiff cross section. As shown in Section 4.7.7, very limited experimental evidence raises questions as to the strength and stiffness near ultimate load of cross sections with an unsupported cross section wall length to thickness ratio of 7.5 or greater. Further examination is required for very thin wall sections.

Within the general limits of this study, it can be concluded that:

(1) Programs BIMPHI, PIER, and FPIER are accurate and useful tools for the analysis of biaxially loaded piers.

(2) BIMPHI is an accurate subroutine for predicting cross section stiffness for a wide range of pier shapes.

(3) PIER is an accurate program for studying single member pier behavior and satisfies all general requirements of AASHTO Article 1.5.34(A)(1) for determination of slenderness effects in compression members.

(4) FPIER is an accurate program for studying multiple member pier bent behavior and satisfies all general requirements of AASHTO Article 1.5.34 (A)(1) for determination of slenderness effects in compression members.

(5) In utilizing these programs, the Hognestad stress-strain diagram should be used for unconfined concrete and the Ford stress-strain diagram may be used for confined concrete. Best agreement was found when the maximum compressive stress is assumed as $0.85f'_c$ for vertically cast members and $0.95f'_c$ for horizontally cast members.

(6) The assumption that plane sections remain plane was verified for biaxially loaded rectangular columns of solid and cellular cross sections in all cases where the cross section unsupported wall length to thickness ratio did not exceed 6.

(7) Limited experimental evidence indicates that for hollow cross sections with wall unsupported length to thickness ratios of approximately 7.5, a 15% decrease in strength occurs and there is appreciable variation of strains from planar section behavior, particularly in the tension zones of the thin wall area. Recent tests reported by Jobse [29] and also shown in Fig. 4.51 indicate as much as 40% decrease in strength for extremely thin wall sections ($X_u/t = 32$).

REFERENCES

1. American Association of State Highway Officials, Standard Specifications for Highway Bridges, 12th Ed., 1977.

2. ACI Committee 318, Building Code Requirements for Reinforced Concrete (ACI 318-77), American Concrete Institute, Detroit, 1977, 102 pp.

3. ACI Committee 318, Commentary on Building Code Requirements for Reinforced Concrete (ACI 318-71), American Concrete Institute, Detroit, 1977, 132 pp.

4. Wood, B. R., Beaulieu, D., and Adams, P. F., "Column Design by P-Delta Method," Proceedings, ASCE, V. 102, No. ST2, February 1976, pp. 411-427.

5. Wood, B. R., Beaulieu, D., and Adams, P. F., "Further Aspects of Design by P-Delta Model," Proceedings, ASCE, No. ST3, March 1976, pp. 487-500.

6. Poston, R. W., "Computer Analysis of Slender Nonprismatic or Hollow Bridge Piers," unpublished M.S. thesis, The University of Texas at Austin, May 1980.

7. Poston, R. W., Diaz, M., Breen, J. E., and Roesset, J. M., "Design of Slender, Nonprismatic, and Hollow Concrete Bridge Piers," Research Report 254-2F, Center for Transportation Research, The University of Texas at Austin, August 1982.

8. Hognestad, E., "A Study of Combined Bending and Axial Load in Reinforced Concrete Members," University of Illinois Bulletin, Engineering Experiment Station Bulletin Series No. 399, November 1951.

9. MacGregor, J. G., Breen, J. E., and Pfrang, E. O., "Design of Slender Concrete Columns," Journal of the American Concrete Institute, Proceedings Vol. 67, No. 1, January 1970, pp. 6-28.

10. Ferguson, P. M., Reinforced Concrete Fundamentals, 3rd Ed., John Wiley and Sons, Inc., New York, 1973.

11. Breen, J. E., "The Restrained Long Concrete Column as a Part of a Rectangular Frame," unpublished Ph.D. dissertation, The University of Texas, Austin, June 1962.

12. Ford, J. S., "Behavior of Concrete Columns in Unbraced Multipanel Frames," unpublished Ph.D. dissertation, The University of Texas at Austin, December 1977.

13. Mavichak, V., "Strength and Stiffness of Reinforced Concrete Columns under Biaxial Bending," unpublished Ph.D. dissertation, The University of Texas at Austin, May 1977.

14. Considère, A., Experimental Researches on Reinforced Concrete, Translated by L. S. Moisseiff, McGraw Publishing Co., 1903.

15. Procter, A. N., "Hollow Concrete Columns," Civil Engineering (London), September 1976, pp. 53-55.

16. Procter, A. N., "Hollow Rectangular Reinforced Concrete Columns," Civil Engineering (London), September 1977, pp. 45-49.

17. Breen, J. E., Cooper, R. L., and Gallaway, T. M., "Minimizing Construction Problems in Segmentally Precast Box Girder Bridges," Research Report No. 121-6F, Center for Highway Research, The University of Texas at Austin, August 1975.

18. Farah, A., and Huggins, M. W., "Analysis of Reinforced Concrete Columns Subjected to Longitudinal Load and Biaxial Bending," ACI Journal, July 1969, pp. 569-575.

19. Wu, Howard, "The Effect of Volume/Surface Ratio on the Behavior of Reinforced Concrete Columns under Sustained Loading," unpublished Ph.D. thesis, University of Toronto, 1973.

20. Drysdale, R. G., "The Behavior of Slender Reinforced Concrete Columns Subjected to Sustained Biaxial Bending," unpublished Ph.D. dissertation, The University of Toronto, 1967.

21. Rüsch, Hubert, "Researches Toward a General Flexural Theory for Structural Concrete," ACI Journal, July 1960, pp. 1-28.

22. Green, R., "Behavior of Unrestrained Reinforced Concrete Columns," Ph.D. dissertation, University of Texas at Austin, 1966.

23. Green, R., and Breen, J. E., "Eccentrically Loaded Concrete Columns Under Sustained Load," ACI Journal, Proceedings V. 66, No. 11, Nov. 1969, pp. 866-874.

24. Chovichien, V., Gutzmiller, M. J., and Lee, R. H., "Analysis of Reinforced Concrete Columns Under Sustained Load," ACI Journal, Proceedings V. 70, No. 10, October 1973, pp. 692-699.

25. Breen, J. E., and Pauw, A., "An Investigation of the Flexural and Shearing Capacity of Reinforced Concrete Beams," Vol. 61, No. 33, Bull. No. 49, Engineering Experimental Station, University of Missouri, 1960.

26. Baron, M. J., and Siess, C. P., "Effect of Axial Load on the Shear Strength of Reinforced Concrete Beams," Civil Engineering Studies, Structural Research Series No. 121, University of Illinois, Urbana, Ill., June 1956.

27. Ernst, C., Smith, M., Riveland, R., and Pierce, N., "Basic Reinforced Concrete Frame Performance Under Vertical and Lateral Loads," ACI Journal, Proceedings V. 70, No. 4, April 1973, pp. 261-269.

28. Repa, J. V., Jr., "Flexural Stiffness Redistribution in Typical Highway Bents," unpublished M.S. thesis, The University of Texas at Austin, August 1970.

29. Jobse, H. J., "Applications of High Strength Concrete for Highway Bridges," Report No. FHWA/RD-82/097, Concrete Technology Corporation, Tacoma, Washington, 1982.